The Interaction Between Chemical and Mechanical Processes During Metamorphism: A Microstructural and Petrologic Study of Amphibolite Shear Zones, Cheyenne Belt, Southeastern Wyoming

by

Matthew W. Nyman

Dissertation submitted to the Faculty of the Virginia Polytechnic Institute and State University in partial fulfillment of the requirements for the degree of

Doctor of Philosophy

in

Geological Sciences

APPROVED:

Robert J. Tracy, Co-Chairman

Richard D. Law, Co-Chairman

David A. Hewitt

Robert J. Bodnar

Ernest M. Duebendorfer

February, 1992

Blacksburg, Virginia

ABSTRACT

Shear zones which deform margins of amphibolite boudins in the Cheyenne Belt, SE Wyoming, record a full strain transition from relatively undeformed amphibolite which has relict igneous textures to mylonitic amphibolite with a strongly developed L-S tectonic fabric. The strain transition is marked by the rotation of amphibole and plagioclase aggregates into parallelism with the shear zone boundary and progressive grain size reduction. These observations indicate that strain magnitude increases across the shear zone. Detailed petrologic and microstructural analysis of a single amphibolite shear zone has been conducted in order to: 1) document the petrologic and microstructural evolution of the shear zone and 2) investigate the interrelationships between mechanical and chemical processes associated with shear zone formation.

Amphibolites throughout the shear zone consist of amphibole + plagioclase with only minor amounts of quartz + chlorite + epidote + sphene + ilmenite. Within the relatively undeformed amphibolite, amphibole and, to a lessor extent, plagioclase has wide compositional variation. Amphibole compositions vary from actinolitic hornblende to magnesio-hornblende which involves increases in Al, Fe, Na and K contents and decreases in Si and Mg. Plagioclase compositions vary from An_{60} in cores of plagioclase grains to An_{30} within grain boundary domains. With increasing strain magnitude across the shear zone variation of amphibole composition decreases and become predominantly magnesio-hornblende. Plagioclase compositions also decrease in range although grain boundary domains still have higher albite content. The observed variation of amphibole compositions indicate that shear zone formation occurred during prograde metamorphism although compositional changes may also be a function of changing grain boundary fluid composition.

These petrologic data indicate that shear zone metamorphism was in part controlled by the magnitude of strain during deformation. Scanning electron microscope back-scattered images and color enhanced X-ray compositional maps indicate that compositional variation in plagioclase and amphibole occurs along margins of highly angular grains of various sizes. These textural observations have been interpreted to indicate that chemical reactions occurred by a dissolution and reprecipitation processes following or during cataclastic deformation. Transmission electron microscope (TEM) images show local zones of high dislocation density adjacent to microcracks suggesting that work hardening may have been an important processes during cataclasis. Alternatively, microcracks may have acted as source for development of dislocations.

The importance of deformation in assisting shear zone chemical processes is evidenced by: 1) the observation of new mineral overgrowth along grain boundaries and 2) TEM images of amphibole which show that actinolitic hornblende has a high defect density whereas magnesio-hornblende overgrowths are relatively defect free. This observation suggests that strain energy associated with dislocations may have contributed to the chemical process. Thermodynamic modelling of reaction progress within the shear zone using the Gibbs Method indicates that observed modal and compositional changes can occur isothermally if strain energy is added to the system. Increases in reaction progress with deformation may have also been due to increases in fluid infiltration or diffusion due to grain size reduction. The general conclusion of this study is that in order to apply petrologic, geochemical and isotopic data to understanding geochemical and tectonic processes, microstructural information on the magnitude of strain and the type of deformation mechanism must be evaluated, quantitatively if possible.

ACKNOWLEDGEMENTS

"When your serious about having fun, it is no fun at all" Calvin and Hobbes

"I was gratified to be able to answer promptly. I said I don't know." Mark Twain

Across these short paragraphs acknowledgements are suppose to flow conveying words of thanks for support, guidance and the occasional kick in the butt. Difficult to say at the least and I apologize at the beginning for any omissions which are surely due to my shortened memory rather than lack of appreciation. For the last six years my parents and family have been a source of continual emotional and financial support. Despite the calls of "Get a job, your 30 years old" they have never-the-less supported my academic pursuits. In addition, my parents are truly responsible for me sticking with my degree programs as they instilled in me tenacity, a good work ethic and the desire to always preform to the best of my ability. In particular I acknowledge my older brother and fellow geologist Mark who always admonished me about field relations and forced me to think how the more esoteric aspects of this study apply to real rocks. I hope that I have served that aspect of my work well.

To my co-advisors I acknowledge their patience with their 'renegade' grad student. No, Wyoming is not even close to the pubs adjacent to the Moine Thrust or the genteel, pastoral settings of Connecticut, but despite my working outside of their geologic and geographic areas of expertises, both Bob and Rick have been a source of intellectual and financial support. I especially thank them for pushing me to stick with this study even when funding fell through or I had an all to frequent lapse of confidence. In addition, I thank my other committee members: Dave Hewitt for forcing me through the perils of thermo as well as updating me on Giant trivia (especially when they were winning). Bob Bodnar for early financial assistance in attending GSA and GAC-MAC meetings and useful comments on various manuscripts. And Ernie Duebendorfer for sharing his extensive knowledge of the Medicine Bow Mountains as well as reviewing my dissertation.

The camaraderie and friendships that I have developed with my fellow grad students have been the true reward of being in graduate school. First the old folks, those that have up and left; the old flink boys, Don Hall and Mike Sterner, Mike and Karen Wizevich, Bill and Alicia Hames, Alan and Susan Hubbard, Maya Elrick, of course Dr. Jean Cline, Celia and Peter Clowe-Hennings and John Groen. The ever observant Charlie Oakes is thanked for many stimulating (and unopinionated) discussions on geologic and

nongeologic topics. And my irrepressible former roomate Senor Ronald Wynn Sheets for, well for being Ron Sheets. My petrologic pals Steve Miller, Barb Munn (and of course Ron Wirgart) and Tom (and Kathleen) Armstrong are thanked for their friendship and supplying added incentive to my petrologic endeavours In particular I thank Tom for fruitful discussions and reflections on petrologic and field aspects of this study especially with respect to application to other geologic settings. My TEM work would not have been completed without the able assistance and friendship of Gene Smelik (and family). Others who have assisted or taught me new things along the way include Rich Whitmarsh, Sven Morgan, Chris Fedo, J. Bret Bennington, Carl Kirby and Mark Williamson. Also many kudos to Todd Solberg for all his microprobe assistance and the ever-pleasant office staff Belinda, Karen, Linda, Carolyn and Dean.

Lastly and most importantly I acknowledge May Nyman, my wife, companion, friend, climbing partner and lover, because of her these last three years have surely been the best yet. Our relationship which started because we had the same shoe size and continued because of Philippino guerrillas is certainly the most important thing in my life and I look forward to sharing the days (daze) ahead together. I consider the completion of this endeavour a joint project which I could not have done without her support and enthusiasm.

TABLE OF CONTENTS

INDEX TO FIGURES

CHAPTER 2

CHAPTER 3

CHAPTER 4

INDEX TO TABLES

CHAPTER 2

CHAPTER 3

CHAPTER 1: INTRODUCTION TO DISSERTATION

The goal of the research reported in this dissertation is to determine the interrelationships between mechanical and chemical processes during metamorphism and in particular, the effects of deformation on the progress of reactions within shear zones which deform amphibolite boudins. This study involves petrologic, geochemical and microstructural characterization of meter-scale shear zones that cut and deform amphibolite boudins in the Cheyenne belt, southeastern Wyoming. In the Cheyenne belt, samples of variably deformed amphibolite contain a full strain transition from relatively undeformed amphibolite with a relict igneous texture to amphibolite with well developed linear and planar fabric elements. Strain magnitude increases across the shear zone, as indicated by the progressive rotation of amphibole + plagioclase aggregates as well as decreasing grain size. Samples which contain the full strain transition provide a natural laboratory for this study in that the full range of mechanical and chemical changes associated with increasing deformation are present. Therefore, this study locale provides an ideal setting to investigate the interaction between chemical and mechanical processes with respect to shear zone evolution, and to make inferences as to the importance of the interaction of these processes during metamorphism in general. The results of this study show that mechanical processes such as grain size reduction and the development of high dislocation densities can exert considerable control on the extent of reactions within such shear zones.

During dynamothermal metamorphism there are two end-member interrelationships between deformation and metamorphism (Brodie and Rutter, 1985). On one hand, mechanical processes can enhance the progress of reactions. This can occur by: 1) grain size reduction which can promote fluid ingress and/or enhancement of

intergranular diffusion rates as well as increase the grain boundary volume available for reaction (Nyman et al., 1991; Koons et al., 1987); 2) increase in dislocation densities of minerals that can in turn change the thermodynamic stability of phases (Wintsch and Andrews, 1985); 3) enhancement of volume diffusion by providing fast diffusion 'pipes' along dislocation cores and other defect microstructures (Yund et al., 1991; Hacker and Christie, 1991); and 4) provision of nucleation sites along defect microstructures that would lessen activation energy barriers for initial stages of grain growth (Smith, 1985, Cahn, 1957). In addition, dislocation creep or cataclasis may significantly alter the physical properties of grain boundaries which could dramatically affect intergranular diffusion rates and hence the progress of chemical processes.

On the other hand, mineral reactions can alter the physical properties of rocks and therefore change the amount of strain which can be accommodated as well as induce changes in deformation mechanisms. The ductility of rocks can be affected by: 1) decreases in the grain size of reaction products, which would facilitate mechanical processes such as grain boundary sliding (reaction enhanced ductility of White and Knipe, 1975; see also Gilotti, 1989; Rubie, 1983) ; 2) release of fluids during dehydration reactions, thereby promoting cataclasis or producing transient changes in strain rate (Kerrich et al., 1980; see review by Murrell, 1985); 3) volume changes that may enhance intracrystalline plasticity (Poirier, 1982); and 4) variation of local chemical potential gradients that can affect diffusive transfer deformation mechanisms (Rutter, 1976).

There have been numerous studies that have outlined the interrelationships between chemical and mechanical processes during metamorphism, especially with respect to shear zones (see review by Brodie and Rutter, 1985). In addition, there also have been studies in a variety of other geologic settings that indicate the interaction

between chemical and mechanical processes is vital in facilitating, as well as instigating, geological and geophysical processes. For example, theoretical studies have indicated that weathering and low-temperature dissolution may occur by preferential solution along etch pits (Lasaga and Blum, 1986) Etch pits are interpreted as representing the intersection of dislocations with the mineral surface. Experimental studies addressing the theory of defect enhanced dissolution have shown that the solubility of minerals increases with increasing strain magnitude (Schott et al., 1989; Bosworth, 1981) , although other studies show that increases in defect density have relatively little effect on solubility (Murphy, 1989; Blum et al., 1990). The increase of solubility with increasing defect density has been explained by: 1) increase in the Gibbs free energy which results in a decrease in the stability of the mineral and 2) changes in kinetic rates due to increases in available sites for dissolution. Examples of increasing solubility with increasing deformation have also been described in naturally deformed rocks (e.g. Engelder, 1982).

The importance of the interaction between mechanical and chemical processes has also been illustrated for deep crustal processes. Several workers have proposed that reconstructive polymorphic phase transformations may be the source for deep focus earthquakes in subducting lithosphere (Kirby et al., 1991;Kirby, 1987; Green and Burnley, 1989; Rubie, 1984). The controversy concerning deep-focus earthquakes is that at deep crustal levels in subduction zones, rocks should deform by creep rather than a frictional mechanism. As shown by study of shallow earthquakes within the brittle regime, frictional processes such as fracture and sliding are required to produce seismic energy (Scholz, 1990). Kirby and co-workers (Kirby, 1987; Kirby et al., 1991) have proposed that faulting within subduction slabs may be due to reconstructive phase transformations of olivine and have called this process 'transformational faulting'. The main tenet of this model is that metastable phases within interior portions of subducting

slabs persist into hotter regions of the mantle. At some critical stress and temperature, faulting occurs due to the creation of shear instabilities associated with reconstructive polymorphic phase transformations. This behavior has been observed in hydrostatic laboratory experiments for ice, tremolite and germanate olivine.

These two examples which cover shallow and deep crustal processes, highlight the obvious importance of the interaction between mechanical and chemical processes in assisting and perhaps controlling geologic and geophysical processes. Other examples of geologic processes where interaction between mechanical and chemical processes are important include: 1) cementation during burial diagenesis where hydrostatic stresses along grain boundaries can promote dissolution and subsequent cementation (de Boer, 1977); 2) development of cleavage and other structural fabrics where nonhydrostatic tectonic stresses control chemical potential gradients and deformation mechanisms (Gray and Durney, 1979; Rutter, 1976); 3) the rheology of rocks, in which it has been shown both experimentally and in field examples that the nature of the chemical environment can control the strength and deformation mechanisms of rocks (Murrell, 1985; Kerrich et al, 1980); and 4) the positioning of paleomagnetic poles, where a recent study by Stamakatos and Kodama (1991) has shown that the magnitude of strain must be considered when evaluating paleomagnetic data.

This dissertation is separated into three chapters. The first chapter describes the petrologic and geochemical evolution of small-scale amphibolite shear zones from the Cheyenne belt, southeastern Wyoming. Chapter 2 details a quantitative treatment of the effects of changing dislocation density on the progress of reactions within the shear zone using the Gibbs Method. Chapter 3 is a report on the deformation mechanisms for the development of core-mantle structures in amphibole. These chapters present comprehensive petrologic, geochemical and microstructural data on the mechanical and

chemical evolution of the small-scale shear zones which allow for a quantitative evaluation of the role of strain energy in the progress of the metamorphism. The general conclusion of this study is that in order to apply petrologic, geochemical and isotopic data to understanding geochemical and tectonic processes, microstructural information on the magnitude of strain and the type of deformation mechanisms must be evaluated, quantitatively if possible.

CHAPTER 2: PETROLOGIC EVOLUTION OF AMPHIBOLITE SHEAR ZONES, CHEYENNE BELT, SOUTHEASTERN WYOMING

ABSTRACT

Meter-scale amphibolite boudins in the Cheyenne belt, southeastern Wyoming are cut and deformed by shear zones which preserve the full strain transition across approximately 7 cm from relatively undeformed amphibolite with a relict igneous texture to amphibolite with a L-S tectonic fabric. The strain transition is marked by the progressive dextral rotation of amphibole + plagioclase aggregates into parallelism with the shear zone boundary. Strain magnitude increases across the shear zone as indicated by the development of the tectonic fabric and progressive reduction of amphibole and plagioclase grain size as a result of cataclasis.

Bulk chemical data for five samples from a single strain transition shows no significant or systematic variation in major element chemistry except for a 1 weight percent loss of SiO_2. This indicates that the shear zone was a closed system to nonvolatile components during metamorphism and deformation.

Amphibolites within the shear zone consist of amphibole + plagioclase with only minor amounts of quartz + chlorite + epidote + sphene + ilmenite. Within the relatively undeformed amphibolite, amphibole and, to a lessor extent, plagioclase has wide compositional variation. Amphibole compositions vary from actinolitic hornblende to magnesio-hornblende which involves increases in Al, Fe, Na and K contents and decreases in Si and Mg. This variation can be modelled as progress along tschermakite, edenite and $FeMg_{-1}$ exchange vectors from tremolite. Plagioclase compositions vary from An_{60} in cores of plagioclase grains to An_{30} within grain boundary domains. With increasing strain magnitude across the shear zone variation of amphibole composition decreases and become predominantly magnesio-hornblende. Plagioclase compositions

also decrease in range although grain boundary domains still have higher albite content. The observed variation of amphibole compositions indicate that shear zone formation occurred during prograde metamorphism although compositional changes may also, in part, be a function of changing grain boundary fluid composition.

These petrologic data indicate that shear zone metamorphism was controlled by the magnitude of strain during deformation. Scanning electron microscope back-scattered images and color enhanced X-ray compositional maps indicate that compositional variation in plagioclase and amphibole occurs along margins of highly angular grains of various sizes. These textural observations have been interpreted to indicate that chemical reactions occurred by a dissolution and reprecipitation process following or during cataclastic deformation. This suggests that grain boundary formation was an important process in the petrologic evolution of the shear zone possibly by providing zones for fluid ingress to facilitate metamorphic reactions. The general implication of the documented interrelationships between metamorphism and deformation within the shear zones highlight the necessity for conducting detailed microstructural evaluation of rocks in order to interpret petrologic, isotopic and geochronologic data.

INTRODUCTION

Since the pioneering work of Beach (1973; 1976) on shear zones in Scourian mafic dikes, northwestern Scotland, there have been numerous studies which have outlined some of the chemical, isotopic and mechanical variations associated with shear zone processes (see Brodie and Rutter, 1985 for a review of the interrelationships between metamorphism and deformation). Detailed study of shear zones offers a unique research opportunity in that shear zones may preserve a complete record from relatively undeformed to highly deformed rocks and thus contain information on the mechanical and

chemical changes associated with deformation and metamorphism. Examination of these changes has been instrumental in characterizing several important shear zone-related phenomena including fluid flow, ore deposition, mechanical behavior of rocks, deformation mechanisms and variation in isotopic compositions due to fluid flow and deformation. Furthermore, petrologic study of variably deformed rocks may provide at least two relative points along a P-T-t path: one for the least deformed rock and one for the highly deformed material (see Swapp 1991). This is especially important in rocks which do not reequilibrate under changing metamorphic conditions without assistance from deformation-related processes such as increased fluid flow or enhanced intracrystalline strain energy due to slow diffusion or reaction rates (Wintsch and Andrews, 1987; Nyman et al.,1991; Koons et al., 1987).

Shear zones which deform margins of amphibolite boudins in the Cheyenne belt, SE Wyoming, record a full strain transition from relatively undeformed amphibolite which has relict igneous textures to deformed amphibolite with a strongly developed L-S tectonic fabric. Detailed petrologic and microstructural analysis of a single amphibolite shear zone has been conducted in order to: 1) document the petrologic evolution of the shear zone, 2) integrate the petrologic model with proposed tectonic models for the Cheyenne belt and, 3) investigate the interrelationships between mechanical and chemical processes associated with shear zone formation.

REGIONAL GEOLOGY OF THE CHEYENNE BELT, SOUTHEASTERN WYOMING

The Cheyenne belt is a major crustal boundary which extends across southeastern Wyoming from the Laramie Range in the east through the Medicine Bow Mountains to the Sierra Madre Range (Fig. 2.1). The Cheyenne belt marks the boundary between the

Figure 2.1. Regional geology of the Cheyenne belt, southeastern Wyoming (adapted from Duebendorfer and Houston, 1987).

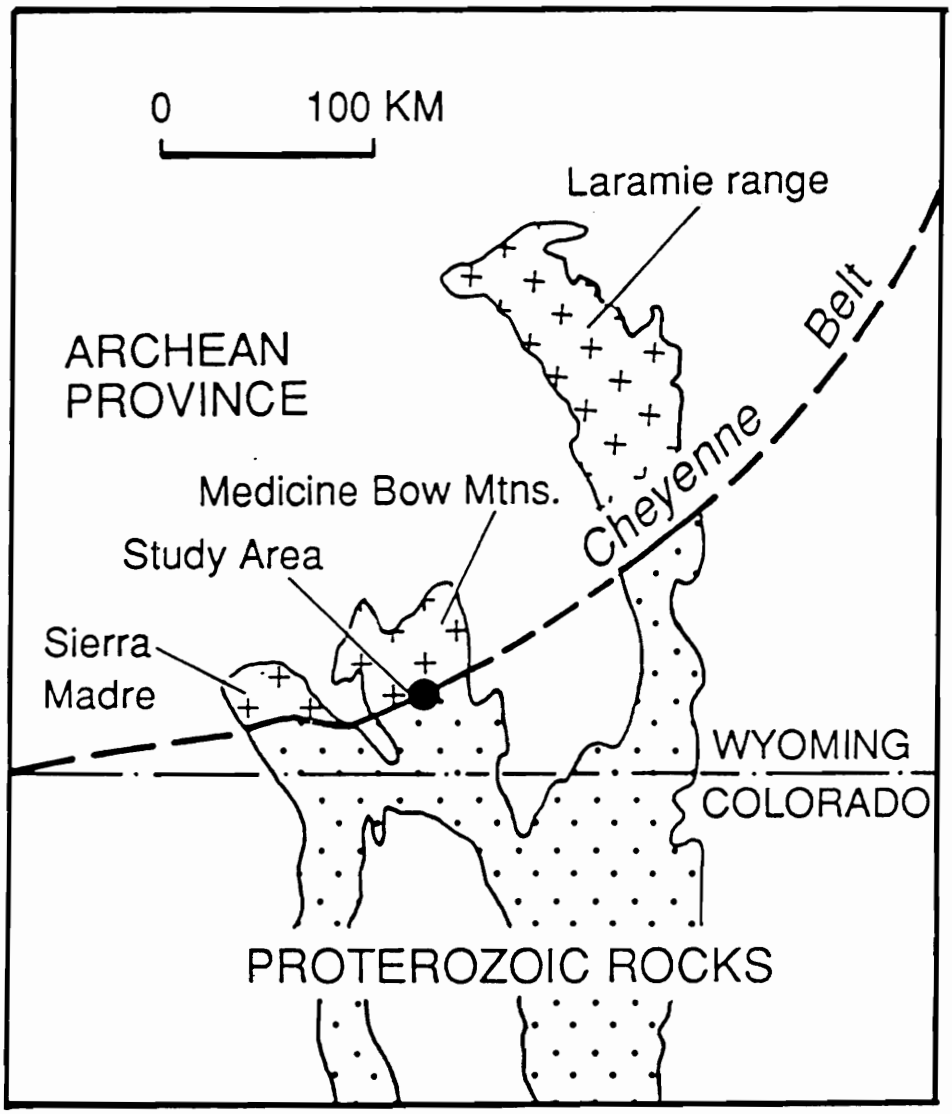
0
100 KM
Laramie range
ARCHEAN
PROVINCE
Medicine Bow Mtns.
Study Area
Cheyenne Belt
Sierra
Madre
WYOMING
COLORADO
PROTEROZOIC ROCKS

Archean Wyoming Province greenschist facies basement and Early Proterozoic supracrustal rocks (2300-2000 Ma) to the north and middle to upper amphibolite facies Proterozoic terranes of the Colorado Province (1800 Ma) to the south (Karlstrom et al., 1983; Duebendorfer and Houston, 1987). The boundary is obscured in the Laramie Range where the younger Laramie anorthosite-syenite complex has been emplaced along the trend of the Cheyenne belt at about 1450 Ma (Hills and Armstrong, 1974). Recent petrologic/geochronologic work has postulated that deformation and metamorphism within Archean rocks north of the Laramie anorthosite could be associated with deformation along the Cheyenne belt (Patel et al., 1991; Chamberlin et al., 1991).

The Cheyenne belt is characterized by intense deformation, localized in shear zones, which accompanied Proterozoic accretionary tectonics. Detailed mapping in the Medicine Bow Mountains by Duebendorfer and Houston (1987) has differentiated six lithotectonic blocks within a 0.7 to 7 km wide zone of crystal plastic and cataclastic deformation (Duebendorfer and Houston, 1987). Kinematic analysis of field and microstructural features by Duebendorfer and Houston (1987) suggested that accretion was characterized by north-directed thrusting at amphibolite-grade conditions, followed by later lower-grade dextral strike-slip reactivation. However, the presence of subhorizontal lineations in the Sand Lake Shear Zone as well as other parts of the East Bear Lake Block suggest an earlier phase of translation movement perhaps during an Archean event (Duebendofer, personal communication, 1992; Ball and Farmer, 1991). The deformation associated with thrusting was concentrated at the margins of lithotectonic blocks in 50-200 m wide shear zones, although localized shear zones also penetrate the blocks. Recent mapping by Duebendorfer and Houston (1990) has shown that a similar regional framework is present in the Sierra Madre Range. Metamorphic temperatures in the Medicine Bow Mountains estimated from synkinematic garnet porphyroblasts and

matrix biotite indicate that thrusting occurred at a minimum of 475°C. Estimates of metamorphic pressure during thrusting are less precise and constrained by the equilibrium (?) coexistence of andalusite and kyanite in a garnet-biotite schist to be approximately 3.5 kbar at 480 °C (Duebendorfer, 1988). Ages of syn- and post-kinematic plutons date Cheyenne belt deformation at approximately 1750 Ma.

FEATURES OF AMPHIBOLITE SHEAR ZONES

Cheyenne belt shear zones are best exposed in the Medicine Bow Mountains. The shear zone investigated in this study is located near the northeastern margin of the Cheyenne belt in the Medicine Bow Mountains and has been designated the Sand Lake shear zone (SLSZ) (Fig. 2.2). The SLSZ deforms the margin of a large amphibolite boudin and has an anastomosing geometry. Relatively undeformed amphibolite has a relict igneous texture consisting of amphibole and plagioclase with a weak linear fabric and no planar component. The complete strain transition from undeformed amphibolite to deformed amphibolite occurs over 7.5 cm (Fig. 2. 3), and is marked by a decrease in grain size, an increase in foliation development and rotation of the amphibole and plagioclase porphyroclasts into parallelism with the shear zone boundary. The progressive development of the tectonic fabric and decrease in grain size are interpreted as indicating that strain magnitude increases across the shear zone. The tectonic fabric in the deformed amphibolite is predominantly a strong L-S fabric, but portions of the outcrop also show only L or S fabric elements. The change in orientation of amphibole and plagioclase porphyroclasts with respect to distance from the shear zone boundary as well as development of an L-S fabric, suggest that the shear zone formed by heterogeneous simple shear (Ramsay and Graham, 1970; Ramsay, 1980). However, variation in the fabric of the deformed amphibolite suggests a more complicated deformation history

Figure 2.2. Sketch map of Sand Lake Shear Zone.

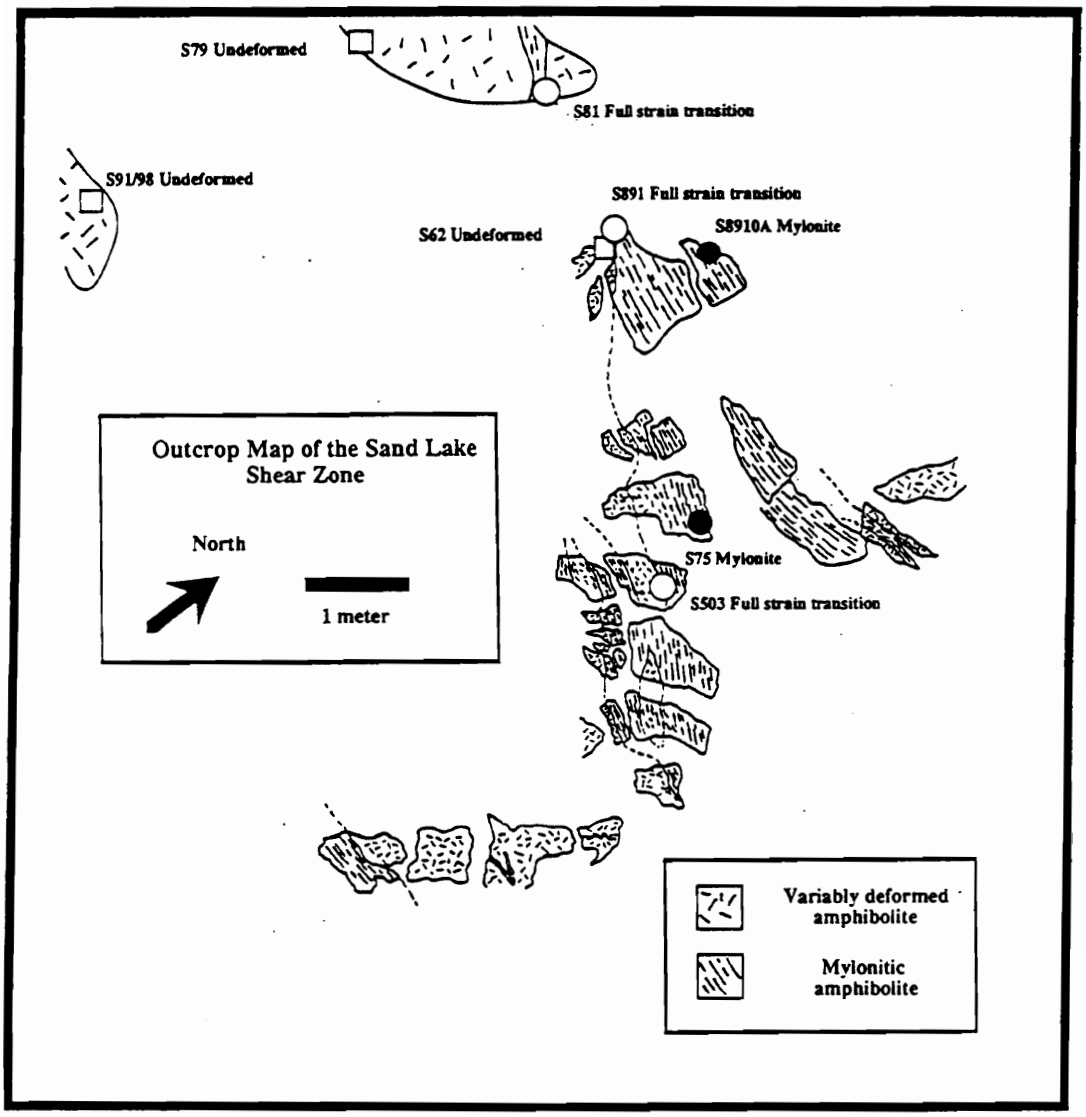
S79 Undeformed
S81 Full strain transition
S91/98 Undeformed
S891 Full strain transition
S8910A Mylonite
S62 Undeformed
Outcrop Map of the Sand Lake Shear Zone
North
1 meter
S75 Mylonite
S503 Full strain transition
Variably deformed amphibolite
Mylonitic amphibolite

Figure 2.3. Field photograph of full strain transition in amphibolites from the Sand Lake shear zone. Shear zone formation is marked by the progressive rotation of amphibole and plagioclase aggregates into parallelism with the shear zone boundary. As discussed in the text, the strain transition can be divided into three zones: 1) a relatively undeformed section (bottom of photo) in which amphibolite has a relict igneous texture; 2) a transitional zone where amphibole and plagioclase aggregates show rotation and; 3) mylonitic zone (top of photo) defined by amphibolite with a L-S tectonic fabric.


MINOLTA

Deformation is inferred to have occurred by a cataclastic deformation mechanism based on: 1) the angular shape of deformed grains, 2) replacement textures observed along grain boundaries of plagioclase and amphibole (see below) and 3) the observation that grain boundaries form along planes of structural weakness (e.g. cleavage planes). See chapter 4 for more details on the deformation mechanism of amphibole.

The strain transition can be divided into three distinct zones based on fabric: undeformed, transitional and mylonitic. In this and subsequent chapters, the term mylonitic is used only as a descriptive term to describe strongly deformed amphibolites with a L-S tectonic fabric and not to infer that deformation occurred by a crystal plastic mechanism (see chapter 4). As will be discussed below, this general division is coincident with compositional variation of amphibole and plagioclase porphyroclasts as well as changes in the microstructures. These relations indicate that mechanical and chemical variations across the strain transition are in part linked to strain intensity.

Petrography

The mineral assemblage across the strain transition is dominated by amphibole and plagioclase which make up to 70-90% of the mode. Minor phases in the assemblage include ilmenite, sphene, chlorite, epidote and quartz. Ilmenite occurs within amphibole clots and is commonly rimmed by a narrow band of sphene. With increasing strain the modal abundance of ilmenite decreases and ilmenite is replaced by sphene. Epidote and chlorite are minor phases and do not show any systematic modal variation across the strain transition.

Plagioclase and amphiboles show distinct microstructural variation across the strain transition. In relatively undeformed amphibolite, plagioclase has a bimodal size

distribution consisting of large 1-3 mm presumed relict plagioclase phenocrysts and $\leq$ 1 mm subequant grains. The larger plagioclase is inferred to be relict phenocrysts based on the core compositions and the textural relationships with mafic phases which resembles an igneous texture. These two morphological types are commonly found in apparent core-mantle structures where the subequant plagioclase grains form an irregular mosaic about relict plagioclase phenocrysts. Both relict phenocrysts and subequant 'subgrains' have deformed albite twin planes and undulatory extinction. In some samples of relatively undeformed amphibolite, all plagioclase phenocrysts have been replaced by fine-grained (< 1 mm), subequant plagioclase.

With increasing strain intensity across the transitional and mylonitic sections of the shear zone plagioclase grains attain a more uniform grain size and shape. The presence of undulatory extinction, deformed albite twin planes and apparent core-mantle structures suggests grain size reduction by an intracrystalline strain mechanism either as a result of dislocation creep or microcracking and cataclasis (Tullis and Yund, 1977; 1987). Back-scattered secondary electron (BSE) images show that large plagioclase grains, which have undulatory extinction, are cut by fractures along which plagioclase has been dissolved and replaced by more albitic plagioclase. This supports a cataclastic deformation mechanism for deformation of the plagioclase.

In the relatively undeformed amphibolite, amphibole porphyroclasts occur as large laths surrounded by a complex array of 'subgrains' (Fig. 2.4a). This microstructure resembles core-mantle structures (White, 1976). Amphibole laths have inclusion-rich cores with both quartz and ilmenite inclusions aligned along cleavage planes. Twinning is common in the porphyroclasts and is similar to (100) twins reported by Biermann (1981). Undulatory and patchy extinction are also evident in some of the laths. Variation in extinction angles of the laths commonly occurs along cleavage traces

Figure 2.4. Photomicrographs of variably deformed amphibolite from across the shear zone. All photomicrographs are shown in plane polarized light. A. Photomicrograph of an amphibole porphyroclast from relatively undeformed amphibolite. Porphyroclasts consist of a lath-shaped actinolitic core mantled by angular to euhedral 'subgrains'. See chapter 4 for additional petrographic details on the core/mantle textures of the porphyroclasts. B. Photomicrograph of highly deformed amphibole porphyroclasts from transitional zone of the full strain transition. In this photomicrograph highly deformed porphyroclasts are surrounded by irregular and lath shaped amphiboles which are aligned parallel to the foliation. The sigmoidal shape of the porphyroclast is consistent with the dextral shear sense defined by the rotation of amphibole and plagioclase aggregates. C. Photomicrograph from mylonitic amphibolite showing layering defined by plagioclase- and amphibole-rich layers.

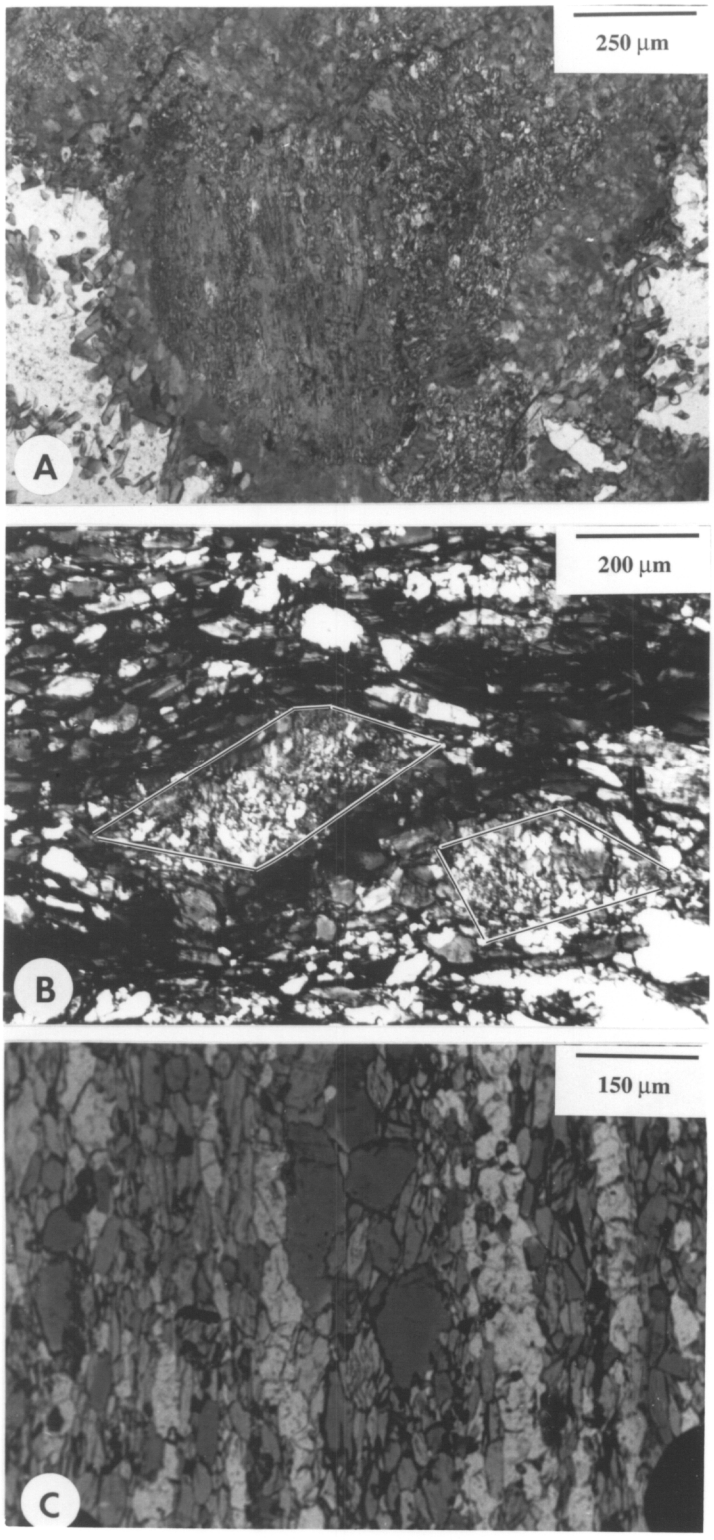
250 μm
A
200 μm
B
150 μm
C

Amphibole 'subgrains' which mantle the laths show microstructural variation as a function of distance from the porphyroclast. Anhedral to subhedral 'subgrains' with irregular grain boundaries occur adjacent to porphyroclast cores, whereas euhedral grains occur at the margins of the core-mantle structure. The boundaries between plagioclase feldspar and the amphibole core-mantle structure are marked by amphibole needles which grow into the surrounding plagioclase feldspar. Additional details of the textural relationships and deformation mechanisms for the amphibole core-mantle structure are discussed in chapter 4.

With increasing strain in the shear zone, there is a decrease in the overall grain size and the fabric becomes dominated by amphibole grains with larger aspect ratios. Where large amphibole porphyroclasts are still present, they have an augen shape, show significant grain size reduction at their margins, and are wrapped around by lath-shaped amphiboles (Fig. 2.4b). The cores of amphibole porphyroclasts have irregular extinction due to slight misorientation along cleavage planes which produces variation in extinction position across a single amphibole grain. Also present in the variably deformed amphibolite are zones of fine grained amphibole+quartz $\pm$ ilmenite which probably represent highly deformed porphyroclasts.

Grain size and microstructural variation of the amphibole continue to decrease into the mylonitic section of the shear zone. The L-S fabric in the mylonite is defined by the alternation of layers rich in amphibole or plagioclase. Amphibole grains are lath-shaped (Length/Width ratios of approximately 2) in XZ sections and are oriented with the long dimension parallel to the foliation (Fig. 2.4C).

Bulk Chemistry

Bulk chemical analyses of five samples (one relatively undeformed, three from a strain transition and one mylonitic) were obtained in order to determine if formation of the SLSZ involved significant mass transfer (Table 2.1). Bulk chemical analyses were performed by Chemex Labs Ltd using the ICP-AES method. Detection limits were 0.01 for all oxides including lost on ignition values which were measured after heating samples in a furnace.

Figure 2.5 shows plots of the major oxides for each sample. This graph shows that there are no significant or systematic variations in the major oxides as a function of strain magnitude. SiO_2 shows the maximum and most systematic variation with a decrease from 51.2 wt % in undeformed amphibolite to 50.4 wt % in mylonitic amphibolite.

Mineral Chemistry

Electron microprobe analyses were made of all mineral phases in samples representing different degrees of strain magnitude. Microprobe analyses were performed on a Cameca SX-50 electron microprobe in the VPI&SU electron microprobe laboratory. Operating conditions were 15 kv accelerating potential and 20 nA beam current. The following mineral standards were used: Amelia albite (Na_2O, SiO_2, Al_2O_3); Benson orthoclase (Na_2O); norbergite (MgO, F); pyrolusite (MnO); rutile (TiO_2); wollastonite (CaO); Rockport fayalite (FeO); $Ba_5(PO_4)_3Cl$ (Cl). Compositional data were corrected using a ZAF program supplied by Cameca, Inc. Quantitative analytical data were coupled with BSE images collect on a Camscan SEM and analog false color X-ray images obtained using a Cameca SX-50 to determine the relationships between textural features, fabric development and compositional variation. The analog false color images are

TABLE 2.1

BULK CHEMISTRY DATA

SAMPLE #	S62	S141 U	S141 T	S141 M	S75
DESCRIPTION	Undeformed	Full Undeformed	Full Transitional	Full Mylonitic	Mylonitic
SiO_2	51.32	51.29	50.98	50.83	50.46
Al_2O_3	13.56	13.32	13.16	12.16	13.52
TiO_2	1.28	.81	.85	1.06	1.19
Fe_2O_3	13.29	12.19	12.50	13.55	13.30
MnO	0.21	0.18	0.18	0.18	0.18
MgO	6.52	7.55	7.71	7.81	6.65
CaO	9.56	10.11	10.40	10.52	10.09
Na_2O	2.14	2.18	2.25	1.93	2.22
K_2O	0.31	0.34	0.28	0.28	0.36
P_2O_5	0.13	0.09	0.10	0.11	0.12
BaO	<0.01	<0.01	<0.01	<0.01	<0.01
LOI	1.30	1.34	1.24	1.22	1.18
TOTAL	99.62	99.39	99.65	99.66	99.28

Figure 2.5. Plots of bulk chemical analyses of variably deformed amphibolite. Note that except for SiO_2, there is no systematic variation of any major oxides across the shear zone suggesting isochemical behavior. Systematic variation in SiO_2 only involves a decrease of 1 wt% across the shear zone. Abbreviations along horizontal axis are as follows: Udef = Relatively undeformed amphibolite (S62) ; FUDef = Undeformed section of full strain transition (S141); FTrans = Transitional section of full strain transition (S141); FMyl = Mylonitic section of full strain transition (S141); Myl = Mylonitic amphibolite (S75)

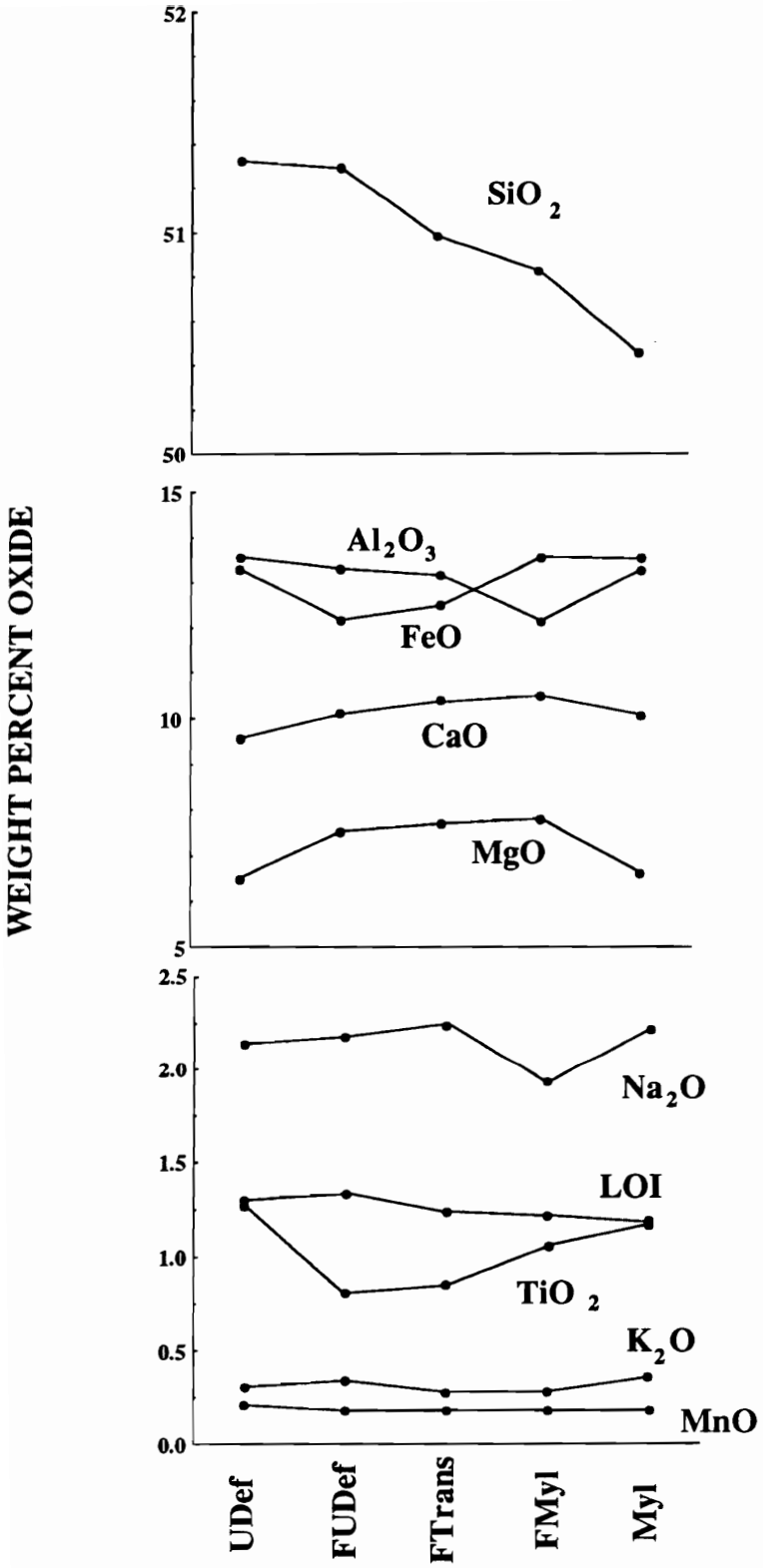
WEIGHT PERCENT OXIDE
52
51
50
SiO 2
15
10
5
Al2O3
FeO
CaO
MgO
2.5
2.0
1.5
1.0
0.5
0.0
Na2O
LOI
TiO 2
K2O
MnO
UDef
FUDef
FTrans
FMyl
Myl

computer generated representations of variation in X-ray intensity . To produce these images, small step scans across mineral grains are conducted during which data on X-ray intensity and relative X-Y position are collected. Image analysis computer programs use this data to produce the images that show variation in X-ray intensity with position.

Amphibole analyses were first recalculated on the basis of 23 oxygens assuming all Fe is Fe^{2+}. Cations were assigned to crystallographic sites following the method of Robinson et al. (1982). Site assignments as prescribed by Robinson et al. (1982) using a 23 oxygen renormalization resulted in Na being excluded from the M4 site and, for these amphiboles, M4 values less than 2. As evident from the blue green color of some of the amphiboles, there is likely to be some Fe^{3+} (Robinson et al., 1982). Formulas were therefore recalculated normalizing to 13 cations excluding Ca, Na and K (13 eCNK). This scheme allows for Na in the M4 site and generally produces a charge balanced stoichiometry for these amphiboles.

Amphibole Compositions

Relatively Undeformed Amphibole

Plots of amphibole compositions from a sample of relatively undeformed amphibolite (S62) are shown in figures 2.6a-2.6c. Amphibole compositions range from actinolitic hornblende to ferrous tschermakitic hornblende (nomenclature after Leake, 1978) and define a linear trend in a plot of Si versus $Mg/(Mg+Fe^{2+})$.

The complex chemistry of amphiboles can be represented by progress along various compositional vectors (representing exchange components) from a single additive component (typically tremolite) (Spear 1981; Thompson, 1982). The actual amounts and types of exchange components that describe a specific composition are dependent on the chosen recalculation scheme as well as choice of exchange components. Describing

Figure 2.6A-D. Plots of amphibole compositions from relatively undeformed amphibolite (sample S62). Amphibole compositions are recalculated on the basis of 13 cations exclusive of Ca, Na and K. See text for discussion.

A
Act Hb
Fe Act Hb
Mg Hb
Fe Hb
Ts Hb
Fe Ts Hb
Ts
Fe Ts
Mg ratio
Si
B
Prg
Ts
Ed
Tr
Al(IV)
Al(VI)
C
Prg
Hb
Ed
Ts
Tr
Al(IV)
A site
D
Tr
Al(IV)
A Site + 2Ti + Al(VI) + Fe3+

complex mineral compositions using exchange and additive components provides a convenient algebraic method to describe chemical variation, but the specific substitutions that control the variation cannot be uniquely ascertained (Hewitt and Abrecht, 1982).

Using the 13 eCNK recalculation scheme, the nature of the exchange components which describe the compositional variation can be deduced from figures 2.6b and 2.6d. In a plot of Al(VI) vs Al(IV), the data for the relatively undeformed amphibolite fall along a linear trend which is subparallel to the pargasite line (slope = 2) with a vertical intercept greater than 0.0. Variation of A site occupancy with Al(IV) also defines a linear trend which is subparallel to the pargasite line but changes slope at lower A site values. The linear fit to data in this plot also has a positive intercept as well as a concentration of data which shows an increase in Al(IV) with no associated A site increase. This suggests that some of the Al(IV) substitution is not linked with an increase in A site occupancy. Both of these plots indicate that the compositional variation can be represented by progress along the tschermakite ($Mg_{-1}Si_{-1}Al(IV)Al(VI)$) and the edenite ($Si_{-1}NaAl(IV)$)exchange vectors. Note that the pargasite vector is the algebraic sum of edenite and tschermakitic components.

As pointed out by Spear (1981), there are several amphibole exchange components which are associated with substitution of Al into the tetrahedral site (tschermakite, ferri-tschermakite, Ti-tschermakite and edenite). If all of these exchanges control the compositional variation, then a plot of Al(IV) vs A site + 2 Ti + Al(VI) $+Fe^{3+}$ should show the data lying on a line with a slope of 1 (Fig. 2.6d). The observed deviation of the linear trend defined by the data from a line with a slope of 1 suggests that part of the substitution of one of the cations (probably Fe^{3+}) may be explained by some other substitution such as glaucophane or richterite.

In summary, using a 13 eCNK recalculation scheme, amphibole compositions from the relatively undeformed amphibolite can be represented by variable progress along tschermakite, edenite and possibly glaucophane exchange vectors. Variation in Fe and Mg may also be a function of simple $FeMg_{-1}$ exchange.

Relationships between amphibole textural types and compositional variations are shown in X-ray compositional maps (Fig. 2.7) and SEM back-scattered images (Fig. 2.8) of a single amphibole porphyroclast and mantling 'subgrains'. Cores of amphibole porphyroclasts are relatively homogeneous, with high Si and Mg contents and lower Fe and Al (Fig. 2.7). Portions of the cores have lamellar-shaped regions which show compositional variation as shown by changes in the analog false-color X-ray intensity from red to yellow. These areas are texturally similar to exsolution lamellae reported for calcic amphiboles (Brady, 1974; Grapes and Graham, 1978). The SEM back-scattered images (Fig. 2.8) and associated microprobe data (Fig. 2.9 and 2.10) also indicate the relatively homogeneous composition of the porphyroclast core with slight composition variation across lamallae-shaped regions.

'Subgrains' in mantles of amphibole porphyroclasts show three types of compositional and textural relationships. The term 'subgrains' is used to describe the apparent core-mantle structure in the relatively undeformed amphibolite where small, angular amphibole fragments surround larger amphibole grains. As will be shown in Chapter 4, this apparent core-mantle structure formed as a result of cataclastic and not crystal plastic deformation. (White, 1976). 'Subgrains' adjacent to the porphyroclast core (marked zone I in Fig. 2.8) have actinolitic cores which are similar in composition to the host amphibole. From the core outward, compositional variation follows a smooth profile with decreasing Fe and Al and increasing Si and Mg contents (Fig. 2.10A). Margins of the 'subgrains' are marked by a sharp compositional break with amphibole

Figure 2.7. False-color-enhanced X-ray compositional maps of an amphibole porphyroclasts from the relatively undeformed amphibolite. Variation in color is an analog representation of compositional changes as measured by changes in count rates during step scans. Note that decreasing Mg and Si content are balanced by increasing Fe and Al. This is the same porphyroclast shown in figure 2.3A and 2.7. Field of view is approximately 2mm. Operating conditions include an accelerating potential of 15 kv and sample current of 200 nA. Sampling resolution (size of steps during scan) was 8 microns. Data was collected on wave length dispersive spectrometers.

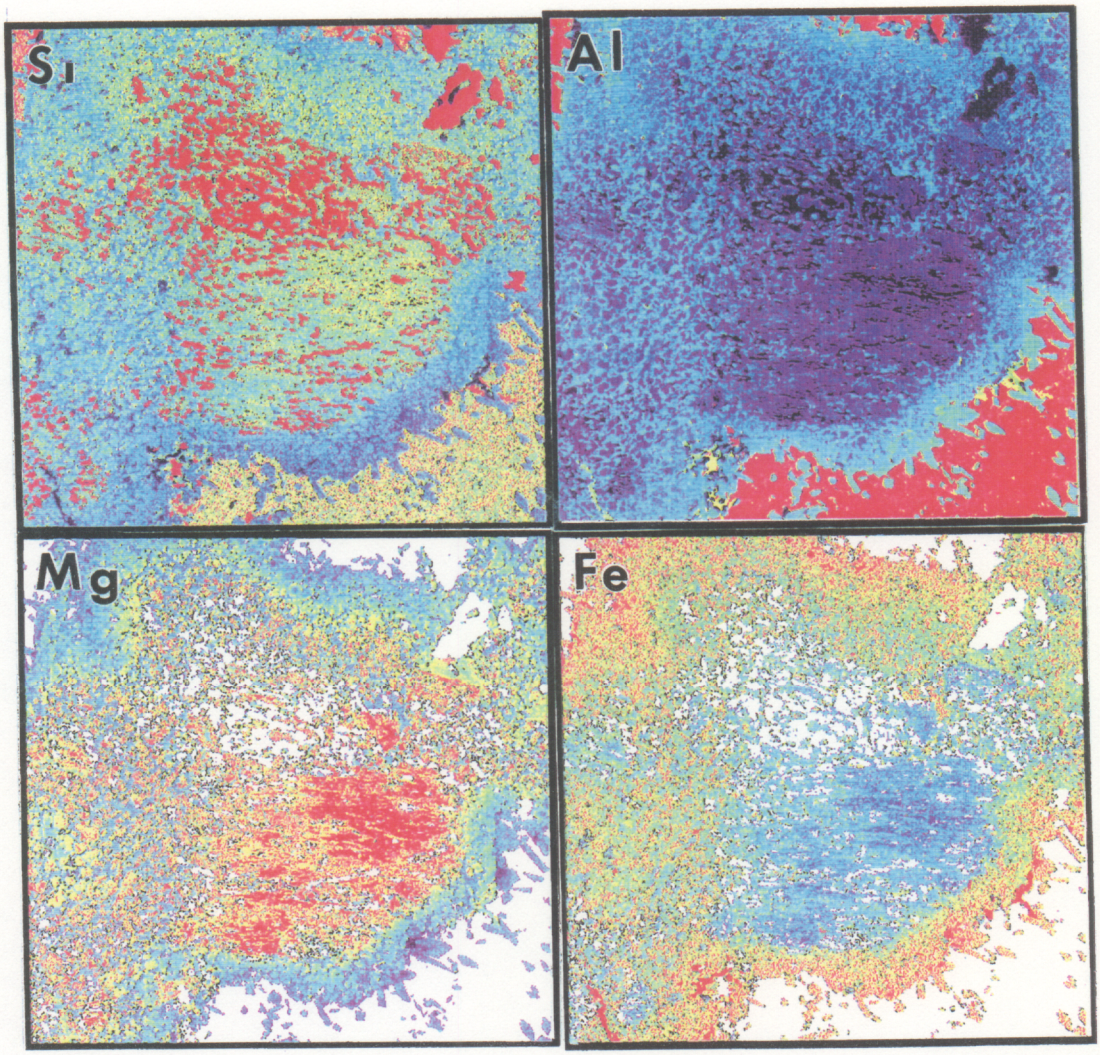
Si
Al
Mg
Fe
Low
Relative Count Rates
High

Figure 2.8 Secondary electron back-scattered image of the same amphibole porphyroclasts shown in figure 2.4A and 2.7. Variation in contrast is due to changes in composition. Paler areas have higher Al and Fe contents with hornblende compositions whereas darker sections have high Mg and Si contents and more actinolitic compositions. Dark inclusions within the porphyroclast are quartz; highly illuminated inclusions are ilmenite. The area around the porphyroclasts consists of plagioclase and appears black due to the contrast conditions required to reveal the compositional variation of amphibole. The line corresponds to the location of an electron microprobe traverse shown in figure 2.9. The arrows correspond to locations of qualitative and quantitative traverses across 'subgrains'shown in figures 2.10 A-C. Note that the 'subgrains' which surround the porphyroclast core can be separated into three zones which have different textural and chemical characteristics (marked zones 1-3 in figure 2.7A; see text for discussion).

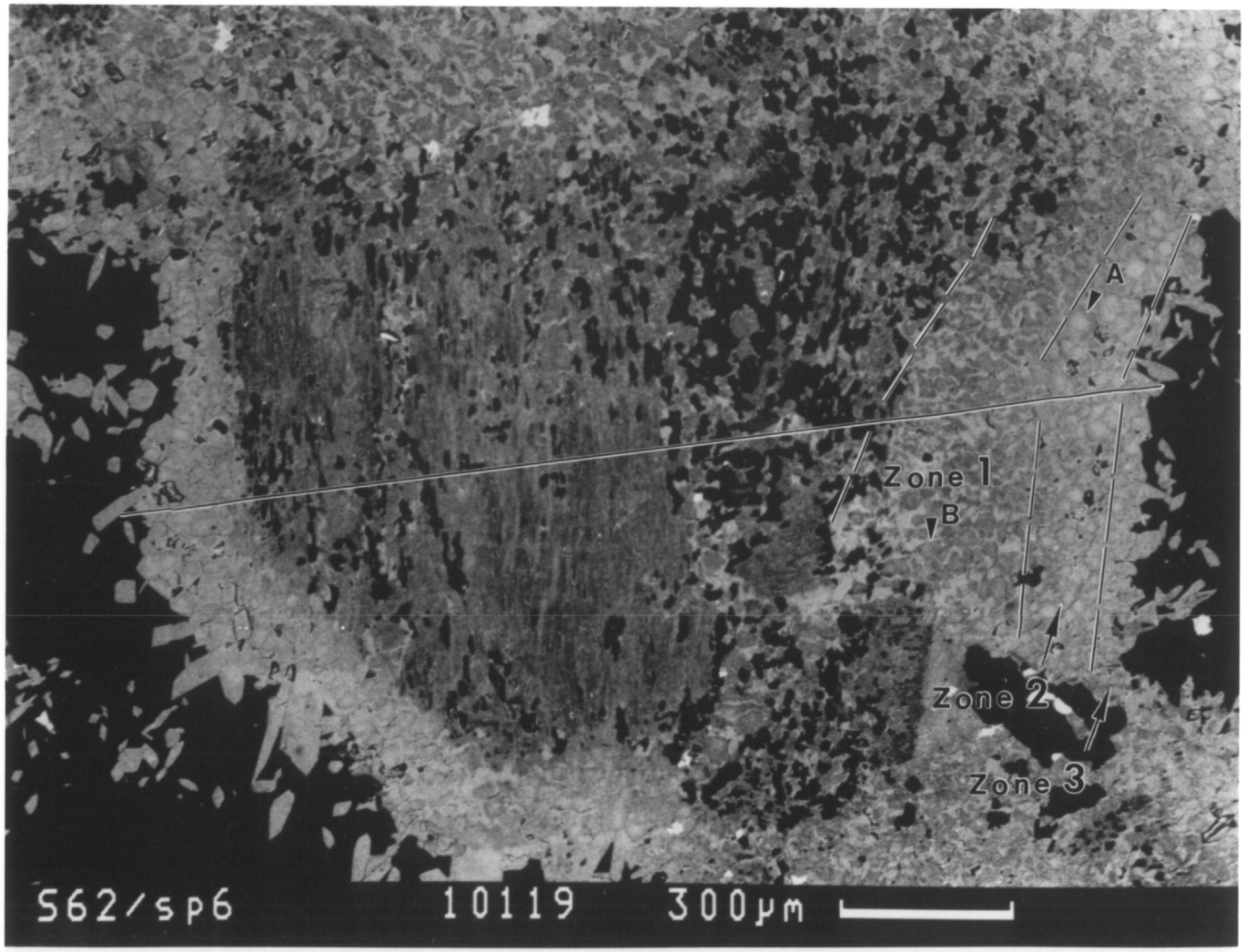
A
Zone 1
B
Zone 2
Zone 3
S62/sp6
10119
300μm

Figure 2.9 Compositional data from electron microprobe traverse across amphibole porphyroclast and 'subgrains' shown in figure 2.8

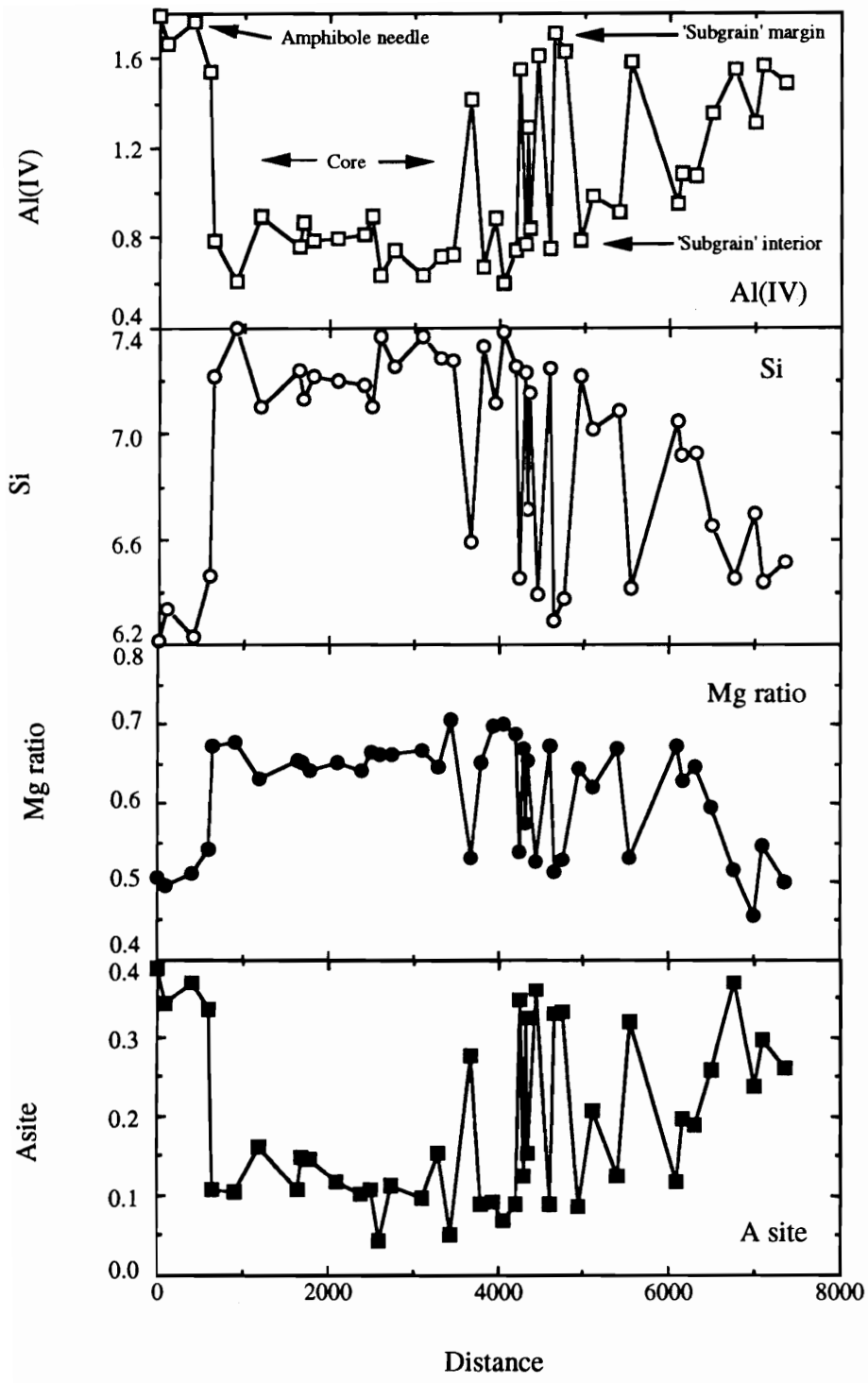
Amphibole needle
'Subgrain' margin
Core
'Subgrain' interior
Al(IV)
Si
Mg ratio
A site
Asite
Distance
0
2000
4000
6000
8000
0.4
0.8
1.2
1.6
6.2
6.6
7.0
7.4
0.4
0.5
0.6
0.7
0.8
0.0
0.1
0.2
0.3
0.4

Figure 2.10 A&B. Qualitative electron microprobe traverse across amphibole porphyroclast and 'subgrains'. Traverse shown in 2.10A is marked by an arrow and the letter B is figure 2.8. Traverse shown in 2.10B and 2.10C is marked by an arrow and the letter A in figure 2.8.

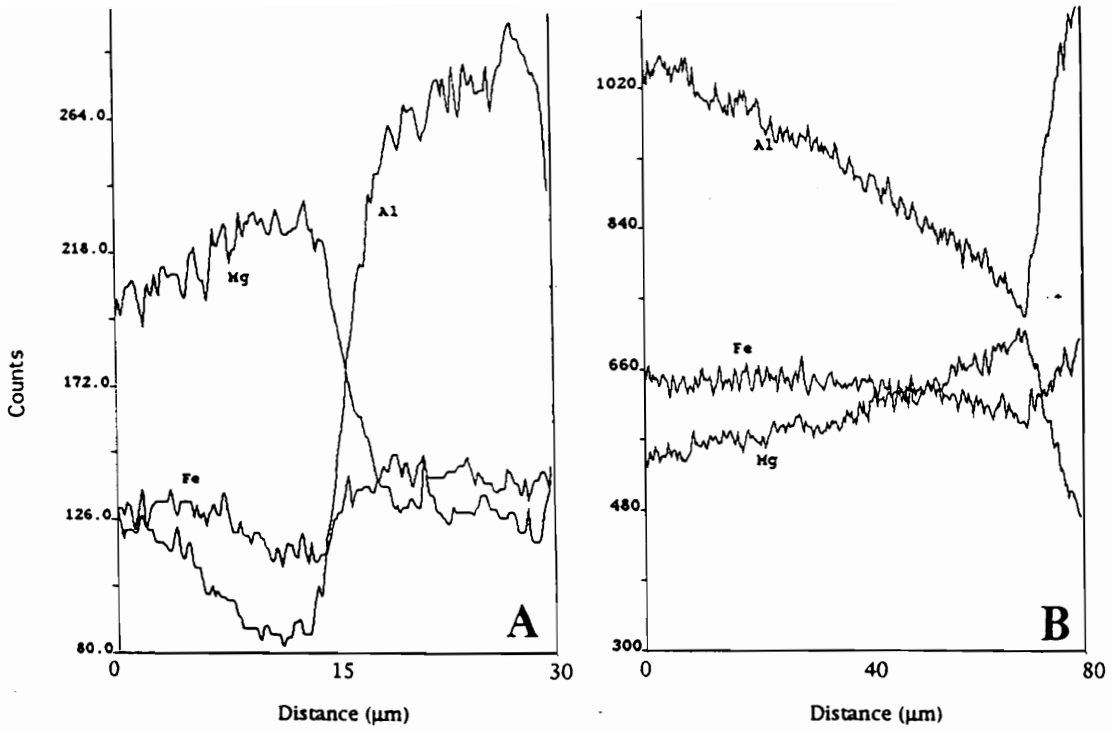
Counts
264.0
218.0
172.0
126.0
80.0
Mg
Al
Fe
A
0
15
30
Distance (μm)
1020
840
660
480
300
Al
Fe
Mg
B
0
40
80
Distance (μm)

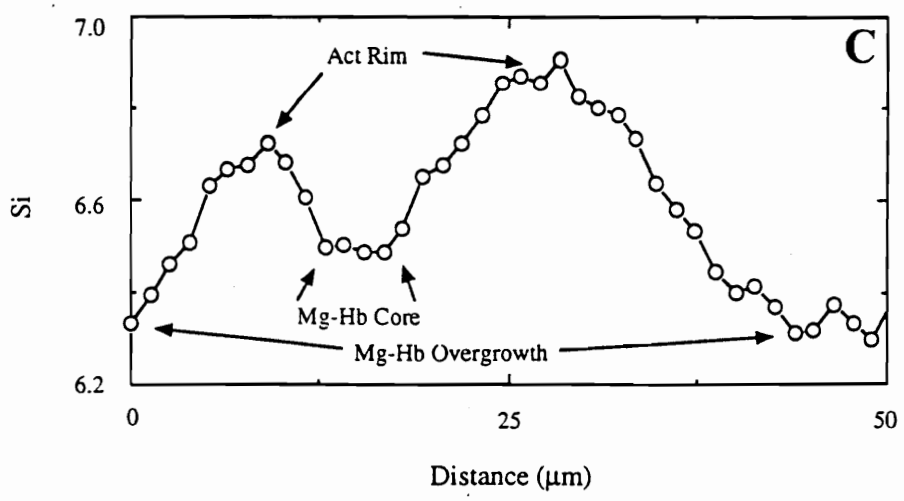
7.0
6.6
6.2
Si
Act Rim
C
Mg-Hb Core
Mg-Hb Overgrowth
0
25
50
Distance (μm)

along the grain boundaries having high tschermakite and edenite components. In zone II, the 'subgrains' have a more equant shape and core to rim microprobe traverses across these 'subgrains' show similar compositional trends to those in zone I. However, cores of 'subgrains' in zone II have higher tschermakite and edenite contents than in zone I, and the compositional profiles show larger compositional changes across each grain (Fig. 2.10B & C). Zone III of the mantling 'subgrains' includes the thin, equant amphibole needles which have a relatively uniform composition and the highest tschermakite and edenite components.

Full strain transition

Plots of amphibole compositions from a single sample which shows the full strain transition (sample 81) are illustrated in figure 2.11. Amphibole compositions have been separated on the basis of the relative strain magnitude: undeformed, transitional and mylonitic.

Amphibole compositions define trends similar to those observed in the relatively undeformed amphibolite, except that the compositional range is smaller and some of the linear trends are less well developed. Most amphibole compositions plot within the magnesio-hornblende field, and in plots of A site vs Al(IV) form a trend subparallel to the hornblende line. The slope of the data, as shown in the Al(VI) vs Al(IV) plot, is shallower than observed in the relatively undeformed amphibolite, although it is still subparallel to the tschermakitic line. Plots of Al(IV) vs [A site + 2 Ti + Al(IV) + Fe^{3+}] show linear trends similar to those displayed in the relatively undeformed amphibolite.

X-ray compositional maps and back-scattered electron SEM images of amphibole from across the strain gradient show textural and compositional relationships like those observed in the relatively undeformed amphibolite. In the undeformed portion of the strain transition, cores of porphyroclasts and 'subgrains' have relatively low tschermakite

Figure 2.11. Plots of amphibole compositional data from full strain transition sample S81. Data is separated into relative strain intensity zones based on criteria outlined in figure 2.3.

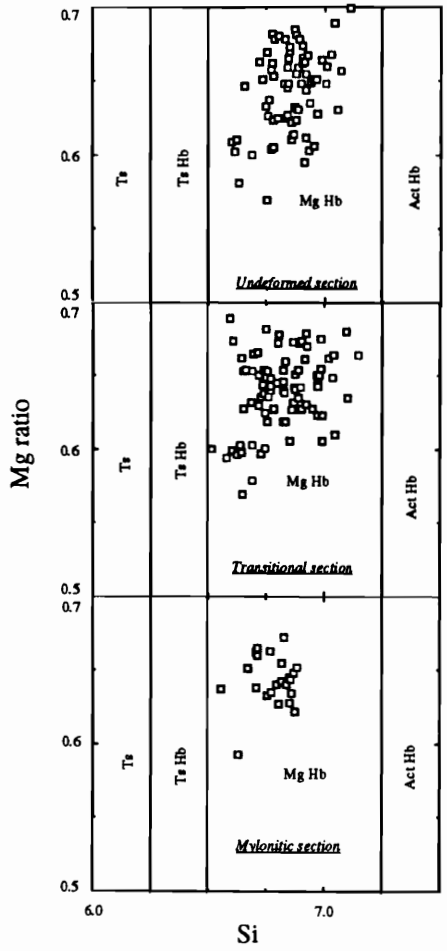
Mg ratio
0.7
0.6
0.5
Ts
Ts Hb
Mg Hb
Act Hb
Undeformed section
Transitional section
Mylonitic section
6.0
7.0
Si

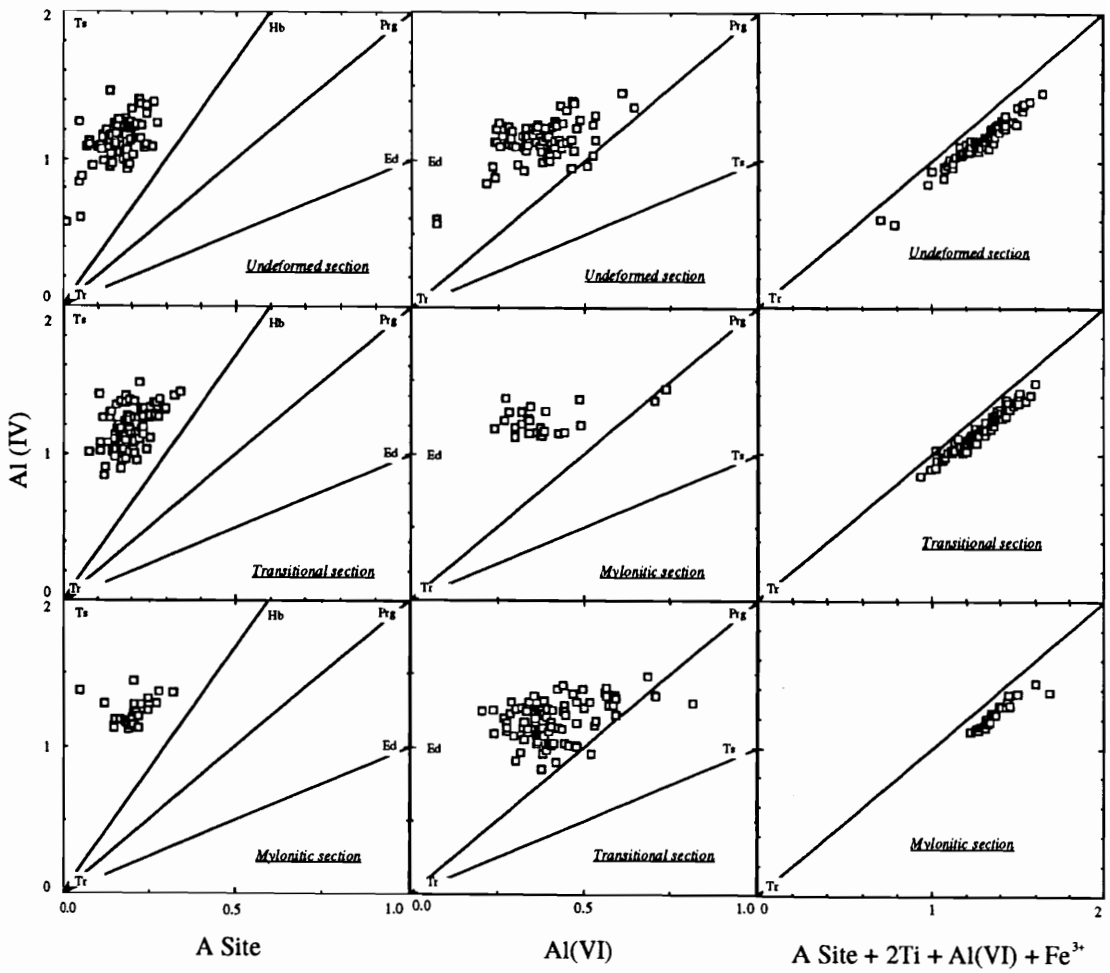
Al (IV)
2
1
0
Ts
Hb
Prg
Ed
Tr
Undeformed section
Transitional section
Mylonitic section
0.0
0.5
1.0
A Site
Al(VI)
1
2
A Site + 2Ti + Al(VI) + Fe3+

and edenite contents compared to grain boundary regions. Subequant and lath-shaped amphibole 'subgrains' in the least deformed amphibolite from the full strain transition have compositional zoning profiles similar to those observed for 'subgrains' in the relatively undeformed amphibolite with sharp compositional gradients at grain boundaries. Smaller amphibole grains are the most homogeneous compositionally.

With increasing strain in the mylonitic section of the strain transition, amphibole compositions become more homogeneous. X-ray compositional maps and BSE images indicate a lack of compositional zoning and no sharp chemical discontinuities along grain boundaries. In some samples, amphibole compositions are variable and porphyroclasts have textural and chemical characteristics similar to those observed in less strained amphibolites. In these samples, amphibole porphyroclasts have irregular, patchy extinction with actinolitic cores and hornblende rims . Lath-shaped amphiboles which wrap the porphyroclasts have the highest tschermakite and edenite contents and the most homogeneous compositions.

Mylonitic amphibolite

Compositions of amphiboles from mylonitic amphibolites are plotted in figures 2.12 through 2.15. Compositions fall along linear trends like those observed in the relatively undeformed and full strain amphibolites. Mylonitic samples have three classes of amphibole compositions: Type 1 amphibole compositions are homogeneous and are magnesio-hornblende to tschermakitic hornblende (samples 75 and 910a), Type 2 amphiboles have actinolitic margins with Al-rich cores (sample 895a) and Type 3 have actinolitic cores and magnesio-hornblende rims (sample 141).

Figure 2.12 and 2.13 shows compositional plots for Type 1 amphiboles. Mylonitic amphibolites which contain Type 1 compositions consist of lath-shaped

Figure 2.12. Plots of amphibole compositions from mylonitic amphibolite sample 75 in which compositions are relatively homogeneous. Note the lack of amphibole compositions which plot in the actinolitic hornblende field as observed in relatively undeformed amphibolite.

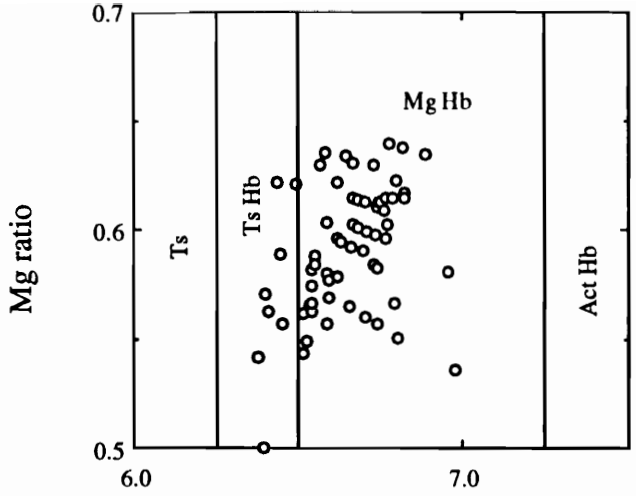
0.7
0.6
0.5
Mg ratio
Ts
Ts Hb
Mg Hb
Act Hb
6.0
7.0
Si

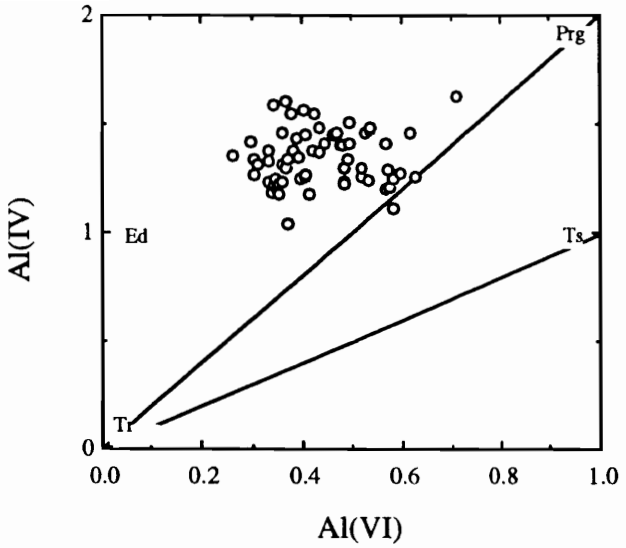
2
1
0
Al(IV)
Prg
Ed
Ts
Tr
0.0
0.2
0.4
0.6
0.8
1.0
Al(VI)

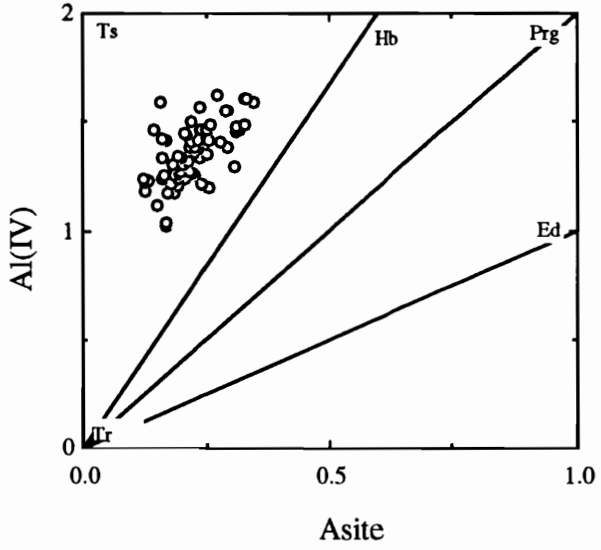
2
1
0
Al(IV)
Ts
Hb
Prg
Ed
Tr
0.0
0.5
1.0
Asite

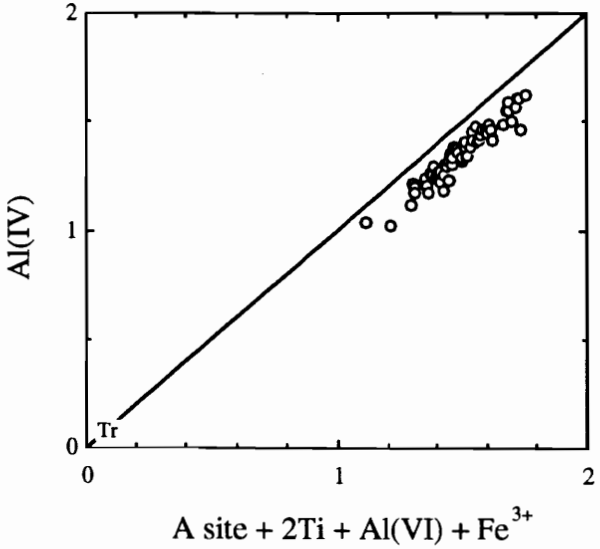
2
1
0
Al(IV)
Tr
0
1
2
A site + 2Ti + Al(VI) + Fe3+

Figure 2.13. Plots of amphibole compositions from mylonitic amphibolite sample 910A in which compositions are relatively homogeneous. Note the lack of amphibole compositions which plot in the actinolitic hornblende field as observed in relatively undeformed amphibolite.

Mg ratio
0.7
0.6
0.5
Ts
Ts Hb
Act Hb
Mg Hb
6
7
Si
Al(IV)
Tr
0
1
2
A site + 2 Ti + Al(VI) + Fe3+
Al(IV)
Al(VI)
Tr
Hb
Prg
Ts
Ed
0.0
0.5
1.0
Asite
Al(IV)
Tr
Prg
Ts
Ed

Figure 2.14. Plots of amphibole compositions from mylonitic amphibolite sample 895a which have actinolitic rims and more hornblende rich cores. This relationship has been interpreted as resulting from retrograde metamorphism.

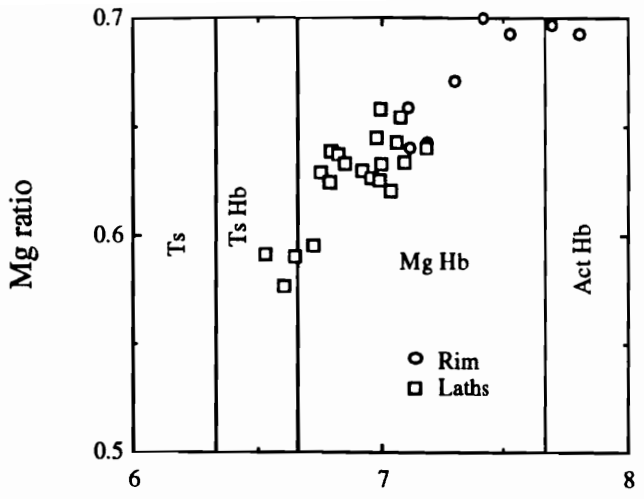
Mg ratio
0.7
0.6
0.5
6
7
8
Si
Ts
Ts Hb
Mg Hb
Act Hb
Rim
Laths

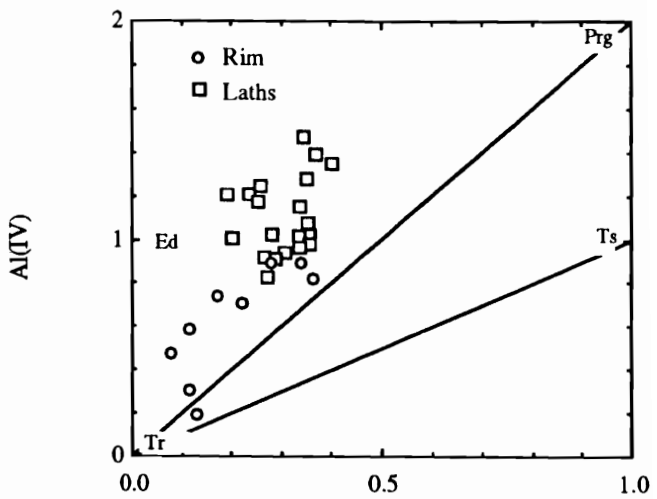
Al(IV)
2
1
0
0.0
0.5
1.0
Al(VI)
Rim
Laths
Prg
Ts
Ed
Tr

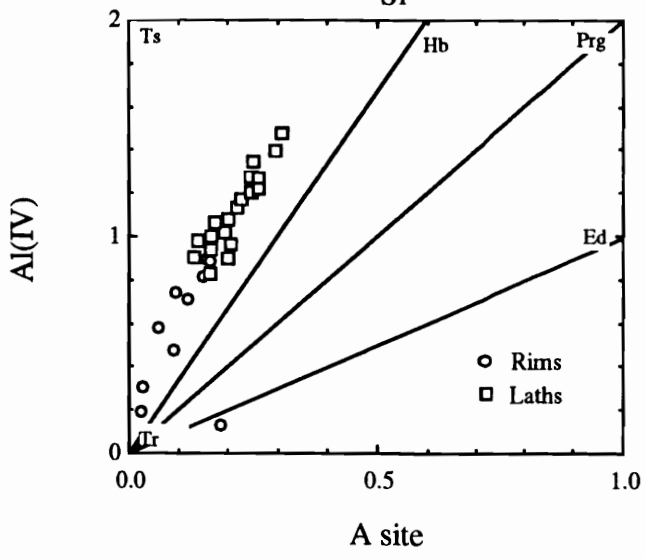
Al(IV)
2
1
0
0.0
0.5
1.0
A site
Ts
Hb
Prg
Ed
Rims
Laths
Tr

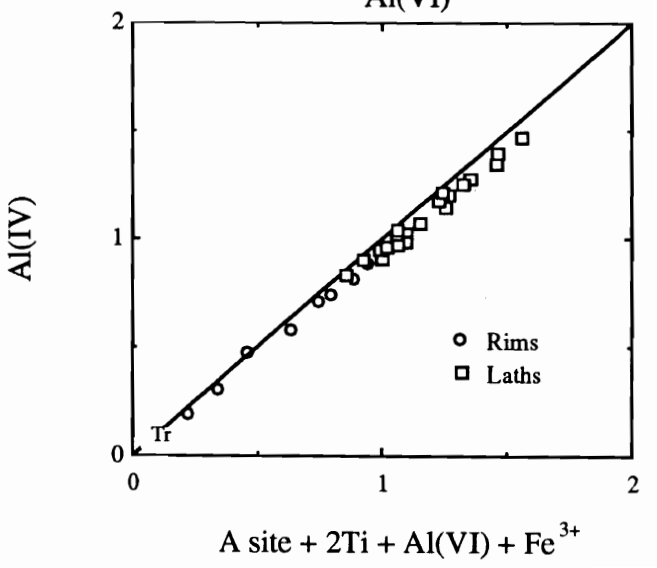
Al(IV)
2
1
0
0
1
2
A site + 2Ti + Al(VI) + Fe3+
Rims
Laths
Tr

Figure 2.15 Plots on the right show the opposite relationship with actinolitic hornblende cores and more hornblende rich rims. This is interpreted as representing amphibole with relict actinolitic hornblende core compositions.

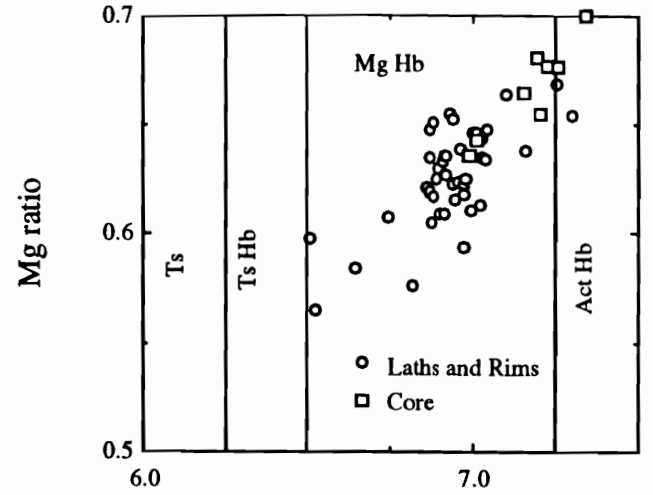
Mg ratio
0.7
0.6
0.5
6.0
7.0
Si
Ts
Ts Hb
Act Hb
Mg Hb
Laths and Rims
Core

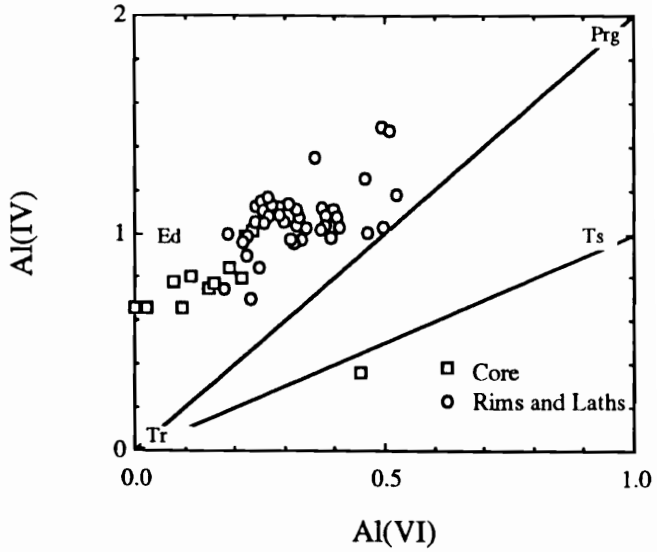
Al(IV)
2
1
0
0.0
0.5
1.0
Al(VI)
Prg
Ts
Ed
Tr
Core
Rims and Laths

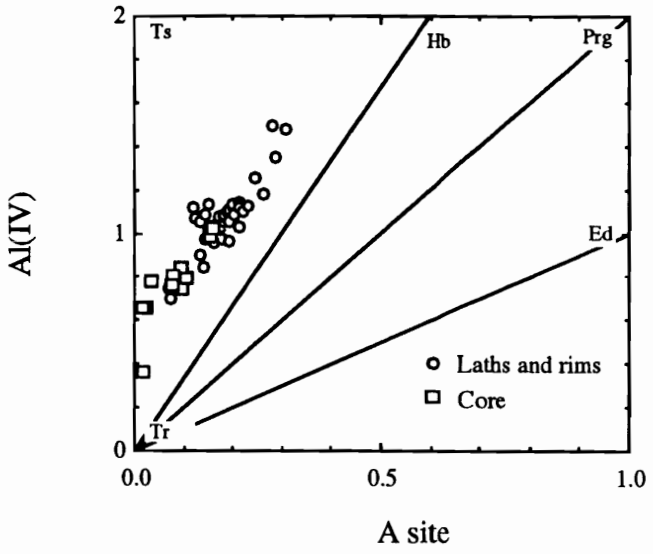
Al(IV)
2
1
0
0.0
0.5
1.0
A site
Ts
Hb
Prg
Ed
Tr
Laths and rims
Core

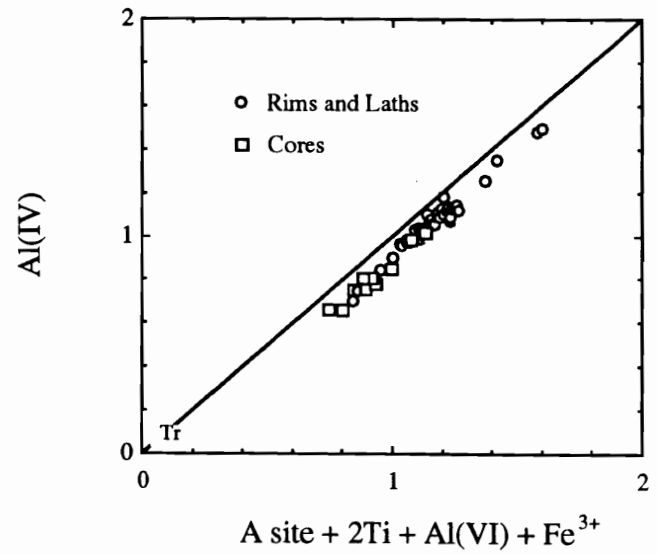
Al(IV)
2
1
0
0
1
2
A site + 2Ti + Al(VI) + Fe3+
Rims and Laths
Cores
Tr

amphiboles interlayered with equant plagioclase feldspar. SEM images andX-ray compositional maps of these amphiboles indicate that they are homogeneous. In outcrop, mylonitic amphibolites which have Type 1 compositions occur farthest from the shear zone boundary (e.g. samples 910a and 75).

Type 2 amphiboles are found in samples which have fine-grained amphibole layers parallel to the foliation (e.g. sample 895). These layers are commonly associated with kink folds which deform the mylonitic fabric. In thin section, amphiboles within these zones have corroded boundaries which have been altered to fine grained amphibole. Adjacent to the late kinks, epidote is more abundant and plagioclase is thoroughly sericitized. BSE images of these areas show that the alteration is discontinuous between amphibole layers and appears along grain boundaries of amphibole laths. Microprobe study of these zones indicates that amphibole laths have Fe-hornblende to Fe-tschermakitic hornblende compositions whereas the altered zones are actinolitic (Fig. 2.14).

Type 3 compositions are found in samples that have porphyroclasts which have irregular extinction and are mantle by amphibole laths. Porphyroclastic cores have actinolitic compositions whereas the margins of the porphryoclasts as well as the amphibole laths have magneiso-hornblende compositions (Fig. 2.15). Amphibolites which have these textures and compositions are found close to the shear zone boundary (sample 141).

Plagioclase Compositions

Plots of plagioclase compositions from samples at different strain magnitudes are shown in figure 2.16. In all samples, plagioclase compositions show significant variation with no systematic change with respect to the degree of strain. Back-scattered

Figure 2.16A-I. Figure 2.16A-C show plots of plagioclase compositions from relatively undeformed amphibolite. Textural relationships are not shown in 2.16A and B whereas figure 2.16C shows textural relationships of representative compositions from sample 62. Figure 2.16D and E are plots of plagioclase compositions from the undeformed and mylonitic sections of sample 81a which is a sample that contains the full strain transition. Note the shift in the bulk of the compositions from An_{60} to An_{50}. Plagioclase compositions in figure 2.16D of approximately An_{35} are from grain boundaries. Figure 2.16F show plagioclase data from sample 81 separated into core and edge compositions. Figure 2.16G-I are plots of plagioclase compositions from mylonitic amphibolite samples. In figure 2.16G note the shift in the range of compositions to lower anorthite contents. Figure 2.16H shows the range of compositions in sample 1.41. Figure 2.16I shows representative analyses of feldspar from mylonitic samples broken down into the different textural settings. Note that from relict igneous and core compositions to edge and grain size reduced plagioclase there is a decrease in anorthite content from An_{60} to An_{30}.

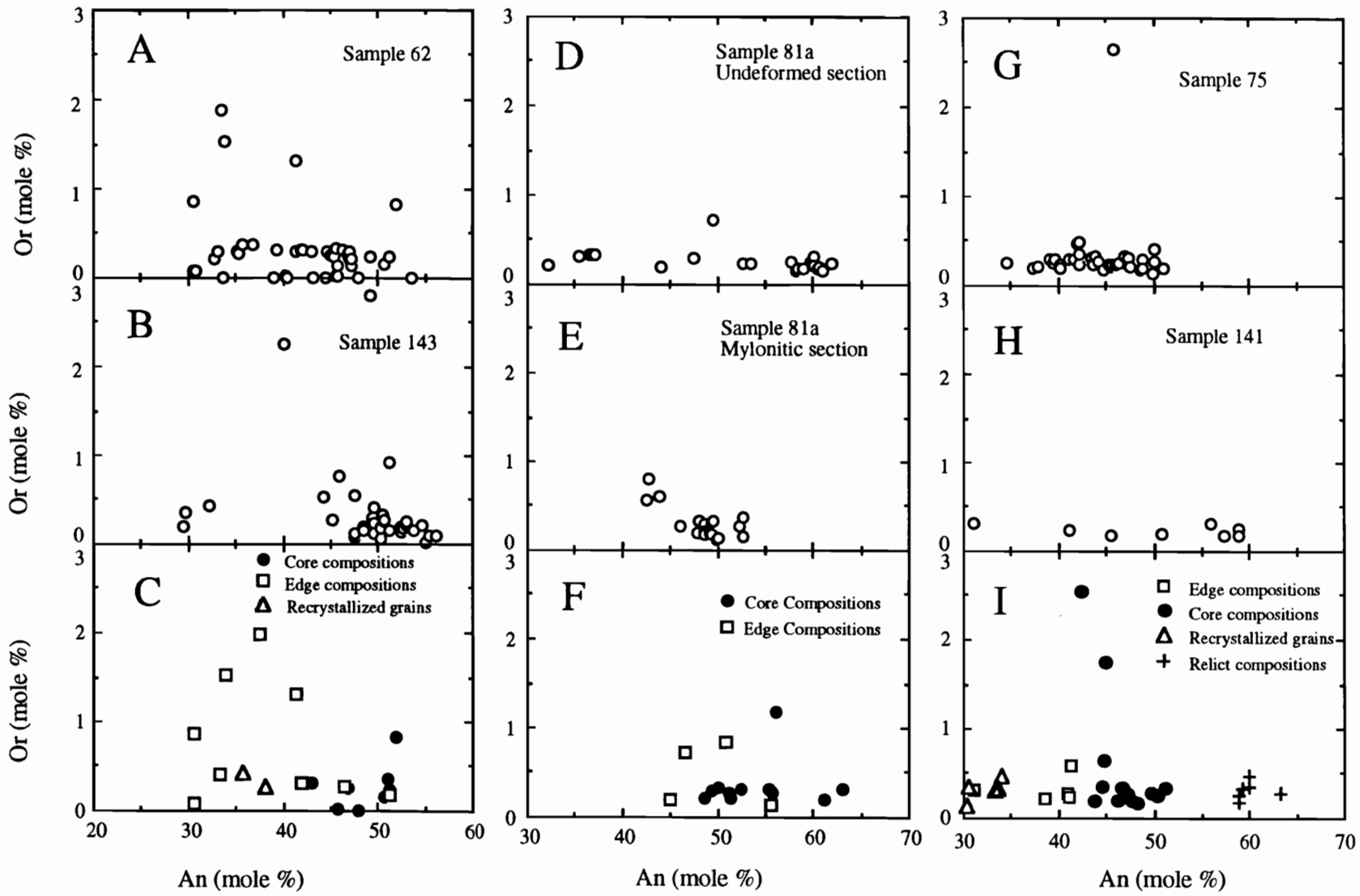
A
Sample 62
B
Sample 143
C
Core compositions
Edge compositions
Recrystallized grains
D
Sample 81a
Undeformed section
E
Sample 81a
Mylonitic section
F
Core Compositions
Edge Compositions
G
Sample 75
H
Sample 141
I
Edge compositions
Core compositions
Recrystallized grains
Relict compositions
Or (mole %)
An (mole %)

Figure 2.17 Back-scattered electron image of deformed plagioclase from sample 62. Note the angular shape and wide variety of grain sizes. Pale areas correspond to more anorthitic plagioclase (An_{50-60}) whereas darker areas have a higher albite component (An_{30-40}). Dusty white contrast along some grain boundaries of plagioclase may represent local increase in anorthite component or edge affects. The white euhedral grains are amphibole.

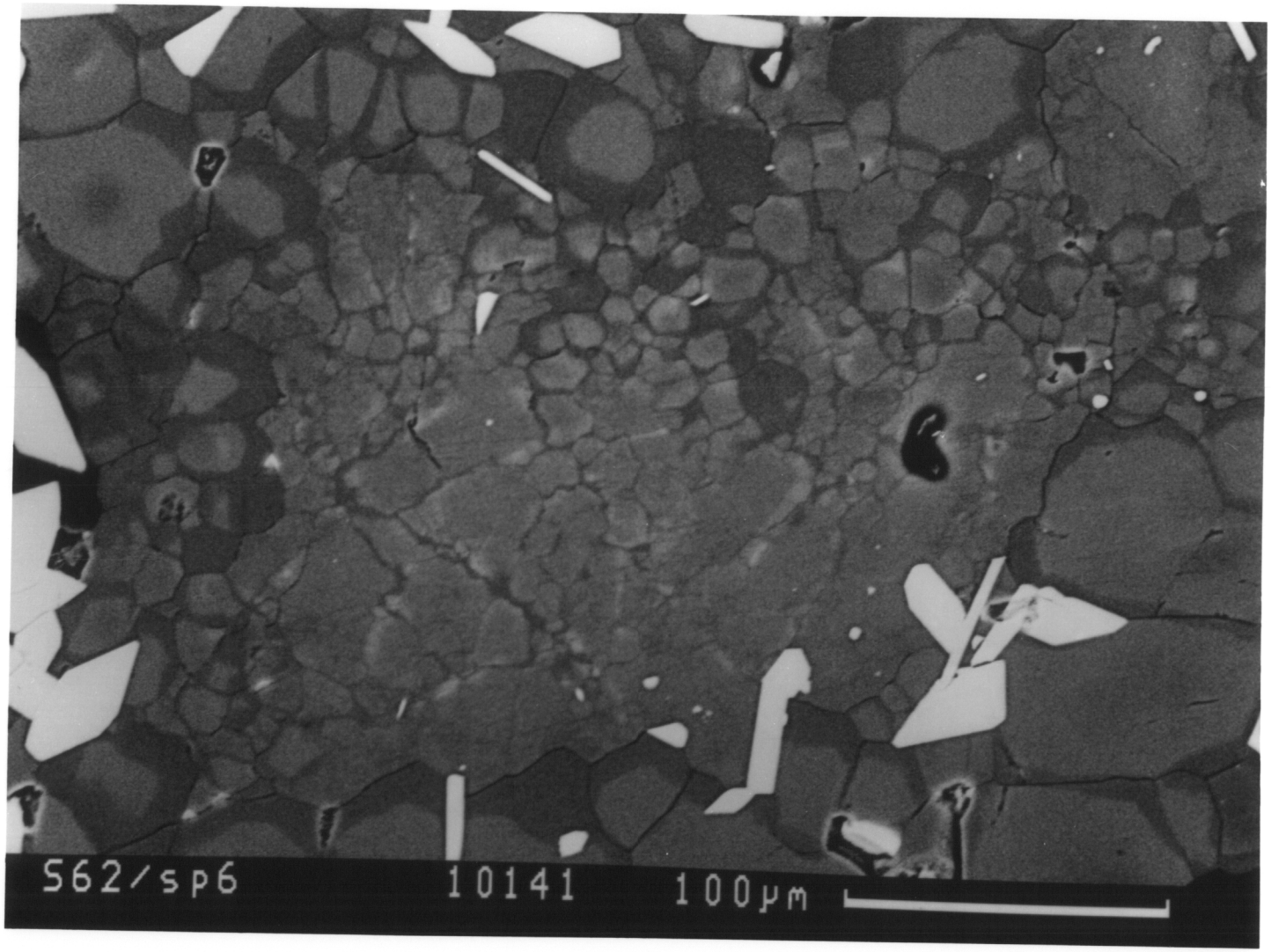
S62/sp6
10141
100µm

electron SEM and X-ray compositional maps of plagioclase at all strain magnitudes show a sharp compositional gradient along grain boundaries, with edges of grains enriched in albite (Fig. 2.17). Across the strain gradient the thickness of albitic rims is related to the degree of grain size reduction and recrystallization: highly recrystallized areas show thicker rims of albitic plagioclase.

Analyses of plagioclase from relatively undeformed amphibolite are shown in figures 2.17A. - 2.11C. The well defined populations for sample 143 at An_{45-55} are from relict plagioclase phenocrysts and cores of recrystallized mantling grains. Highly albitic compositions are from edges of recrystallized grains. Compositions which are intermediate in the range of An_{55}-An_{30} do not have a consistent textural setting and are found at the cores and margins of different grains.

The textural relationship between cores and rims of recrystallized plagioclase grains in the undeformed portion of a single sample that shows the full strain transition is shown in figures 2.16D through 2.16F. Across a single plagioclase grain the composition varies from An_{60} in the cores to An_{35} along the margins. Mylonitic sections of this strain transition show a small range of compositions near An_{50} (Fig. 2.16E).

Plagioclase compositions from mylonitic amphibolites show similar chemical and textural variation as plagioclase from relatively undeformed amphibolite. A few plagioclase grains show variable compositions from core to rim (Fig. 2.16I) whereas most grains show a sharp composition gradient (Fig. 2.16H). Core compositions fall into two groups with An contents of An_{60} and An_{50-55}. Several samples which contain circular spots of plagioclase wrapped by amphibole laths have the highest Ab content (An_{35-30}). Amphibole laths in these samples show replacement along margins of Al-hornblende by actinolite and are commonly associated with fine grained layers adjacent to later kink folds.

Chlorite

The few chlorite analyses from across the shear zone are fairly homogeneous with Mg/(Fe+Mg) ratios of 0.50 to 0.56.

Epidote

Epidote analyses show wide variation across the shear zone with no systematic changes with respect to the degree of strain. Compositions vary from 13 mol % to 42 mol % pistacite with up to 1 mol % piemontite component. Zoned grains are also observed with pistacite content increasing from 8 to 19 mol % from core to rim. Analyses of epidote from late kinks and cross cutting epidote veins have the highest pistacite content.

DISCUSSION

Closed System Behavior of Shear Zones

Shear zone formation may occur either as an open or closed chemical system. Numerous geochemical studies have shown that open-system behavior during shear zone formation involves large scale fluid influx and subsequent changes in bulk, trace and isotopic chemistry of the deformed rocks (e.g. McCaig et al.,1990; Beach,1976; Kerrich et al., 1977; Hickman and Glassley, 1984; Sinha et al. 1985). Shear zones of this nature typically postdate the peak of metamorphism, involve hydration of relatively dry host rock and commonly form at greenschist facies conditions.

Examples of closed-system behavior during shear zone formation include the Ivrea shear zone in Italy (Brodie,1981), shear zones which deform adamellite in the Yellowknife area (Kerrich et al., 1977) and metagabbro shear zones in the Southeastern Adirondacks (Nyman and Swapp,1987). In comparison to open-system shear zones,

isochemical systems occur at higher metamorphic grades and commonly form during prograde metamorphism (Brodie, 1981).

Bulk chemical analyses of samples from across the Cheyenne belt shear zone demonstrate that on this scale the shear zone formed under closed-system conditions with no apparent metasomatism. As will be discussed in a section below, this is consistent with the inference that the shear zone formed during increasing temperature near the peak metamorphic conditions.

Although the bulk chemical data indicate isochemical and isovolumetric processes during shear zone formation, SEM back-scattered images and X-ray compositional maps of amphibole and plagioclase from across the strain transition indicate that element redistribution was active at least on the grain boundary scale. This is supported by the observations of aluminous hornblende overgrowths on actinolitic fragments and albitic rims on plagioclase grains which are interpreted as forming as a result of a dissolution/re-precipitation during metamorphism and deformation. As will be discussed in a section below, the replacement of actinolitic amphibole by more aluminous hornblende requires mobility of several cations within the grain boundary regions at the centimeter scale, presumably in the presence of a grain boundary fluid (cf, Carmichael, 1969).

Shear Zone Metamorphism

Numerous studies of regional metamorphism of mafic rocks have summarized the important chemical changes that occur in response to changing P-T conditions (e.g., Cooper, 1972; Grapes et al., 1977; Harte and Graham, 1975; Laird and Albee, 1981; Laird, 1980). Unlike pelitic rocks, which may undergo various divariant exchange reactions separated by discontinuous univariant reactions, mafic assemblages have a relatively constant mineralogical composition over a substantial range in metamorphic

grade. Reactions during metamorphism of mafic rocks are typically continuous and result in compositional changes of mineral solid solutions with progressive modal decreases in some phases (e.g. chlorite and epidote).

Laird and Albee (1981) outlined the metamorphism of the "common assemblage" which is found in worldwide occurrences of mafic rocks, and identified a systematic mineral compositional variation which occurs in response to changing metamorphic conditions. During regional metamorphism of mafic rocks, amphibole and plagioclase compositions show the most systematic compositional variation. With increasing P and T, amphibole becomes enriched in Al, Ti and A-site cations and depleted in Si and Mg. These compositional changes can be represented as progress along tschermakite, edenite and glaucophane exchange vectors (Thompson et al, 1981). Compositional change of amphibole during prograde metamorphism can also be a function of the mineral assemblage (Leger and Ferry, 1991; Cho and Ernst, 1991). Plagioclase feldspar compositions become more anorthitic with increasing grade and show discrete compositional jumps at the peristerite gap (albite to oligoclase) in medium and low pressure facies series (Laird and Albee, 1981). The production of anorthite component during metamorphism is associated with the disappearance of epidote which is a complex function of P,T and fO_2 during metamorphism (Holdaway, 1972). Liou et al. (1974) note that the disappearance of chlorite marks the upper limit of the greenschist facies. The disappearance of chlorite is probably through is a divariant reaction and a function of temperature and fO_2 (Spear, 1981; Liou et al., 1974).

The observed chemical zonation in amphibole porphyroclasts from the least deformed amphibolite is consistent with their formation during prograde metamorphism. As shown by the BSE images and X-ray compositional maps, the cores of the amphibolite porphyroclasts are relatively homogeneous. Minor variation occurs as

localized, poorly defined patches which may represent incipient exsolution of Al-poor and Al-rich amphiboles in response to cooling. Exsolution of calcic amphiboles observed on the TEM scale (see Smelik et al. 1991) will be discussed below. The bulk of compositional variation is observed along the grain boundaries of the angular 'subgrains' which mantle porphyroclasts. The angular morphology of the 'subgrains' and the sharp compositional gradient both suggest a dissolution/precipitation reaction mechanism involving replacement of actinolitic compositions with more aluminous hornblende.

With increasing strain across the shear zone the range of amphibole compositions decreases as indicated by the progressive elimination of actinolitic amphibole compositions. This trend is interpreted as indicating that deformation within the shear zone enhanced the progress of metamorphic reactions towards the attainment of equilibrium at peak metamorphic conditions. The most aluminous amphiboles (Fe-tschermakitic hornblende) occur in mylonitic rocks which are found farthest from the shear zone boundary (sample 75) and amphibole needles at the margins of amphibole porphyroclasts in relatively undeformed amphibolite. These compositions probably represent the equilibrium composition for the peak of metamorphism. This inference is made primarily on the basis of the high aluminum content of the amphibole which has been shown to increase at higher metamorphic grade (Spear, 1981; Laird and Albee, 1981). However, Al content of amphibole may also be a function of the local assemblage. (Leger and Ferry, 1991; Cho and Ernst, 1991). If the local assemblage controlled the composition, the composition of amphibole may have been limited by the extent of the plagioclase breakdown. For the mylonitic amphibolite, mechanical processes such as intracrystalline strain and/or grain size reduction may have facilitated equilibration to the equilibrium conditions (cf., Koons et al. 1987). Details of the role of deformation in affecting the shear zone chemical processes will be discussed in chapter 3.

The low-Al actinolitic compositions (type 2) observed in other samples of the deformed amphibolite are the result of retrograde metamorphism associated with later kink folds which deform the L-S fabric. Kink folds are also associated with other retrograde features including epidote veins, chloritization of amphibole and sericitization and saussuritization of plagioclase.

Submicron scale exsolution of the calcic amphiboles has been observed throughout the strain transition. Cummingtonite exsolution lamellae are observed in the relatively undeformed amphibolite and found in amphiboles which have actinolitic compositions. Submicron-scale exsolution of Al-poor actinolite and Al-rich hornblende is also found in a narrow range of compositions and is observed in samples from across the strain transition (Smelik et al., 1991). The localized, poorly defined compositional contrast observed in amphibole porphyroclasts is similar to reported occurrences of coexisting calcic amphiboles which have been interpreted as representing both an exsolution product (Brady, 1974) as well as a disequilibrium coexistence (Grapes and Graham, 1978). Lack of detailed crystallographic study precludes any definitive interpretation of this feature.

The range of plagioclase compositions here is remarkably different from that reported in other studies of mafic rocks. For medium-pressure facies series mafic schists from Vermont, Laird and Albee (1981) reported that plagioclase composition varied from nearly pure albite at approximately 500 °C to oligoclase at 550 °C. This is consistent with mafic schists from the Haast schists in New Zealand as well as Dalradian rocks in Scotland (Cooper, 1972; Harte and Graham, 1975). Compared to these earlier studies, plagioclase from the variably deformed Cheyenne belt amphibolites are unusually anorthitic and have nearly igneous compositions (An_{50} to An_{95} ; Barker, 1983). Relict plagioclase phenocrysts in relatively undeformed amphibolite have the highest anorthite content and a relatively constant composition (sample 143). Where plagioclase has

undergone grain size reduction, margins of grains and domains of grain size reduction show an increase in albite component with sharp compositional gradients along grain boundaries. The distribution of plagioclase feldspar compositions represents incomplete reequilibration of igneous compositions under the prevailing metamorphic conditions. Plagioclase compositions similar to those observed in amphibolites from the Cheyenne belt have been reported by Grapes et al. (1977) for variably deformed and metamorphosed gabbros in Japan and by Mongoltkip and Ashworth (1986) in metagabbros from Scotland. Both studies concluded that the compositions represent relict igneous compositions and did not reequilibrate during metamorphism.

Phase Equilibria and Metamorphic Reactions

Amphibolites from the SLSZ have several petrographic characteristics which differ from other reports of mafic rocks. Across the strain transition, amphibolites contain relatively small amounts of chlorite and epidote, even in the relatively undeformed amphibolite where the actinolitic amphibole has a composition characteristic of greenschist facies conditions. In addition, petrographic characteristics of the amphibole porphyroclasts in the relatively undeformed amphibolite suggest that amphibole may have directly and passively replaced pyroxene. These characteristics include; 1) the observation of (100) twins which may represent relict pyroxene twins and 2) tabular outlines that appear to be pseudomorphs of igneous pyroxene grains. This observation is interpreted as indicating that amphibole directly and passively replaced the pyroxene phenocrysts and did not coexist with abundant chlorite or epidote.

The lack of abundant chlorite and epidote in the shear zone amphibolite must primarily be a result of bulk chemical control. Figure 2.18 shows expanded tetrahedral plots of the mineral compositions for the relatively undeformed amphibolite. Plots for

Figure 2.18. Exploded tetrahedral plots Al_2O_3-Na_2O-CaO -FMO (FeO + MgO) of amphibole, plagioclase, chlorite and epidote compositions from relatively undeformed amphibolite (S62). Small plus sign represents location of bulk chemical composition of sample. Note that trend of amphibole compositions is towards the bulk composition and tie lines that connect the hornblende composition with the most albitic plagioclase pass through the bulk composition.

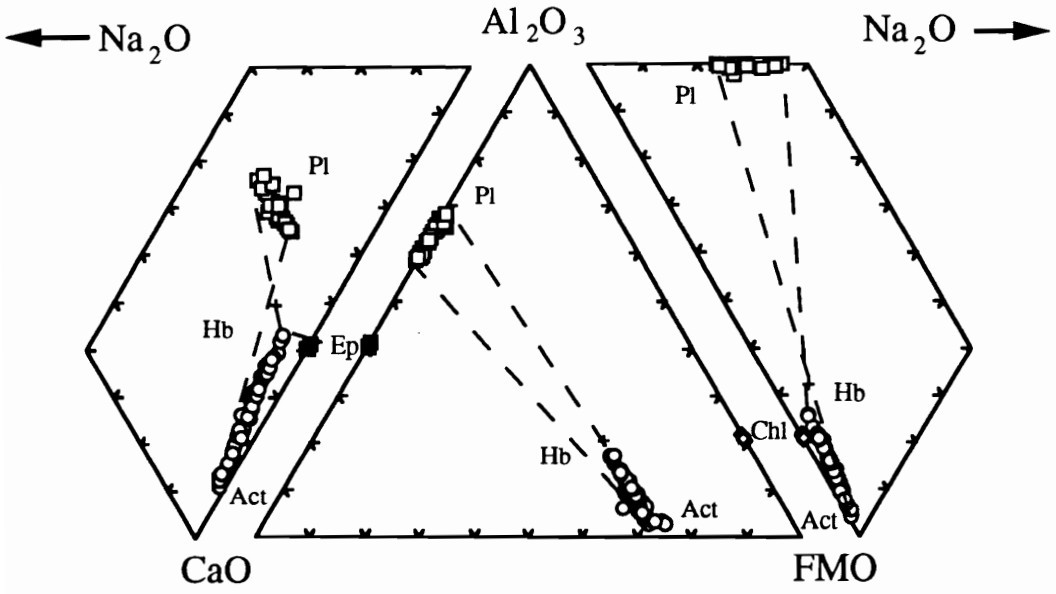
Na2O
Al2O3
Na2O
Pl
Hb
Ep
Act
Pl
Hb
Act
Pl
Hb
Chl
Act
CaO
FMO

progressively more deformed amphibolites show similar but less varied trends. In all plots examined, tie lines that connect actinolitic amphibole with the most calcic plagioclase and aluminous hornblende with the most albitic plagioclase pass through or near the bulk composition which explains the paucity of chlorite and epidote in the amphibolites.

Reactions during prograde metamorphism of mafic rocks involve: 1) increases in tschermakite, edenite, glaucophane and $FeMg_{-1}$ components of amphibole; 2) increase in the anorthite component of plagioclase; and 3) gradual decrease in the modal proportions of epidote and chlorite. Due to the relatively simple modes of amphibolites from the SLSZ, reactions which model the shear zone metamorphism must differ from those reported by other workers. The main differences include: 1) the calcic compositions of the plagioclase feldspar; 2) the progression towards more albitic plagioclase associated with more aluminous amphibole; 3) the appearance of sphene replacing ilmenite with increasing strain; and 4) the lack of chlorite as a source of Al and Fe and epidote as a source of Ca and Al.

One possible mass balance reaction which models the observed petrographic and chemical variation observed is:

(1) 1.14 Amphibole I + 5 Plagioclase I + 0.214 Ilmenite + 0.187 Quartz + 0.069 Water
$\Leftrightarrow$ 1.636 Amphibole II + 4.611 Plagioclase II + 0.330 Sphene

where amphibole II has higher tschermakite, edenite and $FeMg_{-1}$ contents than amphibole I and plagioclase II is more albitic than plagioclase I (see Table 2.2). In this reaction, the breakdown of the anorthitic plagioclase (plagioclase I) along grain boundaries in response to both deformation and heating provides a source of Al and Na for amphibole II as well as Ca for the reaction of ilmenite to sphene. This results in a slight decrease in the amount

of plagioclase. The remaining plagioclase would have a more albitic composition with additional Si supplied from quartz and the replacement of amphibole I (rich in Si) by amphibole II (lower Si content).

Reactions for shear zone metamorphism also can be formulated using a simplified reaction space in the CNMASH system . The reaction matrix for this system contains 8 phase components and 6 system components which results in two linearly independent reactions (Table 2.3). The reaction matrix was solved using a Gibbs method computer program (Spear 1989) which formulates reactions using a Gauss-Jordan reduction as outlined by Thompson (1982). Two possible linearly independent reactions for this system are (see Table 2.3 for abbreviations):

$$(2) \quad .66\ \text{Fe-Tr} + 1.0\ \text{Mg-Hb} \Leftrightarrow 1.0\ \text{Fe-Hb} + .66\ \text{Tr}$$

$$(3) \quad .44\ \text{Tr} + .20\ \text{Ab} + .10\ \text{An} + .20\ \text{Qtz} + .50\ H_2O \Leftrightarrow .667\ \text{Mg-Hb} + .273\ \text{Fe-Tr}$$

Reaction 2 is the Fe-Mg exchange reaction between actinolite/tremolite with aluminous hornblende. Reaction 3 describes a reaction where plagioclase components react with tremolite to produce a more Fe-rich tremolite and Mg- hornblende. Given that the mineral compositions are simplified for this model, these two reactions provide a general outline for the shear zone metamorphism and support the observation that amphibole compositional variation is controlled by changes in plagioclase composition.

With increasing deformation, reaction progress in more highly strained rocks would be greater, eliminating the amphibole I and plagioclase I compositions. This suggests that mechanical processes such as intracrystalline strain (resulting in increases in defect density), grain size reduction and grain boundary formation are the major controlling factors in the reaction history and progress of these rocks. In these

TABLE 2.2 : PARAMETERS USED IN MASS BALANCE CALCULATIONS

Mass balance calculations were completed using Singular Value Decomposition matrix analysis (Fisher, 1990).

Components: K_20-Na_2O-CaO-MgO-FeO-MnO-TiO_2-Al_2O_3-SiO_2

Phases: Sphene, quartz and ilmenite are assumed to have endmember compositions

Compositions of plagioclase and amphibole are averages of several analyses from relatively undeformed amphibolite.

	Act Hb	Mg Hb	Ca-Plag	Na-Plag
SiO_2	49.48	43.26	55.97	59.41
Al_2O_3	5.60	12.48	27.26	23.14
TiO_2	0.35	0.39	0.01	0.01
FeO	15.56	18.67	0.20	0.19
MnO	0.24	0.22	0.01	0.01
MgO	13.04	8.76	0.04	0.03
CaO	12.33	11.97	10.22	7.27
Na_2O	0.54	1.18	5.75	7.12
K_2O	0.13	0.34	0.06	0.14
Sum	97.27	97.27	99.52	97.32

TABLE 2.3 : REACTION SPACE PARAMETERS

System Components (NC): Na_2O-CaO-MgO-Al_2O_3-SiO_2 (Note that FeO = 1- MgO)

Phase components (NP):

Tremolite (Tr)
Fe-Tremolite (Fe-Tr)
Mg-Hornblende (Hb)
Fe-Hornblende (Fe-Hb)
Anorthite (An)
Albite (Ab)
Quartz (Qtz)
Water (H_2O)

Phase component compositions were taken from Gibbs method program of Spear (1989).

PC	Si	Al	Mg	Ca	Na	H_2O
Tr	8.0	0.0	5.0	2.0	0.0	1.0
Fe-Tr	8.0	0.0	0.0	2.0	0.0	1.0
Mg-Hb	6.2	3.3	3.3	2.0	0.3	1.0
Fe-Hb	6.2	3.3	0.0	2.0	0.3	1.0
Ab	3.0	1.0	0.0	0.0	1.0	0.0
An	2.0	2.0	0.0	1.0	0.0	0.0
Qtz	1.0	0.0	0.0	0.0	0.0	0.0
Water	0.0	0.0	0.0	0.0	0.0	1.0

The number of linearly independent reaction is PC-NC = 2

amphibolites, and possibly other metamorphic rocks, chemical processes are ultimately controlled by deformation and, in the absence of deformation, reaction progress would be limited (Nyman et al., 1991; Koons et al., 1987).

These observations have several important implications. Amphibole zonation has been used to model polymetamorphism (Laird and Albee, 1981) and P-T-t paths (Holland and Richardson, 1979; Triboulet and Auden, 1988). From this study, it is apparent that variation in amphibole composition within a single porphyroclast is a function of: 1) grain boundary formation; 2) local phase assemblage; and 3) the composition of the grain boundary fluid (cf Rubie, 1986). For example, zoned 'subgrains' which are observed at the boundaries of amphibole porphyroclasts (Fig. 2.8; zone II) show a compositional progression from hornblende-rich cores to actinolite interiors and back to hornblende-rich margins. Experimental and field studies have shown that Al content of amphiboles increases with increasing temperature (Spear, 1981; Laird and Albee, 1981) which would suggest a complex heating/cooling path for these rocks. Alternatively, this variation as may be interpreted as indicating amphibole growth in which the compositions are controlled by the available chemical species in the grain boundary region (Yardley et al., 1991). In this case, the low-Al amphibole compositions represent growth during a stage in the metamorphism where Al was not being liberated from the plagioclase. Growth of the more aluminous hornblende represents stages where deformation and dissolution of plagioclase resulted in local transport of the calcic components, precipitation of a more albitic feldspar and growth of a more Al-rich amphibole.

The interpretation that reaction progress was a function of grain boundary formation suggests that the chemical processes within the shear zone may be diffusion controlled (Fisher, 1978). The chemical variation of plagioclase and amphibole is therefore a function of availability of chemical species at the developing interfaces during

grain boundary formation. With increasing deformation, grain boundary formation would facilitate fluid infiltration, increasing rates of dissolution and migration of necessary chemical constituents.

REGIONAL IMPLICATIONS

Pressure and Temperature Estimates

Temperature estimates using amphibole and plagioclase compositions are hindered by a paucity of thermodynamic data on even simple end member compositions as well as a lack of understanding of the mixing properties of amphibole (see Graham et al., 1989 for review). Temperature estimation for the SLSZ is also hindered by difficulty in choosing the equilibrium compositions for amphibole and plagioclase. Using Spear's (1980) empirical calibration and compositions from mylonitic amphibolite (sample 75), estimates range from 490-530 °C which are roughly consistent with temperatures reported by Duebendorfer (1988). Temperature estimates using the thermometer calculated by Blundy and Holland (1990) yield temperatures in the range of 800-850 °C. These latter estimates far exceed the reported temperatures and are clearly inconsistent with phase equilibria in the amphibolites. Therefore the peak metamorphic temperature is taken as approximately equal to 500 °C.

Quantitative pressure estimates for the amphibolites cannot be made. Estimates from pelites from the French Slate approximately 1 km across strike from the SLSZ indicate a pressure of 3.5-4 kb (Duebendorfer 1988).

Implications of Field and Petrologic Data for Tectonic Models for the Cheyenne belt

Duebendorfer and Houston (1987) proposed a tectonic model for the Cheyenne belt which involves oblique convergence between an island arc and the Archean continental margin. This resulted in accretion of several different lithotectonic blocks with deformation concentrated along mylonite zones which separate the crustal segments.

Structural features along the SLSZ have orientations which are similar to the D1 structures of Duebendorfer and Houston (1987), with lineations defined by alignment of amphibole porphyroclasts trending NE-SW at a shallow to moderate plunge. D1 structures have been interpreted by Duebendorfer and Houston (1987) as forming early in the accretionary history of the area. These authors suggest the D1 structures represent a preliminary phase of dextral strike slip or low-angle thrusting associated with oblique convergence. Dextral movement is consistent with the observed rotation of amphibole and feldspar porphyroclasts into parallelism with the shear zone boundary (Fig. 2.2b).

Compositional variations of amphibole and plagioclase are difficult to interpret in terms of regional-scale processes due to the local control that deformation and the phase assemblage have on the chemistry of the two phases. Regional and experimental studies of amphibolites have shown that tschermakite, edenite and $FeMg_{-1}$ contents of amphibole increases with increasing metamorphic grade (Laird and Albee, 1981; Spear, 1981). Assuming this, amphibole compositions from across the SLSZ therefore indicate that shear zone formation occurred during an increase in metamorphic grade. Petrographic observations in the relatively undeformed amphibolite suggest that amphibole directly and passively replaced igneous clinopyroxene and that with increasing deformation, amphibole and plagioclase compositions equilibrated to the peak metamorphic conditions. Attainment of peak metamorphic temperature probably postdated deformation as indicated

by: 1) the presence of amphibole needles, which have the most aluminous (and therefore peak temperature compositions) at the margins of amphibole porphyroclasts that grow into deformed plagioclase and, 2) TEM images which show that aluminous hornblende that replaces actinolite is nearly devoid of defect microstructures whereas actinolite has zones of dislocation tangles and abundant microcracks (see Chapter 3 and 4). This observation suggests that the growth of aluminous hornblende postdated most of the deformation. The regional tectonic implication of these observations is that the development of the shear zone must have been associated with a heating event, possibly during thermal relaxation of isotherms following burial by low angle thrusting as suggested by tectonic models of Duebendorfer and Houston (1987). These observations are the first to recognize that in the Medicine Bow Mountains metamorphism outlasted the deformation. In addition, these data substantiate models that propose convergence of several different thrust sheets during tectonic development of the Medicine Bow Mountains.

Asymmetric dextral folds which deform the mylonitic foliation of the amphibolite have a morphology and orientation similar to late strike-slip (D2) structures reported by Duebendorfer and Houston (1987). In the SLSZ, dextral kinks are associated with epidote veins and narrow fine-grained zones oriented parallel to the mylonitic foliation. In thin sections of the kink bands, epidote replaces amphibole and plagioclase is highly altered to sericite. Fine-grained bands parallel to the mylonitic fabric consist of hornblende partially altered to fine-grained actinolite (type 3 amphibole from mylonitic amphibolite). These observations are consistent with the argument of Duebendorfer and Houston that these structures formed late in the tectonic development of the Cheyenne belt at lower metamorphic grade.

SUMMARY

Detailed study of variably deformed amphibolite in the Cheyenne belt, southeastern Wyoming, indicates that microstructural and chemical characteristics vary as a function of strain intensity. Microstructural changes across the shear zone include progressive grain size reduction and development of a L-S fabric defined by alternating amphibole- and plagioclase-rich layers. Textures that indicate microcracking of plagioclase and amphibole suggest deformation occurred via a cataclastic deformation mechanism. Bulk chemical analyses of amphibolite from across the shear zone as well as mass balance reactions indicate that shear zone processes were essentially isochemical. Within relatively undeformed amphibolite, actinolitic hornblende was replaced along grain boundaries by magnesio-hornblende, with concomitant replacement of calcic plagioclase by albitic plagioclase. Replacement textures along grain boundaries suggest that reactions occurred by dissolution and precipitation processes. Increased reaction progress occurs with increasing strain as indicated by the progressive elimination of actinolitic hornblende compositions. Ilmenite is also progressively replaced by sphene across the shear zone, indicating local transport of Ca, Si and Fe.

The occurrence of textures which indicate dissolution and precipitation along amphibole and plagioclase grain boundaries suggests that reactions are in part controlled by chemical and mechanical processes at grain boundaries. Also, homogenization of compositions with increasing strain indicates a link between the chemical and mechanical evolution of the shear zone. Shear zone formation occurred during increasing metamorphic grade, possibly related to loading along the Cheyenne belt, as indicated by increases in tschermakite, edenite and $FeMg_{-1}$ of amphibole,. This input of mechanical and thermal energy was insufficient, however, to drive reactions to completion within the relatively undeformed amphibolite as shown by the large range of amphibole and

plagioclase compositions. However, in more highly strained amphibolite, the observed decrease in the range of amphibole compositions and complete replacement of ilmenite by sphene indicates an increase in reaction progress. These observations suggest that the petrologic evolution of amphibolite in the SLSZ is controlled by mechanical processes associated with the progressive development of the mylonitic amphibolite.

The strong interrelationship between chemical and mechanical processes during metamorphism described in this and other studies of variably deformed mafic rocks (Brodie and Rutter, 1985) emphasizes the importance of deformation in controlling chemical processes in rocks. Mechanical processes contribute to the total energy of the system either as strain energy associated with increases in intracrystalline defect density (Wintsch and Dunning, 1985), or as enhancement of reaction rates due to increases in fluid infiltration or intergranular diffusion. In either case, the chemical evolution of the rock may be strongly influenced by the degree of deformation, the strain path, or variation in deformation mechanism. Addition of energy through deformation may be especially important in overcoming activation energy barriers in systems which are close to equilibrium and require additional energy to drive chemical processes. These documented interrelationships between deformation and metamorphism highlight the necessity for considering the mechanical evolution of rocks in order to apply petrologic, isotopic and geochronologic data in constraining geologic processes and tectonic models.

CHAPTER 3: AN EVALUATION OF THE ROLE OF STRAIN ENERGY DURING METAMORPHIC REACTIONS: AN EXAMPLE FROM AN AMPHIBOLITE SHEAR ZONE, CHEYENNE BELT, SOUTHEASTERN WYOMING

ABSTRACT

Petrologic investigation of meter-scale shear zones which deform amphibolite boudins indicates that the progress of metamorphic reactions increases with increasing strain magnitude. This is evidenced by the progressive elimination of actinolitic hornblende, and replacement by magnesio-hornblende, across the shear zone. Back-scattered electron images of amphibole and plagioclase show that replacement occurred along boundaries of angular shaped grains. Compositional gradients across these regions are steep. Replacement of plagioclase and amphibole along grain boundaries is interpreted as occurring by a dissolution/reprecipitation mechanism. TEM observations of amphibole grains reveals that boundaries between actinolitic and magnesio-hornblende are marked by an abrupt change in dislocation density; actinolitic hornblende having relatively high dislocation density whereas magnesio-hornblende is nearly defect free. These observations suggest that strain energy associated with increases in dislocation density may have contributed to the progress of metamorphic reactions. Models derived using the Gibbs Method indicate that observed modal and compositional changes of amphibole and plagioclase can occur isothermally when strain energy associated with dislocations in amphibole or plagioclase is added to the system. These results suggest that the progress of reactions during syndeformational metamorphism may in part be controlled by mechanical processes such as increases in dislocation density.

INTRODUCTION

Increases in dislocation density have been shown to affect a wide variety of geochemical processes including volume diffusion (Yund et al., 1981; 1989), dissolution (Wintsch and Dunning, 1985), weathering (Blum et al., 1990), nucleation (Smith, 1985) and polymorphic phase transformations (Snow and Yund, 1987). One way in which variation of dislocation density can affect geochemical and petrologic processes is by increasing the Gibbs free energy and thereby altering the equilibrium conditions of the mineral (Helgesen et al., 1978; Wintsch and Dunning, 1985; Kerrick, 1986). Dislocations have also been shown to cause variation in kinetic rates of chemical processes by providing a larger number of active sites for dissolution (Blum et al., 1990) or zones of enhanced volume diffusion along dislocation cores. For most geologic conditions however, the effect on volume diffusion has been shown to be minor (Yund et al., 1981; 1989).

Although theoretical, experimental and field studies have shown that increased dislocation densities can enhance the rates of chemical processes, the magnitude of the effect is controversial and it is commonly difficult to ascribe variation in geochemical rates to dislocation density alone. This may especially be true in metamorphic environments where variation in other factors such as heat conduction, pressure changes, fluid flow and chemical potential gradients may overwhelm any contribution from dislocation-related processes (Rubie and Thompson, 1985). Experimental studies of the effect of dislocations on low-temperature dissolution also have been inconclusive. This is primarily due to the fact that experiments are performed far from equilibrium (Blum et al., 1990) and precipitation of new phases during experiments inhibits subsequent dissolution, thereby masking any potential effects of deformation (Murphy, 1989).

The objective of this paper is to quantitatively determine the effect of dislocation-induced strain energy on the progress of metamorphic reactions within an amphibolite shear

zone located in the Cheyenne belt, southeastern Wyoming. This paper will address only the possible importance of strain energy associated with dislocations recognizing that other processes also may significantly contribute to the chemical processes. Across centimeter-scale shear zones, petrologic data indicate a strong correlation between the progress of metamorphic reactions and the intensity of cataclastic deformation. This is shown by the progressive homogenization of amphibole and plagioclase compositions with increasing deformation across the shear zone. The progress of metamorphic reactions within the shear zone must therefore be at least partly controlled by some process associated with increasing deformation intensity across the strain transition. Possible processes include: 1) variation of the thermodynamic stability of phases due to increases in dislocation density; 2) increases in volume diffusion along dislocation cores and; 3) increases in fluid infiltration and/or intergranular diffusion which would increase kinetic rates of reactions.

Additional evidence for deformation control of reactions in amphibolite shear zones is provided by back-scattered electron (BSE) images and X-ray compositional maps that show compositional variation of plagioclase and amphibole grains occurs mainly along grain boundaries. In amphibole grains, actinolitic hornblende is replaced by magnesio-hornblende, and anorthitic plagioclase (XAn = 0.50) is replaced by more albitic plagioclase (XAn = 0.30). The observation of mineral overgrowths on angular grains suggests that reactions occurred by a dissolution and reprecipitation process. Furthermore, transmission electron microscope (TEM) images of grain boundary areas of amphibole show that the compositional boundaries between actinolite and magnesio-hornblende are marked by an abrupt change in dislocation density; actinolite has high dislocation densities whereas magnesio-hornblende is relatively defect-free. This texture can be interpreted to indicate a relationship between the development of the dislocations and the replacement of actinolite by magnesio-hornblende.

The effect of strain energy on the progress of reactions within the shear zone has been evaluated using the Gibbs Method (Spear, 1988; 1989) and conservative estimates of strain energy for various dislocation densities. Gibbs Method calculations were completed using computer programs developed by Spear and others (1989, 1991). Modification of the chemical system due to strain energy has been determined by correlating strain energy with the activity of plagioclase and amphibole. Details of the model will be discussed in a later section. The results of this modelling show that for the first increments of temperature increase (5-10 °C), additional energy provided by a dislocation density of 10^{11} cm^{-2} for plagioclase and 10^{10} cm^{-2} for amphibole could double the magnitude of modal and compositional changes. The general implication of this result is that during dynamothermal metamorphism, deformation by dislocation creep may increase the progress of metamorphic reactions. This process could be especially important in rocks subjected to conditions where dislocation climb is difficult, leading to pile-up of dislocations and possibly larger changes in Gibbs free energy.

The results of this study are broadly consistent with other studies which have demonstrated the importance of strain energy in affecting chemical processes during metamorphism (Wintsch and Andrews, 1989; Wintsch and Dunning, 1985; Kerrick, 1986). Although these studies did include quantitative estimates of strain energy, they did not demonstrate a precise correlation between observed chemical variation, strain magnitude and dislocation density. The present study outlines a quantitative model of strain energy contributions in naturally deformed rocks where correlation between the progress of chemical reactions and strain magnitude can be clearly demonstrated. In addition, TEM observations of amphibole indicate a direct correlation between dislocation density (and therefore strain energy) and the replacement of actinolitic hornblende by magnesio-hornblende. These petrologic and microstructural characteristics of the variably

deformed amphibolite provide a unique opportunity to outline the general importance of deformation during shear zone metamorphism.

PETROLOGIC AND MICROSTRUCTURAL CHARACTERISTICS OF AMPHIBOLITE SHEAR ZONES

Increasing deformation across the amphibolite shear zone is marked by the progressive development of a L-S tectonic fabric and grain size reduction of plagioclase and amphibole. Associated with increasing deformation across the shear zone, compositional variation of amphibole and, to a lessor extent plagioclase, decreases (Fig. 3.1). This observation indicates that increases in reaction progress during shear zone formation are possibly a result of some deformation-related process.

Details of the reaction and deformation mechanisms during shear zone deformation can be inferred from scanning and transmission electron microscope (SEM and TEM) images of amphibole and plagioclase. Back-scattered electron (BSE) images of both amphibole and plagioclase from across the strain transition show steep compositional gradients at grain boundaries (Fig. 3.2). Compositional changes along amphibole grain boundaries show that actinolitic amphibole has been replaced by magnesio-hornblende. This replacement involves a decrease in Si and Mg contents of the amphibole and concomitant increases in Al, Fe and minor amounts of Na (Fig. 3.2A). Plagioclase shows textural features similar to amphibole (Fig. 3.2B) where calcic plagioclase has been replaced along grain boundaries by plagioclase with a higher albite content. These replacement textures are interpreted to have resulted from a dissolution and precipitation processes involving transport of Si, Mg, Al, Fe, Mg and Na within intergranular regions (cf Carmichael, 1969). Based on the wide variety of grain sizes and the angular shape of grains, deformation of both plagioclase and amphibole has been interpreted as due to a cataclastic deformation mechanism (Nyman et al., 1991; Nyman et al., 1992).

Figure 3.1 Amphibole compositional plots showing decreasing range of amphibole compositions with increasing strain across the shear zone. This trend has been interpreted to indicate that reaction progress is in part, a function of strain magnitude. Amphibole formulas were calculated on the basis of 13 cations excluding Ca, Na and K.

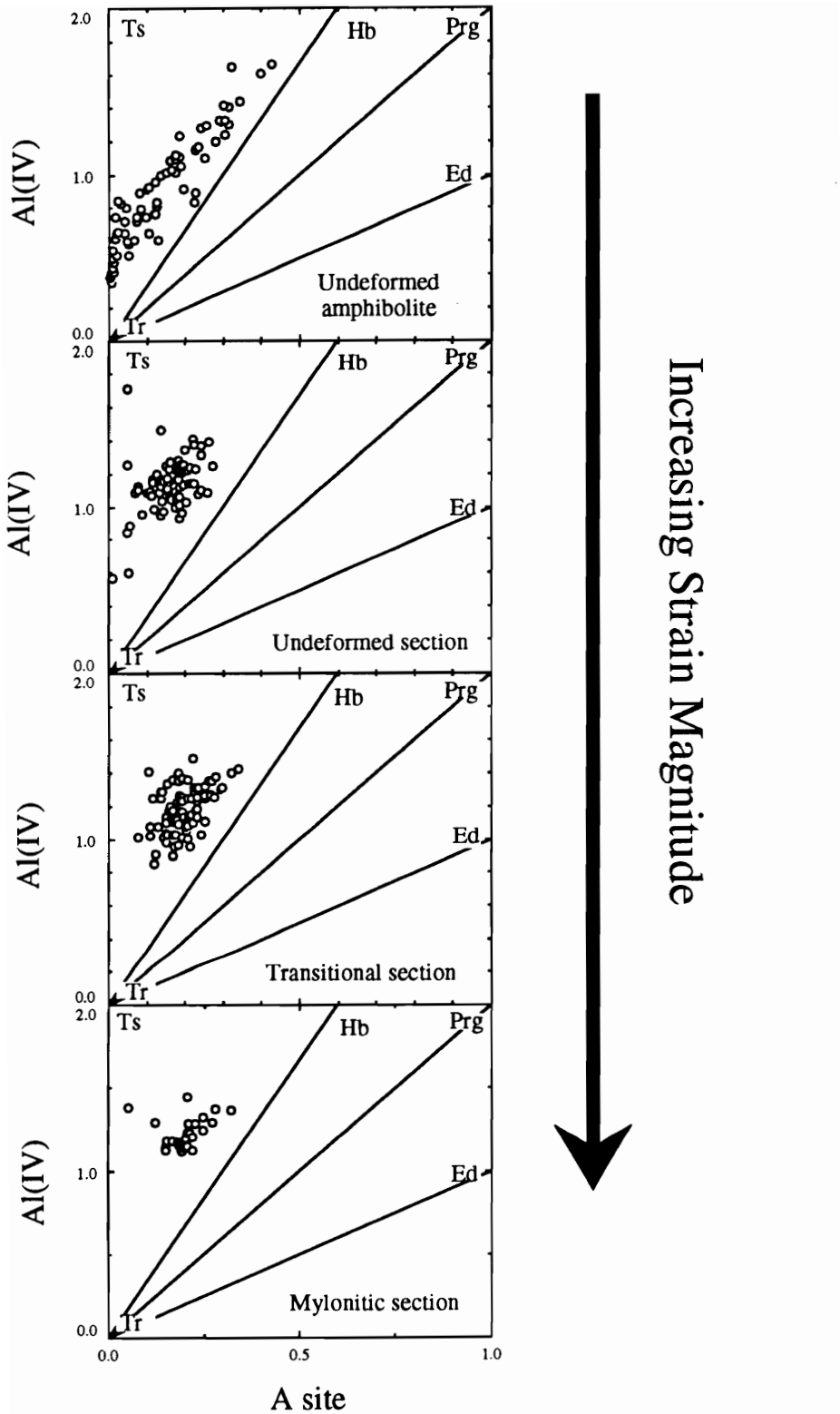
Ts
Hb
Prg
Ed
Tr
Undeformed amphibolite
Undeformed section
Transitional section
Mylonitic section
Al(IV)
A site
2.0
1.0
0.0
0.5
Increasing Strain Magnitude

Figure 3.2. Back-scattered electron images. A. 'Subgrain' microstructure around an amphibole porphyroclast within relatively undeformed amphibolite. Note that for angular 'subgrains' in the left portion of the photomicrograph, compositional variation occurs along grain boundaries. More equant 'subgrains' at the margins of the porphryoclast have more complex compositional zoning although borders of these grains are also magnesio-hornblende. B. Strongly deformed plagioclase within relatively undeformed amphibolite. Note angular shape and wide variety of grain sizes suggesting cataclastic deformation. Darker contrast at margins of grains indicate zones of higher albite content.

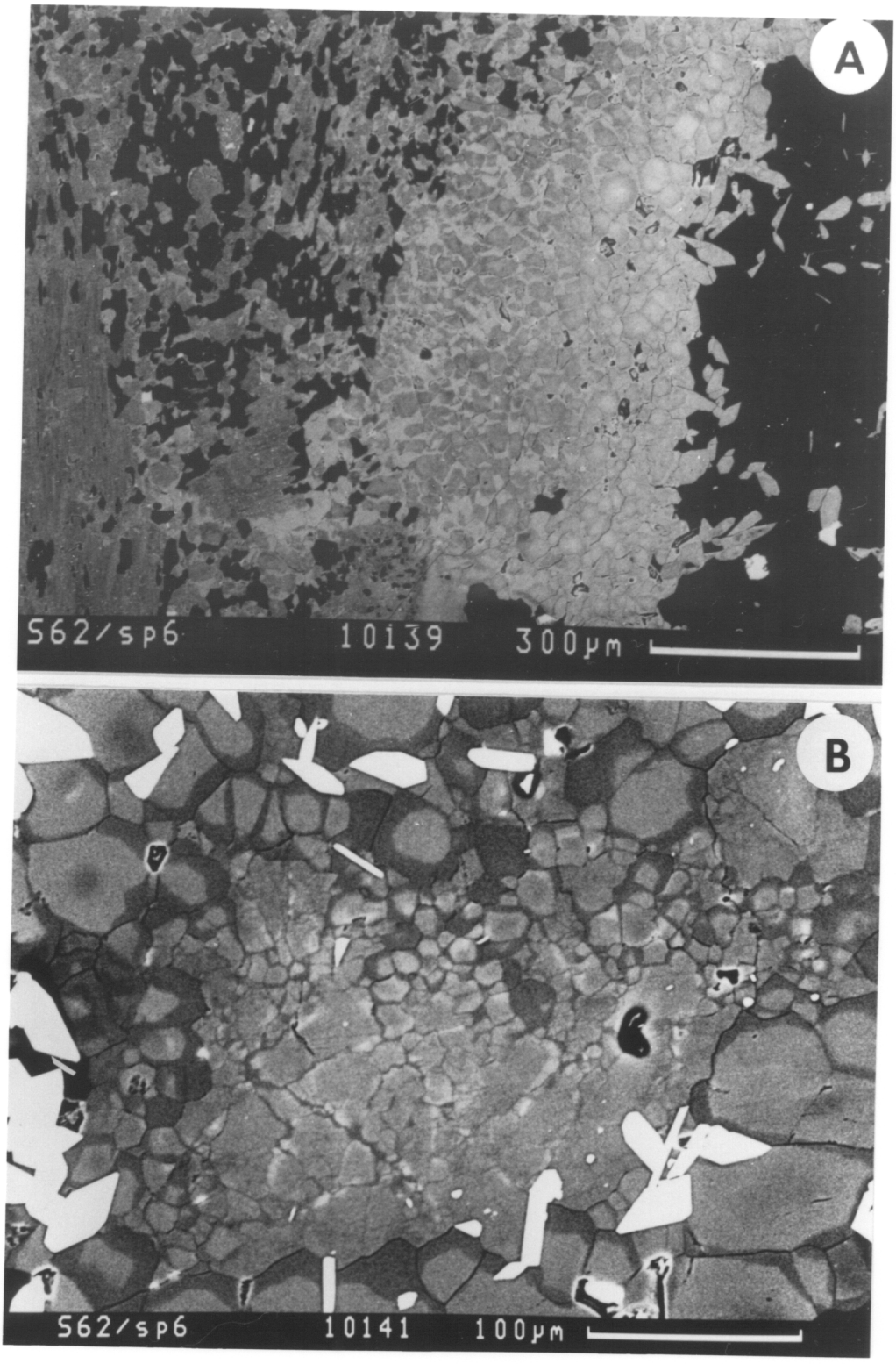
A
S62/sp6 10139 300µm
B
S62/sp6 10141 100µm

Preliminary TEM investigation of amphibole from across the strain transition revealed a wide variety of defect microstructures and densities. Defect microstructures predominantly consist of linear dislocations that are generally parallel to cleavage orientations. These dislocations resemble (100) screw dislocations reported by Cumbest et al. (1989a,b). Dislocation tangles also are common and occur mostly adjacent to microcracks. Areas away from the microcracks generally have a lower density of dislocations and may locally be totally devoid of defect microstructures. Other defect microstructures include dislocation networks, partial dislocations, dislocation loops and stacking faults.

TEM observations of boundaries of amphibole grains where actinolitic hornblende is replaced by magnesio-hornblende indicate a significant change in dislocation density. Figure 3.3 shows a TEM photomicrograph of this relationship; amphibole in the upper right section has a magnesio-hornblende composition and is nearly free of dislocations whereas the lower left of the photomicrograph shows actinolitic amphibole with a relatively high dislocation density. This relationship of relatively low dislocation density in magnesio-hornblende relative to actinolitic compositions has been observed in amphiboles throughout the strain transition.

Replacement of phases along grain boundaries suggests that reaction progress is in part a function of grain boundary development. The abrupt compositional changes along the grain boundary indicate that chemical processes occurred by a dissolution and precipitation mechanism with actinolitic hornblende and calcic plagioclase dissolution and replacement by magnesio-hornblende and more albitic plagioclase. Furthermore, the dramatic increases in density of defect microstructures across these boundaries as observed in TEM images suggest that strain energy related to the development of the microstructure may in part be a driving mechanism for this chemical process. In the following section,

Figure 3.3 Photomicrograph of transmission electron microscope image near grain boundary regions of an amphibole 'subgrain'. Note that actinolitic (Act) portion of grain has a much higher dislocation density than hornblende (Hb). Arrows point to boundary between compositional zones. Defect microstructures include curved and straight dislocations which occur in tangles.

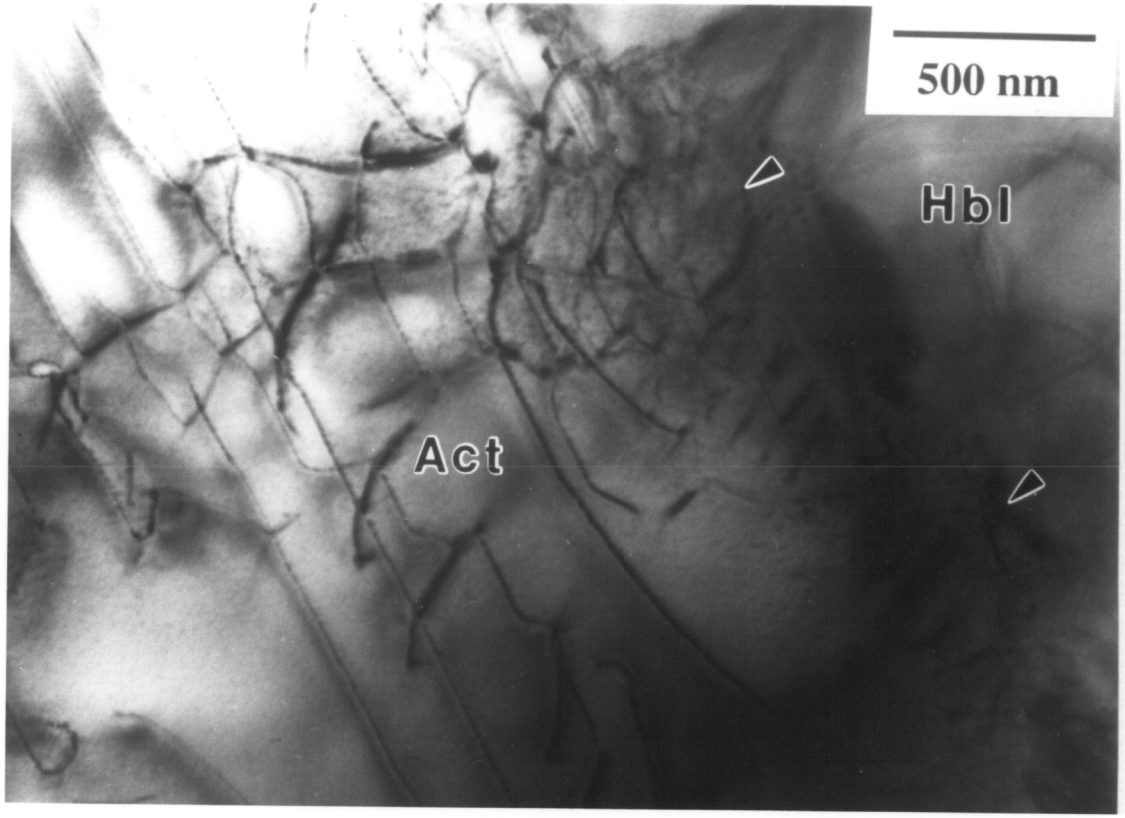
500 nm
Hbl
Act

calculations of strain energy associated with defect microstructures in amphibole and plagioclase will be presented. This data will than be evaluated with respect to the progress of reactions in the shear zone.

STRAIN ENERGY CALCULATIONS

Theory

Calculation of strain energy associated with dislocations in deformed materials involves integrating strain energy functions over the area affected by the dislocation (Hirth and Lothe, 1982). Strain energy functions are derived using: 1) the amount of displacement due to the dislocations (i.e. length of the Burgers vector | b |); 2) the stresses required to produce the displacement; 3) the extent of the strain field around the dislocation; and 4) the material properties (i.e. shear modulus). For calculations of strain energy, the deformed material is assumed to have mechanical properties consistent with standard elastic theory where strain is a linear function of stress (Hirth and Lothe, 1982). However, estimates of energy for the complex, highly distorted cores of dislocations are problematic in that standard elastic theory is inadequate in modelling the physical properties of the core region (Hirth and Lothe, 1982; van der Hoek et al., 1982). This is evident in equation (1) by the fact that as r_0 approaches 0 the first term on the right side of the equation becomes undefined. Therefore, the equation is no longer valid for calculation of strain energy and additional terms are required to account for the inelastic inner core (see below).

For a cylindrical model and screw dislocation, the energy associated with a unit length of dislocation is given by (Hirth and Lothe, 1982):

$$U_{line} = (\tau b^2/4\pi) \ln (R/r_0) + \alpha\tau b^2 \qquad (1)$$

where τ is the shear modulus, b is the Burgers vector length, R is the radius around the dislocation in which the crystal lattice is distorted, r_0 is the radius of the dislocation core, and α is a factor used to approximate the core energy . In this equation, the first term on the right side of the equation is related to the energy of the distorted part of the lattice around the dislocation (R) and the second part is associated with the core region (r_0). The total energy associated with dislocations in a unit volume is:

$$U_{total} = U_{line} \rho V \qquad (2)$$

where ρ is the dislocation density and V is the molar volume (Schott et al., 1989).

The relation between U_{total} and Gibbs free energy can be determined by:

$$G = U + PV - TS \qquad (3)$$

and taking the total derivative:

$$dG = dU + PdV + VdP - SdT - TdS. \qquad (4)$$

Changes in dV, dP and dT due to strain associated with dislocations are probably small and assumed to be 0. Entropy effects of a dislocation were estimated by Cottrell (1953) to be not larger than 10^{-6} eV per K per atom plane that the dislocation pierces. This is an extremely small value compared to internal energy values for dislocations which are calculated as approximately 10^4 eV per K per atom plane. Therefore, entropy effects of dislocations can be ignored and internal energy is assumed to be equal to Gibbs free energy.

Table 3.1 lists the parameters used to calculate strain energy for plagioclase and amphibole. Calculations using Eq. 1 require several simplifications for the values of R and r_o. The value R is taken as a measure of the distance between dislocations and is approximated by $\rho^{-1/2}/2$ whereas the radius of the nonlinear core (r_o) is assumed to be equal to | b | (Hirth and Lothe, 1982). For these calculations the value for α is taken as 0.1 which results in the most conservative estimates for strain energy associated with the core. For these calculations, all dislocations are assumed to be of the same type, i.e. screw dislocations for both amphibole and plagioclase, and interaction between dislocations is neglected.

Sources of Data for Amphibole and Plagioclase Dislocations

Burgers vector determinations for naturally deformed amphiboles have been presented by Cumbest et al. (1989a). They determined that over 90 % of all observed dislocations were screw with a Burgers vector direction of [001]. The length of the Burgers vector was not determined in this study nor are there any other reports of Burgers vector lengths for clinoamphibole. Therefore, in the present study a value of 0.50 nm (5 Å) was used which is approximately equal to the shortest unit cell dimension and therefore the smallest unit cell translation distance for clinoamphibole. In addition to determination of Burgers vectors, Cumbest et al. (1989a) reported dislocation densities for amphibole porphyroclasts of 5×10^8 cm^{-2}. Metamorphic conditions during deformation were reported as 520-540 °C and 6.5 kb (Cumbest et al., 1989b). In a TEM study of deformed glaucophane, Reynard et al. (1989) have reported dislocation densities as high as 10^{13} cm^{-2}. Conditions during deformation were reported as 15-18 kb and 550-600 °C.

Determination of slip systems and Burgers vector lengths for feldspar have been reported by Olsen and Kohlstedt (1984) and White (1975) (see also reviews by Tullis,

TABLE 3.1 STRAIN ENERGY AND ACTIVITY CALCULATIONS

Dislocation density (cm^{-2})	Amphibole Line Energy (J/cm^3)	Amphibole Total Energy (J/mole)	Activity	Plagioclase Line Energy (J/cm^3)	Plagioclase Total Energy (J/mole)	Activity
10^6	2.08×10^{-10}	0.057	1.000	3.65×10^{-10}	0.0367	1.000
10^7	1.85×10^{-10}	0.506	1.000	3.24×10^{-10}	0.326	1.000
10^8	1.62×10^{-10}	4.435	1.000	2.82×10^{-10}	2.844	1.000
10^9	1.40×10^{-10}	38.094	1.005	2.41×10^{-10}	24.251	1.004
10^{10}	1.17×10^{-10}	318.398	1.051	1.99×10^{-10}	200.602	1.032
10^{11}	9.37×10^{-11}	2558.559	1.489	1.57×10^{-10}	1586.911	1.280
10^{12}	7.08×10^{-11}	19331.390	20.246	1.16×10^{-10}	11678.003	6.154

Physical parameters:

AMPHIBOLE	PLAGIOCLASE
$\tau = 1.0 \times 10^5$ J/cm^3	$\tau = 9.0 \times 10^4$ J/cm^3
$\lvert b \rvert = 5.0$ Å	$\lvert b \rvert = 7.1$ Å
V = 272.92 cm^3/mole	V = 100.8 cm^3/mole

1983 and Gandais and Willaime, 1984). For plagioclase (An_{25}-An_{48}) deformed at granulite facies conditions, Olsen and Kohlstedt (1984) determined that dislocations were predominantly screw dislocations parallel to [001] with a Burgers vector length of 7.1 Å. This length is consistent with the c unit cell dimension for plagioclase of approximately 7.0 Å. They also reported large variations in dislocation density (4×10^7 - 7×10^8 cm^{-2}) with evidence of dislocation climb and cross-slip indicated by the occurrence of subgrain boundaries composed of well organized dislocation networks.

For oligoclase deformed during amphibolite grade retrogressive metamorphism, White (1975) determined that the predominant slip system was in the [100] direction along {010} planes with a predominant screw character. White (1975) observed little evidence of recovery with highly variable dislocation densities of 10^7 - 10^9 cm^{-2} in relatively unstrained areas and 10^{10} - 10^{12} cm^{-2} in highly strained areas. White postulated that observed chemical variation in feldspar may have been partially driven by enhanced diffusion associated with increases in dislocation energy. For the present study, Burgers vector data provided by Olsen and Kohlstedt (1984) have been used for calculations of plagioclase strain energy assuming that dislocations are predominantly screw.

Results of Calculations

Results of strain energy calculations for plagioclase and amphibole are shown in Figure 3.4. For dislocation densities of 10^6 to 10^{10} cm^{-2}, energy values range up to 0.300 KJ/mole for amphibole and 0.200 KJ/mole for plagioclase. At higher values of dislocation density (10^{11} to 10^{12} cm^{-2}), energy values reach 20 KJ/mole for amphibole and 12 KJ/mole for plagioclase. The magnitudes of the strain energy values are somewhat larger than values calculated for quartz (Wintsch and Dunning, 1985; Blum et al., 1990), rutile (Casey et al., 1988) and strained calcite (Schott et al., 1989). This variation is in part due

Figure 3.4. Plot of strain energy as a function of dislocation density for amphibole and plagioclase.

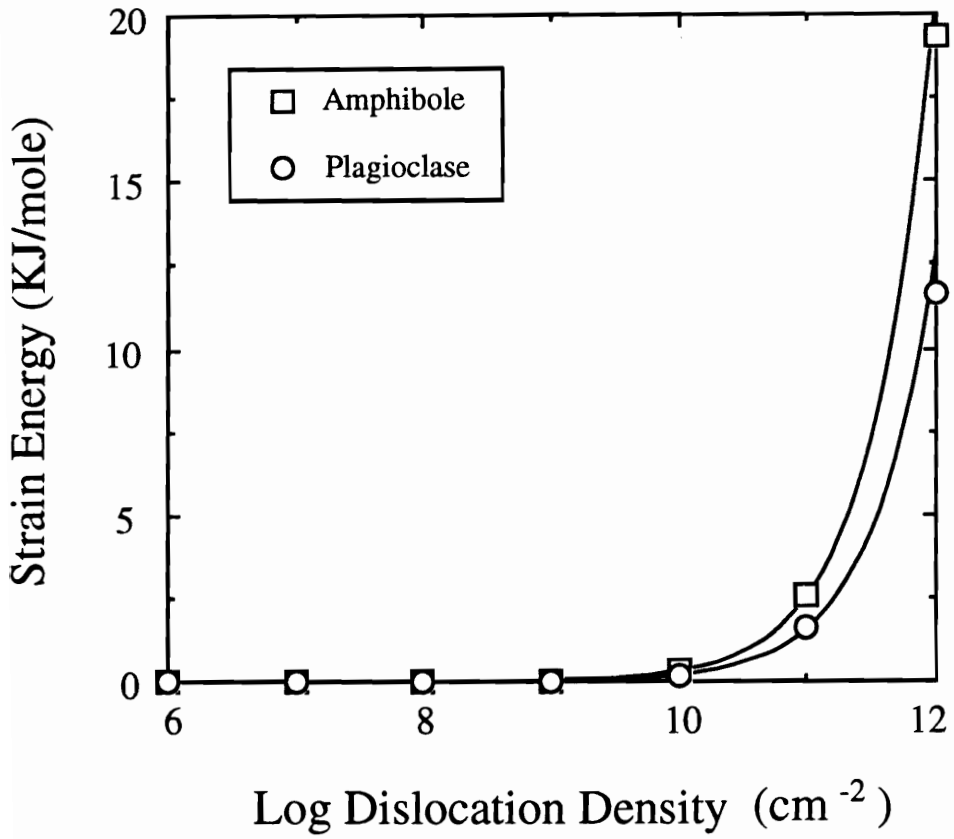
Strain Energy (KJ/mole)
20
15
10
5
0
Amphibole
Plagioclase
6
8
10
12
Log Dislocation Density (cm -2)

to the larger molar volumes of plagioclase and amphibole relative to the other phases.

In order to assess the validity of the calculated values, the effects of order-of-magnitude changes for the values used in Eq. 1 must be considered. Assuming that the values for shear moduli are appropriate, the factors in Eq. 1 which can vary are | b |, R, (which is a function of the dislocation density) and r_0 (which is assumed to be equal to the length of the Burgers vector). Due to the logarithmic dependence of R and r_0 in Eq. 1, the energy calculations are relatively insensitive to variations in R and r_0. As stated previously, values of | b | for plagioclase were taken from TEM investigation of naturally deformed plagioclase whereas for amphibole | b | is taken as equal to the smallest unit cell dimension. The choice of | b | equal to c for amphibole is necessarily a minimum, because for straight, linear dislocations (not partials), the smallest possible displacement of the crystal lattice must involve translation which is equal to some integral multiple of a unit cell dimension. The value of | b | for plagioclase is also close to the c unit cell dimension which also indicates that it is a minimum. Therefore, the choices of | b | for plagioclase and amphibole are necessarily minimums and should give the most conservative estimates of energy.

The other variable which must be considered is the dislocation density. Dislocation densities in deformed minerals range from 10^6 cm^{-2}, which corresponds to relatively defect-free material, to as high as 10^{12} cm^{-2} in which it is difficult to measure individual dislocation segments and dislocation tangles are abundant. However, these values may actually represent minimum densities because dynamic or static recovery by dislocation climb or cross-slip may remove evidence of even higher dislocation densities (Brodie and Rutter, 1985; Wintsch and Dunning, 1985). Rigorous evaluation of dislocation densities for amphibole and plagioclase for the variably deformed amphibolite have yet to be completed . TEM investigation of relatively undeformed and mylonitic amphibole form the Medicine Bow amphibolites indicates that dislocation densities are highly variable with

large dislocation densities adjacent to microcracks and boundaries between actinolitic hornblende and magnesio-hornblende overgrowths (Fig. 3.3). From TEM images of amphibole, estimates in regions of high dislocation density range from 10^7 to 10^9 cm^{-2}. These values are based on visual comparison with TEM images reported by Cumbest et al. (1989a,b) for clinoamphibole and Reyard et al. (1989) for glaucophane.

Details of defect structures and densities in plagioclase from the shear zone are not known at this time. However, petrographic evidence suggests that plagioclase has been deformed by a deformation mechanism similar to that in amphibole and may have a similar distribution of defect microstructures. Plagioclase throughout the shear zone has undulatory extinction and bent albite twins which indicating that the crystal lattice has been distorted by intracrystalline strain associated with either dislocations or microcracks (Tullis and Yund, 1977). In addition, in zones where plagioclase grain size is greatly reduced, BSE images show that plagioclase has textures very similar to amphibole, with an angular morphology and wide variety of grain sizes. The similarity between plagioclase and amphibole textures suggests that the two phases probably deformed by the same cataclastic deformation mechanism. Therefore, compositional variation along plagioclase grain boundaries may show distribution of defect densities similar to that observed in TEM images of amphibole. The similarity of observed plagioclase optical microstructures to those reported by White (1975) for plagioclase deformed at a similar metamorphic grade provides evidence to support this assertion. White reported that defect microstructures in the plagioclase have an inhomogeneous distribution, with areas of high dislocation densities separated by zones of nearly defect-free plagioclase. He also reported a close association between dislocation density and chemical variation of plagioclase. The reported compositional range and textural setting of the variation in plagioclase composition is

similar to that which is observed along plagioclase grain boundaries in shear zone samples of the present study.

MODEL FOR STRAIN-ASSISTED REACTIONS IN AMPHIBOLITE SHEAR ZONES

Strain energy associated with dislocations can affect chemical processes in two ways: 1) by increasing the Gibbs free energy of deformed phases, and 2) by enhancing kinetics through changing the dissolution or diffusion rates of the deformed material. The Gibbs Method (Spear et al., 1982; 1991) can be used to calculate the effects of increasing strain energy on the activity of plagioclase and of amphibole and to correlate increasing strain energy with changes in reaction progress.

Changes in Activity Associated with Strain Energy

Increases in Gibbs free energy of a mineral as a result of increased strain energy can be expressed as a change in the activity of the deformed mineral (Casey et al., 1988; Wintsch and Dunning, 1985). At a constant pressure, the molar Gibbs free energy or chemical potential of a strained material is:

$$G_{strained} = G_{unstrained} + RT \ln a \qquad (5)$$

and the activity of the strained material is :

$$a = \exp(G_{strained} - G_{unstrained})/RT \qquad (6)$$

where T is temperature and R is the gas constant. Values for $(G_{strained} - G_{unstrained})$ are simply the calculated strain energy values for plagioclase and amphibole in Table 3.1 and

Figure 3.3. The resulting changes in activity for plagioclase and amphibole from the addition of strain energy are shown in Table 3.1. The changes in activity show a large increase at high dislocation densities consistent with the logarithmic form of the strain energy function (Eq. 1) and expression for activity (Eq. 5 & 6).

Effects of Strain Energy on the Progress of Reactions

Increase in reaction progress within the amphibolite shear zone due to strain energy was evaluated using the Gibbs Method (Spear et al, 1982; Spear, 1988; 1989). Model parameters and one set of linearly independent reactions (conditions of heterogeneous equilibria) used in this model are listed in Table 3.2. The Gibbs Method involves solving a set of linearly independent equations where changes in intensive variables (P,T and μ) are calculated using changes in phase composition. The set of linearly independent equations includes a Gibbs-Duhem equation for each phase in the system and a set of heterogeneous equilibria such that the variance of the system of equations (number of unknowns - number of equations) is equal to the thermodynamic variance calculated from the phase rule. The heterogeneous equilibria include both exchange and net transfer reactions where the number of equilibria is equal to the number of system components minus the number of phase components (Spear et al., 1982; Spear 1988, 1989). With mass balance constraints and assuming a closed system, changes in volume percents of the phases can be evaluated and therefore the progress of reactions can be monitored (Spear, 1988).

The main interest in this model is in evaluating the effects due to strain energy of increasing activity of plagioclase and amphibole on the resulting phase compositions and volume percents. The procedure used to evaluate the effect of changing plagioclase and

TABLE 3.2 GIBBS METHOD PARAMETERS

System Components (NC):

Na_2O-CaO-MgO-Al_2O_3-SiO_2-H_2O

(Note that FeO = 1- MgO)

Phase components (NP):

Tremolite (Tr)
Fe-Tremolite (Fe-Tr)
Mg-Hornblende (Mg-Hb)
Fe-Hornblende (Fe-Hb)
Albite (Ab)
Anorthite (An)
Quartz (Qtz)
Water

Number of linearly independent reaction is PC-NC = 2

Linearly independent reactions:

$$0.66\ \text{Fe-Tr} + 1.0\ \text{Mg-Hb} \leftrightarrow 1.0\ \text{Fe-Hb} + 0.66\ \text{Tr}$$

$$0.44\ \text{Tr} + 0.20\ \text{Ab} + 0.10\ \text{An} + 0.20\ \text{Qtz} + 0.50\ H_2O \leftrightarrow 0.667\ \text{Mg-Hb} + 0.273\ \text{Fe-Tr}$$

amphibole activity on reaction progress is as follows. Starting conditions were chosen as 500 °C and 3500 bars with phase modes and compositions approximated using amphibole and plagioclase data from relatively undeformed amphibolite (Table 3.2). These starting conditions assume that the relatively undeformed rock consists of two amphiboles (actinolite and hornblende), plagioclase (An_{50}), quartz and pure water. These calculations also are conducted where variation in activity due to strain energy is evaluated by decreasing the anorthite component of plagioclase and tremolite component of actinolite. These compositional trends are consistent with observed variation in plagioclase and amphibole with increasing strain.

Using the Gibbs Method computer program developed by Spear and others (1989; 1991), changes in composition and volume proportions (modes) of plagioclase and hornblende were calculated for temperature increments of 5 °C. Results of this procedure using 'unstrained' plagioclase and amphibole are shown by the line denoted with large open circles in Figure 3.5 and 3.6. As expected, there is a decrease in XAn and volume proportion of plagioclase with an increase in volume proportion of hornblende. The composition of hornblende stays relatively constant due to the fact that the starting composition was chosen as Fe-rich hornblende and therefore does not undergo much change in composition in the calculations.

To evaluate the effects of changes in the activity of plagioclase and amphibole due to strain energy, an ideal model was used where the percent change in the activity corresponds directly to an equal percent change in composition. To monitor the changes in volume proportion and phase composition with the increasing activities associated with increased strain energy, the albite component of plagioclase was increased (or anorthite component decreased) for each temperature increment by a factor of 0.4, 3 and 28% which corresponds to dislocation densities of plagioclase of 10^9, 10^{10} and 10^{11}, respectively

(Table 3.2). The Gibbs Method was than used to monitor the changes in volume proportions and compositions that would occur with a change to the new 'strained' plagioclase composition. A similar procedure was used for amphibole by changing the composition of tremolite (decreasing Mg content) by 3% which approximately corresponds to a dislocation density of 10^9-10^{10} cm^{-2} in amphibole.

Results of this model are shown in Figure 3.5 and 3.6. With the addition of strain energy associated with dislocation densities for plagioclase of 10^9 and 10^{10} cm^{-2} the resulting changes from normal reaction progress in volume proportions and phase composition are very small. As discussed above, the lack of variation of hornblende compositions is due to the choice of starting composition. However, at strain energy associated with a dislocation density of 10^{11} cm^{-2} there is a two-fold increase in the change in volume proportions of hornblende and plagioclase as well as anorthite component in plagioclase. This variation is especially pronounced at the first increment of temperature. Similar changes are observed when the activity of tremolite is changed. However, large variations in modal and chemical values occur with relatively small changes of tremolite activity due to strain energy (Fig. 3.5). In Figure 3.5 tremolite activity was changed by only 3%, corresponding to a dislocation density of 10^9-10^{10} cm^{-2}, resulting in approximately a doubling of volume changes and XAn with only minor changes in hornblende composition. The reason for the discrepancy between changing tremolite or plagioclase activities is probably due to the stoichiometry of the net transfer reaction (Table 3.2) where the coefficient for tremolite is larger (0.40) than the coefficient for plagioclase (0.10).

Figure 3.5 A & B. Result of Gibbs Method modelling for amphibolite shear zones. A. Amphibole and plagioclase compositional variation as a function of temperature and strain energy of plagioclase. Variation in strain energy is expressed as fractions of anorthite activity. B. Volume percent changes of hornblende and plagioclase using same temperature and strain energy values as A.

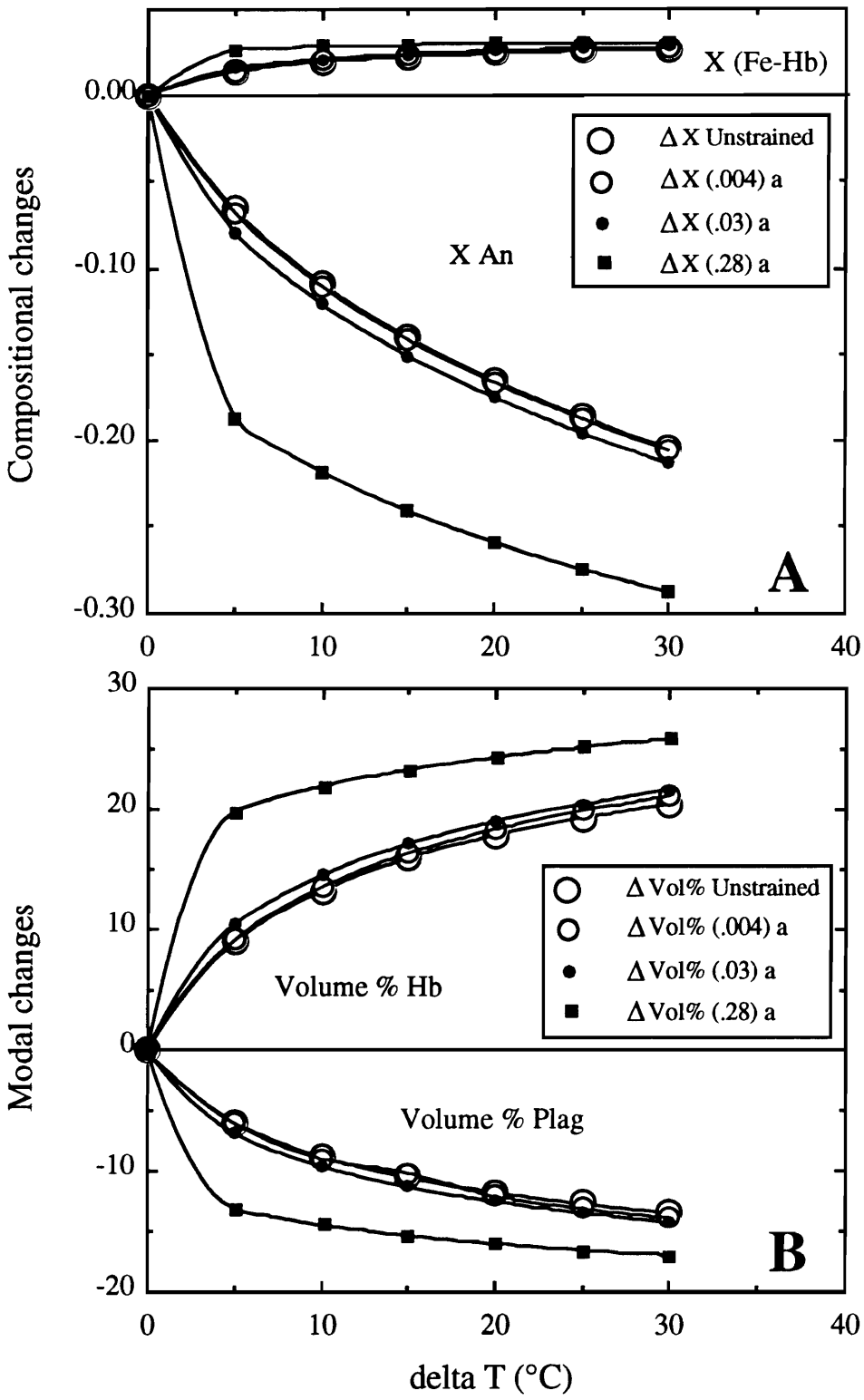
X (Fe-Hb)
0.00
ΔX Unstrained
ΔX (.004) a
ΔX (.03) a
ΔX (.28) a
X An
-0.10
-0.20
-0.30
Compositional changes
A
0
10
20
30
40
30
20
10
0
ΔVol% Unstrained
ΔVol% (.004) a
ΔVol% (.03) a
ΔVol% (.28) a
Volume % Hb
Volume % Plag
-10
-20
Modal changes
B
delta T (°C)

Figure 3.6 A & B. Result of Gibbs Method modelling for amphibolite shear zones. A. Amphibole and plagioclase compositional changes for variation in strain energy, and therefore activity, of tremolite. B. Variation in volume percent for same conditions used in A.

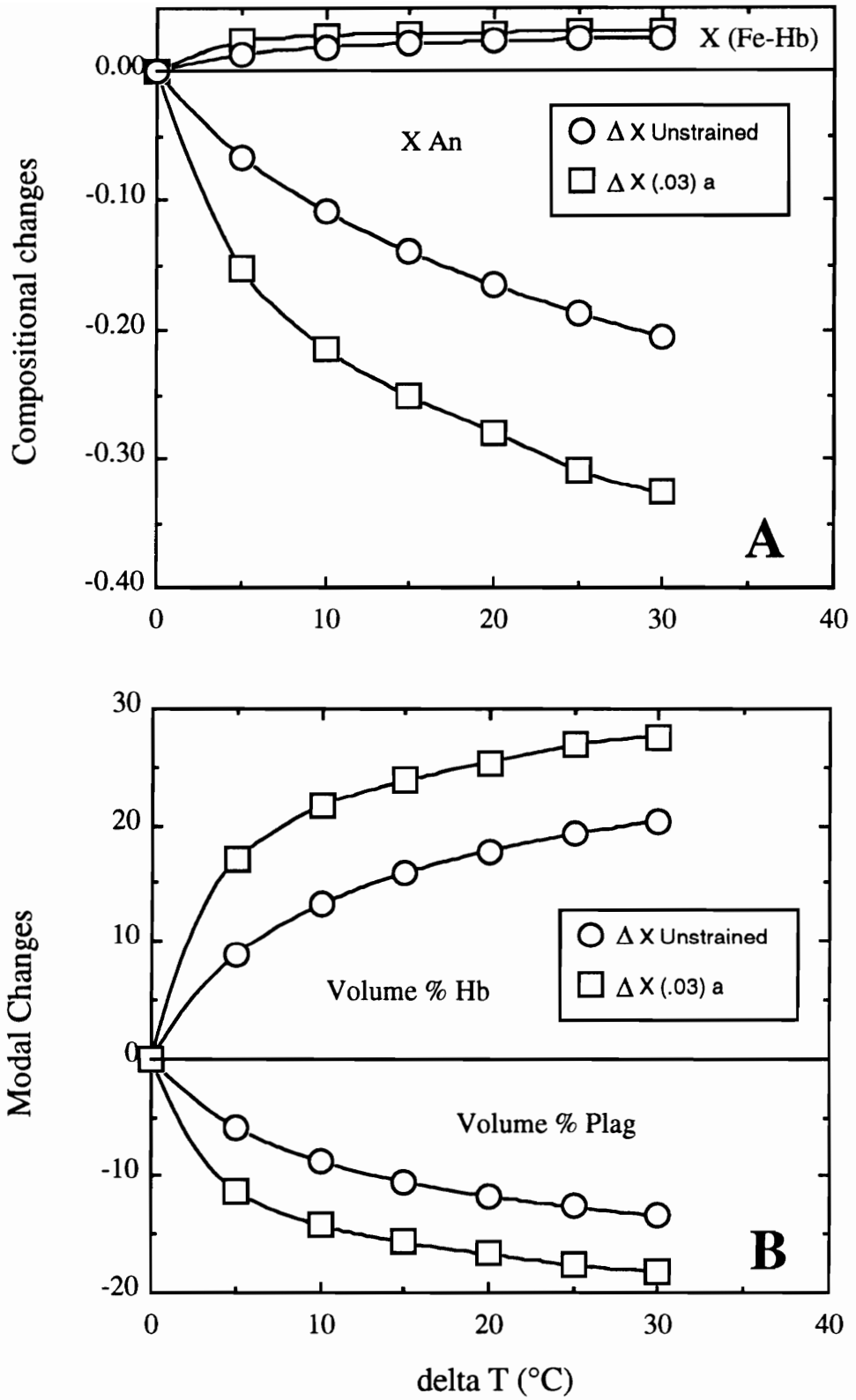
X (Fe-Hb)
0.00
X An
Δ X Unstrained
Δ X (.03) a
-0.10
-0.20
-0.30
-0.40
Compositional changes
A
0
10
20
30
40
30
20
10
0
Volume % Hb
Volume % Plag
-10
-20
Modal Changes
B
delta T (°C)

DISCUSSION

Results of Modelling

The model results presented in figures 3.5 and 3.6 emphasize the potential for strain energy to increase the progress of metamorphic reactions within the shear zone by changing the activities, and therefore stabilities, of the anorthite component of plagioclase or the tremolite component of amphibole. As shown in figures 3.5 and 3.6, the resulting modal and compositional changes with the addition of strain energy are the largest in the first increments of increasing temperature.

To test the validity of these results with respect to actual compositional and modal changes across the strain transition, the following two cases have been considered. Precise estimates of modal variation across the shear zone are hindered by the presence of different amphibole and plagioclase compositions from grain to grain which are difficult to distinguish. However, image analysis of bulk amphibole and plagioclase proportions across a sample which contains a full strain transition over 7 cm indicates that there is approximately a 20% increase in amphibole from undeformed to mylonitic amphibolite. This modal variation is observed in other samples although there are examples where modal behavior is less systematic or shows no variation with respect to distance across the strain transition. With reference to figure 3.5 and 3.6, in the unstrained model this variation could have occurred over a 25° temperature interval whereas at dislocation densities of 10^{11} cm^{-2}, the same change would occur after only a 5° change.

As presented in chapter 1, relict igneous plagioclase has a composition of approximately XAn = 0.50 whereas plagioclase along grain boundaries and in areas where grains show evidence for grain size reduction by cataclasis has anorthite mole fractions as low as 0.30. For the shear zone system, this compositional change for unstrained plagioclase would require an increase in temperature of approximately 30 °C whereas at a

dislocation density of 10^{11} cm^{-2} for plagioclase, an equivalent compositional change would require only 5-7 °C of heating (Figure 3.5A). These two examples indicate that very little additional thermal energy is required to increase reaction progress within the more deformed sections of the shear zone considering the contribution from strain energy.

General Application to Metamorphic Processes

The progress of metamorphic reactions is a complex interplay between equilibrium and mechanical processes controlled by kinetic rates, and it is frequently difficult to pinpoint the exact source(s) of energy that control the progress of metamorphism. Energy sources during metamorphism include heat, surface energy, chemical energy as well as defect energy and, in actively deforming rocks, it is likely that all of these processes may contribute to progress of metamorphic reactions (Wintsch, 1985). However, for these amphibolite shear zones several of these energy sources can be eliminated as candidates for providing the energy to enhance reaction progress during deformation.

Heat

Due to the small size of the amphibolite shear zones it is unlikely that there were any significant thermal gradients between relatively undeformed and highly deformed rocks and it is therefore probable that rocks throughout the shear zone were subjected to the same P-T conditions and increases in temperature (or pressure) could not have been a driving force for increased reaction progress in the shear zone. This is supported by the fact that amphibole in both the relatively undeformed and mylonitic amphibolite have similar, high-Al compositions suggesting that temperature (and pressure ?) were uniform across the shear zone.

It has been proposed that localized deformation can produce shear heating and contribute to the thermal evolution of thrust zones (e.g., Scholz et al., 1979). However,

for small scale shear zones Brodie (1981) has shown that shear heating at reasonable strain rates would contribute approximately 1 °C of temperature rise during deformation. For these shear zones this temperature increase would not have been sufficient to increase reaction progress within the mylonite section of the shear zone.

Surface Energy

Estimates of surface energy in minerals range from 10^{-5} to 10^{-7} J/cm^2 although these values would be even smaller in the presence of a fluid (Wintsch, 1985). However, even small values of surface energy may be important in chemical processes such as dissolution and nucleation along phase boundaries (Vernon, 1975). In addition, with decreasing grain size across the shear zone the ratio of surface area to volume would increase and possibly increase the contribution of surface energy. Therefore, it cannot be ruled out that surface energy may have played a role in dissolution/precipitation mechanisms although the small magnitudes of surface energy make it unlikely that contributions were very significant.

Fluid-related processes

In several articles Ferry (1980, 1986, 1988a, 1988b) and co-workers (Ferry and Symmes, 1991) have proposed that increases in regional metamorphic grade may be driven by fluid infiltration. In addition, geochemical studies of shear zones have shown that increases in permeability due to grain size reduction in shear zones enhance fluid flow which can drive shear zone metamorphism. Typically this results in retrogression of the country rock within the shear zone (e.g., Beach, 1976; Sinha et al., 1989).

For the amphibolite shear zones of this study, preliminary calculations show that with decreasing grain size across the shear zone, diffusion coefficients and values for fluid

flux increase by orders of magnitude. Using flux equations from Walther and Wood (1984) and measured grain size variation across the amphibolite shear zones it was found that for an order of magnitude decrease in grain size there is a two order of magnitude increase in flux values. Application of the same grain size data to Brady's (1983) equations for effective diffusivity produced results of similar magnitude. It is therefore possible that reaction rates within highly deformed amphibolite, and resulting increases in reaction progress, could have been due to enhancement of diffusion or fluid influx as a result of grain size reduction. In addition, influx of hot fluids along the shear zone could potentially have contributed to the enhanced reaction progress within the mylonitic amphibolite by either producing an actual increase in temperature or contributing to reaction enthalpy without raising the temperature.

Despite the obvious potential for fluid-related processes to control the progress of reactions there are several indications that shear zone evolution did not involve large amounts of fluid infiltration. This evidence includes: 1) the lack of even centimeter scale metasomatism across the shear zone as indicated by mass balance and bulk chemistry (see chapter 2); and 2) the lack of retrogression within highly deformed rocks. However, textural and compositional relationships do indicate that transport of several cations must occur at least on the grain boundary scale, presumably in the presence of an intergranular fluid (Brady, 1983). In addition, the lack of bulk chemical variation is not *a priori* evidence for lack of fluid infiltration in that if infiltrating fluid was in equilibrium with the rocks there may be no metasomatic affects. Infiltration and/or intergranular diffusion could have been enhanced due to grain size reduction during deformation, resulting in an increase in reaction progress within the highly strain rocks. Therefore, enhanced fluid infiltration or diffusion in response to grain size reduction cannot be ruled out as an important shear zone process.

SUMMARY AND CONCLUSIONS

The results of these calculations show that the observed increase in reaction progress within the amphibolite shear zones may involve, but does not require, additional thermal energy. The sole driving force for reaction could be strain energy due to dislocations. It has been shown that observed modal and compositional changes within the shear zone which ordinarily require an approximately 30 °C temperature increase can be modelled to occur with only a 5 °C change when strain energy associated with dislocations is considered. The possibility that strain energy associated with dislocations contributed to the progress of reactions with increasing deformation across the shear zone is supported by TEM observations of actinolitic hornblende having high dislocation densities whereas magnesio-hornblende is relatively defect free. This microstructure is interpreted to indicate that magnesio-hornblende replaced actinolite which had a high dislocation density and was therefore relatively unstable.

These model results combined with the well constrained microstructural and petrologic framework provide a basis to support the contention that strain energy can assist chemical processes during metamorphism. However, due to the complexity of metamorphic processes it is difficult to state definitively that strain energy was the **only** driving force that produced increased reaction progress within the shear zone. Increased reaction rates due to increases in fluid infiltration and/or intergranular diffusion rates during grain size reduction may have also played a significant role in the evolution of the shear zone.

The implication of the results of this study is that in rocks which are undergoing syndeformational reactions, the extent of reaction may be affected by the amount of strain. Therefore, in reaction progress studies (e.g., Ferry, 1986) the amount of deformation, the exact deformation mechanism and variation in grain size should all be considered in order

to assess the role of mechanical processes during metamorphism. The role of strain energy may be especially important at conditions during metamorphism where even small changes in the stability of a single phase may cause reactions to occur (Wintsch and Andrews, 1987). During inhomogeneous nucleation, strain energy may also be important in overcoming activation energy barriers, a phenomenon which is usually ascribed to thermal overstepping (Ridley, 1985). The general conclusion of this study is that in order to apply petrologic, geochemical and isotopic data to understanding geochemical and tectonic processes, microstructural information on the magnitude of strain and the type of deformation mechanism should be evaluated, quantitatively if possible.

CHAPTER 4: CATACLASTIC DEFORMATION MECHANISM FOR THE DEVELOPMENT OF CORE-MANTLE STRUCTURES IN AMPHIBOLE

ABSTRACT

Core-mantle structures in mineral grains have typically been interpreted as forming during crystal plastic deformation. Optical, scanning electron and transmission electron microscope investigation of what appear to be core-mantle structures in amphibole from the Cheyenne belt, southeastern Wyoming, indicate that subgrain-like structures formed as a result of cataclastic rather than crystal plastic deformation. Optical and SEM evidence to support a cataclastic origin include (1) the angular shape of 'subgrains' with boundaries commonly parallel to (110) cleavage, (2) the wide variety of 'subgrain' sizes, (3) the compositional zonation of the amphibole 'subgrains' with actinolitic hornblende interiors overgrown by magnesio-hornblende, and (4) the observation that some of the undulatory extinction in porphyroclast cores is due to slip along cleavage planes. Whether dislocations observed in the amphibole grains were formed prior to cataclastic deformation (work hardening) or formed in response to crack propagation is unknown. The implication of these observations is that core-mantle structures in other minerals may, at least in some cases, have also formed during cataclastic deformation rather than during recovery and/or recrystallization. Therefore, optical identification of core-mantle structures is not a priori evidence for a crystal plastic deformation mechanism.

INTRODUCTION

Optically, core-mantle structures consist of a core with intragranular strain features such as undulatory extinction surrounded by a mantle of subgrains and new grains. On the basis of transmission electron microscope (TEM) observations, core-mantle structures in quartz were first demonstrated to be associated with crystal plastic deformation by White

(1976) who proposed that recovery and resultant rotation were important processes in subgrain formation and recrystallization of new grains. Yund and Tullis (1991) have referred to this mechanism as climb-accommodated dislocation creep. This process operates at conditions where dislocation climb is relatively easy. Similar optical microstructures have been taken as evidence for crystal plasticity in other minerals. Core-mantle structures have been reported for feldspar (White, 1975), pyroxene (Mercier, 1985), olivine (Ave Lallement and Carter, 1970) and amphibole (Cumbest et al., 1989a,b). However, as pointed out by Brodie and Rutter (1985) minerals such as amphibole are relatively resistant to crystal plastic deformation, even at high metamorphic grades. Can the presence of core-mantle like structures in such minerals therefore be taken as evidence for crystal plastic deformation ?

Amphibole porphyroclasts from variably deformed amphibolite in the Cheyenne belt, southeast Wyoming display core-mantle structures which, on the basis of optical characteristics, were originally interpreted as forming as a result of crystal plastic deformation (Nyman et al., 1990). However, detailed scanning electron microscopy (SEM) of these porphyroclasts indicates that the mantling subgrains are in fact angular actinolitic hornblende fragments which have been overgrown by magnesio-hornblende. We interpret the angular grains, which will be referred to as 'subgrains' in this paper, as being formed during cataclastic deformation and subsequently overgrown by magnesio-hornblende. Therefore, as previously demonstrated for feldspar by Tullis and Yund (1977, 1987) the presence of core-mantle or subgrain structures, as well as optical scale undulatory extinction, cannot be taken as unequivocal evidence for crystal plastic deformation.

GEOLOGIC FRAMEWORK

The samples for this study were collected from the Cheyenne belt, Medicine Bow Mountains, southeast Wyoming. The Cheyenne belt is a major tectonic feature which separates Wyoming province Archean rocks to the northwest and Proterozoic Colorado province rocks to the southeast. In the Medicine Bow Mountains the Cheyenne belt consists of a variety of lithotectonic blocks separated by major shear zones (Duebendorfer and Houston, 1987). Metamorphic conditions during shear zone formation have been estimated at approximately 500 °C and 3.5 kbar (Duebendorfer, 1988; Nyman et al.,1990).

Amphibolite boudins in the Medicine Bow Mountains commonly display well-developed strain gradients as indicated by the progressive rotation of amphibole + plagioclase aggregates into parallelism with shear zone boundaries. The least deformed amphibolite has an igneous texture with a poorly defined linear fabric. Mylonitic amphibolites have a strong linear and planar tectonic fabric. Microstructures from two amphibolite samples are reported in this paper. These samples include mylonitic amphibolite collected about 5 cm within a 1 m wide shear zone and a relatively undeformed amphibolite from 8 cm outside the same shear zone.

OPTICAL PETROGRAPHY

Relatively undeformed amphibolite from near the margins of the shear zone has a relict igneous texture with no planar fabric and a weak linear alignment of amphibole porphyroclasts. Plagioclase is present as 1-3 mm laths with undulatory extinction and bent albite twins. In samples closer to the shear zone boundary, relict plagioclase phenocrysts have undergone grain size reduction producing small (20-100 μm) subequant grains. Throughout the shear zone, plagioclase grains have anorthitic cores, with domains of higher albite content along grain boundaries (Nyman et al., 1990).

Amphibole porphyroclasts from relatively undeformed amphibolite display an apparent core-mantle structure with lath-shaped cores and a mantle of 'subgrains' (Fig. 4.1A). Amphibole porphyroclast cores have wavy and patchy extinction and frequent twins (possibly [100]). The mantling 'subgrains' are texturally gradational with the porphyroclast cores and show a progression from angular, subequant grains adjacent to the core to equant grains at the margins of the porphyroclasts (Fig. 4.2B). Some angular 'subgrains' that are adjacent to the core are lath shaped and have grain boundaries that are parallel to (110) cleavage planes (see arrows in Fig. 4.1B).

Amphibole porphyroclasts, with textural and compositional variations similar to those found in the relatively undeformed sample, are also present in the mylonitic sample. Cores of the porphyroclasts have patchy extinction and are mantled by lath-shaped grains (Fig. 4.1C). Figure 4.1D shows that extinction variation in the porphyroclast core follows sharp, angular boundaries, some of which outline the (110) cleavage planes.

ANALYTICAL METHODS

Scanning electron microscopy in back-scattered electron mode using a Camscan Series II microscope was employed to investigate the relation between the mantling 'subgrains' and the porphyroclast cores. Textural and compositional variation observed in SEM were confirmed by analysis of false-color-enhanced X-ray images collected on a Cameca SX-50 electron microprobe. TEM of the amphibole porphyroclasts from both undeformed and deformed samples was conducted with a Philips 420ST microscope operating at 120 Kev. Details of TEM procedures are given by Veblen and Bish (1988).

Figure 4.1. Optical photomicrographs (plane polarized light) of amphibole textures. A: Amphibole porphyroclast from relatively undeformed amphibolite with core-mantle texture. Arrows correspond to location of 1B. B: High-magnification photomicrograph of transition from actinolitic core to mantling 'subgrains'; shows angular geometry and wide variety of sizes of amphibole 'subgrains'. Arrows point to boundaries which are parallel to (110) cleavage planes. C: Amphibole porphyroclast, outlined by black lines, from mylonitic amphibolite which shows irregular extinction. Porphyroclast is surrounded by amphibole laths which are parallel to foliation. Arrow points to area shown in 1D. D: High-magnification photomicrograph showing that irregular extinction in porphyroclasts shown in 1C is due to crystallographic misorientation along angular (110) cleavage surfaces. Arrows point to one such surface.

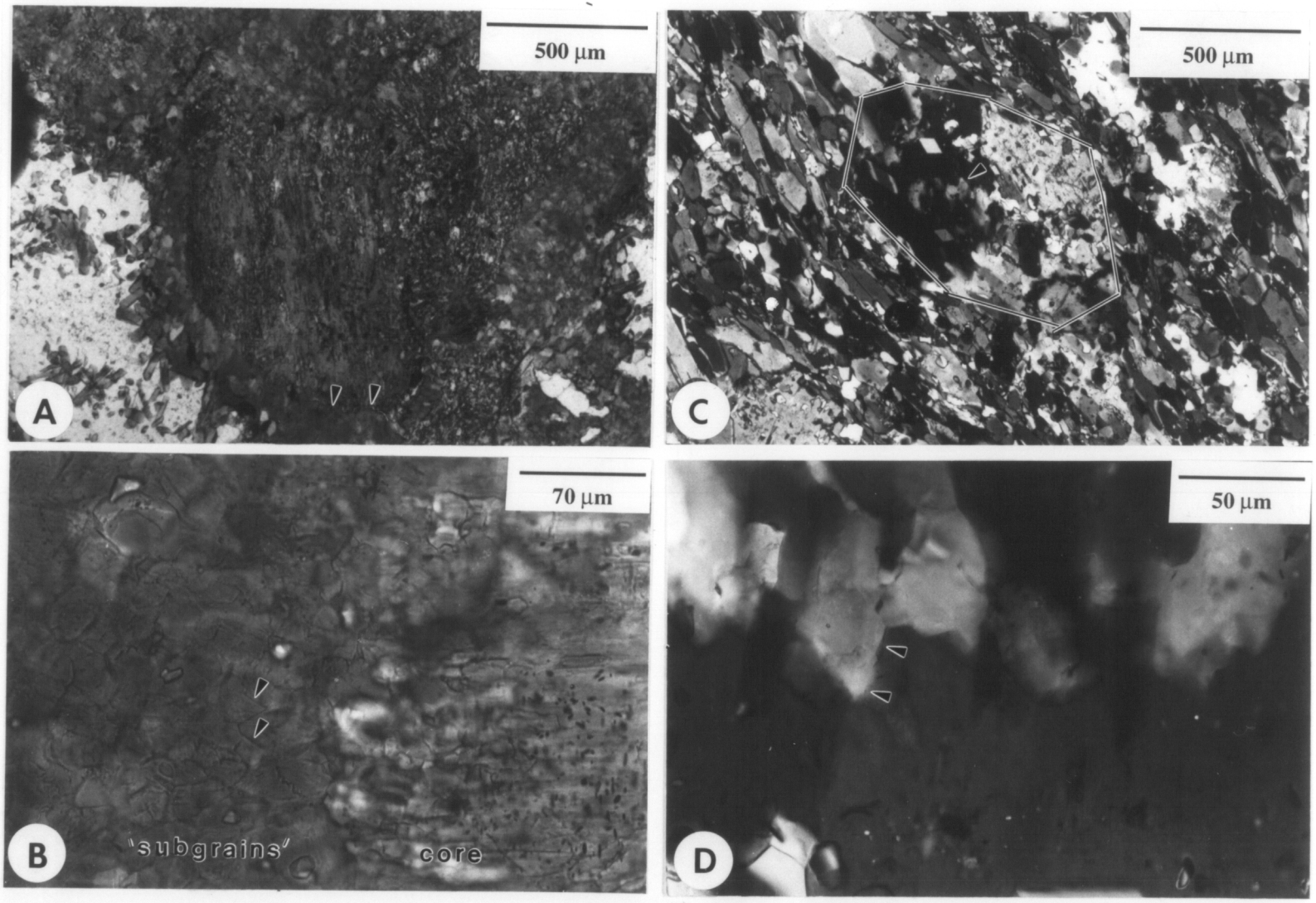
500 μm
A
500 μm
C
70 μm
B
'subgrains'
core
50 μm
D

SEM

Figure 4.2A shows a representative example of the porphyroclast microstructure from a relatively undeformed sample. Cores of amphibole porphyroclasts have a relatively homogeneous composition, although SEM images show slight compositional variation indicated by irregular patches and streaks (Figs. 2A). The 'subgrains' adjacent to the porphyroclast core have irregular shapes and a wide variety of sizes. Margins of 'subgrains' are marked by sharp compositional gradients (Fig. 4.2B). Interior portions of 'subgrains' have dark contrast relative to their boundary regions, corresponding to an actinolitic hornblende composition similar to the core composition. Lighter contrast amphibole along the boundaries of 'subgrains' has a magnesio-hornblende composition. Electron microprobe analyses of these amphibole compositions have been presented by Smelik et al. (1991). In contrast to the 'subgrains' adjacent to the porphyroclast core, amphibole 'subgrains' along the margins of the porphyroclast have a more equant shape. These equant shaped amphibole 'subgrains' are compositionally zoned with a outward progression from magnesio-hornblende in the interior of the 'subgrains' to actinolitic hornblende and back to amphibole with a magnesio-hornblende composition at their margins.

TEM

A wide variety of dislocation microstructures were observed within the amphibole porphyroclasts. The actinolitic hornblende porphyroclast cores contain predominantly linear dislocations that are generally parallel to cleavage orientations. Dislocation tangles are also common in the porphyroclast cores, occurring mostly adjacent to microcracks (Fig. 4.3A). Areas away from the microcracks generally have a lower density of dislocations

Figure 4.2. SEM photomicrographs; back-scattered electrons. Arrow in both photomicrographs are for reference and point to the same feature. A: Porphyroclast shown in figure 1A. Dark areas correspond to actinolitic hornblende compositions. Lighter areas have a magnesio-hornblende composition. B: Higher magnification images of 'subgrain' structures of same porphyroclast. Note that actinolitic hornblende interiors of 'subgrains' have an angular shape and wide variety of sizes. 'Subgrains' in outer margins of mantle are more equant and are compositionally zoned.

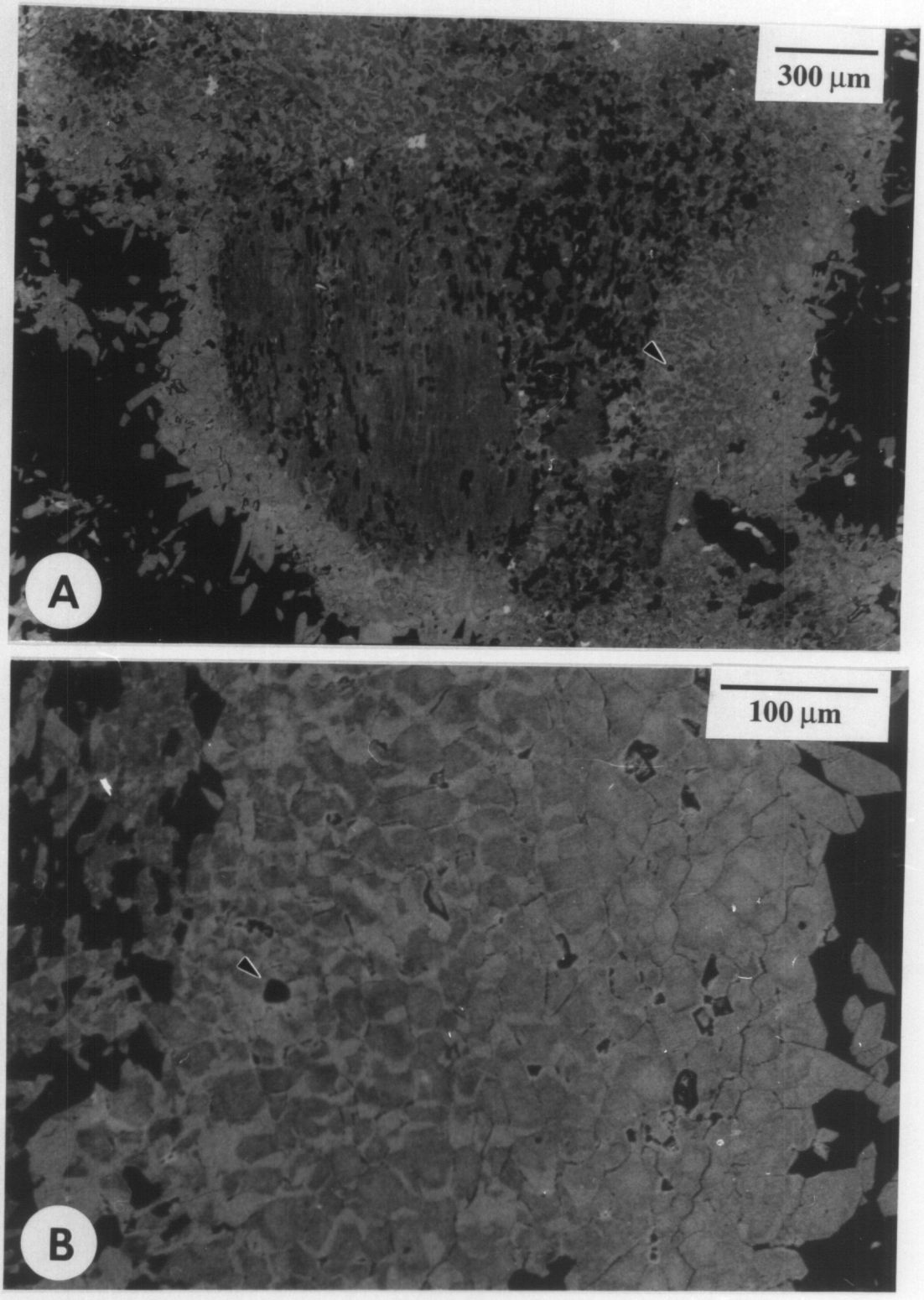
300 μm
A
100 μm
B

Figure 4.3. TEM photomicrographs. A: Dislocation tangles associated with microcracks (arrows) in amphibole. Areas farther away from microcracks have lower dislocation density with isolated linear dislocations. B: Straight and curved dislocations at boundary between actinolitic hornblende interiors and magnesio-hornblende rims of amphibole 'subgrains'. Note that magnesio-hornblende is relatively defect free.

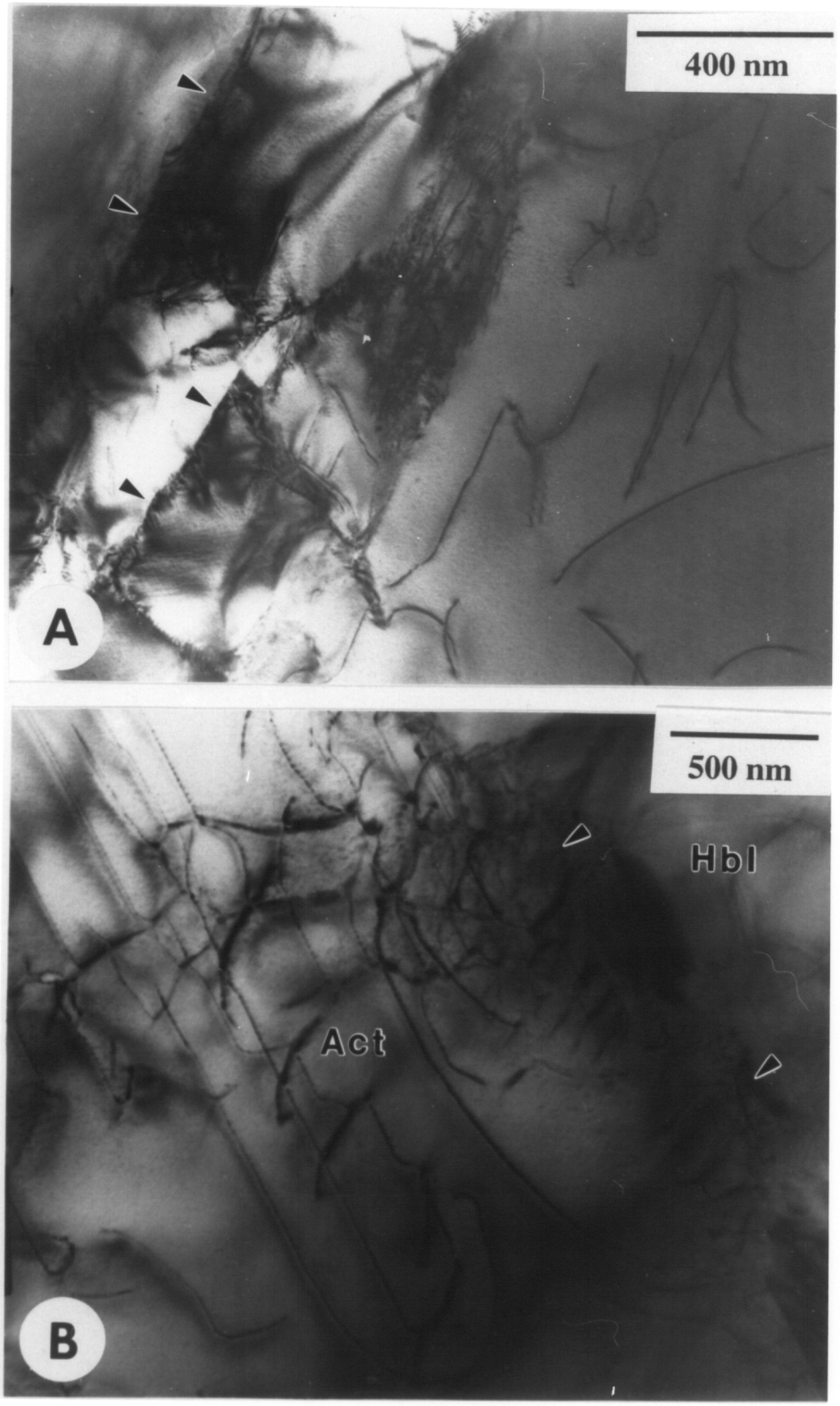
400 nm
A
500 nm
Hbl
Act
B

and locally may be totally devoid of defects. Other defect microstructures include dislocation networks, partial dislocations, dislocation loops and stacking faults.

The actinolitic hornblende interiors of the angular 'subgrains' adjacent to the porphyroclast cores have microstructures similar to those of the cores; many isolated as well as tangled straight dislocations were observed. Stacking faults are also common in the 'subgrain' interiors . The boundary between actinolitic hornblende interiors and magnesio-hornblende rims of the 'subgrains' are marked by an increase in dislocation density. Figure 4.3B shows a TEM photomicrograph of this relation; amphibole in the upper right section has a magnesio-hornblende composition and is nearly free of dislocations, whereas the lower left of the photomicrograph shows actinolitic hornblende with a relatively higher dislocation density. This relation of magnesio-hornblende having relatively low dislocation density compared to actinolitic hornblende compositions has been observed in amphiboles throughout the strain transition.

DISCUSSION

Amphibole porphyroclasts from the Cheyenne belt appear to have a well-defined core-mantle geometry. The cores, which commonly display both undulatory extinction and deformation twins, are mantled by 'subgrains' that, from their extinction positions, are seen to be crystallographically misoriented with respect to the cores. The mantling 'subgrains' also show a progression from highly angular shapes adjacent to the core to more equant shaped grains along the margins of the porphyroclast. This type of textural variation of 'subgrains' is, at least geometrically, similar to core-mantle structure in quartz (cf. White, 1976, fig. 2). Closer inspection of porphyroclasts in both the relatively undeformed and mylonitic amphibolite (Fig. 4.1 C and D) show that undulatory extinction of the cores is, at least in part, due to slight misorientation along planes that commonly

parallel (110). In these porphyroclasts, irregular extinction may not be the product of crystal plastic deformation and bending of the lattice, but rather crystallographic misorientation along planes of structural weakness (e.g., cleavage). Similar optical scale undulatory extinction in feldspar has also been shown to be the result of microfracturing and rotation of the fragments during cataclastic deformation (Tullis and Yund, 1977; 1987).

The mechanism for subgrain formation during crystal plastic deformation generally involves angular rotation in response to the pile up of dislocations and their subsequent rearrangement to a stable configuration (White, 1976). On the basis of (1) the angular shape of the 'subgrains' adjacent to the porphyroclast core (Figs. 4.1B, 4.2 B and C), and (2) the fact that some 'subgrains' boundaries are parallel to (110) cleavage surfaces (Fig. 4.1C), we interpret 'subgrain' formation in the Cheyenne belt amphibolites as occurring as a result of cataclasis, possibly associated with dislocation pile-up and/or fluid infiltration during prograde metamorphic reactions. Details of the role of dislocations and fluid infiltration are discussed below. In addition, the back-scattered SEM photomicrographs of the 'subgrain' structure adjacent to the amphibole porphyroclast show angular actinolitic hornblende fragments that have been overgrown by magnesio-hornblende. This texture resembles many cataclastic fabrics observed in fault zones (House and Gray, 1982; Blenkinsop and Rutter, 1986; Stel, 1986). The outer margin of equant amphibole 'subgrains' represents new amphibole growth in response to increasing metamorphic grade or changing fluid composition.

MODELS FOR OBSERVED CORE-MANTLE STRUCTURES

The role of dislocations in the cataclastic deformation of the Cheyenne belt amphiboles is difficult to evaluate, especially in terms of the relative timing between dislocation processes and 'subgrain' formation. The main TEM observations which are

germane to interpreting the core-mantle structures from the variably deformed amphibolite include (1) the distinct lack of dislocation structures in the magnesio-hornblende overgrowths, (2) the pile-up of dislocation at the boundary between the two amphibole composition regions, and (3) the increase in dislocation density along microcracks.

The observed 'subgrain' structure could have been produced by at least three different interrelationships between cataclastic and dislocation-related processes. First, dislocation processes could be independent of the cataclastic mechanism and represent a temporally separate event that exerted no control over the development of the cataclastic texture (Kranz, 1983). However, the association of dislocations with boundaries between the actinolitic hornblende cores and overgrowths of magnesio-hornblende suggests some causal relation between dislocation processes and development of the cataclastic (brecciated) texture. The possibility that the compositional boundaries acted as barriers to post-cataclasis dislocation motion is preclude by the absence of dislocations in the magnesio-hornblende overgrowths.

A second possibility is that during deformation, dislocation build-up led to strain hardening, facilitating cataclastic processes. Evidence to support this model includes (1) the build-up of dislocations along microcracks that are parallel to cleavage directions, (2) the large proportion of straight dislocations in the porphyroclast core as well as in the actinolitic hornblende interiors of the 'subgrains', and (3) the relatively low temperature and pressure (approximately 500 °C and 3.5 kbar) estimated for the Cheyenne belt amphibolites. Under such conditions climb in amphibole is difficult (Brodie and Rutter, 1985). Microstructural evidence for lack of climb in these amphiboles includes the abundance of straight dislocations and dislocation tangles, although the local presence of dislocation networks and loops does indicate that some climb has occurred. In addition,

the abundance of straight dislocations may indicate that a single Burgers vector dominates the amphibole microstructure (J. D. Fitz Gerald, 1991 personal commun.).

A third possibility is that the observed dislocation structures nucleated around the microcracks during crack development; this interpretation implies that crack formation preceded dislocation development (Atkinson and Meredith, 1987; Hirth and Tullis, 1991). In this model, the development and propagation of cracks would serve as a nucleation source for dislocations, especially along crack tips.

Our preferred model is as follows. Grain boundaries produced by cataclasis of the actinolitic hornblende porphyroclasts provided pathways for intergranular fluids which allowed for the dissolution of actinolitic hornblende and calcic plagioclase (An50) and precipitation of magnesio-hornblende and more albitic plagioclase (An30) in response to increasing metamorphic grade. Evidence for the presence of an intergranular fluid includes (1) chemical reactions which require the addition of water to model the observed variation of amphibole and plagioclase compositions, (2) the presence of fluid inclusions within quartz and plagioclase, and (3) the replacement of ilmenite by sphene, which requires transport of Ca, Fe, and Si (cf. Carmichael, 1969). Fluids may also have been important in reducing the effective confining pressure and thereby facilitating cataclasis. Equant amphibole 'subgrains' at the margins of the porphyroclasts which have variable composition represent new amphibole growth near peak metamorphic conditions with some growth postdating the deformation. As outlined above, the role of dislocations during cataclasis is problematic. However, grain boundary areas of the actinolitic hornblende 'subgrains' that have relatively high dislocation densities would have a higher free energy due to strain energy associated with dislocations. Increases in free energy could enhance the dissolution of actinolitic hornblende and contribute to the progress of the metamorphic reactions (cf., Wintsch and Andrews, 1989).

CONCLUSIONS

Optical and SEM examination of amphibole core-mantle structures in Cheyenne belt tectonites indicate formation by a cataclastic rather than crystal plastic deformation mechanism. Evidence to support this interpretation includes (1) the angular shape of amphibole 'subgrains', (2) the observation that patchy extinction in amphibole porphyroclasts is due to rotation along cleavage planes, (3) the presence of textures suggesting dissolution of actinolitic hornblende and subsequent replacement by magnesio-hornblende along 'subgrain' boundaries, and (4) the observation that 'subgrain' boundaries parallel (110) cleavage planes. The role of dislocations during cataclasis is unknown although the build-up of dislocation tangles along microcracks and at boundaries between actinolitic hornblende and magnesio-hornblende suggests some causal relationship.

We suggest that further investigation of core-mantle structures and application to understanding deformation mechanisms should include study of compositional variation, especially along grain boundary regions. This can be readily conducted on minerals, such as feldspar and amphibole, that undergo systematic chemical variation during metamorphism. Core-mantle structures in quartz may require detailed investigation using techniques such as cathodoluminescence (Blenkinsop and Rutter, 1986) to detect subtle chemical variations that may outline additional evidence for the dominant deformation mechanism.

REFERENCES

Atkinson, B.K. and Meredith, P.G., 1987, The theory of subcritical crack growth with applications to minerals and rocks, in Atkinson, B.K., ed., Fracture mechanics of rocks, Academic Press, p. 111-166.

Ave'Lallement, H.G. and Carter, N.L., 1970, Syntectonic recrystallization of olivine and modes of flow in the upper mantle, Geological Society of America Bulletin, 81, p. 2203-2220.

Ball, T.,T. and Farmer, G.L., 1991, Identification of 2.0 to 2.4 Ga Nd model age crustal material in the Cheyenne belt, southeastern Wyoming: Implications for Proterozoic accretionary tectonics at the southern margin of the Wyoming craton, Geology, 19, p. 360-363.

Barker, D.S., 1983, Igneous Rocks, Prentice-Hall, Inc., New Jersey, 417 P.

Beach, A., 1973, The Mineralogy of High Temperature Shear Zones at Scourie, N.W. Scotland, Journal of Petrology, 14, p. 231-248.

Beach, A., 1976, The interrelations of fluid transport, deformation, geochemistry and heat flow in early Proterozoic shear zones in the Lewisian complex, Philosophical Transactions of the Royal Society of London, A280 , p. 569-604.

Biermann, 1981, (100) Deformation twins in naturally deformed amphiboles, Nature, 272, 821-823.

Biermann, C. and Van Roermund, H.L.M., 1983, Defect structures in naturally deformed clinoamphiboles - A TEM study, Tectonophysics, 95, p. 267-278.

Blenkinsop, T.G. and Rutter, E.H., 1986, Cataclastic deformation of quartzite in the Moine thrust zone, Journal of Structural Geology, 8, p. 669-681.

Blum, A.E., Yund, R.A. and Lasaga, A.C., 1990, The effect of dislocation density on the dissolution rate of quartz, Geochimica Cosmochimica Acta, 54, p. 283-297.

Blundy, J.D. and Holland, T.J.B., 1990, Calcic amphibole equilibria and a new amphibole-plagiocalse geothermometer, Contributions to Mineralogy and Petrology, 104, p. 208-224.

Bosworth, W., 1981, Strain-induced preferential dissolution of halite, Tectonophysics, 78, p. 509-525.

Brady, J.B., 1974, Coexisting actinolite and hornblende from west-central New Hampshire, American Mineralogist, 59, p. 529-535.

Brady, J.B., 1983, Intergranular diffusion in metamorphic rocks, American Journal of Science, 283A, p. 181-200.

Brodie, K.H., 1980, Variations in mineral chemistry across a shear zone in phlogopite peridotite, Journal of Structural Geology, 2, p. 265-272.

Brodie, K.H., 1981, Variation in amphibole and plagioclase composition with deformation, Tectonophysics, 78, p. 385-402.

Brodie, K.H. and Rutter, E.H., 1985, On the Relationship between Deformation and Metamorphism, with Special Reference to the Behavoir of Basic Rocks, in Thompson, A.B. and Rubie, D.C., eds., Metamorphic Reactions: Kinetics, Textures, and Deformation: Springer-Verlag , p. 138-179.

Cahn, J.W., 1957, Nucleation on dislocations, Acta Metallurgica, 5, p. 169-172.

Carmichael, D.M., 1969, On the mechanism of prograde metamorphic reactions in quartz-bearing pelitic rocks, Contributions to Mineralogy and Petrology, 20, p. 244-267.

Chamberlin, K.R., Frost, B.R., Patel, S.C. and Snyder, G.L., 1991, New U-Pb geochronological and thermobarometric constraints on Proterozoic tectonic processes along the SE margin of the Wyoming craton, Geological Society of America Abstracts with Programs, 23, P. 59.

Casey, W.H., Carr, M.J. and Graham, R.A., 1988, Crystal defects and the dissolution kinetics of rutile, Geochimica Cosmochimica Acta, 52, p. 1545-1556.

Cho, M. and Ernst, W.G., 1991, An experimental determination of calcic amphibole solid solution along the join tremolite-tschermakite, American Mineralogist, 76, p. 985-1001.

Cooper, A.F., 1972, Progressive metamorphism of metabasic rocks from the Haast schist group of southern New Zealand, Journal of Petrology, 13, p. 457-492.

Cottrell, A.H., 1953, Dislocations and Plastic Flow in Crystals, Oxford University Press, New Jersey, 345 P.

Cumbest, R.J., Van Roermund, H.L.M., Drury, M.R. and Simpson, C., 1989a, Burgers vector determination in clinoamphiboles by computer simulation, American Mineralogist, 74, p. 586-592.

Cumbest, R.J., Drury, M.R., Van Roermund, H.L.M. and Simpson, C., 1989b, Dynamic recrystallization and chemical evolution of clinoamphibole from Senja, Norway, Contributions to Mineralogy and Petrology, 101, p. 339-349 .

De Boer, R.B., 1977, On the thermodynamics of pressure solution - interaction between chemical and mechanical forces, Geochimica Cosmochimica Acta, 41, p. 249-256.

Duebendorfer, E.M and Houston, R.S., 1987, Proterozoic accretionary tectonics at the southern margin of the Archean Wyoming craton, Geological Society of America Bulletin, 98, p. 554-568.

Duebendorfer, E.M, 1988, Evidence for an inverted metamorphic gradient associated with a Precambrian suture, southern Wyoming, Journal of Metamorphic Geology, 6, p. 41-63.

Duebendorfer, E.M. and Houston, R.S., 1990, Structural analysis of a ductile-brittle Precambrian shear zone in the Sierra Madre, Wyoming: western extension of the Cheyenne belt ?, Precambrian Research, 48, p. 21-39.

Engelder, T., 1982, A natural example of the simultaneous operation of free-face dissolution and pressure solution, Geochimica Cosmochimica Acta, 46, p. 69-74.

Ferry, J.M., 1980, A case study of the amount and distribution of heat and fluid during metamorphism, Contributions to Mineralogy and Petrology, 71, p. 373-385.

Ferry, J.M., 1986, Reaction progress: a monitor of fluid-rock interaction during metamorphic and hydrothermal events, in Walther J.V. and Wood, B.J. eds., Fluid-rock interaction during metamorphism: Springer-Verlag, p. 60-88.

Ferry, J. M., 1988a, Infiltration-driven metamorphism in Northern New England, USA, Journal of Petrology, 29, p. 1121-1159.

Ferry, J.M, 1988b, Contrasting mechanisms of fluid flow through adjacent stratigraphic units during metamorphism, south-central Maine, USA, Contributions to Mineralogy and Petrology, 98, p. 1-12.

Fisher, G.W., 1978, Rate laws in metamorphism, Geochemica Cosmochimica Acta, 42, p. 1035-1050.

Fisher, G.W., 1989, Matrix analysis of metamorphic mineral assemblages and reactions, Contributions to Mineralogy and Petrology, 102, p. 69-77.

Gandais, M. and Willaime, C., 1984, Mechanical properties of feldspars, in Brown, W.L., ed., Feldspars and Feldspathoids, Reidel Publishing, p. 207-246.

Gilotti, J., 1989, Reaction progress during mylonitization of basaltic dikes along the Sarv thrust, Swedish Caledonides, Contributions to Mineralogy and Petrology, 101. p. 30-45.

Graham, C.M., Maresch, W.V., Welch, M.D. and Pawley, A.R., 1989, Experimental studies on amphiboles: a review of thermodynamic perspectives, European Journal of Mineralogy, 1, p. 535-555.

Grapes, R.H., Hashimoto, S. and Miyashita, S., 1977, Amphiboles of a metagabbro-amphibolite sequence, Hidaka metamorphic belt, Hokkaido, Journal of Petrology, 18, p. 285-318.

Grapes, R.H. and Graham, C.M., 1978, The actinolite-hornblende series in metabasites and the so-called miscibility gap: A review, Lithos, 11, p. 85-97.

Gray, D.R. and Durney, D.W., 1979, Crenulation cleavage differentiation: implications of solution-deposition processes, Journal of Structural Geology, 1, p. 73-80.

Green III, H.W. and Burnley, P.C., 1989, A new self-organizing mechanism for deep-focus earthquakes, Nature, 341, , p. 733-737.

Hacker, B. and Christie, J.M., 1990, Observational evidence for a possible new diffusion path, Science, 251, p. 67-70.

Harte, B. and Graham, C.M., 1975, The graphical analysis of greenschist to amphibolite facies mineral asseblages in metambasites, Journal of Petrology, 16, p. 347-370.

Hay, R.S. and Evans, B., 1987, Chemically induced grain boundary migration in calcite: temperature dependence, phenomenology and possible applications to geologic systems, Contributions to Mineralogy and Petrology, 97, p. 127-141.

Helgesen, H.,C., Delany, J.M., Nesbitt, H.W. and Bird, D.K., 1978, Summary and critique of the thermodynamic properties of rock-forming minerals, American Journal of Science, 278A, 229 p.

Hewitt, D.A. and Abrecht, J., 1986, Limitations on the interpretation of biotite substitutions from chemical analyses of natural samples, American Mineralogist, 71, p. 1126-1128.

Hickman, M.H. and Glassley, W.E., 1984, The role of metamorphic fluid transport in the Rb-Sr isotopic resetting of shear zones: evidence from Norde Stromfjord, West Greenland, Contributions to Mineralogy and Petrology, 87, p. 265-281.

Hills, F.A. and Armstrong, R.L., 1974, Geochronology of Precambrian Rocks in the Laramie Range and Implications for the Tectonic Framework of Precambrian Southern Wyoming, Precambrian Research, 1, p.213-225.

Hirth, J.P. and Loth, J., 1982, Theory of Dislocations, McGraw-Hill Book Company, 780 pp.

Hirth, G. and Tullis, J., 1991, Mechanisms responsible for the brittle-ductile transition in experimentally deformed quartz aggregates, EOS, 72, p. 286.

Holland, J.B. and Richardson, 1979, Amphibole zonation in metabasites as as guide to the evolution of metamorphic conditions, Contributions to Mineralogy and Petrology, 70, p. 143-148.

Holdaway, M.J., 1972, Thermal stability of Al-Fe epidote as a function of fO_2 and Fe content, Contributions to Mineralogy and Petrology, 37, p. 307-340.

House, W.M. and Gray, D.R., 1982, Cataclasites along the Saltville thrust, U.S.A. and their implications for thrust-sheet emplacement, Journal of Structural Geology, 4, p. 257-269.

Karlstrom, K.E., Flurkey, A.J., Houston, R.S., 1983, Stratigraphy and depositional setting of Proterozoic metasedimentary rocks in southeastern Wyoming: record of an Early Proterozoic Atlantic-type cratonic margin, Geological Society of America Bulletin, 94, p. 1257-1294.

Kirby, S.H., 1987, Localized polymorphic phase transformations in high-pressure faults and applications to the physical mechanism of deep earthquakes, Journal of Geophysical Research, 92, p. 13,789-13,800.

Kirby, S.H., Durham, W.B. and Stern, L.A., 1991, Phase changes and deep-earthquake faulting in subducting lithosphere, Science, 252, p. 216-225.

Kerrich, R., Fyfe, W.S., Gorman, B.E., and Allison, I., 1977, Local modification of rock chemistry by deformation, Contributions to Mineralogy and Petrology, 65, p. 183-190.

Kerrich, R., Allison, I., Barnett, R.L., Moss, S. and Starkey, J., 1980, Microstructural and chemical transformations accompanying deformation of granite in a shear zone at Mieville, Switzerland: With implications for stress corrosion cracking and superplastic flow, Contributions to Mineralogy and Petrology, 73, p. 221-242.

Kerrich, R., LaTour, T.E. and Barnett, R.L., 1981, Mineral reactions participating in intragranular fracture propagation: implications for stress corrosion cracking, Journal of Structural Geology, 3, p. 77-87.

Kerrick, D.M., 1986, Dislocation strain energy in the Al_2SiO_5 polymorphs, Physics and Chemistry of Minerals, 13, p. 221-226.

Koons, P.O., Rubie, D.C. and Frueh-Green, G., 1987, The effects of disequilibrium and deformation on the mineralogical evolution of quartz diorite during metamorphism in the eclogite facies, Journal of Petrology, 28, p. 679-700.

Kranz, R.L., 1983, Microcracks in Rocks: A Review, Tectonophysics,100, p. 449-480.

Laird, J., 1980, Phase equilibria in mafic schist from Vermont, Journal of Petrology, 21, p. 1-37.

Laird, J. and Albee, A.L., 1981, Pressure, temperature and time indicators in mafic schist: Their application to reconstructing the polymetamorphic history of Vermont, American Journal of Science, 281, p. 127-175.

Lasaga, A.C. and Blum, A.E., 1986, Surface chemistry, etch pits and mineral-water reactions, Geochimica Cosmochimica Acta, 50, p. 2363-2379.

Leake, 1978, Nomenclature of amphiboles, Canadian Mineralogist, 16, p. 501-520.

Leger, A. and Ferry, J.M., 1991, Highly aluminous hornblende from low-pressure metacarbonates and a preliminary thermodynamic model of the Al content of calcic amphibole, American Mineralogist, 76, p. 1002-1017.

Liou, J.G., Kuniyoshi, S. and Ito, K., 1974, Experimental studies of the phase relations between greenschist and amphibolite in a basaltic system, American Journal of Science, 274, p. 613-632.

Livi, K.J.T. and Veblen, D.R., 1987, "Eastonite" from Easton, Pennsylvania: A mixture of phlogopite and a new form of serpentine, American Mineralogist, 72, p. 113-125.

Lloyd, G., 1985, Review of instrumentation techniques and applications of SEM in mineralogy, in White, J.C., ed., Application of electron microscopy in the earth sciences: Mineralogical Association of Canada Short Course Handbook, 11, p. 151-188.

McCaig, A.M., Wickham, S.M. and Taylor, H.P., Jr., 1990, Deep fluid circulation in alpine shear zones, Pyrenees, France: field and oxygen isotope stuides, Contributions to Mineralogy and Petrology, 106, p. 41-60.

Mercier, J.-C., C., 1985, Olivine and Pyroxenes, in Wenk, H-R, ed., Preferred orientation in deformed metals and rocks: An introduction to modern texture analysis, Academic Press, p. 407-430.

Mongoltkip, P. and Ashworth, J.R., 1986, Amphibolitization of metagabbros in the Scottish Highlands, Journal of Metamorphic Geology, 4, p. 261-283.

Murphy, W.M., 1989, Dislocations and feldspar dissolution, European Journal of Mineralogy, 1, p. 315-326.

Murrell, S.A.F., 1985, Aspects of relationships between deformation and prograde metamorphism that causes the evolution of water, in Thompson, A.B. and Rubie, D.C., eds., Metamorphic Reactions: Kinetics, Textures, and Deformation: Springer-Verlag, p. 211-241.

Nyman, M.W., Law, R.D. and Smelik, E.A., 1992, Cataclastic deformation mechanism for the development of core-mantle structures in amphibole, accepted for publication in Geology.

Nyman, M.W., Law, R.D., Smelik, E.A.and Veblen, D.R., 1991, Deformation mechanisms of amphibole: Evidence form an amphibolite shear zone, EOS, p. 286.

Nyman, M.W., Armstrong, T.R. and Tracy, R.J., 1991, A comparative study of deformation-assisted reactions in pelites and amphibolites, Geological Society of America Abstracts with Programs, 23, P. 449.

Nyman, M.W., 1988, Petrology and Geologic Relationships of Metagabbro Shear Zones, Southeastern Adirondack Mountains, Whitehall/Fort Anne, New York, unpublished M.A. thesis, SUNY-Binghamton, 105 p.

Nyman, M.W. and Swapp, S.,M., 1987, Southeastern Adirondack Metagabbros: Field and Petrographic Relationships, Geological Society of America Abstracts with Programs, 19, P. 49.

Olsen, T.S. and Kohlstedt, D.L., 1984, Analysis of dislocations in some naturally deformed plagioclase feldspars, Physics and Chemistry of Minerals, 11, p. 153-160.

Patel, S.C., Frost, B.R. and Snyder, G.L., 1991, Extensive early Proterozoic Barrovian metamorphism in the southeastern Wyoming province, Laramie Range, Wyoming, Geological Society of America Abstracts with Programs, 23, P. 59.

Poirier, J.P., 1982, On transformation plasticity, Journal of Geophysical Research, 87, p. 6791-6797.

Ramsay, J.G. and Graham, R.H., 1970, Strain variation in shear belts, Canadian Journal of Earth Sciences, 7, p. 786-813.

Ramsay, J.G., 1980, Shear zone geometry: a review, Journal of Structural Geology, 2, p. 83-99.

Reyard, B., Gillet, P. and Willaime, C., 1989, Deformation mechanisms in naturally deformed glaucophanes: a TEM and HREM study, European Journal of Mineralogy, 1, p. 611-624.

Ridley, J., 1985, The effect of reaction enthalpy on the progress of a metamorphic reaction, in Thompson, A.B. and Rubie, D.C., eds., Metamorphic Reactions: Kinetics, Textures, and Deformation: Springer-Verlag p. 80-97.

Robinson, P.R., Spear, F.S., Schumacher, J.C., Laird, J., Klein, C., Evans, B.W. and Doolan, B.L., 1982, Phase relations of metamorphic amphiboles: Natural occurrence and theory, in Reviews in Mineralogy, vol. 9B, eds. Veblen, D and Ribbe, P.H., p. 1-211.

Rubie, D.C., 1983, Reaction-enhanced ductility: The role of solid-solid univariant reactions in the deformation of the crust and mantle, Tectonophysics, 96, p. 331-352.

Rubie, D.C., 1984, The olivine to spinel transformation and the rheology of subducting lithosphere, Nature, 308, p. 505-508.

Rubie, D.C. and Thompson, A.B., 1985, Kinetics of metamorphic reactions at elevated temperatures and pressures: An appraisal of available experimental data, in Thompson, A.B. and Rubie, D.C., eds., Metamorphic Reactions: Kinetics, Textures, and Deformation: Springer-Verlag p. 27-79.

Rubie, D.C. , 1986, The catalysis of mineral reactions by water and restrictions on the presence of aqueous fluid during metamorphism, Mineralogical Magazine, 50, p. 399-415.

Rutter, E.H., 1976, The kinetics of rock deformation by pressure solution, Philosophical Transactions of the Royal Society of London, 283A, p. 203-219.

Scholz, C.H., Beavan, J. and Hanks, T.C., 1979, Frictional metamorphism, argon depletion and tectonic stress on the Alpine fault, New Zealand, Journal of Geophysical Research, 84, p. 6770-6782.

Scholz, C.H., 1990, The Mechanics of Earthquakes and Faulting, Cambridge University Press

Schott, J., Brantley, S., Crerar, D., Guy, C., Borcsik, M. and Willaime, C., 1989, Dissolution kinetics of strained calcite, Geochimica Cosmochimica Acta, 53, p. 373-382.

Simpson, C. and Wintsch, R.P., 1989, Evidence for deformation-induced K-feldspar replacement by myrmekite, Journal of Metamorphic Geology, 7, p. 261-275.

Sinha, A.K., Hewitt, D.A., and Rimstidt, J.D, 1986, Fluid interaction and element mobility in the development of ultramylonites, Geology,14, p. 883-886.

Smelik, E.A., Nyman, M.W. and Veblen, D.R., 1991, Pervasive exsolution within the calcic amphibole series: TEM evidence for a miscibility gap between actinolite and hornblende in natural samples, American Mineralogist, 76, p. 1184-1204.

Smith, B.K., 1985, The influence of defect crystallography on some properties of orthosilicates, in Thompson, A.B. and Rubie, D.C., eds., Metamorphic Reactions: Kinetics, Textures, and Deformation: Springer-Verlag, p. 98-117.

Snow, E. and Yund, R.A., 1987, The effect of ductile deformation on the kinetics and mechanisms of the aragonite-calcite transformatoin, Journal of Metamorphic Geology, 5, p. 141-153.

Spear, F.S., 1980, NaSi⇔CaAl exchange equilibrium between plagioclase and amphibole, Contributions to Mineralogy and Petrology, 72, p. 33-41.

Spear, F.S., 1981, An experimental study of hornblende stability and compositional variability in amphibolite, American Journal of Science, 281, p. 697-734.

Spear, F.S., Ferry, J.M. and Rumble III, D., 1982, Analytical formulation of phase equilibria: The Gibbs' Method: in Characterization of metamorphism through mineral equilibria, Reviews in Mineralogy, vol. 10, ed. J.M. Ferry, p. 105-152.

Spear, F.S., 1988, The Gibbs method and Duhem's theorem: The quantitative relationships among P,T, chemical potential, phase compositions and reaction progress in igneous and metamorphic systems, Contributions to Mineralogy and Petrology, 99, p. 249-256.

Spear, F.S., 1989, Petrologic determination of metamorphic pressure-temperature-time paths, Short course in geology, vol. 7, American Geophysical Union, p. 1-56.

Spear, F.S., Peacock, S.M., Kohn M.J., Florence, F.P. and Menard, T., 1991, Computer programs for petrologic P-T-t path calculations, American Mineralogist, 76, p. 2009-2012.

Stamatakos, J. and Kodama, K.P., 1991, The effects of grain-scale deformation on the Bloomsburg Formation pole, Journal of Geophysical Research, 96, p. 17,919 - 17,933.

Stel, H., 1986, The effect of cyclic operation of brittle and ductile deformation on the metamorphic assemblage in cataclasites and mylonites, PAGEOPH, 124, p. 289-307.

Swapp, S.M., 1991, Heterogeneous Deformation and Metamorphism in Mafic Granulites, accepted for publication in Journal of Metamorphic Geology.

Symmes, G.H. and Ferry, J.M., 1991, Evidence from mineral assemblages for infiltration of pelitic schists by aqueous fluids during metamorphism, Contributions to Mineralogy and Petrology, 108, p. 419-438.

Thompson, J.B.,Jr., 1982, Composition space: An algebraic and geometrical approach: in Characterization of metamorphism through mineral equilibria, Reviews in Mineralogy, vol. 10, ed. J.M. Ferry, p. 1-32.

Thompson, J.B, Jr., Laird, J. and Thompson, A.B., 1982, Reactions in amphibolite, greenschist and blueschist, Journal of Petrology, 23, p. 1-27.

Triboulet and Auden, 1988, Controls on P-T-t deformation path form amphibole zonation during progressive metamorphism of basic rocks, estuary of the River Vilaine, South Brittany, France, Journal of Metamorphic Geology, 6, p. 117-133.

Tullis, J. and Yund, R.A., 1987, Transition from cataclastic flow to dislocation creep of feldspar: Mechanism and microstructure, Geology,15, p. 606-609.

Tullis, J., 1983, Deformation of feldspars, in Feldspar Mineralogy, Reviews in Mineralogy, vol. 2, 2nd Edition, P.H. Ribbe ed., p. 297-341.

Tullis, J. and Yund, R.A., 1977, Experimental deformation of dry Westerly granite, Journal of Geophysical Research, 82, p. 5707-5718.

van der Hoek, B., van der Eerden, J.P. and Bennema, P., 1982, Thermodynamic stability conditions for the occurrence of hollow cores caused by stress of line and planar defects, Journal of Crystal Growth, 56, p. 621-632.

Veblen, D.R. and Bish, D.L., 1988, TEM and X-ray study of orthopyroxene megacrysts: Microstructures and crystal chemistry, American Mineralogist, 73, 677-691.

Vernon, R.H., 1975, Metamorphic Processes, Reactions and Microstructure Development, Halshed Press, New York, 324 P.

Vernon, R.H., 1990, Questions about myrmekite in deformed rocks, Journal of Structural Geology, 13, p. 979-985.

Walther, J.V. and Wood, B.J., 1984, Rate and mechanism of prograde metamorphism, Contributions to Mineralogy and Petrology, 88, p. 2246-259.

White, S., 1975, Tectonic deformation and recrystallization of oligoclase, Contributions to Mineralogy and Petrology, 50, p. 287-304.

White, S., 1976, The effects of strain on the microstructures, fabrics and deformation mechanisms in quartzites, Philosophical Transactions of the Royal Society of London, A283, p. 69-86.

White, S. and Knipe, S, 1978, Transformation and reaction enhanced ductility in rocks, Journal of the Geological Society of London, 135, p. 513-516.

Wintsch, R.P., 1985, The Possible Effects of Deformation on Chemical Processes, in Thompson, A.B. and Rubie, D.C., eds., Metamorphic Reactions: Kinetics, Textures, and Deformation: Springer-Verlag , p. 251-269.

Wintsch, R.P. and Dunning, J., 1985, The Effect of Dislocation Density on the Aqueous Solubility on Quartz and Some Geologic Implications: A Theoretical Approach, Journal of Geophysical Research, 90, p. 3649-3657.

Wintsch, R.P. and Andrews, M.S., 1987, Deformation induced growth of sillimanite: "Stress" Minerals Revisited, Journal of Geology, 96, p. 143-161.

Yardely, B.W.D., Rochelle, C.A., Barnicoat, A.C. and Lloyd, G.E., 1991, Oscillatory zoning in metamorphic minerals: an indicator of infiltration metasomatism, Mineralogical Magazine, 55, p. 357-365.

Yund, R.A., Quigley, J. and Tullis, J., 1989, The effect of dislocations on bulk diffusion in feldspars during metamorphism, Journal of Metamorphic Geology, 7, p. 337-341.

Yund, R.A., Smith, B.M. and Tullis, J., 1981, Dislocation-Assisted Diffusion of Oxygen in Albite, Physics and Chemistry of Minerals, 7, p. 185-189.

APPENDICES

APPENDIX A: Amphibole Compositions

Amphibole analyses are normalized to 13 cations exclusive of Ca, Na and K. Compositions are separated into categories based on relative strain magnitude as discussed in the text. Several different label schemes have been used to describe the sample and spot location for the analyses. The location of the probe analyses have been noted on photomicrographs and SEM images which are available from the author. Examples of each label type are as follows:

UTR2.1	Undeformed amphibolite traverse in spot 2 on grain 1
AMTR3.3	Amphibole traverse grain 3 spot 3.
(S)62.6a1.1	Sample 62, spot 6, Amphibole 1, Analyses 1
143.1a1.2	Sample 143, Spot 1, Amphibole 1, Analysis 2
141.4a1tr	Sample 141, Spot 4, Amphibole traverse 1

APPENDIX A: Amphibole composition Sample 62 Undeformed amphibolite

		am1	UNK1.1	UNK1.2	UNK1.3	UNK1.4	UTR2.1	UTR2.2	UTR2.3	UTR2.4	UTR2.5	UTR2.6	UTR2.7	UTR2.8
	SiO2	42.225	49.699	50.951	49.964	46.765	50.967	50.163	50.872	49.203	51.203	50.885	50.777	52.025
	Al2O3	14.064	6.632	5.467	6.269	9.550	4.228	5.386	5.582	6.302	4.985	5.249	5.723	4.184
	TiO2	0.000	0.000	0.000	0.000	0.000	0.000	0.000	0.000	0.000	0.000	0.000	0.000	0.000
	FeO	17.918	14.755	14.282	14.535	16.040	13.511	16.634	14.118	13.950	13.928	13.764	14.072	13.364
	MnO	0.234	0.220	0.283	0.221	0.238	0.271	0.274	0.224	0.218	0.227	0.212	0.221	0.296
	MgO	7.972	12.876	13.773	13.096	10.955	14.657	13.764	13.750	13.201	14.213	13.891	13.389	14.618
	CaO	11.923	12.374	12.031	12.073	11.789	12.336	12.252	12.108	11.591	14.233	12.206	11.957	12.237
	Na2O	1.327	0.601	0.509	0.595	0.960	0.396	0.489	0.533	0.521	0.407	0.469	0.497	0.391
	K2O	0.394	0.107	0.099	0.111	0.178	0.088	0.104	0.093	0.089	0.083	0.093	0.083	0.055
	Cl	0.136	0.092	0.082	0.091	0.124	0.130	0.165	0.177	0.150	0.122	0.121	0.134	0.171
	F	0.020	0.259	0.122	0.154	0.173	0.049	0.047	0.000	0.061	0.000	0.165	0.000	0.032
	Total	96.213	97.616	97.598	97.109	96.772	96.633	99.277	97.456	95.286	99.399	97.054	96.852	97.372
Tetrahedral	Si	6.393	7.240	7.351	7.280	6.911	7.417	7.153	7.353	7.255	7.387	7.394	7.381	7.500
	Al(IV)	1.607	0.760	0.649	0.720	1.089	0.583	0.847	0.647	0.745	0.613	0.606	0.619	0.500
	Fe3+	0.000	0.000	0.000	0.000	0.000	0.000	0.000	0.000	0.000	0.000	0.000	0.000	0.000
	total T site	8.000	8.000	8.000	8.000	8.000	8.000	8.000	8.000	8.000	8.000	8.000	8.000	8.000
Octahedral	Al(VI)	0.902	0.379	0.280	0.357	0.574	0.142	0.058	0.304	0.351	0.235	0.293	0.361	0.211
M1,M2,M3	Ti	0.000	0.000	0.000	0.000	0.000	0.000	0.000	0.000	0.000	0.000	0.000	0.000	0.000
	Fe3+	0.372	0.329	0.490	0.404	0.473	0.465	0.892	0.427	0.566	0.000	0.364	0.379	0.389
	Mg	1.799	2.796	2.962	2.845	2.414	3.180	2.926	2.963	2.902	3.057	3.009	2.901	3.142
	Fe2+	1.897	1.469	1.233	1.367	1.509	1.179	1.091	1.279	1.155	1.708	1.309	1.332	1.222
	Mn	0.030	0.027	0.035	0.027	0.030	0.033	0.033	0.027	0.027	0.000	0.026	0.027	0.036
	total M1-M3	5.000	5.000	5.000	5.000	5.000	5.000	5.000	5.000	5.000	5.000	5.000	5.000	5.000
Octahedral	Ca	1.934	1.931	1.860	1.885	1.867	1.924	1.872	1.875	1.831	2.200	1.900	1.862	1.890
M4	Na	0.066	0.069	0.140	0.115	0.133	0.076	0.128	0.125	0.149	0.000	0.100	0.138	0.109
	Fe2+	0.000	0.000	0.000	0.000	0.000	0.000	0.000	0.000	0.000	0.124	0.000	0.000	0.000
	Mn	0.000	0.000	0.000	0.000	0.000	0.000	0.000	0.000	0.000	0.028	0.000	0.000	0.000
	Mg	0.000	0.000	0.000	0.000	0.000	0.000	0.000	0.000	0.000	0.000	0.000	0.000	0.000
	total M4 site	2.000	2.000	2.000	2.000	2.000	2.000	2.000	2.000	1.980	2.352	2.000	2.000	1.999
A site	Na	0.324	0.101	0.002	0.053	0.142	0.035	0.007	0.024	0.000	0.114	0.032	0.002	0.000
	K	0.076	0.020	0.018	0.021	0.034	0.016	0.019	0.017	0.017	0.015	0.017	0.015	0.010
	total A site	0.400	0.121	0.020	0.074	0.175	0.052	0.026	0.041	0.017	0.129	0.050	0.018	0.010
	Mg/Mg+Fe2+	0.487	0.656	0.706	0.675	0.615	0.729	0.728	0.698	0.715	0.625	0.697	0.685	0.720

APPENDIX A: Amphibole composition Sample 62 Undeformed amphibolite

		UTR2.9	UTR2.10	sg1	AM1	ACT1	AMTR1.1	AMTR1.3	AMTR1.4	AMTR1.6	AMTR1.7	AMTR1.8	AMTR1.9	AMTR1.10
	SiO2	53.724	52.580	49.413	45.134	49.887	43.575	41.774	44.149	45.934	43.677	44.769	44.602	45.924
	Al2O3	2.444	2.878	5.898	10.061	5.963	12.602	13.859	10.594	9.086	11.599	10.503	11.249	8.561
	TiO2	0.000	0.000	0.000	0.367	0.000	0.000	0.000	0.000	0.134	0.000	0.000	0.000	0.119
	FeO	13.320	13.587	15.772	16.790	13.998	18.244	18.133	17.482	17.350	17.667	17.035	16.964	16.770
	MnO	0.249	0.265	0.325	0.243	0.301	0.231	0.280	0.235	0.278	0.271	0.278	0.263	0.226
	MgO	15.670	14.901	13.054	9.858	12.971	8.344	8.140	9.525	10.627	9.247	9.687	9.514	10.905
	CaO	12.264	12.316	11.686	11.672	12.196	12.009	12.183	11.828	11.802	11.794	11.704	11.646	11.912
	Na2O	0.186	0.235	0.657	1.094	0.582	1.145	1.246	1.067	0.958	1.142	1.172	1.129	0.942
	K2O	0.035	0.043	0.193	0.393	0.073	0.358	0.415	0.394	0.393	0.371	0.345	0.265	0.325
	Cl	0.182	0.107	0.171	0.134	0.089	0.099	0.096	0.194	0.165	0.184	0.183	0.117	0.096
	F	0.076	0.142	0.242	0.119	0.095	0.101	0.118	0.717	0.132	0.003	0.050	0.000	0.000
	Total	98.151	97.055	97.410	95.866	96.156	96.708	96.243	96.185	96.858	95.957	95.725	95.747	95.780
Tetrahedral	Si	7.648	7.614	7.194	6.806	7.352	6.563	6.341	6.701	6.838	6.592	6.762	6.707	6.896
	Al(IV)	0.352	0.386	0.806	1.194	0.648	1.437	1.659	1.299	1.162	1.408	1.238	1.293	1.104
	Fe3+	0.000	0.000	0.000	0.000	0.000	0.000	0.000	0.000	0.000	0.000	0.000	0.000	0.000
	total T site	8.000	8.000	8.000	8.000	8.000	8.000	8.000	8.000	8.000	8.000	8.000	8.000	8.000
Octahedral	Al(VI)	0.058	0.105	0.206	0.594	0.387	0.799	0.820	0.596	0.432	0.655	0.632	0.701	0.411
M1,M2,M3	Ti	0.000	0.000	0.000	0.042	0.000	0.000	0.000	0.000	0.015	0.000	0.000	0.000	0.013
	Fe3+	0.494	0.385	0.732	0.350	0.229	0.360	0.429	0.466	0.585	0.534	0.409	0.460	0.497
	Mg	3.326	3.217	2.833	2.216	2.850	1.873	1.842	2.155	2.358	2.081	2.181	2.133	2.441
	Fe2+	1.092	1.261	1.188	1.767	1.496	1.938	1.873	1.753	1.575	1.696	1.743	1.674	1.609
	Mn	0.030	0.032	0.040	0.031	0.038	0.029	0.036	0.030	0.035	0.035	0.036	0.033	0.029
	total M1-M3	5.000	5.000	5.000	5.000	5.000	5.000	5.000	5.000	5.000	5.000	5.000	5.000	5.000
Octahedral	Ca	1.871	1.911	1.823	1.886	1.926	1.938	1.981	1.923	1.882	1.907	1.894	1.876	1.916
M4	Na	0.051	0.066	0.177	0.114	0.074	0.062	0.019	0.077	0.118	0.093	0.106	0.124	0.084
	Fe2+	0.000	0.000	0.000	0.000	0.000	0.000	0.000	0.000	0.000	0.000	0.000	0.000	0.000
	Mn	0.000	0.000	0.000	0.000	0.000	0.000	0.000	0.000	0.000	0.000	0.000	0.000	0.000
	Mg	0.000	0.000	0.000	0.000	0.000	0.000	0.000	0.000	0.000	0.000	0.000	0.000	0.000
	total M4 site	1.922	1.977	2.000	2.000	2.000	2.000	2.000	2.000	2.000	2.000	2.000	2.000	2.000
A site	Na	0.000	0.000	0.008	0.206	0.092	0.272	0.348	0.237	0.159	0.241	0.237	0.206	0.191
	K	0.006	0.008	0.036	0.076	0.014	0.069	0.080	0.076	0.075	0.071	0.067	0.051	0.062
	total A site	0.006	0.008	0.044	0.281	0.106	0.341	0.428	0.314	0.233	0.313	0.304	0.256	0.253
	Mg/Mg+Fe2+	0.753	0.718	0.705	0.556	0.656	0.492	0.496	0.552	0.600	0.551	0.556	0.560	0.603

APPENDIX A: Amphibole composition Sample 62 Undeformed amphibolite

		AMTR1	AMTR1	AMTR3.1	AMTR3.2	AMTR3.3	AMTR3.4	AMTR3.5	AMTR3.6	AMTR3.16	AMTR3.17	AMTR3.20	AMTR3.22	AMTR3.23
	SiO2	44.300	1.359	52.638	52.558	51.547	53.083	52.201	52.469	51.753	50.774	48.860	47.961	46.364
	Al2O3	11.007	1.740	3.313	3.030	4.467	2.482	2.285	2.785	4.542	4.804	9.126	7.254	9.014
	TiO2	0.032	0.059	0.000	0.000	0.000	0.000	0.000	0.000	0.000	0.000	0.000	0.000	0.000
	FeO	17.456	0.538	13.655	13.707	13.834	14.350	15.131	14.083	13.848	14.230	15.840	14.823	16.101
	MnO	0.258	0.023	0.280	0.339	0.209	0.493	0.462	0.413	0.255	0.382	0.220	0.239	0.229
	MgO	9.499	0.966	14.781	14.896	14.056	15.041	15.073	15.031	14.095	13.865	9.731	11.999	11.054
	CaO	11.860	0.172	12.139	11.794	12.377	10.790	10.467	11.270	12.075	12.227	11.163	12.469	11.634
	Na2O	1.100	0.105	0.336	0.315	0.419	0.289	0.253	0.327	0.416	0.491	0.971	0.669	0.923
	K2O	0.358	0.048	0.071	0.037	0.052	0.042	0.030	0.053	0.117	0.116	0.223	0.172	0.182
	Cl	0.089	0.119	0.078	0.104	0.096	0.087	0.125	0.074	0.068	0.069	0.106	0.110	0.061
	F	0.123	0.186	0.078	0.184	0.251	0.292	0.278	0.091	0.074	0.061	0.059	0.259	0.003
	Total	96.080	5.315	97.368	96.963	97.306	96.950	96.304	96.595	97.243	97.019	96.299	95.954	95.565
Tetrahedral	Si	6.675	3.295	7.584	7.585	7.486	7.596	7.506	7.555	7.482	7.389	7.255	7.167	6.918
	Al(IV)	1.325	4.705	0.416	0.415	0.514	0.404	0.387	0.445	0.518	0.611	0.745	0.833	1.082
	Fe3+	0.000	0.000	0.000	0.000	0.000	0.000	0.107	0.000	0.000	0.000	0.000	0.000	0.000
	total T site	8.000	8.000	8.000	8.000	8.000	8.000	8.000	8.000	8.000	8.000	8.000	8.000	8.000
Octahedral	Al(VI)	0.630	0.265	0.146	0.100	0.251	0.014	0.000	0.027	0.256	0.213	0.852	0.444	0.503
M1,M2,M3	Ti	0.004	0.107	0.000	0.000	0.000	0.000	0.000	0.000	0.000	0.000	0.000	0.000	0.000
	Fe3+	0.468	1.090	0.416	0.573	0.283	0.994	1.300	0.839	0.382	0.425	0.021	0.169	0.558
	Mg	2.134	3.490	3.175	3.205	3.043	3.209	3.231	3.226	3.038	3.008	2.154	2.673	2.459
	Fe2+	1.732	0.000	1.229	1.081	1.397	0.724	0.469	0.856	1.292	1.307	1.946	1.683	1.452
	Mn	0.033	0.048	0.034	0.041	0.026	0.060	0.000	0.050	0.031	0.047	0.028	0.030	0.029
	total M1-M3	5.000	5.000	5.000	5.000	5.000	5.000	5.000	5.000	5.000	5.000	5.000	5.000	5.000
Octahedral	Ca	1.915	0.447	1.874	1.824	1.926	1.654	1.613	1.739	1.870	1.906	1.776	1.996	1.860
M4	Na	0.085	0.494	0.094	0.088	0.074	0.080	0.070	0.091	0.117	0.094	0.224	0.004	0.140
	Fe2+	0.000	0.000	0.000	0.000	0.000	0.000	0.050	0.000	0.000	0.000	0.000	0.000	0.000
	Mn	0.000	0.000	0.000	0.000	0.000	0.000	0.056	0.000	0.000	0.000	0.000	0.000	0.000
	Mg	0.000	0.000	0.000	0.000	0.000	0.000	0.000	0.000	0.000	0.000	0.000	0.000	0.000
	total M4 site	2.000	0.941	1.967	1.912	2.000	1.734	1.790	1.830	1.987	2.000	2.000	2.000	2.000
A site	Na	0.236	0.000	0.000	0.000	0.044	0.000	0.000	0.000	0.000	0.045	0.055	0.190	0.127
	K	0.069	0.147	0.013	0.007	0.010	0.008	0.005	0.010	0.022	0.021	0.042	0.033	0.035
	total A site	0.305	0.147	0.013	0.007	0.053	0.008	0.005	0.010	0.022	0.067	0.097	0.223	0.162
	Mg/Mg+Fe2+	0.552	1.000	0.721	0.748	0.685	0.816	0.861	0.790	0.702	0.697	0.525	0.614	0.629

APPENDIX A: Amphibole composition Sample 62 Undeformed amphibolite

		AMTR3.24	AMTR3.25	AMTR3.29	AMTR3.30	AMTR3.31	AMTR3.32	AMTR3.33	AMTR3.35	AMTR3.38	AMTR3.39	AMTR3.40	AMTR1	AMTR2
	SiO2	50.590	47.573	54.457	47.807	49.689	47.984	46.633	48.764	47.472	45.598	44.254	46.678	52.381
	Al2O3	4.900	7.226	5.797	8.195	6.732	8.265	8.686	6.239	8.634	9.525	10.674	8.418	3.723
	TiO2	0.000	0.000	0.000	0.000	0.000	0.000	0.000	0.000	0.000	0.000	0.000	0.702	0.000
	FeO	15.453	16.520	13.515	15.126	14.804	15.684	17.503	15.673	16.584	17.028	17.698	16.789	13.962
	MnO	0.347	0.362	0.209	0.257	0.248	0.180	0.179	0.310	0.321	0.281	0.278	0.239	0.256
	MgO	13.391	11.795	11.350	11.474	12.746	11.423	10.454	12.734	11.114	10.225	9.575	11.239	14.606
	CaO	11.538	11.423	10.825	12.247	12.230	12.003	11.795	11.720	11.630	11.483	11.749	11.932	12.042
	Na2O	0.578	0.903	0.582	0.827	0.644	0.886	0.850	0.839	0.889	1.016	1.089	0.846	0.338
	K2O	0.122	0.264	0.157	0.208	0.149	0.222	0.314	0.220	0.330	0.438	0.370	0.254	0.076
	Cl	0.119	0.157	0.194	0.177	0.148	0.091	0.067	0.071	0.040	0.047	0.141	0.109	0.072
	F	0.000	0.028	0.173	0.073	0.093	0.104	0.344	0.230	0.092	0.122	0.168	0.125	0.112
	Total	97.037	96.249	97.258	96.392	97.483	96.841	96.825	96.800	97.106	95.763	95.996	97.329	97.568
Tetrahedral	Si	7.345	7.044	7.893	7.108	7.240	7.087	6.949	7.165	6.985	6.849	6.678	6.886	7.530
	Al(IV)	0.655	0.956	0.107	0.892	0.760	0.913	1.051	0.835	1.015	1.151	1.322	1.114	0.470
	Fe3+	0.000	0.000	0.000	0.000	0.000	0.000	0.000	0.000	0.000	0.000	0.000	0.000	0.000
	total T site	8.000	8.000	8.000	8.000	8.000	8.000	8.000	8.000	8.000	8.000	8.000	8.000	8.000
Octahedral	Al(VI)	0.183	0.305	0.884	0.544	0.397	0.525	0.474	0.246	0.482	0.536	0.577	0.350	0.160
M1,M2,M3	Ti	0.000	0.000	0.000	0.000	0.000	0.000	0.000	0.000	0.000	0.000	0.000	0.078	0.000
	Fe3+	0.698	0.717	0.000	0.169	0.335	0.294	0.506	0.618	0.551	0.539	0.556	0.547	0.493
	Mg	2.898	2.604	2.453	2.543	2.769	2.515	2.322	2.790	2.438	2.290	2.154	2.472	3.130
	Fe2+	1.178	1.329	1.664	1.712	1.469	1.643	1.675	1.308	1.489	1.600	1.678	1.524	1.186
	Mn	0.043	0.045	0.000	0.032	0.031	0.023	0.023	0.039	0.040	0.036	0.035	0.030	0.031
	total M1-M3	5.000	5.000	5.000	5.000	5.000	5.000	5.000	5.000	5.000	5.000	5.000	5.000	5.000
Octahedral	Ca	1.795	1.812	1.681	1.951	1.909	1.899	1.883	1.845	1.833	1.848	1.900	1.886	1.855
M4	Na	0.163	0.188	0.000	0.049	0.091	0.101	0.117	0.155	0.167	0.152	0.100	0.114	0.094
	Fe2+	0.000	0.000	0.306	0.000	0.000	0.000	0.000	0.000	0.000	0.000	0.000	0.000	0.000
	Mn	0.000	0.000	0.026	0.000	0.000	0.000	0.000	0.000	0.000	0.000	0.000	0.000	0.000
	Mg	0.000	0.000	0.000	0.000	0.000	0.000	0.000	0.000	0.000	0.000	0.000	0.000	0.000
	total M4 site	1.957	2.000	2.013	2.000	2.000	2.000	2.000	2.000	2.000	2.000	2.000	2.000	1.949
A site	Na	0.000	0.071	0.164	0.189	0.091	0.153	0.128	0.084	0.087	0.144	0.218	0.128	0.000
	K	0.023	0.050	0.029	0.039	0.028	0.042	0.060	0.041	0.062	0.084	0.071	0.048	0.014
	total A site	0.023	0.121	0.193	0.229	0.119	0.195	0.188	0.125	0.149	0.228	0.290	0.175	0.014
	Mg/Mg+Fe2+	0.711	0.662	0.555	0.598	0.653	0.605	0.581	0.681	0.621	0.589	0.562	0.619	0.725

APPENDIX A: Amphibole composition Sample 62 Undeformed amphibolite

		AMTR3.1	AMTR3.3	AMTR3.4	AMTR3.6	AMTR3.7	AMTR3.8	AMTR3.9	AMTR3.10	AMTR3.11	AMTR3.12	AMTR3.13	AMTR3.14	AMTR3.15
	SiO2	42.397	49.216	49.738	49.805	51.806	45.619	48.311	47.973	49.232	49.232	48.313	45.762	48.471
	Al2O3	14.048	5.298	7.235	5.298	4.318	11.618	7.792	8.198	6.519	7.268	6.686	10.127	7.240
	TiO2	0.000	0.000	0.000	0.000	0.000	0.000	0.000	0.000	0.000	0.000	0.000	0.000	0.000
	FeO	19.061	16.017	14.809	14.497	14.198	17.477	15.905	15.932	15.200	15.521	15.237	17.359	15.561
	MnO	0.218	0.260	0.224	0.273	0.168	0.228	0.245	0.251	0.242	0.196	0.258	0.204	0.301
	MgO	7.864	13.530	12.273	13.778	14.396	9.437	11.930	11.963	12.768	12.144	13.092	10.387	12.322
	CaO	11.674	11.541	11.942	12.138	12.256	11.877	11.791	12.038	11.930	12.111	12.072	11.788	11.778
	Na2O	1.281	0.597	0.650	0.454	0.384	1.108	0.770	0.790	0.645	0.715	0.628	0.948	0.702
	K2O	0.408	0.164	0.117	0.066	0.056	0.260	0.203	0.158	0.169	0.154	0.151	0.242	0.166
	Cl	0.088	0.083	0.044	0.050	0.062	0.030	0.089	0.114	0.134	0.149	0.128	0.118	0.106
	F	0.104	0.128	0.039	0.000	0.029	0.087	0.002	0.095	0.328	0.231	0.182	0.283	0.042
	Total	97.142	96.834	97.069	96.359	97.673	97.740	97.038	97.511	97.165	97.720	96.745	97.218	96.689
Tetrahedral	Si	6.350	7.169	7.254	7.280	7.452	6.725	7.074	7.007	7.202	7.187	7.083	6.770	7.109
	Al(IV)	1.650	0.831	0.746	0.720	0.548	1.275	0.926	0.993	0.798	0.813	0.917	1.230	0.891
	Fe3+	0.000	0.000	0.000	0.000	0.000	0.000	0.000	0.000	0.000	0.000	0.000	0.000	0.000
	total T site	8.000	8.000	8.000	8.000	8.000	8.000	8.000	8.000	8.000	8.000	8.000	8.000	8.000
Octahedral M1,M2,M3	Al(VI)	0.829	0.079	0.498	0.192	0.184	0.743	0.418	0.418	0.326	0.438	0.238	0.536	0.360
	Ti	0.000	0.000	0.000	0.000	0.000	0.000	0.000	0.000	0.000	0.000	0.000	0.000	0.000
	Fe3+	0.625	0.950	0.310	0.586	0.468	0.415	0.552	0.554	0.518	0.355	0.679	0.640	0.599
	Mg	1.756	2.938	2.668	3.002	3.087	2.074	2.604	2.605	2.784	2.643	2.861	2.291	2.694
	Fe2+	1.762	1.001	1.496	1.186	1.240	1.740	1.395	1.392	1.342	1.540	1.189	1.508	1.309
	Mn	0.028	0.032	0.028	0.034	0.020	0.029	0.030	0.031	0.030	0.024	0.032	0.026	0.037
	total M1-M3	5.000	5.000	5.000	5.000	5.000	5.000	5.000	5.000	5.000	5.000	5.000	5.000	5.000
Octahedral M4	Ca	1.873	1.801	1.866	1.901	1.889	1.876	1.850	1.884	1.870	1.894	1.896	1.868	1.851
	Na	0.127	0.169	0.134	0.099	0.107	0.124	0.150	0.116	0.130	0.106	0.104	0.132	0.149
	Fe2+	0.000	0.000	0.000	0.000	0.000	0.000	0.000	0.000	0.000	0.000	0.000	0.000	0.000
	Mn	0.000	0.000	0.000	0.000	0.000	0.000	0.000	0.000	0.000	0.000	0.000	0.000	0.000
	Mg	0.000	0.000	0.000	0.000	0.000	0.000	0.000	0.000	0.000	0.000	0.000	0.000	0.000
	total M4 site	2.000	1.970	2.000	2.000	1.996	2.000	2.000	2.000	2.000	2.000	2.000	2.000	2.000
A site	Na	0.245	0.000	0.050	0.029	0.000	0.192	0.068	0.107	0.053	0.097	0.075	0.140	0.050
	K	0.078	0.030	0.022	0.012	0.010	0.049	0.038	0.029	0.032	0.029	0.028	0.046	0.031
	total A site	0.323	0.030	0.072	0.042	0.010	0.241	0.106	0.137	0.084	0.125	0.103	0.186	0.081
	Mg/Mg+Fe2+	0.499	0.746	0.641	0.717	0.714	0.544	0.651	0.652	0.675	0.632	0.706	0.603	0.673

APPENDIX A: Amphibole composition Sample 62 Undeformed amphibolite

		AMTR3.16	AMTR3.17	AMTR3.18	AMTR3.19	AMTR3.20
	SiO2	46.922	44.668	47.604	43.546	46.339
	Al2O3	8.082	10.926	8.399	11.335	8.518
	TiO2	0.011	0.284	0.000	0.000	0.228
	FeO	16.211	17.604	16.202	18.753	16.521
	MnO	0.334	0.198	0.260	0.197	0.269
	MgO	11.563	9.580	11.617	8.822	11.275
	CaO	11.625	12.088	12.147	11.777	11.707
	Na2O	0.919	1.043	0.780	1.128	0.866
	K2O	0.254	0.294	0.228	0.310	0.361
	Cl	0.103	0.102	0.105	0.040	0.103
	F	0.182	0.272	0.278	0.091	0.020
	Total	96.206	97.059	97.620	95.999	96.207
Tetrahedral	Si	6.969	6.680	6.985	6.590	6.892
	Al(IV)	1.031	1.320	1.015	1.410	1.108
	Fe3+	0.000	0.000	0.000	0.000	0.000
	total T site	8.000	8.000	8.000	8.000	8.000
Octahedral	Al(VI)	0.383	0.606	0.438	0.611	0.386
M1,M2,M3	Ti	0.001	0.032	0.000	0.000	0.025
	Fe3+	0.633	0.418	0.492	0.589	0.622
	Mg	2.560	2.136	2.541	1.990	2.500
	Fe2+	1.380	1.783	1.496	1.784	1.433
	Mn	0.042	0.025	0.032	0.025	0.034
	total M1-M3	5.000	5.000	5.000	5.000	5.000
Octahedral	Ca	1.850	1.937	1.910	1.909	1.866
M4	Na	0.150	0.063	0.090	0.091	0.134
	Fe2+	0.000	0.000	0.000	0.000	0.000
	Mn	0.000	0.000	0.000	0.000	0.000
	Mg	0.000	0.000	0.000	0.000	0.000
	total M4 site	2.000	2.000	2.000	2.000	2.000
A site	Na	0.114	0.239	0.132	0.240	0.115
	K	0.048	0.056	0.043	0.060	0.068
	total A site	0.163	0.295	0.174	0.300	0.184
	Mg/Mg+Fe2+	0.650	0.545	0.629	0.527	0.636

APPENDIX A: Amphibole Compositions; Sample 62 Undeformed amphiboilte

		62.6a1.1	62.6a1.2	62.6a1.3	62.6a1.4	62.6a1.6	62.6a1.8	62.6a1.9	62.6a1.10	62.6a1.11	62.6a1.12	62.6a1.13	62.6a1.14	62.6a1.15
	SiO2	41.174	42.992	41.486	42.99	49.145	50.976	48.433	49.243	48.907	48.889	48.945	49.337	48.152
	Al2O3	14.12	13.975	13.736	11.865	5.551	4.418	6.821	5.902	6.498	5.585	5.342	6.789	6.427
	TiO2	0.338	0.289	0.286	0.576	0.206	0.139	0.392	0.177	0.249	0.402	0.514	0.172	0.398
	FeO	19.169	19.445	19.689	18.451	15.489	14.652	16.207	15.396	15.932	15.77	16.464	15.617	16
	MnO	0.192	0.179	0.294	0.195	0.213	0.214	0.218	0.177	0.152	0.191	0.32	0.231	0.222
	MgO	7.98	8.1	7.984	9.073	13.116	13.996	12.173	12.799	12.676	12.693	12.521	12.41	12.434
	CaO	11.98	12.08	11.773	11.895	12.357	12.726	12.279	12.378	12.432	12.432	11.934	12.294	11.993
	Na2O	1.326	1.291	1.383	1.182	0.505	0.398	0.673	0.503	0.624	0.518	0.697	0.579	0.628
	K2O	0.341	0.347	0.384	0.408	0.101	0.08	0.22	0.083	0.151	0.165	0.203	0.109	0.176
	Cl	0.189	0.165	0.269	0.166	0.151	0.048	0.063	0.038	0.074	0.066	0.053	0.056	0.065
	F	0.001	0	0.009	0	0	0.02	0.036	0.083	0.002	0	0.019	0.103	0
	Total	96.81	98.863	97.293	96.801	96.834	97.667	97.515	96.779	97.697	96.711	97.012	97.697	96.495
Tetrahedral	Si	6.212	6.339	6.234	6.459	7.217	7.397	7.102	7.239	7.136	7.218	7.203	7.188	7.103
	Al(IV)	1.788	1.661	1.766	1.541	0.783	0.603	0.898	0.761	0.864	0.782	0.797	0.812	0.897
	Fe3+	0.000	0.000	0.000	0.000	0.000	0.000	0.000	0.000	0.000	0.000	0.000	0.000	0.000
	total T site	8.000	8.000	8.000	8.000	8.000	8.000	8.000	8.000	8.000	8.000	8.000	8.000	8.000
Octahedral M1,M2,M3	Al(VI)	0.723	0.767	0.667	0.560	0.177	0.153	0.281	0.261	0.253	0.190	0.130	0.354	0.220
	Ti	0.038	0.032	0.032	0.065	0.023	0.015	0.043	0.020	0.027	0.045	0.057	0.019	0.044
	Fe3+	0.661	0.578	0.766	0.599	0.509	0.336	0.439	0.403	0.466	0.389	0.553	0.397	0.585
	Mg	1.795	1.780	1.789	2.032	2.871	3.028	2.661	2.805	2.757	2.794	2.747	2.696	2.734
	Fe2+	1.758	1.819	1.708	1.719	1.393	1.442	1.548	1.489	1.478	1.558	1.474	1.505	1.389
	Mn	0.025	0.022	0.037	0.025	0.026	0.026	0.027	0.022	0.019	0.024	0.040	0.029	0.028
	total M1-M3	5.000	5.000	5.000	5.000	5.000	5.000	5.000	5.000	5.000	5.000	5.000	5.000	5.000
Octahedral M4	Ca	1.937	1.908	1.896	1.915	1.944	1.979	1.929	1.949	1.943	1.967	1.882	1.919	1.895
	Na	0.063	0.092	0.104	0.085	0.056	0.021	0.071	0.051	0.057	0.033	0.118	0.081	0.105
	Fe2+	0.000	0.000	0.000	0.000	0.000	0.000	0.000	0.000	0.000	0.000	0.000	0.000	0.000
	Mn	0.000	0.000	0.000	0.000	0.000	0.000	0.000	0.000	0.000	0.000	0.000	0.000	0.000
	Mg	0.000	0.000	0.000	0.000	0.000	0.000	0.000	0.000	0.000	0.000	0.000	0.000	0.000
	total M4 site	2.000	2.000	2.000	2.000	2.000	2.000	2.000	2.000	2.000	2.000	2.000	2.000	2.000
A site	Na	0.325	0.277	0.299	0.259	0.088	0.091	0.121	0.093	0.120	0.115	0.081	0.083	0.075
	K	0.066	0.065	0.074	0.078	0.019	0.015	0.041	0.016	0.028	0.031	0.038	0.020	0.033
	total A site	0.390	0.343	0.372	0.337	0.107	0.105	0.162	0.108	0.148	0.146	0.119	0.103	0.108
	Mg/Mg+Fe	0.505	0.495	0.511	0.542	0.673	0.677	0.632	0.653	0.651	0.642	0.651	0.642	0.663

APPENDIX A: Amphibole Compositions; Sample 62 Undeformed amphiboilte

		62.6a1.16	62.6a1.17	62.6a1.18	62.6a1.19	62.6a1.21	62.6a1.22	62.6a1.23	62.6a1.24	62.6a1.25	62.6a1.26	62.6a1.27	62.6a1.28	62.6a1.29
	SiO2	50.365	51.011	50.855	49.982	49.778	44.535	50.437	48.306	50.874	49.011	44.904	49.123	42.949
	Al2O3	5.896	5.505	5.005	5.43	4.432	11.874	5.255	5.918	3.473	6.154	9.55	5.272	12.063
	TiO2	0.26	0.187	0.116	0.251	0.432	0.399	0.418	0.3	0.871	0.343	0.474	0.206	0.416
	FeO	15.332	14.871	14.777	15.435	15.415	18.252	15.223	15.542	14.839	15.672	17.586	15.551	18.413
	MnO	0.24	0.237	0.236	0.169	0.299	0.175	0.238	0.256	0.266	0.246	0.176	0.275	0.259
	MgO	13.209	13.247	13.61	13.138	13.701	9.139	13.139	13.083	14.317	12.865	10.493	13.122	9.024
	CaO	12.435	12.369	12.622	12.589	12.072	11.996	12.484	12.054	12.431	12.495	12.474	12.406	12.072
	Na2O	0.598	0.416	0.46	0.587	0.466	1.137	0.455	0.557	0.36	0.602	0.96	0.511	1.202
	K2O	0.14	0.068	0.041	0.126	0.144	0.267	0.096	0.166	0.055	0.153	0.268	0.121	0.286
	Cl	0.07	0.061	0.058	0.031	0.045	0.041	0.183	0.054	0.114	0.075	0.066	0.026	0.075
	F	0	0	0	0.031	0.01	0	0	0	0	0.047	0.089	0	0.029
	Total	98.545	97.972	97.78	97.769	96.794	97.815	97.928	96.236	97.6	97.663	97.04	96.613	96.788
Tetrahedral	Si	7.257	7.366	7.371	7.284	7.279	6.589	7.329	7.118	7.381	7.158	6.709	7.233	6.451
	Al(IV)	0.743	0.634	0.629	0.716	0.721	1.411	0.671	0.882	0.594	0.842	1.291	0.767	1.549
	Fe3+	0.000	0.000	0.000	0.000	0.000	0.000	0.000	0.000	0.025	0.000	0.000	0.000	0.000
	total T site	8.000	8.000	8.000	8.000	8.000	8.000	8.000	8.000	8.000	8.000	8.000	8.000	8.000
Octahedral	Al(VI)	0.258	0.303	0.226	0.216	0.043	0.660	0.229	0.146	0.000	0.217	0.390	0.148	0.587
M1,M2,M3	Ti	0.028	0.020	0.013	0.028	0.048	0.044	0.046	0.033	0.095	0.038	0.053	0.023	0.047
	Fe3+	0.397	0.334	0.320	0.324	0.640	0.483	0.318	0.673	0.477	0.441	0.472	0.491	0.578
	Mg	2.837	2.852	2.941	2.854	2.987	2.016	2.846	2.874	3.097	2.801	2.337	2.880	2.021
	Fe2+	1.450	1.462	1.471	1.557	1.245	1.776	1.532	1.242	1.323	1.473	1.725	1.424	1.735
	Mn	0.029	0.029	0.029	0.021	0.037	0.022	0.029	0.032	0.008	0.030	0.022	0.034	0.033
	total M1-M3	5.000	5.000	5.000	5.000	5.000	5.000	5.000	5.000	5.000	5.000	5.000	5.000	5.000
Octahedral	Ca	1.920	1.914	1.960	1.966	1.891	1.902	1.944	1.903	1.932	1.955	1.997	1.957	1.943
M4	Na	0.080	0.086	0.040	0.034	0.109	0.098	0.056	0.097	0.043	0.045	0.003	0.043	0.057
	Fe2+	0.000	0.000	0.000	0.000	0.000	0.000	0.000	0.000	0.000	0.000	0.000	0.000	0.000
	Mn	0.000	0.000	0.000	0.000	0.000	0.000	0.000	0.000	0.025	0.000	0.000	0.000	0.000
	Mg	0.000	0.000	0.000	0.000	0.000	0.000	0.000	0.000	0.000	0.000	0.000	0.000	0.000
	total M4 site	2.000	2.000	2.000	2.000	2.000	2.000	2.000	2.000	2.000	2.000	2.000	2.000	2.000
A site	Na	0.087	0.030	0.089	0.131	0.024	0.228	0.072	0.062	0.059	0.126	0.275	0.103	0.293
	K	0.026	0.013	0.008	0.023	0.027	0.050	0.018	0.031	0.010	0.029	0.051	0.023	0.055
	total A site	0.112	0.043	0.097	0.155	0.050	0.278	0.090	0.093	0.069	0.154	0.326	0.126	0.348
	Mg/Mg+Fe	0.662	0.661	0.667	0.647	0.706	0.532	0.650	0.698	0.701	0.655	0.575	0.669	0.538

APPENDIX A: Amphibole Compositions; Sample 62 Undeformed amphiboilte

		62.6a1.30	62.6a1.31	62.6a1.32	62.6a1.33	62.6a1.34	62.6a1.35	62.6a1.36	62.6a1.37	62.6a1.38	62.6a1.39	62.6a1.40	62.6a1.50	62.6a1.51
	SiO2	50.034	49.548	42.646	41.702	42.629	49.865	47.408	48.219	42.888	46.477	48.151	46.705	44.769
	Al2O3	5.369	5.019	12.799	13.685	13.124	5.775	7.583	6.253	12.551	7.461	6.418	7.546	10.093
	TiO2	0.254	0.791	0.419	0.344	0.423	0.603	0.361	0.391	0.42	0.597	0.439	0.521	0.467
	FeO	15.151	15.018	18.491	18.961	18.549	16.384	16.095	16.178	18.874	16.825	16.679	16.545	17.745
	MnO	0.189	0.242	0.179	0.235	0.182	0.299	0.222	0.242	0.239	0.26	0.307	0.298	0.23
	MgO	13.583	13.443	8.775	8.047	8.628	12.585	11.784	12.659	8.714	11.596	12.433	11.818	10.393
	CaO	12.437	12.55	12.168	11.706	11.981	12.189	12.306	12.226	11.879	12.142	11.846	12.012	12.188
	Na2O	0.492	0.383	1.204	1.26	1.203	0.557	0.757	0.606	1.219	0.727	0.795	0.792	0.908
	K2O	0.104	0.072	0.307	0.357	0.345	0.218	0.208	0.15	0.337	0.263	0.188	0.288	0.31
	Cl	0.127	0.072	0.122	0.035	0.042	0.159	0.189	0.155	0.072	0.122	0.092	0.177	0.1
	F	0	0.048	0.025	0.022	0	0	0	0.027	0.043	0	0.038	0.007	0.044
	Total	97.74	97.186	97.135	96.354	97.106	98.634	96.913	97.106	97.236	96.47	97.386	96.709	97.247
Tetrahedral	Si	7.257	7.249	6.391	6.293	6.374	7.215	7.017	7.084	6.411	6.921	7.050	6.923	6.648
	Al(IV)	0.743	0.751	1.609	1.707	1.626	0.785	0.983	0.916	1.589	1.079	0.950	1.077	1.352
	Fe3+	0.000	0.000	0.000	0.000	0.000	0.000	0.000	0.000	0.000	0.000	0.000	0.000	0.000
	total T site	8.000	8.000	8.000	8.000	8.000	8.000	8.000	8.000	8.000	8.000	8.000	8.000	8.000
Octahedral	Al(VI)	0.175	0.114	0.652	0.727	0.687	0.200	0.340	0.167	0.622	0.231	0.158	0.242	0.414
M1,M2,M3	Ti	0.028	0.087	0.047	0.039	0.048	0.066	0.040	0.043	0.047	0.067	0.048	0.058	0.052
	Fe3+	0.490	0.407	0.546	0.678	0.591	0.477	0.404	0.614	0.651	0.580	0.718	0.621	0.635
	Mg	2.937	2.932	1.961	1.810	1.923	2.715	2.600	2.772	1.942	2.574	2.714	2.612	2.301
	Fe2+	1.347	1.430	1.772	1.715	1.729	1.506	1.589	1.374	1.708	1.515	1.324	1.430	1.569
	Mn	0.023	0.030	0.023	0.030	0.023	0.037	0.028	0.030	0.030	0.033	0.038	0.037	0.029
	total M1-M3	5.000	5.000	5.000	5.000	5.000	5.000	5.000	5.000	5.000	5.000	5.000	5.000	5.000
Octahedral	Ca	1.933	1.967	1.954	1.893	1.919	1.890	1.951	1.924	1.902	1.937	1.858	1.908	1.939
M4	Na	0.067	0.033	0.046	0.107	0.081	0.110	0.049	0.076	0.098	0.063	0.142	0.092	0.061
	Fe2+	0.000	0.000	0.000	0.000	0.000	0.000	0.000	0.000	0.000	0.000	0.000	0.000	0.000
	Mn	0.000	0.000	0.000	0.000	0.000	0.000	0.000	0.000	0.000	0.000	0.000	0.000	0.000
	Mg	0.000	0.000	0.000	0.000	0.000	0.000	0.000	0.000	0.000	0.000	0.000	0.000	0.000
	total M4 site	2.000	2.000	2.000	2.000	2.000	2.000	2.000	2.000	2.000	2.000	2.000	2.000	2.000
A site	Na	0.071	0.076	0.304	0.261	0.268	0.046	0.169	0.097	0.256	0.147	0.084	0.135	0.201
	K	0.019	0.013	0.059	0.069	0.066	0.040	0.039	0.028	0.064	0.050	0.035	0.054	0.059
	total A site	0.090	0.089	0.362	0.330	0.334	0.086	0.208	0.125	0.320	0.197	0.119	0.190	0.259
	Mg/Mg+Fe	0.686	0.672	0.525	0.514	0.527	0.643	0.621	0.669	0.532	0.629	0.672	0.646	0.595

APPENDIX A: Amphibole Compositions; Sample 62 U

		62.6a1.51	62.6a1.52	62.6a1.53	62.6a1.55
	SiO2	42.959	45.923	43.07	43.949
	Al2O3	12.414	12.878	12.222	12.999
	TiO2	0.43	0.387	0.344	0.302
	FeO	18.478	18.91	18.958	18.634
	MnO	0.231	0.198	0.238	0.257
	MgO	8.745	7.929	8.871	8.303
	CaO	12.164	11.69	11.774	11.873
	Na2O	1.175	1.174	1.185	1.106
	K2O	0.38	0.436	0.37	0.3
	Cl	0.07	0.103	0.113	0.22
	F	0.005	0	0	0
	Total	97.051	99.628	97.145	97.943
Tetrahedral	Si	6.449	6.693	6.435	6.517
	Al(IV)	1.551	1.307	1.565	1.483
	Fe3+	0.000	0.000	0.000	0.000
	total T site	8.000	8.000	8.000	8.000
Octahedral	Al(VI)	0.645	0.905	0.587	0.788
M1,M2,M3	Ti	0.049	0.042	0.039	0.034
	Fe3+	0.481	0.253	0.718	0.481
	Mg	1.957	1.723	1.976	1.835
	Fe2+	1.839	2.052	1.651	1.830
	Mn	0.029	0.024	0.030	0.032
	total M1-M3	5.000	5.000	5.000	5.000
Octahedral	Ca	1.956	1.826	1.885	1.886
M4	Na	0.044	0.174	0.115	0.114
	Fe2+	0.000	0.000	0.000	0.000
	Mn	0.000	0.000	0.000	0.000
	Mg	0.000	0.000	0.000	0.000
	total M4 site	2.000	2.000	2.000	2.000
A site	Na	0.298	0.157	0.228	0.204
	K	0.073	0.081	0.071	0.057
	total A site	0.371	0.238	0.298	0.261
	Mg/Mg+Fe	0.516	0.456	0.545	0.501

APPENDIX A: Amphibole Compositions: S143 Undeformed amphibolite

		143.1a1.2	143.1a1.3	143.1a2.1	143.1a2.2	143.1a2.3	143.1a2.4	143.1a3.1	143.1a3.2	143.1a3.3	143.1ukn	143.1a9.1	143.1a9.2	143.1a9.3
	SiO2	44.382	45.230	46.363	46.724	45.776	45.145	46.333	48.227	46.185	47.140	45.185	48.805	49.075
	Al2O3	9.167	9.231	9.193	8.970	8.905	9.121	8.716	6.797	8.580	8.010	9.619	6.863	6.262
	TiO2	0.713	0.738	0.535	0.438	0.604	0.735	0.588	0.434	0.607	0.378	0.472	0.375	0.368
	FeO	17.439	17.296	17.135	17.106	17.446	17.784	17.163	15.780	17.014	16.109	17.655	16.009	15.973
	MnO	0.226	0.227	0.266	0.277	0.269	0.320	0.252	0.326	0.292	0.203	0.290	0.224	0.232
	MgO	10.829	10.845	11.307	10.929	11.249	10.710	11.233	12.745	11.030	11.922	10.616	12.319	12.574
	CaO	11.853	11.979	11.794	12.036	11.806	11.714	11.904	12.168	11.742	12.100	11.912	12.194	12.131
	Na2O	1.045	1.085	0.925	0.823	1.094	1.118	0.904	0.714	0.984	0.839	1.012	0.691	0.773
	K2O	0.274	0.289	0.230	0.248	0.237	0.269	0.234	0.154	0.230	0.178	0.233	0.170	0.150
	Cl	0.144	0.146	0.131	0.140	0.132	0.132	0.000	0.073	0.109	0.000	0.183	0.107	0.074
	F	0.000	0.019	0.072	0.000	0.078	0.000	0.000	0.037	0.000	0.084	0.000	0.075	0.000
	Total	96.072	97.085	97.951	97.691	97.596	97.048	97.327	97.455	96.773	96.963	97.177	97.832	97.612
Tetrahedral	Si	6.659	6.721	6.771	6.867	6.738	6.703	6.817	7.041	6.848	6.942	6.697	7.119	7.166
	Al	1.341	1.279	1.229	1.133	1.262	1.297	1.183	0.959	1.152	1.058	1.303	0.881	0.834
	Fe3+	0.000	0.000	0.000	0.000	0.000	0.000	0.000	0.000	0.000	0.000	0.000	0.000	0.000
	total T site	8.000	8.000	8.000	8.000	8.000	8.000	8.000	8.000	8.000	8.000	8.000	8.000	8.000
Octahedral	Al	0.280	0.337	0.354	0.420	0.283	0.299	0.328	0.211	0.348	0.332	0.377	0.299	0.243
M1,M2,M3	Ti	0.080	0.082	0.059	0.048	0.067	0.082	0.065	0.048	0.068	0.042	0.053	0.041	0.040
	Fe3+	0.732	0.595	0.762	0.545	0.764	0.734	0.670	0.614	0.611	0.552	0.703	0.460	0.468
	Mg	2.422	2.402	2.462	2.394	2.469	2.371	2.464	2.774	2.438	2.617	2.346	2.679	2.737
	Fe2+	1.456	1.554	1.331	1.558	1.384	1.474	1.441	1.313	1.498	1.432	1.486	1.493	1.483
	Mn	0.029	0.029	0.033	0.034	0.034	0.040	0.031	0.040	0.037	0.025	0.036	0.028	0.029
	total M1-M3	5.000	5.000	5.000	5.000	5.000	5.000	5.000	5.000	5.000	5.000	5.000	5.000	5.000
Octahedral	Ca	1.905	1.907	1.846	1.895	1.862	1.863	1.876	1.903	1.865	1.909	1.892	1.906	1.898
M4	Na	0.095	0.093	0.154	0.105	0.138	0.137	0.124	0.097	0.135	0.091	0.108	0.094	0.102
	Fe2+	0.000	0.000	0.000	0.000	0.000	0.000	0.000	0.000	0.000	0.000	0.000	0.000	0.000
	Mn	0.000	0.000	0.000	0.000	0.000	0.000	0.000	0.000	0.000	0.000	0.000	0.000	0.000
	Mg	0.000	0.000	0.000	0.000	0.000	0.000	0.000	0.000	0.000	0.000	0.000	0.000	0.000
	total M4 site	2.000	2.000	2.000	2.000	2.000	2.000	2.000	2.000	2.000	2.000	2.000	2.000	2.000
A site	Na	0.209	0.220	0.107	0.130	0.174	0.185	0.134	0.106	0.148	0.149	0.182	0.101	0.117
	K	0.052	0.055	0.043	0.046	0.045	0.051	0.044	0.029	0.044	0.033	0.044	0.032	0.028
	total A site	0.262	0.274	0.150	0.176	0.219	0.236	0.178	0.134	0.192	0.182	0.226	0.133	0.145
	Mg/(Mg+Fe)	0.625	0.607	0.649	0.606	0.641	0.617	0.631	0.679	0.619	0.646	0.612	0.642	0.649

APPENDIX A: Amphibole Compositions: S143 Undeformed amphibolite

		143.1a10.1	143.1a10.2	143.1a10.3	143.1a4.1	143.1a4.2	143.1a4.3	143.1A4.4	143.1a4.4	143.1a4.5	143.3a2.1	143.3a2.2	143.3a2.3	143.3a2.4
	SiO2	46.570	45.731	46.684	47.695	47.289	46.177	54.295	54.007	46.847	43.788	42.468	41.941	44.994
	Al2O3	7.979	8.127	8.158	8.434	8.681	9.440	7.700	7.513	8.533	13.061	13.635	13.670	10.022
	TiO2	0.630	0.607	0.563	0.413	0.366	0.340	0.301	0.252	0.390	0.334	0.357	0.501	1.038
	FeO	17.340	17.593	17.401	16.342	15.985	16.471	14.257	13.967	16.380	18.257	18.582	18.947	18.227
	MnO	0.280	0.197	0.306	0.286	0.244	0.269	0.237	0.197	0.285	0.279	0.284	0.225	0.253
	MgO	11.355	11.375	11.524	11.556	11.642	11.159	10.017	10.091	11.205	9.096	8.753	8.297	10.423
	CaO	11.996	11.781	11.875	11.685	12.350	12.194	10.655	10.607	11.934	12.233	12.000	11.948	12.036
	Na2O	1.032	0.967	0.934	1.004	0.885	0.879	0.740	0.644	0.889	1.259	1.331	1.270	1.121
	K2O	0.216	0.197	0.225	0.210	0.215	0.228	0.205	0.235	0.241	0.345	0.360	0.542	0.318
	Cl	0.117	0.133	0.114	0.102	0.087	0.122	0.057	0.064	0.111	0.155	0.220	0.319	0.164
	F	0.000	0.061	0.007	0.048	0.000	0.007	0.099	0.011	0.079	0.000	0.061	0.048	0.104
	Total	97.515	96.769	97.791	97.775	97.744	97.286	98.563	97.588	96.894	98.807	98.051	97.708	98.700
Tetrahedral	Si	6.871	6.786	6.841	6.960	6.929	6.806	7.786	7.806	6.933	6.432	6.300	6.279	6.603
	Al	1.129	1.214	1.159	1.040	1.071	1.194	0.214	0.194	1.067	1.568	1.700	1.721	1.397
	Fe3+	0.000	0.000	0.000	0.000	0.000	0.000	0.000	0.000	0.000	0.000	0.000	0.000	0.000
	total T site	8.000	8.000	8.000	8.000	8.000	8.000	8.000	8.000	8.000	8.000	8.000	8.000	8.000
Octahedral M1,M2,M3	Al	0.258	0.208	0.250	0.411	0.428	0.446	1.087	1.086	0.421	0.694	0.684	0.691	0.337
	Ti	0.070	0.068	0.062	0.045	0.040	0.038	0.032	0.027	0.043	0.037	0.040	0.056	0.115
	Fe3+	0.603	0.809	0.749	0.561	0.394	0.526	0.000	0.000	0.473	0.526	0.672	0.612	0.668
	Mg	2.497	2.516	2.517	2.514	2.543	2.452	2.141	2.174	2.472	1.992	1.936	1.852	2.280
	Fe2+	1.537	1.375	1.384	1.433	1.565	1.504	1.739	1.712	1.554	1.717	1.634	1.760	1.569
	Mn	0.035	0.025	0.038	0.035	0.030	0.034	0.000	0.000	0.036	0.035	0.036	0.029	0.031
	total M1-M3	5.000	5.000	5.000	5.000	5.000	5.000	5.000	5.000	5.000	5.000	5.000	5.000	5.000
Octahedral M4	Ca	1.896	1.873	1.864	1.827	1.939	1.926	1.637	1.643	1.892	1.925	1.907	1.917	1.893
	Na	0.104	0.127	0.136	0.173	0.061	0.074	0.000	0.000	0.108	0.075	0.093	0.083	0.107
	Fe2+	0.000	0.000	0.000	0.000	0.000	0.000	0.427	0.432	0.000	0.000	0.000	0.000	0.000
	Mn	0.000	0.000	0.000	0.000	0.000	0.000	0.029	0.024	0.000	0.000	0.000	0.000	0.000
	Mg	0.000	0.000	0.000	0.000	0.000	0.000	0.000	0.000	0.000	0.000	0.000	0.000	0.000
	total M4 site	2.000	2.000	2.000	2.000	2.000	2.000	2.093	2.098	2.000	2.000	2.000	2.000	2.000
A site	Na	0.191	0.151	0.130	0.111	0.190	0.177	0.206	0.180	0.147	0.284	0.290	0.285	0.211
	K	0.041	0.037	0.042	0.039	0.040	0.043	0.038	0.043	0.046	0.065	0.068	0.104	0.060
	total A site	0.232	0.189	0.172	0.150	0.230	0.220	0.243	0.224	0.193	0.349	0.358	0.389	0.271
	Mg/(Mg+Fe)	0.619	0.647	0.645	0.637	0.619	0.620	0.552	0.559	0.614	0.537	0.542	0.513	0.592

APPENDIX A: Amphibole Compositions: S143 Undeformed amphibolite

		143.3a2.5	143.3a1.1	143.3a1.2	143.3a1.3	143.3a1.4	143.3a3.1	143.3a3.2	143.3a3.3	143.3a6.1	143.3a6.2	143.3a6.3	143.3a6.4	143.3a8.1
	SiO2	43.187	42.498	47.013	46.140	45.084	45.722	44.782	45.086	46.150	45.506	45.265	46.156	47.569
	Al2O3	10.849	12.660	9.560	9.510	9.508	9.043	9.662	9.677	8.753	9.704	9.129	8.489	7.839
	TiO2	1.062	0.462	0.656	0.620	0.818	0.770	0.915	0.681	0.669	0.778	0.745	0.744	0.522
	FeO	18.297	17.743	16.906	16.665	16.951	17.131	17.712	17.327	17.458	17.876	17.905	17.396	16.171
	MnO	0.322	0.239	0.272	0.313	0.307	0.280	0.246	0.270	0.321	0.256	0.288	0.278	0.258
	MgO	9.644	9.135	11.076	10.893	10.761	11.014	10.615	10.803	11.132	10.487	10.877	11.296	11.857
	CaO	12.124	11.812	12.031	12.148	12.000	12.076	12.033	11.975	11.987	11.769	11.878	11.983	12.163
	Na2O	1.063	1.000	0.924	0.957	0.961	0.895	0.982	0.975	0.991	1.148	1.112	0.975	0.796
	K2O	0.377	0.406	0.269	0.275	0.245	0.248	0.319	0.269	0.273	0.322	0.258	0.252	0.185
	Cl	0.200	0.400	0.107	0.149	0.111	0.121	0.155	0.141	0.141	0.147	0.141	0.130	0.100
	F	0.001	0.072	0.011	0.000	0.043	0.000	0.000	0.011	0.032	0.038	0.054	0.090	0.006
	Total	97.126	96.427	98.825	97.670	96.789	97.300	97.421	97.215	97.907	98.031	97.652	97.789	97.466
Tetrahedral	Si	6.474	6.393	6.817	6.796	6.707	6.759	6.638	6.674	6.784	6.698	6.686	6.792	6.978
	Al	1.526	1.607	1.183	1.204	1.293	1.241	1.362	1.326	1.216	1.302	1.314	1.208	1.022
	Fe3+	0.000	0.000	0.000	0.000	0.000	0.000	0.000	0.000	0.000	0.000	0.000	0.000	0.000
	total T site	8.000	8.000	8.000	8.000	8.000	8.000	8.000	8.000	8.000	8.000	8.000	8.000	8.000
Octahedral M1,M2,M3	Al	0.391	0.637	0.451	0.447	0.374	0.334	0.326	0.362	0.300	0.381	0.275	0.264	0.333
	Ti	0.120	0.052	0.072	0.069	0.092	0.086	0.102	0.076	0.074	0.086	0.083	0.082	0.058
	Fe3+	0.621	0.689	0.541	0.459	0.586	0.607	0.668	0.684	0.658	0.650	0.748	0.675	0.489
	Mg	2.155	2.048	2.394	2.392	2.387	2.427	2.346	2.384	2.439	2.301	2.395	2.478	2.593
	Fe2+	1.673	1.543	1.509	1.593	1.523	1.511	1.528	1.461	1.488	1.551	1.464	1.466	1.495
	Mn	0.041	0.030	0.033	0.039	0.039	0.035	0.031	0.034	0.040	0.032	0.036	0.035	0.032
	total M1-M3	5.000	5.000	5.000	5.000	5.000	5.000	5.000	5.000	5.000	5.000	5.000	5.000	5.000
Octahedral M4	Ca	1.947	1.904	1.869	1.917	1.913	1.913	1.911	1.899	1.888	1.856	1.880	1.889	1.912
	Na	0.053	0.096	0.131	0.083	0.087	0.087	0.089	0.101	0.112	0.144	0.120	0.111	0.088
	Fe2+	0.000	0.000	0.000	0.000	0.000	0.000	0.000	0.000	0.000	0.000	0.000	0.000	0.000
	Mn	0.000	0.000	0.000	0.000	0.000	0.000	0.000	0.000	0.000	0.000	0.000	0.000	0.000
	Mg	0.000	0.000	0.000	0.000	0.000	0.000	0.000	0.000	0.000	0.000	0.000	0.000	0.000
	total M4 site	2.000	2.000	2.000	2.000	2.000	2.000	2.000	2.000	2.000	2.000	2.000	2.000	2.000
A site	Na	0.256	0.195	0.129	0.191	0.190	0.169	0.193	0.179	0.170	0.183	0.198	0.167	0.138
	K	0.072	0.078	0.050	0.052	0.046	0.047	0.060	0.051	0.051	0.060	0.049	0.047	0.035
	total A site	0.328	0.273	0.179	0.242	0.236	0.216	0.254	0.230	0.222	0.244	0.247	0.215	0.173
	Mg/(Mg+Fe)	0.563	0.570	0.613	0.600	0.611	0.616	0.606	0.620	0.621	0.597	0.621	0.628	0.634

APPENDIX A: Amphibole Compositions: S143 Undeformed amphibolite

		143.3a8.2	143.3a8.4	143.3a9.1	143.3a9.2	143.3a10.1	143.3a10.2	143.3a10.3	143.3a10.4	143.5a10tr	143.5a10tr	143.5a10tr	143.5a10tr	143.5a10tr
	SiO2	47.710	46.764	46.717	48.464	46.731	46.753	47.133	47.242	47.407	46.837	51.312	45.698	44.261
	Al2O3	8.214	7.848	8.844	7.572	8.141	8.637	8.994	8.770	8.169	8.321	7.612	9.419	11.249
	TiO2	0.637	0.706	0.599	0.485	0.518	0.492	0.458	0.417	0.564	0.481	2.548	0.738	0.373
	FeO	17.136	17.379	17.467	16.065	16.896	16.204	16.683	16.211	16.793	15.955	16.127	17.105	17.500
	MnO	0.264	0.239	0.328	0.261	0.323	0.256	0.276	0.286	0.241	0.189	0.269	0.253	0.229
	MgO	11.243	11.407	11.302	12.396	11.397	11.649	11.217	11.328	11.917	11.506	9.792	10.956	9.980
	CaO	12.206	12.054	11.720	12.134	11.454	12.156	12.029	12.049	12.093	12.080	10.714	12.091	12.116
	Na2O	0.914	0.980	0.882	0.737	1.127	0.738	0.843	0.832	0.849	0.775	0.729	0.873	0.992
	K2O	0.198	0.216	0.195	0.160	0.220	0.199	0.260	0.204	0.192	0.215	0.177	0.266	0.249
	Cl	0.103	0.135	0.107	0.106	0.099	0.088	0.121	0.108	0.090	0.089	0.100	0.154	0.122
	F	0.011	0.000	0.000	0.091	0.013	0.000	0.000	0.000	0.005	0.000	0.030	0.011	0.109
	Total	98.636	97.728	98.161	98.471	96.919	97.172	98.014	97.447	98.320	96.448	99.410	97.564	97.180
Tetrahedral	Si	6.954	6.886	6.799	7.009	6.895	6.873	6.886	6.933	6.888	6.946	7.370	6.735	6.575
	Al	1.046	1.114	1.201	0.991	1.105	1.127	1.114	1.067	1.112	1.054	0.630	1.265	1.425
	Fe3+	0.000	0.000	0.000	0.000	0.000	0.000	0.000	0.000	0.000	0.000	0.000	0.000	0.000
	total T site	8.000	8.000	8.000	8.000	8.000	8.000	8.000	8.000	8.000	8.000	8.000	8.000	8.000
Octahedral	Al	0.366	0.248	0.316	0.300	0.311	0.369	0.434	0.450	0.287	0.400	0.658	0.371	0.545
M1,M2,M3	Ti	0.070	0.078	0.066	0.053	0.057	0.054	0.050	0.046	0.062	0.054	0.275	0.082	0.042
	Fe3+	0.433	0.586	0.814	0.589	0.694	0.573	0.526	0.460	0.662	0.444	0.000	0.612	0.606
	Mg	2.443	2.504	2.452	2.673	2.507	2.553	2.443	2.478	2.581	2.544	2.097	2.407	2.210
	Fe2+	1.656	1.554	1.312	1.354	1.390	1.419	1.512	1.530	1.379	1.534	1.970	1.496	1.568
	Mn	0.033	0.030	0.040	0.032	0.040	0.032	0.034	0.036	0.030	0.024	0.000	0.032	0.029
	total M1-M3	5.000	5.000	5.000	5.000	5.000	5.000	5.000	5.000	5.000	5.000	5.000	5.000	5.000
Octahedral	Ca	1.906	1.902	1.828	1.880	1.811	1.915	1.883	1.895	1.883	1.919	1.649	1.909	1.929
M4	Na	0.094	0.098	0.172	0.120	0.189	0.085	0.117	0.105	0.117	0.081	0.203	0.091	0.071
	Fe2+	0.000	0.000	0.000	0.000	0.000	0.000	0.000	0.000	0.000	0.000	0.079	0.000	0.000
	Mn	0.000	0.000	0.000	0.000	0.000	0.000	0.000	0.000	0.000	0.000	0.033	0.000	0.000
	Mg	0.000	0.000	0.000	0.000	0.000	0.000	0.000	0.000	0.000	0.000	0.000	0.000	0.000
	total M4 site	2.000	2.000	2.000	2.000	2.000	2.000	2.000	2.000	2.000	2.000	1.963	2.000	2.000
A site	Na	0.165	0.181	0.076	0.087	0.133	0.125	0.122	0.131	0.122	0.142	0.000	0.159	0.214
	K	0.037	0.041	0.036	0.030	0.041	0.037	0.048	0.038	0.036	0.041	0.032	0.050	0.047
	total A site	0.201	0.222	0.113	0.116	0.174	0.162	0.170	0.170	0.157	0.183	0.032	0.209	0.261
	Mg/(Mg+Fe)	0.596	0.617	0.651	0.664	0.643	0.643	0.618	0.618	0.652	0.624	0.516	0.617	0.585

APPENDIX A: Amphibole Compositions: S143 Undeformed amphibolite

		143.5a11tr	143.5a11tr	143.5a11tr	143.5a11tr	143.5a11tr	143.5a14tr	143.5a14tr	143.5a14tr	143.5a2.1	143.5a2.2	143.5a3.1	143.5a3.2	143.5a3.3
	SiO2	48.145	44.788	46.495	46.203	45.861	47.059	47.454	46.389	42.074	44.616	44.633	43.192	46.720
	Al2O3	10.645	9.542	8.661	9.182	9.374	8.442	8.508	8.628	13.293	11.205	9.599	10.167	8.206
	TiO2	0.158	0.934	0.633	0.706	0.368	0.487	0.366	0.600	0.372	0.379	0.718	0.753	0.634
	FeO	16.485	18.103	16.880	16.794	16.610	16.603	16.249	16.582	18.745	18.101	17.830	18.327	18.114
	MnO	0.163	0.299	0.305	0.225	0.280	0.239	0.226	0.263	0.261	0.267	0.317	0.284	0.297
	MgO	8.697	10.548	11.291	11.090	11.060	11.603	11.428	11.414	9.088	9.753	10.399	10.063	11.142
	CaO	9.766	11.779	11.902	12.026	12.193	12.206	12.088	12.285	11.357	12.069	11.892	11.834	11.904
	Na2O	2.271	1.081	0.925	0.961	0.898	0.927	0.749	0.884	1.151	1.156	1.163	1.200	0.924
	K2O	0.241	0.373	0.232	0.271	0.224	0.226	0.204	0.245	0.285	0.277	0.286	0.368	0.257
	Cl	0.072	0.159	0.101	0.146	0.088	0.098	0.090	0.119	0.149	0.100	0.145	0.201	0.132
	F	0.002	0.000	0.053	0.000	0.000	0.050	0.000	0.012	0.000	0.000	0.000	0.038	0.000
	Total	96.645	97.606	97.478	97.604	96.956	97.940	97.362	97.421	96.775	97.923	96.982	96.427	98.330
Tetrahedral	Si	7.137	6.627	6.839	6.800	6.790	6.892	6.965	6.844	6.253	6.590	6.656	6.506	6.834
	Al	0.863	1.373	1.161	1.200	1.210	1.108	1.035	1.156	1.747	1.410	1.344	1.494	1.166
	Fe3+	0.000	0.000	0.000	0.000	0.000	0.000	0.000	0.000	0.000	0.000	0.000	0.000	0.000
	total T site	8.000	8.000	8.000	8.000	8.000	8.000	8.000	8.000	8.000	8.000	8.000	8.000	8.000
Octahedral M1,M2,M3	Al	0.996	0.292	0.340	0.393	0.426	0.350	0.437	0.344	0.582	0.541	0.344	0.310	0.248
	Ti	0.018	0.104	0.070	0.078	0.041	0.054	0.040	0.067	0.042	0.042	0.081	0.085	0.070
	Fe3+	0.031	0.758	0.623	0.532	0.533	0.514	0.465	0.496	1.079	0.581	0.648	0.773	0.738
	Mg	1.922	2.327	2.476	2.433	2.441	2.533	2.500	2.510	2.014	2.148	2.312	2.260	2.430
	Fe2+	2.012	1.483	1.453	1.535	1.523	1.519	1.530	1.550	1.251	1.655	1.576	1.536	1.478
	Mn	0.020	0.037	0.038	0.028	0.035	0.030	0.028	0.033	0.033	0.033	0.040	0.036	0.037
	total M1-M3	5.000	5.000	5.000	5.000	5.000	5.000	5.000	5.000	5.000	5.000	5.000	5.000	5.000
Octahedral M4	Ca	1.551	1.867	1.876	1.896	1.934	1.915	1.901	1.942	1.809	1.910	1.900	1.910	1.866
	Na	0.449	0.133	0.124	0.104	0.066	0.085	0.099	0.058	0.191	0.090	0.100	0.090	0.134
	Fe2+	0.000	0.000	0.000	0.000	0.000	0.000	0.000	0.000	0.000	0.000	0.000	0.000	0.000
	Mn	0.000	0.000	0.000	0.000	0.000	0.000	0.000	0.000	0.000	0.000	0.000	0.000	0.000
	Mg	0.000	0.000	0.000	0.000	0.000	0.000	0.000	0.000	0.000	0.000	0.000	0.000	0.000
	total M4 site	2.000	2.000	2.000	2.000	2.000	2.000	2.000	2.000	2.000	2.000	2.000	2.000	2.000
A site	Na	0.204	0.178	0.139	0.171	0.192	0.179	0.114	0.195	0.140	0.241	0.236	0.260	0.128
	K	0.046	0.070	0.044	0.051	0.042	0.042	0.038	0.046	0.054	0.052	0.054	0.071	0.048
	total A site	0.249	0.248	0.183	0.222	0.234	0.221	0.152	0.241	0.194	0.293	0.291	0.331	0.176
	Mg/(Mg+Fe)	0.489	0.611	0.630	0.613	0.616	0.625	0.620	0.618	0.617	0.565	0.595	0.595	0.622

APPENDIX A: Amphibole Compositions: S143 Undeformed amphibolite

		143.5a5.1	143.5a5.2	143.5a5.3	143.5a1.1	143.5a1.2	143.5a1.3	143.5a1.4	143.5a1.5	143.5a4.1	143.5a4.2	143.5a4.3	143.5a7.1	143.5a7.2
	SiO2	46.246	46.439	45.647	46.878	45.822	47.123	47.198	46.941	47.218	46.203	46.798	43.272	46.938
	Al2O3	8.187	8.519	8.309	8.471	9.413	8.370	8.406	8.822	8.171	8.507	8.354	13.080	8.746
	TiO2	0.548	0.586	0.542	0.518	0.702	0.433	0.578	0.349	0.575	0.512	0.591	0.309	0.532
	FeO	18.166	18.284	17.533	16.802	17.971	16.747	17.364	16.639	18.148	17.847	17.822	18.536	17.410
	MnO	0.227	0.251	0.280	0.204	0.236	0.236	0.304	0.261	0.318	0.313	0.286	0.244	0.327
	MgO	11.113	10.986	11.491	11.553	10.495	11.679	11.383	11.596	11.219	11.004	11.054	8.739	11.138
	CaO	12.088	11.826	12.183	12.255	11.979	12.206	12.082	12.326	11.751	11.971	11.970	11.901	12.180
	Na2O	0.992	1.008	0.928	0.840	1.043	0.824	0.936	0.887	0.988	1.009	0.998	1.245	0.921
	K2O	0.221	0.266	0.199	0.213	0.287	0.227	0.201	0.233	0.238	0.231	0.234	0.387	0.253
	Cl	0.166	0.157	0.125	0.123	0.189	0.093	0.120	0.087	0.130	0.137	0.119	0.212	0.135
	F	0.004	0.046	0.000	0.013	0.019	0.041	0.034	0.000	0.024	0.000	0.000	0.083	0.008
	Total	97.958	98.368	97.237	97.870	98.156	97.979	98.606	98.141	98.780	97.734	98.226	98.008	98.588
Tetrahedral	Si	6.812	6.798	6.753	6.871	6.745	6.889	6.872	6.855	6.862	6.809	6.858	6.418	6.849
	Al	1.188	1.202	1.247	1.129	1.255	1.111	1.128	1.145	1.138	1.191	1.142	1.582	1.151
	Fe3+	0.000	0.000	0.000	0.000	0.000	0.000	0.000	0.000	0.000	0.000	0.000	0.000	0.000
	total T site	8.000	8.000	8.000	8.000	8.000	8.000	8.000	8.000	8.000	8.000	8.000	8.000	8.000
Octahedral M1,M2,M3	Al	0.233	0.268	0.201	0.334	0.378	0.331	0.314	0.373	0.262	0.287	0.300	0.704	0.354
	Ti	0.061	0.065	0.060	0.057	0.078	0.048	0.063	0.038	0.063	0.057	0.065	0.034	0.058
	Fe3+	0.694	0.759	0.760	0.554	0.592	0.586	0.616	0.544	0.768	0.678	0.626	0.596	0.564
	Mg	2.440	2.398	2.534	2.524	2.303	2.545	2.471	2.524	2.431	2.418	2.415	1.932	2.423
	Fe2+	1.544	1.480	1.409	1.506	1.620	1.461	1.498	1.488	1.437	1.522	1.559	1.703	1.561
	Mn	0.028	0.031	0.035	0.025	0.029	0.029	0.037	0.032	0.039	0.039	0.035	0.031	0.040
	total M1-M3	5.000	5.000	5.000	5.000	5.000	5.000	5.000	5.000	5.000	5.000	5.000	5.000	5.000
Octahedral M4	Ca	1.908	1.855	1.931	1.924	1.889	1.912	1.885	1.928	1.830	1.890	1.879	1.891	1.904
	Na	0.092	0.145	0.069	0.076	0.111	0.088	0.115	0.072	0.170	0.110	0.121	0.109	0.096
	Fe2+	0.000	0.000	0.000	0.000	0.000	0.000	0.000	0.000	0.000	0.000	0.000	0.000	0.000
	Mn	0.000	0.000	0.000	0.000	0.000	0.000	0.000	0.000	0.000	0.000	0.000	0.000	0.000
	Mg	0.000	0.000	0.000	0.000	0.000	0.000	0.000	0.000	0.000	0.000	0.000	0.000	0.000
	total M4 site	2.000	2.000	2.000	2.000	2.000	2.000	2.000	2.000	2.000	2.000	2.000	2.000	2.000
A site	Na	0.191	0.141	0.197	0.163	0.187	0.145	0.149	0.180	0.108	0.179	0.163	0.249	0.165
	K	0.042	0.050	0.038	0.040	0.054	0.042	0.037	0.043	0.044	0.043	0.044	0.073	0.047
	total A site	0.232	0.191	0.235	0.203	0.241	0.188	0.186	0.223	0.152	0.222	0.207	0.322	0.212
	Mg/(Mg+Fe)	0.612	0.618	0.643	0.626	0.587	0.635	0.623	0.629	0.628	0.614	0.608	0.532	0.608

APPENDIX A: Amphibole Compositions: S143 Undeformed amphibolite

		143.5a7.3	143.5a7.4	143.5a1.5	143.6a7.1	143.6a7.2	143.6a7.3	143.6a7.4	143.6a5.1	143.6a5.2	143.6a5.3	143.6a8.1	143.6a8.2	143.6a8.3
	SiO2	44.115	46.437	55.257	39.732	46.017	44.477	47.127	42.890	43.557	47.526	47.455	47.045	45.423
	Al2O3	10.591	8.721	27.809	15.987	9.211	9.489	8.275	13.300	13.536	9.012	8.292	9.403	10.085
	TiO2	0.649	0.596	0.000	0.378	0.704	0.763	0.681	0.277	0.286	0.670	0.554	0.639	0.769
	FeO	18.219	17.217	0.000	19.667	17.883	18.273	17.612	19.423	18.377	17.238	16.745	16.996	18.104
	MnO	0.236	0.310	0.000	0.275	0.313	0.266	0.290	0.229	0.267	0.222	0.322	0.262	0.283
	MgO	9.791	11.244	0.000	6.849	10.864	10.432	11.339	8.843	8.628	11.163	11.251	10.664	10.182
	CaO	11.940	12.074	10.390	11.824	11.850	11.762	11.815	11.072	12.001	12.073	11.943	12.098	11.918
	Na2O	1.118	1.037	5.941	1.393	1.022	1.165	1.032	1.183	1.325	0.943	0.841	0.987	1.227
	K2O	0.337	0.237	0.026	0.547	0.271	0.295	0.244	0.303	0.362	0.243	0.254	0.290	0.320
	Cl	0.170	0.137	0.001	0.328	0.117	0.128	0.143	0.129	0.196	0.157	0.116	0.129	0.193
	F	0.006	0.099	0.015	0.000	0.090	0.040	0.000	0.000	0.000	0.043	0.010	0.000	0.043
	Total	97.172	98.109	99.439	96.980	98.342	97.090	98.558	97.649	98.535	99.290	97.783	98.513	98.547
Tetrahedral	Si	6.583	6.815	8.160	6.024	6.735	6.624	6.863	6.308	6.421	6.873	6.956	6.876	6.676
	Al	1.417	1.185	0.000	1.976	1.265	1.376	1.137	1.692	1.579	1.127	1.044	1.124	1.324
	Fe3+	0.000	0.000	0.000	0.000	0.000	0.000	0.000	0.000	0.000	0.000	0.000	0.000	0.000
	total T site	8.000	8.000	8.160	8.000	8.000	8.000	8.000	8.000	8.000	8.000	8.000	8.000	8.000
Octahedral	Al	0.446	0.323	4.840	0.880	0.324	0.289	0.283	0.613	0.773	0.409	0.388	0.496	0.423
M1,M2,M3	Ti	0.073	0.066	0.000	0.043	0.077	0.085	0.075	0.031	0.032	0.073	0.061	0.070	0.085
	Fe3+	0.620	0.595	0.000	0.654	0.728	0.770	0.681	1.134	0.504	0.522	0.497	0.364	0.567
	Mg	2.178	2.460	0.000	1.548	2.371	2.316	2.462	1.939	1.896	2.407	2.458	2.324	2.231
	Fe2+	1.653	1.518	0.160	1.840	1.461	1.506	1.464	1.255	1.761	1.562	1.556	1.713	1.658
	Mn	0.030	0.039	0.000	0.035	0.039	0.034	0.036	0.029	0.033	0.027	0.040	0.032	0.035
	total M1-M3	5.000	5.000	5.000	5.000	5.000	5.000	5.000	5.000	5.000	5.000	5.000	5.000	5.000
Octahedral	Ca	1.909	1.898	1.644	1.921	1.858	1.877	1.843	1.745	1.896	1.871	1.876	1.895	1.877
M4	Na	0.091	0.102	0.000	0.079	0.142	0.123	0.157	0.255	0.104	0.129	0.124	0.105	0.123
	Fe2+	0.000	0.000	5.994	0.000	0.000	0.000	0.000	0.000	0.000	0.000	0.000	0.000	0.000
	Mn	0.000	0.000	0.000	0.000	0.000	0.000	0.000	0.000	0.000	0.000	0.000	0.000	0.000
	Mg	0.000	0.000	0.000	0.000	0.000	0.000	0.000	0.000	0.000	0.000	0.000	0.000	0.000
	total M4 site	2.000	2.000	7.638	2.000	2.000	2.000	2.000	2.000	2.000	2.000	2.000	2.000	2.000
A site	Na	0.232	0.193	1.701	0.330	0.148	0.213	0.135	0.082	0.274	0.135	0.115	0.174	0.227
	K	0.064	0.044	0.005	0.106	0.051	0.056	0.045	0.057	0.068	0.045	0.047	0.054	0.060
	total A site	0.297	0.238	1.706	0.436	0.199	0.269	0.180	0.139	0.342	0.180	0.162	0.228	0.287
	Mg/(Mg+Fe)	0.568	0.618	0.000	0.457	0.619	0.606	0.627	0.607	0.518	0.606	0.612	0.576	0.574

APPENDIX A: Amphibole Compositions: S143 Undeformed amphibolite

		143.6a8.4	143.6a8.5	143.6a12.1	143.6a12.2	143.6a12.3	143.6altr	143.6altr	143.6altr	143.6altr	143.6altr	143.6ukntr	143.6ukntr	143.6ukntr
	SiO2	45.570	57.393	45.253	46.262	45.566	47.136	46.290	46.446	45.982	46.127	54.704	55.433	54.814
	Al2O3	10.303	26.874	10.481	8.416	9.404	8.371	8.062	8.051	8.050	7.949	27.936	27.852	28.280
	TiO2	0.816	0.013	0.322	0.560	0.705	0.684	0.617	0.695	0.651	0.648	0.020	0.008	0.021
	FeO	17.701	0.310	17.234	16.679	17.386	17.332	17.303	17.502	17.509	17.671	0.097	0.101	0.077
	MnO	0.223	0.020	0.278	0.306	0.339	0.299	0.313	0.322	0.299	0.248	0.006	0.014	0.000
	MgO	10.077	0.006	10.520	11.481	10.572	11.273	11.359	11.320	11.179	11.530	0.007	0.000	0.000
	CaO	11.983	9.054	12.039	11.915	12.085	12.030	11.915	11.955	11.963	11.992	10.501	10.684	10.456
	Na2O	1.156	6.526	1.029	0.895	0.930	0.827	0.931	1.005	0.984	1.038	5.807	5.804	5.785
	K2O	0.315	0.042	0.231	0.279	0.270	0.264	0.247	0.201	0.270	0.219	0.036	0.031	0.014
	Cl	0.169	0.000	0.088	0.123	0.120	0.123	0.145	0.096	0.108	0.114	0.000	0.006	0.002
	F	0.060	0.000	0.000	0.028	0.000	0.031	0.015	0.000	0.000	0.035	0.030	0.000	0.003
	Total	98.373	100.238	97.475	96.944	97.377	98.370	97.197	97.593	96.995	97.571	99.144	99.933	99.452
Tetrahedral	Si	6.706	8.349	6.672	6.840	6.749	6.880	6.844	6.843	6.830	6.802	8.105	8.156	8.077
	Al	1.294	0.000	1.328	1.160	1.251	1.120	1.156	1.157	1.170	1.198	0.000	0.000	0.000
	Fe3+	0.000	0.000	0.000	0.000	0.000	0.000	0.000	0.000	0.000	0.000	0.000	0.000	0.000
	total T site	8.000	8.349	8.000	8.000	8.000	8.000	8.000	8.000	8.000	8.000	8.105	8.156	8.077
Octahedral	Al	0.493	4.608	0.493	0.307	0.391	0.320	0.249	0.240	0.239	0.183	4.878	4.829	4.911
M1,M2,M3	Ti	0.090	0.001	0.036	0.062	0.079	0.075	0.069	0.077	0.073	0.072	0.002	0.001	0.002
	Fe3+	0.453	0.000	0.624	0.645	0.549	0.605	0.681	0.664	0.643	0.744	0.000	0.000	0.000
	Mg	2.211	0.001	2.312	2.531	2.334	2.453	2.504	2.486	2.475	2.535	0.002	0.000	0.000
	Fe2+	1.725	0.390	1.501	1.418	1.605	1.511	1.458	1.492	1.532	1.435	0.118	0.170	0.086
	Mn	0.028	0.000	0.035	0.038	0.043	0.037	0.039	0.040	0.038	0.031	0.000	0.000	0.000
	total M1-M3	5.000	5.000	5.000	5.000	5.000	5.000	5.000	5.000	5.000	5.000	5.000	5.000	5.000
Octahedral	Ca	1.889	1.411	1.902	1.887	1.918	1.881	1.887	1.887	1.904	1.895	1.667	1.684	1.651
M4	Na	0.111	0.000	0.098	0.113	0.082	0.119	0.113	0.113	0.096	0.105	0.000	0.000	0.000
	Fe2+	0.000	5.628	0.000	0.000	0.000	0.000	0.000	0.000	0.000	0.000	5.996	6.015	5.950
	Mn	0.000	0.002	0.000	0.000	0.000	0.000	0.000	0.000	0.000	0.000	0.001	0.002	0.000
	Mg	0.000	0.000	0.000	0.000	0.000	0.000	0.000	0.000	0.000	0.000	0.000	0.000	0.000
	total M4 site	2.000	7.042	2.000	2.000	2.000	2.000	2.000	2.000	2.000	2.000	7.664	7.701	7.600
A site	Na	0.219	1.841	0.196	0.144	0.185	0.115	0.154	0.174	0.187	0.191	1.668	1.656	1.653
	K	0.059	0.008	0.043	0.053	0.051	0.049	0.047	0.038	0.051	0.041	0.007	0.006	0.003
	total A site	0.278	1.849	0.239	0.197	0.236	0.164	0.201	0.212	0.238	0.233	1.675	1.661	1.655
	Mg/(Mg+Fe)	0.562	0.003	0.606	0.641	0.593	0.619	0.632	0.625	0.618	0.638	0.013	0.000	0.000

APPENDIX A: Amphibole Compositions: S143 Unde

		143.6a2tr	143.6a2tr	143.6a2tr
	SiO2	45.972	45.243	46.757
	Al2O3	9.245	9.210	7.684
	TiO2	0.739	0.751	0.591
	FeO	17.522	17.489	17.291
	MnO	0.219	0.265	0.299
	MgO	10.740	10.692	11.315
	CaO	11.905	11.976	12.113
	Na2O	1.039	1.061	0.891
	K2O	0.306	0.301	0.242
	Cl	0.158	0.133	0.127
	F	0.053	0.056	0.014
	Total	97.898	97.177	97.324
Tetrahedral	Si	6.770	6.726	6.920
	Al	1.230	1.274	1.080
	Fe3+	0.000	0.000	0.000
	total T site	8.000	8.000	8.000
Octahedral	Al	0.375	0.339	0.260
M1,M2,M3	Ti	0.082	0.084	0.066
	Fe3+	0.580	0.590	0.545
	Mg	2.358	2.369	2.496
	Fe2+	1.578	1.584	1.595
	Mn	0.027	0.033	0.037
	total M1-M3	5.000	5.000	5.000
Octahedral	Ca	1.878	1.907	1.921
M4	Na	0.122	0.093	0.079
	Fe2+	0.000	0.000	0.000
	Mn	0.000	0.000	0.000
	Mg	0.000	0.000	0.000
	total M4 site	2.000	2.000	2.000
A site	Na	0.175	0.213	0.176
	K	0.057	0.057	0.046
	total A site	0.233	0.270	0.222
	Mg/(Mg+Fe)	0.599	0.599	0.610

APPENDIX A: Amphibole Compositions; S81 Full Strain Transition Undeformed Section

		8AM2.1	8AM2.2	AM3.2	8AM3.2	8AM3.3	8AM3.4	8AM3.4	TR1AM1	TR1AM1	TR2AM1	TR2AM1	TR2AM1	TR2AM1
	SiO2	46.110	45.420	46.200	45.530	45.900	46.960	46.300	46.250	47.130	47.480	47.900	47.330	47.680
	Al2O3	8.590	9.520	9.160	9.670	9.540	8.170	9.090	8.370	8.990	8.430	8.090	7.310	9.060
	TiO2	0.780	0.670	0.680	0.720	0.790	0.770	0.830	0.620	0.590	0.710	0.650	0.660	0.420
	FeO	15.920	15.740	15.650	16.420	16.040	15.330	16.130	14.940	14.900	15.790	14.910	14.910	14.780
	MnO	0.270	0.300	0.250	0.370	0.330	0.270	0.270	0.270	0.370	0.340	0.390	0.330	0.250
	MgO	10.950	11.390	11.250	10.590	11.270	11.670	11.670	11.970	12.090	11.750	12.190	12.320	11.910
	CaO	11.730	11.040	11.860	11.710	11.810	11.890	11.850	12.080	12.190	11.950	12.120	11.810	11.900
	Na2O	1.110	0.850	0.950	0.980	1.050	0.940	1.060	0.930	0.820	0.930	0.840	0.790	0.830
	K2O	0.270	0.250	0.270	0.270	0.270	0.220	0.240	0.230	0.230	0.270	0.210	0.200	0.230
	Cl	0.182	0.107	0.171	0.134	0.089	0.099	0.096	0.194	0.165	0.184	0.183	0.117	0.096
	F	0.076	0.142	0.242	0.119	0.095	0.101	0.118	0.717	0.132	0.003	0.05	0	0
	Total	95.988	95.429	96.683	96.513	97.184	96.420	97.654	96.571	97.607	97.837	97.533	95.777	97.156
Tetrahedral	Si	6.915	6.745	6.858	6.780	6.763	6.968	6.782	6.899	6.887	6.939	7.005	7.027	6.964
	Al	1.085	1.255	1.142	1.220	1.237	1.032	1.218	1.101	1.113	1.061	0.995	0.973	1.036
	Fe3+	0.000	0.000	0.000	0.000	0.000	0.000	0.000	0.000	0.000	0.000	0.000	0.000	0.000
	total T site	8.000	8.000	8.000	8.000	8.000	8.000	8.000	8.000	8.000	8.000	8.000	8.000	8.000
Octahedral	Al	0.433	0.411	0.460	0.477	0.419	0.397	0.351	0.371	0.435	0.390	0.399	0.307	0.524
M1,M2,M3	Ti	0.088	0.075	0.076	0.081	0.088	0.086	0.091	0.070	0.065	0.078	0.071	0.074	0.046
	Fe3+	0.332	0.889	0.433	0.511	0.563	0.371	0.619	0.417	0.457	0.459	0.378	0.496	0.417
	Mg	2.448	2.522	2.490	2.351	2.475	2.581	2.548	2.662	2.634	2.560	2.658	2.727	2.593
	Fe2+	1.664	1.066	1.510	1.534	1.413	1.531	1.357	1.447	1.364	1.471	1.446	1.355	1.389
	Mn	0.034	0.038	0.031	0.047	0.041	0.034	0.033	0.034	0.046	0.042	0.048	0.042	0.031
	total M1-M3	5.000	5.000	5.000	5.000	5.000	5.000	5.000	5.000	5.000	5.000	5.000	5.000	5.000
Octahedral	Ca	1.885	1.757	1.886	1.868	1.864	1.890	1.860	1.931	1.908	1.871	1.899	1.879	1.862
M4	Na	0.115	0.243	0.114	0.132	0.136	0.110	0.140	0.069	0.092	0.129	0.101	0.121	0.138
	Fe2+	0.000	0.000	0.000	0.000	0.000	0.000	0.000	0.000	0.000	0.000	0.000	0.000	0.000
	Mn	0.000	0.000	0.000	0.000	0.000	0.000	0.000	0.000	0.000	0.000	0.000	0.000	0.000
	Mg	0.000	0.000	0.000	0.000	0.000	0.000	0.000	0.000	0.000	0.000	0.000	0.000	0.000
	total M4 site	2.000	2.000	2.000	2.000	2.000	2.000	2.000	2.000	2.000	2.000	2.000	2.000	2.000
A site	Na	0.207	0.001	0.160	0.151	0.164	0.161	0.161	0.200	0.141	0.135	0.137	0.106	0.097
	K	0.052	0.047	0.051	0.051	0.051	0.042	0.045	0.044	0.043	0.050	0.039	0.038	0.043
	total A site	0.259	0.049	0.211	0.203	0.215	0.202	0.206	0.243	0.184	0.185	0.176	0.144	0.140
	Mg/Mg+Fe2+	0.595	0.703	0.622	0.605	0.637	0.628	0.653	0.648	0.659	0.635	0.648	0.668	0.651

APPENDIX A: Amphibole Compositions; S81 Full Strain Transition Undeformed Section

		TR2AM1	TR2AM1	8AM5.1	8AM5.2	8AM6.1	8AM6.2	8AM6.3	8AM6.4	TR1AM7	TR1AM7	TR1AM7	TR1AM7	TR1AM7
	SiO2	43.250	44.500	46.000	47.180	51.080	51.730	48.150	49.570	46.460	46.120	46.380	46.680	46.490
	Al2O3	15.860	11.980	9.500	8.690	3.940	3.800	7.960	6.230	7.810	8.410	8.630	8.520	8.980
	TiO2	0.520	0.480	0.560	0.710	0.370	0.370	0.650	0.510	0.700	0.670	0.680	0.670	0.670
	FeO	14.840	15.120	15.270	15.470	13.490	14.010	15.240	14.720	15.550	16.330	16.080	16.090	16.060
	MnO	0.260	0.290	0.320	0.300	0.340	0.440	0.330	0.390	0.330	0.260	0.310	0.220	0.280
	MgO	9.690	11.170	11.070	11.800	14.870	14.710	12.220	13.490	12.290	12.030	11.390	11.290	11.490
	CaO	10.800	11.550	11.930	11.660	12.220	11.900	11.910	12.040	11.800	11.850	11.830	11.810	11.690
	Na2O	0.600	0.950	0.930	0.810	0.500	0.450	0.800	0.590	0.980	1.020	0.950	1.090	1.030
	K2O	0.260	0.250	0.250	0.230	0.080	0.060	0.180	0.110	0.220	0.200	0.240	0.240	0.250
	Cl	0.136	0.092	0.082	0.091	0.124	0.13	0.165	0.177	0.15	0.122	0.121	0.134	0.171
	F	0.02	0.259	0.122	0.154	0.173	0.049	0.047	0	0.061	0	0.165	0	0.032
	Total	96.236	96.641	96.034	97.095	97.187	97.649	97.652	97.827	96.351	97.012	96.776	96.744	97.143
Tetrahedral	Si	6.288	6.535	6.861	6.912	7.400	7.430	7.013	7.156	6.879	6.786	6.871	6.920	6.839
	Al	1.712	1.465	1.139	1.088	0.600	0.570	0.987	0.844	1.121	1.214	1.129	1.080	1.161
	Fe3+	0.000	0.000	0.000	0.000	0.000	0.000	0.000	0.000	0.000	0.000	0.000	0.000	0.000
	total T site	8.000	8.000	8.000	8.000	8.000	8.000	8.000	8.000	8.000	8.000	8.000	8.000	8.000
Octahedral	Al	1.006	0.609	0.531	0.412	0.072	0.074	0.379	0.216	0.242	0.245	0.378	0.408	0.396
M1,M2,M3	Ti	0.057	0.053	0.063	0.078	0.040	0.040	0.071	0.055	0.078	0.074	0.076	0.075	0.074
	Fe3+	1.009	0.798	0.353	0.586	0.499	0.617	0.490	0.606	0.656	0.755	0.526	0.413	0.592
	Mg	2.100	2.445	2.461	2.577	3.211	3.150	2.653	2.903	2.713	2.639	2.515	2.495	2.520
	Fe2+	0.795	1.059	1.551	1.309	1.136	1.066	1.366	1.171	1.270	1.254	1.466	1.582	1.384
	Mn	0.032	0.036	0.040	0.037	0.042	0.054	0.041	0.048	0.041	0.032	0.039	0.028	0.035
	total M1-M3	5.000	5.000	5.000	5.000	5.000	5.000	5.000	5.000	5.000	5.000	5.000	5.000	5.000
Octahedral	Ca	1.682	1.817	1.906	1.830	1.897	1.831	1.858	1.862	1.872	1.868	1.878	1.876	1.842
M4	Na	0.169	0.183	0.094	0.170	0.103	0.125	0.142	0.138	0.128	0.132	0.122	0.124	0.158
	Fe2+	0.000	0.000	0.000	0.000	0.000	0.000	0.000	0.000	0.000	0.000	0.000	0.000	0.000
	Mn	0.000	0.000	0.000	0.000	0.000	0.000	0.000	0.000	0.000	0.000	0.000	0.000	0.000
	Mg	0.000	0.000	0.000	0.000	0.000	0.000	0.000	0.000	0.000	0.000	0.000	0.000	0.000
	total M4 site	1.852	2.000	2.000	2.000	2.000	1.957	2.000	2.000	2.000	2.000	2.000	2.000	2.000
A site	Na	0.000	0.088	0.175	0.060	0.037	0.000	0.084	0.027	0.153	0.159	0.151	0.189	0.136
	K	0.048	0.047	0.048	0.043	0.015	0.011	0.033	0.020	0.042	0.038	0.045	0.045	0.047
	total A site	0.048	0.135	0.223	0.103	0.052	0.011	0.118	0.048	0.195	0.197	0.196	0.234	0.183
	Mg/Mg+Fe2+	0.725	0.698	0.613	0.663	0.739	0.747	0.660	0.713	0.681	0.678	0.632	0.612	0.645

APPENDIX A: Amphibole Compositions; S81 Full Strain Transition Undeformed Section

		TR1AM7	8AM8.2	TR1AM9	TR1AM9	TR1AM9	TR1AM9	TR1AM9	8AM10.	8AM10.	S1AM6	S1AM6	S1AM6	S1AM6
	SiO2	47.070	47.870	47.960	46.690	47.040	47.760	47.350	45.490	46.630	45.064	45.168	45.856	46.562
	Al2O3	7.810	8.400	7.220	7.960	8.250	8.070	8.080	8.570	8.920	10.810	10.738	10.605	9.073
	TiO2	0.670	0.730	0.610	0.790	0.720	0.730	0.590	0.780	0.740	0.669	0.955	0.789	0.678
	FeO	15.860	15.300	14.650	15.540	15.590	14.820	14.380	15.740	16.200	17.856	17.248	17.949	16.604
	MnO	0.380	0.320	0.180	0.320	0.320	0.300	0.320	0.330	0.340	0.220	0.257	0.235	0.310
	MgO	12.250	12.130	12.640	12.160	11.740	11.760	12.400	11.860	11.420	10.301	10.461	10.612	11.679
	CaO	11.900	12.050	12.210	11.700	11.640	11.810	12.090	11.610	11.680	11.663	11.777	11.895	11.777
	Na2O	0.950	0.870	0.780	0.920	0.980	0.800	0.820	1.010	0.900	1.162	1.266	1.157	1.066
	K2O	0.180	0.230	0.170	0.210	0.220	0.210	0.200	0.220	0.230	0.317	0.289	0.318	0.222
	Cl	0.089	0.119	0.078	0.104	0.096	0.087	0.125	0.074	0.068	0.069	0.106	0.11	0.061
	F	0.123	0.186	0.078	0.184	0.251	0.292	0.278	0.091	0.074	0.061	0.059	0.259	0.003
	Total	97.282	98.205	96.576	96.578	96.847	96.639	96.633	95.775	97.202	98.193	98.323	99.787	98.034
Tetrahedral	Si	6.904	6.956	7.071	6.893	6.940	7.056	6.987	6.774	6.845	6.598	6.614	6.625	6.777
	Al	1.096	1.044	0.929	1.107	1.060	0.944	1.013	1.226	1.155	1.402	1.386	1.375	1.223
	Fe3+	0.000	0.000	0.000	0.000	0.000	0.000	0.000	0.000	0.000	0.000	0.000	0.000	0.000
	total T site	8.000	8.000	8.000	8.000	8.000	8.000	8.000	8.000	8.000	8.000	8.000	8.000	8.000
Octahedral	Al	0.255	0.394	0.325	0.278	0.375	0.461	0.392	0.278	0.388	0.464	0.467	0.431	0.333
M1,M2,M3	Ti	0.074	0.080	0.068	0.088	0.080	0.081	0.065	0.087	0.082	0.074	0.105	0.086	0.074
	Fe3+	0.649	0.451	0.356	0.650	0.524	0.314	0.395	0.735	0.630	0.742	0.600	0.707	0.727
	Mg	2.679	2.628	2.778	2.676	2.582	2.590	2.728	2.633	2.499	2.249	2.284	2.286	2.534
	Fe2+	1.297	1.408	1.450	1.268	1.399	1.516	1.380	1.225	1.359	1.445	1.512	1.462	1.294
	Mn	0.047	0.039	0.022	0.040	0.040	0.038	0.040	0.042	0.042	0.027	0.032	0.029	0.038
	total M1-M3	5.000	5.000	5.000	5.000	5.000	5.000	5.000	5.000	5.000	5.000	5.000	5.000	5.000
Octahedral	Ca	1.870	1.876	1.929	1.851	1.840	1.869	1.911	1.852	1.837	1.830	1.848	1.841	1.836
M4	Na	0.130	0.124	0.071	0.149	0.160	0.131	0.089	0.148	0.163	0.170	0.152	0.159	0.164
	Fe2+	0.000	0.000	0.000	0.000	0.000	0.000	0.000	0.000	0.000	0.000	0.000	0.000	0.000
	Mn	0.000	0.000	0.000	0.000	0.000	0.000	0.000	0.000	0.000	0.000	0.000	0.000	0.000
	Mg	0.000	0.000	0.000	0.000	0.000	0.000	0.000	0.000	0.000	0.000	0.000	0.000	0.000
	total M4 site	2.000	2.000	2.000	2.000	2.000	2.000	2.000	2.000	2.000	2.000	2.000	2.000	2.000
A site	Na	0.140	0.121	0.152	0.114	0.120	0.098	0.146	0.144	0.093	0.160	0.207	0.165	0.137
	K	0.034	0.043	0.032	0.040	0.041	0.040	0.038	0.042	0.043	0.059	0.054	0.059	0.041
	total A site	0.174	0.164	0.184	0.153	0.162	0.138	0.184	0.186	0.136	0.219	0.261	0.224	0.179
	Mg/Mg+Fe2+	0.674	0.651	0.657	0.678	0.649	0.631	0.664	0.682	0.648	0.609	0.602	0.610	0.662

APPENDIX A: Amphibole Compositions; S81 Full Strain Transition Undeformed Section

		S5AM4	S5AM4	S5AM4	S5AM4	S5AM2	S5AM2	S5AM2	S5AM2	S5AM2	S5AM2	S5AM2	S5AM5	S5AM5
	SiO2	46.597	46.110	46.354	46.566	46.548	45.707	45.389	46.915	46.607	47.029	46.640	46.143	46.439
	Al2O3	8.637	8.994	8.759	9.408	8.636	9.187	9.297	8.371	8.896	8.629	8.549	8.955	8.653
	TiO2	0.836	0.810	0.659	1.031	0.848	0.835	0.664	0.615	0.735	0.703	0.760	0.799	0.723
	FeO	17.026	16.917	16.614	17.411	17.101	17.038	17.155	16.439	16.788	16.592	16.772	16.151	16.095
	MnO	0.251	0.298	0.313	0.266	0.347	0.291	0.341	0.255	0.252	0.249	0.310	0.240	0.261
	MgO	11.231	11.043	11.349	10.995	11.083	10.722	10.505	11.045	10.957	11.109	11.145	11.032	11.256
	CaO	11.786	11.647	11.576	11.646	11.594	11.253	11.475	11.706	11.585	11.083	11.642	11.731	11.660
	Na2O	0.991	1.085	1.017	1.062	1.035	1.198	1.205	0.980	1.049	0.995	1.035	1.058	0.895
	K2O	0.227	0.227	0.202	0.221	0.186	0.251	0.238	0.192	0.234	0.216	0.203	0.238	0.237
	Cl	0.119	0.157	0.194	0.177	0.148	0.091	0.067	0.071	0.04	0.047	0.141	0.109	0.072
	F	0	0.028	0.173	0.073	0.093	0.104	0.344	0.23	0.092	0.122	0.168	0.125	0.112
	Total	97.700	97.314	97.208	98.856	97.619	96.676	96.680	96.817	97.233	96.774	97.365	96.581	96.403
Tetrahedral	Si	6.837	6.798	6.828	6.756	6.839	6.780	6.771	6.957	6.867	6.918	6.875	6.859	6.888
	Al	1.163	1.202	1.172	1.244	1.161	1.220	1.229	1.043	1.133	1.082	1.125	1.141	1.112
	Fe3+	0.000	0.000	0.000	0.000	0.000	0.000	0.000	0.000	0.000	0.000	0.000	0.000	0.000
	total T site	8.000	8.000	8.000	8.000	8.000	8.000	8.000	8.000	8.000	8.000	8.000	8.000	8.000
Octahedral M1,M2,M3	Al	0.331	0.360	0.349	0.364	0.334	0.386	0.406	0.419	0.412	0.414	0.360	0.428	0.401
	Ti	0.092	0.090	0.073	0.112	0.094	0.093	0.075	0.069	0.081	0.078	0.084	0.089	0.081
	Fe3+	0.618	0.630	0.694	0.695	0.659	0.680	0.611	0.450	0.557	0.695	0.585	0.448	0.541
	Mg	2.457	2.427	2.492	2.378	2.428	2.371	2.336	2.442	2.407	2.436	2.449	2.445	2.489
	Fe2+	1.472	1.455	1.352	1.418	1.442	1.434	1.529	1.589	1.512	1.347	1.483	1.560	1.456
	Mn	0.031	0.037	0.039	0.033	0.043	0.037	0.043	0.032	0.031	0.031	0.039	0.030	0.033
	total M1-M3	5.000	5.000	5.000	5.000	5.000	5.000	5.000	5.000	5.000	5.000	5.000	5.000	5.000
Octahedral M4	Ca	1.853	1.840	1.827	1.810	1.825	1.788	1.834	1.860	1.829	1.747	1.839	1.868	1.853
	Na	0.147	0.160	0.173	0.190	0.175	0.212	0.166	0.140	0.171	0.253	0.161	0.132	0.147
	Fe2+	0.000	0.000	0.000	0.000	0.000	0.000	0.000	0.000	0.000	0.000	0.000	0.000	0.000
	Mn	0.000	0.000	0.000	0.000	0.000	0.000	0.000	0.000	0.000	0.000	0.000	0.000	0.000
	Mg	0.000	0.000	0.000	0.000	0.000	0.000	0.000	0.000	0.000	0.000	0.000	0.000	0.000
	total M4 site	2.000	2.000	2.000	2.000	2.000	2.000	2.000	2.000	2.000	2.000	2.000	2.000	2.000
A site	Na	0.135	0.150	0.117	0.109	0.120	0.133	0.183	0.141	0.128	0.031	0.134	0.173	0.110
	K	0.042	0.043	0.038	0.041	0.035	0.047	0.045	0.036	0.044	0.041	0.038	0.045	0.045
	total A site	0.177	0.192	0.155	0.150	0.155	0.180	0.228	0.178	0.172	0.071	0.173	0.218	0.155
	Mg/Mg+Fe2+	0.625	0.625	0.648	0.626	0.627	0.623	0.604	0.606	0.614	0.644	0.623	0.610	0.631

APPENDIX A: Amphibole Compositions; S81 Full Strain Transition Undeformed Section

		S5AM5	S5AM5	S4TR1.2	S4TR1.2	S4TR1.2	S4TR1.2	S4TR1.2	S4TR1.2	S4TR1.2	S4TR1.2	S4TR1.2	S4TR1.2	S4TR1.2
	SiO2	47.009	45.174	47.620	46.663	47.319	46.350	45.600	46.785	46.532	47.427	46.898	46.779	48.134
	Al2O3	8.824	10.050	8.237	8.562	8.765	9.810	10.400	9.917	9.282	9.073	8.313	9.057	8.476
	TiO2	0.812	0.957	0.609	0.628	0.620	0.493	0.424	0.544	0.513	0.342	0.614	0.526	0.614
	FeO	16.148	16.645	16.622	16.237	17.039	17.173	17.120	17.107	17.031	16.678	17.200	16.403	17.002
	MnO	0.255	0.227	0.233	0.258	0.334	0.331	0.294	0.295	0.215	0.289	0.267	0.203	0.233
	MgO	11.005	10.138	11.815	11.766	11.909	11.124	10.937	11.176	11.425	11.743	9.967	11.196	11.838
	CaO	11.660	11.658	11.690	11.504	11.643	11.514	11.583	11.814	11.574	11.693	11.773	11.164	11.585
	Na2O	1.026	1.202	0.975	0.996	1.069	1.168	1.207	1.171	1.113	1.055	0.885	0.973	0.958
	K2O	0.239	0.295	0.219	0.209	0.192	0.223	0.255	0.224	0.217	0.215	0.217	0.217	0.167
	Cl	0.088	0.083	0.044	0.05	0.062	0.03	0.089	0.114	0.134	0.149	0.128	0.118	0.106
	F	0.104	0.128	0.039	0	0.029	0.087	0.002	0.095	0.328	0.231	0.182	0.283	0.042
	Total	97.170	96.557	98.103	96.872	98.982	98.303	97.910	99.241	98.363	98.893	96.444	96.919	99.156
Tetrahedral	Si	6.933	6.753	6.917	6.849	6.805	6.732	6.657	6.750	6.773	6.845	7.038	6.877	6.903
	Al	1.067	1.247	1.083	1.151	1.195	1.268	1.343	1.250	1.227	1.155	0.962	1.123	1.097
	Fe3+	0.000	0.000	0.000	0.000	0.000	0.000	0.000	0.000	0.000	0.000	0.000	0.000	0.000
	total T site	8.000	8.000	8.000	8.000	8.000	8.000	8.000	8.000	8.000	8.000	8.000	8.000	8.000
Octahedral	Al	0.467	0.524	0.327	0.331	0.290	0.411	0.447	0.437	0.365	0.388	0.508	0.446	0.335
M1,M2,M3	Ti	0.090	0.108	0.066	0.069	0.067	0.054	0.047	0.059	0.056	0.037	0.069	0.058	0.066
	Fe3+	0.397	0.369	0.669	0.741	0.850	0.796	0.790	0.673	0.785	0.742	0.230	0.726	0.772
	Mg	2.420	2.259	2.558	2.575	2.553	2.409	2.380	2.404	2.479	2.527	2.230	2.454	2.531
	Fe2+	1.595	1.711	1.350	1.253	1.199	1.290	1.300	1.391	1.288	1.271	1.929	1.291	1.267
	Mn	0.032	0.029	0.029	0.032	0.041	0.041	0.036	0.036	0.026	0.035	0.034	0.025	0.028
	total M1-M3	5.000	5.000	5.000	5.000	5.000	5.000	5.000	5.000	5.000	5.000	5.000	5.000	5.000
Octahedral	Ca	1.842	1.867	1.819	1.809	1.794	1.792	1.812	1.826	1.805	1.808	1.893	1.758	1.780
M4	Na	0.158	0.133	0.181	0.191	0.206	0.208	0.188	0.174	0.195	0.192	0.107	0.242	0.220
	Fe2+	0.000	0.000	0.000	0.000	0.000	0.000	0.000	0.000	0.000	0.000	0.000	0.000	0.000
	Mn	0.000	0.000	0.000	0.000	0.000	0.000	0.000	0.000	0.000	0.000	0.000	0.000	0.000
	Mg	0.000	0.000	0.000	0.000	0.000	0.000	0.000	0.000	0.000	0.000	0.000	0.000	0.000
	total M4 site	2.000	2.000	2.000	2.000	2.000	2.000	2.000	2.000	2.000	2.000	2.000	2.000	2.000
A site	Na	0.136	0.215	0.094	0.093	0.092	0.121	0.154	0.154	0.119	0.103	0.151	0.036	0.047
	K	0.045	0.056	0.041	0.039	0.035	0.041	0.047	0.041	0.040	0.040	0.042	0.041	0.031
	total A site	0.181	0.272	0.134	0.132	0.127	0.162	0.201	0.195	0.159	0.143	0.192	0.076	0.077
	Mg/Mg+Fe2+	0.603	0.569	0.655	0.673	0.680	0.651	0.647	0.633	0.658	0.665	0.536	0.655	0.666

APPENDIX A: Amphibole Compositions; S81 Full Strain Transition Undeformed Section

		S4TR1.2	S4TR1.2	S4TR1.2	S4TRAM3	S4TRAM3	S4TRAM3	S4TRAM3	S4TRAM3	S4TRAM3	S4TRAM3	S4TRAM3	S4TRAM3	S4TRAM3
	SiO2	47.010	45.641	45.548	47.796	47.560	47.574	47.335	48.683	49.898	46.033	47.411	47.597	45.864
	Al2O3	8.339	11.727	10.654	8.212	8.137	8.492	8.071	6.992	6.704	8.671	8.731	8.074	10.221
	TiO2	0.614	0.367	0.659	0.545	0.634	0.646	0.456	0.476	0.362	0.494	0.583	0.577	0.317
	FeO	17.074	17.338	16.684	16.470	16.852	17.110	16.505	16.030	15.905	17.197	16.995	16.525	15.905
	MnO	0.233	0.230	0.285	0.313	0.270	0.298	0.236	0.264	0.292	0.218	0.341	0.304	0.320
	MgO	11.846	10.064	10.552	11.918	11.792	11.865	12.037	12.725	13.128	11.708	11.732	12.356	11.409
	CaO	11.536	11.972	11.951	11.589	11.602	11.698	11.940	11.838	11.903	11.828	11.867	11.959	11.881
	Na2O	1.008	1.117	1.052	0.987	0.958	0.967	0.901	0.819	0.783	1.027	0.965	0.905	0.974
	K2O	0.189	0.330	0.332	0.189	0.184	0.233	0.167	0.136	0.124	0.205	0.176	0.187	0.210
	Cl	0.136	0.092	0.082	0.091	0.124	0.13	0.165	0.177	0.15	0.122	0.121	0.134	0.171
	F	0.02	0.259	0.122	0.154	0.173	0.049	0.047	0	0.061	0	0.165	0	0.032
	Total	98.005	99.137	97.922	98.263	98.286	99.063	97.861	98.141	99.309	97.501	99.086	98.617	97.303
Tetrahedral	Si	6.833	6.634	6.689	6.928	6.906	6.848	6.903	7.041	7.113	6.751	6.838	6.872	6.720
	Al	1.167	1.366	1.311	1.072	1.094	1.152	1.097	0.959	0.887	1.249	1.162	1.128	1.280
	Fe3+	0.000	0.000	0.000	0.000	0.000	0.000	0.000	0.000	0.000	0.000	0.000	0.000	0.000
	total T site	8.000	8.000	8.000	8.000	8.000	8.000	8.000	8.000	8.000	8.000	8.000	8.000	8.000
Octahedral M1,M2,M3	Al	0.262	0.643	0.533	0.331	0.299	0.288	0.291	0.233	0.240	0.250	0.323	0.246	0.485
	Ti	0.067	0.040	0.073	0.059	0.069	0.070	0.050	0.052	0.039	0.054	0.063	0.063	0.035
	Fe3+	0.859	0.537	0.510	0.711	0.743	0.804	0.689	0.698	0.694	0.843	0.743	0.770	0.680
	Mg	2.567	2.181	2.310	2.575	2.553	2.546	2.617	2.744	2.790	2.560	2.523	2.659	2.492
	Fe2+	1.217	1.570	1.539	1.285	1.303	1.256	1.324	1.241	1.202	1.266	1.307	1.225	1.269
	Mn	0.029	0.028	0.035	0.038	0.033	0.036	0.029	0.032	0.035	0.027	0.042	0.037	0.040
	total M1-M3	5.000	5.000	5.000	5.000	5.000	5.000	5.000	5.000	5.000	5.000	5.000	5.000	5.000
Octahedral M4	Ca	1.797	1.865	1.880	1.800	1.805	1.804	1.866	1.835	1.818	1.858	1.834	1.850	1.865
	Na	0.203	0.135	0.120	0.200	0.195	0.196	0.134	0.165	0.182	0.142	0.166	0.150	0.135
	Fe2+	0.000	0.000	0.000	0.000	0.000	0.000	0.000	0.000	0.000	0.000	0.000	0.000	0.000
	Mn	0.000	0.000	0.000	0.000	0.000	0.000	0.000	0.000	0.000	0.000	0.000	0.000	0.000
	Mg	0.000	0.000	0.000	0.000	0.000	0.000	0.000	0.000	0.000	0.000	0.000	0.000	0.000
	total M4 site	2.000	2.000	2.000	2.000	2.000	2.000	2.000	2.000	2.000	2.000	2.000	2.000	2.000
A site	Na	0.080	0.179	0.180	0.077	0.075	0.074	0.121	0.064	0.034	0.151	0.104	0.103	0.142
	K	0.035	0.061	0.062	0.035	0.034	0.043	0.031	0.025	0.023	0.038	0.032	0.034	0.039
	total A site	0.116	0.241	0.242	0.112	0.109	0.117	0.152	0.089	0.057	0.189	0.136	0.138	0.181
	Mg/Mg+Fe2+	0.678	0.581	0.600	0.667	0.662	0.670	0.664	0.689	0.699	0.669	0.659	0.685	0.663

APPENDIX A: Amphibole Compositions; S81 Full Strain Transition Transitional Section

		12ASM1	12AM1.	12AM1.	12AM2.	12AM2.	12AM2.	13AM2.	13AM2.	13AM3.	13AM3.	TR1AM1	TR1AM1	TR1AM1
	SiO2	47.600	46.550	47.190	46.480	44.590	44.660	47.010	46.660	45.980	46.250	45.830	47.950	45.860
	Al2O3	7.340	8.220	8.450	8.350	11.760	9.040	7.920	8.970	8.240	9.240	10.410	8.570	9.780
	TiO2	0.720	0.860	0.710	0.740	0.500	0.790	0.680	0.730	0.730	0.760	0.540	0.560	0.580
	FeO	15.060	16.470	15.470	15.540	15.730	16.170	15.420	15.600	16.200	16.140	15.330	14.710	15.130
	MnO	0.380	0.310	0.270	0.320	0.340	0.410	0.370	0.400	0.260	0.370	0.310	0.300	0.280
	MgO	12.220	11.240	11.500	11.520	10 060	11.380	12.220	11.500	11.730	11.390	10.920	12.200	11.190
	CaO	11.980	11.600	11.970	11.810	11.740	11.620	11.830	11.890	11.730	11.760	11.770	12.120	12.090
	Na2O	0.850	0.930	0.750	0.970	0.940	1.070	0.780	1.050	0.950	1.020	0.880	0.740	0.890
	K2O	0.220	0.220	0.230	0.210	0.320	0.260	0.220	0.220	0.240	0.240	0.310	0.220	0.250
	Cl	0.136	0.092	0.082	0.091	0.124	0.13	0.165	0.177	0.15	0.122	0.121	0.134	0.171
	F	0.02	0.259	0.122	0.154	0.173	0.049	0.047	0	0.061	0	0.165	0	0.032
	Total	96.526	96.751	96.744	96.185	96.277	95.579	96.662	97.197	96.271	97.292	96.586	97.504	96.253
Tetrahedral	Si	7.038	6.902	6.972	6.920	6.643	6.693	6.922	6.869	6.832	6.794	6.781	6.987	6.822
	Al	0.962	1.098	1.028	1.080	1.357	1.307	1.078	1.131	1.168	1.206	1.219	1.013	1.178
	Fe3+	0.000	0.000	0.000	0.000	0.000	0.000	0.000	0.000	0.000	0.000	0.000	0.000	0.000
	total T site	8.000	8.000	8.000	8.000	8.000	8.000	8.000	8.000	8.000	8.000	8.000	8.000	8.000
Octahedral	Al	0.317	0.338	0.443	0.385	0.707	0.290	0.297	0.425	0.275	0.393	0.596	0.459	0.536
M1,M2,M3	Ti	0.080	0.096	0.079	0.083	0.056	0.089	0.075	0.081	0.082	0.084	0.060	0.061	0.065
	Fe3+	0.405	0.573	0.380	0.442	0.458	0.747	0.633	0.453	0.677	0.608	0.461	0.397	0.354
	Mg	2.693	2.484	2.533	2.557	2.234	2.542	2.683	2.524	2.598	2.494	2.409	2.650	2.481
	Fe2+	1.457	1.469	1.532	1.493	1.502	1.280	1.266	1.468	1.336	1.374	1.436	1.396	1.528
	Mn	0.048	0.039	0.034	0.040	0.043	0.052	0.046	0.050	0.033	0.046	0.039	0.037	0.035
	total M1-M3	5.000	5.000	5.000	5.000	5.000	5.000	5.000	5.000	5.000	5.000	5.000	5.000	5.000
Octahedral	Ca	1.898	1.843	1.895	1.884	1.874	1.866	1.866	1.875	1.867	1.851	1.866	1.892	1.927
M4	Na	0.102	0.157	0.105	0.116	0.126	0.134	0.134	0.125	0.133	0.149	0.134	0.108	0.073
	Fe2+	0.000	0.000	0.000	0.000	0.000	0.000	0.000	0.000	0.000	0.000	0.000	0.000	0.000
	Mn	0.000	0.000	0.000	0.000	0.000	0.000	0.000	0.000	0.000	0.000	0.000	0.000	0.000
	Mg	0.000	0.000	0.000	0.000	0.000	0.000	0.000	0.000	0.000	0.000	0.000	0.000	0.000
	total M4 site	2.000	2.000	2.000	2.000	2.000	2.000	2.000	2.000	2.000	2.000	2.000	2.000	2.000
A site	Na	0.141	0.110	0.110	0.164	0.145	0.177	0.089	0.175	0.141	0.141	0.118	0.101	0.184
	K	0.041	0.042	0.043	0.040	0.061	0.050	0.041	0.041	0.045	0.045	0.059	0.041	0.047
	total A site	0.183	0.152	0.153	0.204	0.206	0.226	0.130	0.216	0.186	0.186	0.177	0.142	0.231
Mg/Mg+Fe2+		0.649	0.628	0.623	0.631	0.598	0.665	0.679	0.632	0.660	0.645	0.627	0.655	0.619

APPENDIX A: Amphibole Compositions; S81 Full Strain Transition Transitional Section

		TR1AM1	TR1AM1	TR1AM1	13AM5.	13AM5.	13AM4.	13AM4.	15AM1.	15AM1.	15AM1.	15AM2.	15AM2.	15AM15
	SiO2	45.380	47.910	46.586	45.230	43.490	45.140	46.310	47.740	48.010	47.240	45.860	46.590	47.350
	Al2O3	8.250	7.950	8.992	8.470	10.450	9.250	8.950	8.490	7.560	8.440	8.560	7.930	8.070
	TiO2	2.480	0.610	0.954	0.800	0.980	0.780	0.720	0.600	0.700	0.650	0.820	0.760	0.830
	FeO	15.400	14.590	15.032	16.140	16.550	15.840	15.800	14.640	14.490	14.720	16.180	15.520	15.390
	MnO	0.400	0.340	0.326	0.290	0.310	0.390	0.310	0.280	0.300	0.280	0.320	0.310	0.320
	MgO	11.470	12.420	11.640	11.790	10.270	11.300	11.620	11.680	12.120	11.960	11.390	12.150	11.890
	CaO	11.700	12.120	11.960	11.580	11.790	11.940	11.840	12.170	12.010	12.110	11.810	11.850	11.700
	Na2O	0.740	0.730	0.796	1.020	1.240	1.030	0.910	0.860	0.780	0.740	0.910	0.880	0.910
	K2O	0.190	0.220	0.238	0.240	0.340	0.230	0.210	0.220	0.210	0.210	0.220	0.200	0.240
	Cl	0.182	0.107	0.171	0.134	0.089	0.099	0.096	0.194	0.165	0.184	0.183	0.117	0.096
	F	1.976	0.142	0.242	0.119	0.095	0.101	0.118	0.717	0.132	0.003	0.05	0	0
	Total	98.168	97.139	96.937	95.813	95.604	96.1	96.884	97.591	96.477	96.537	96.303	96.307	96.796
Tetrahedral	Si	6.759	7.018	6.874	6.748	6.577	6.741	6.826	7.045	7.102	6.974	6.825	6.893	6.967
	Al	1.241	0.982	1.126	1.252	1.423	1.259	1.174	0.955	0.898	1.026	1.175	1.107	1.033
	Fe3+	0.000	0.000	0.000	0.000	0.000	0.000	0.000	0.000	0.000	0.000	0.000	0.000	0.000
	total T site	8.000	8.000	8.000	8.000	8.000	8.000	8.000	8.000	8.000	8.000	8.000	8.000	8.000
Octahedral	Al	0.207	0.391	0.438	0.237	0.440	0.369	0.381	0.522	0.419	0.443	0.327	0.276	0.366
M1,M2,M3	Ti	0.278	0.067	0.106	0.090	0.111	0.088	0.080	0.067	0.078	0.072	0.092	0.085	0.092
	Fe3+	0.495	0.403	0.422	0.792	0.509	0.552	0.595	0.164	0.253	0.356	0.593	0.614	0.489
	Mg	2.547	2.712	2.561	2.622	2.316	2.516	2.553	2.570	2.673	2.632	2.527	2.680	2.608
	Fe2+	1.423	1.384	1.433	1.222	1.584	1.427	1.353	1.643	1.539	1.462	1.421	1.306	1.405
	Mn	0.050	0.042	0.041	0.037	0.040	0.049	0.039	0.035	0.038	0.035	0.040	0.039	0.040
	total M1-M3	5.000	5.000	5.000	5.000	5.000	5.000	5.000	5.000	5.000	5.000	5.000	5.000	5.000
Octahedral	Ca	1.867	1.902	1.891	1.851	1.910	1.910	1.870	1.924	1.903	1.916	1.883	1.879	1.844
M4	Na	0.133	0.098	0.109	0.149	0.090	0.090	0.130	0.076	0.097	0.084	0.117	0.121	0.156
	Fe2+	0.000	0.000	0.000	0.000	0.000	0.000	0.000	0.000	0.000	0.000	0.000	0.000	0.000
	Mn	0.000	0.000	0.000	0.000	0.000	0.000	0.000	0.000	0.000	0.000	0.000	0.000	0.000
	Mg	0.000	0.000	0.000	0.000	0.000	0.000	0.000	0.000	0.000	0.000	0.000	0.000	0.000
	total M4 site	2.000	2.000	2.000	2.000	2.000	2.000	2.000	2.000	2.000	2.000	2.000	2.000	2.000
A site	Na	0.081	0.110	0.119	0.146	0.274	0.209	0.130	0.170	0.127	0.127	0.146	0.131	0.104
	K	0.036	0.041	0.045	0.046	0.066	0.044	0.039	0.041	0.040	0.040	0.042	0.038	0.045
	total A site	0.117	0.151	0.163	0.192	0.340	0.252	0.169	0.212	0.167	0.167	0.188	0.169	0.149
Mg/Mg+Fe2+		0.641	0.662	0.641	0.682	0.594	0.638	0.654	0.610	0.635	0.643	0.640	0.672	0.650

APPENDIX A: Amphibole Compositions; S81 Full Strain Transition Transitional Section

		15AM3.	15AM3.	15AM4.	15AM4.	15AM4.	15AM5.	15AM5.	15AM5.	2AM1.1	2AM1.2	TR1AM2	TR1AM2	TR1AM2
	SiO2	46.070	47.410	44.830	46.110	45.570	45.000	44.790	46.240	46.290	45.590	44.890	45.400	45.130
	Al2O3	8.950	8.370	9.010	9.350	9.370	11.840	9.520	7.800	8.860	9.090	11.410	10.690	11.220
	TiO2	0.800	0.700	0.990	0.910	1.060	0.490	0.700	0.770	0.810	1.080	0.630	0.610	0.560
	FeO	15.430	15.680	16.050	16.060	16.180	16.310	15.880	15.720	15.750	15.910	15.210	14.790	15.090
	MnO	0.460	0.290	0.400	0.370	0.300	0.280	0.370	0.330	0.360	0.320	0.320	0.270	0.320
	MgO	11.750	11.980	11.190	11.410	11.160	9.930	10.790	11.450	11.350	11.320	11.220	11.330	11.160
	CaO	11.720	11.620	11.830	11.860	11.880	12.110	11.650	11.710	11.880	11.810	11.670	11.770	11.830
	Na2O	0.910	0.890	1.010	0.980	1.030	1.010	1.070	0.960	0.960	0.910	0.770	0.810	0.870
	K2O	0.240	0.200	0.270	0.260	0.280	0.300	0.290	0.200	0.250	0.260	0.270	0.240	0.290
	Cl	0.089	0.119	0.078	0.104	0.096	0.087	0.125	0.074	0.068	0.069	0.106	0.11	0.061
	F	0.123	0.186	0.078	0.184	0.251	0.292	0.278	0.091	0.074	0.061	0.059	0.259	0.003
	Total	96.542	97.445	95.736	97.598	97.177	97.649	95.463	95.345	96.652	96.42	96.555	96.279	96.534
Tetrahedral	Si	6.803	6.924	6.727	6.768	6.745	6.648	6.754	6.949	6.859	6.768	6.592	6.711	6.644
	Al	1.197	1.076	1.273	1.232	1.255	1.352	1.246	1.051	1.141	1.232	1.408	1.289	1.356
	Fe3+	0.000	0.000	0.000	0.000	0.000	0.000	0.000	0.000	0.000	0.000	0.000	0.000	0.000
	total T site	8.000	8.000	8.000	8.000	8.000	8.000	8.000	8.000	8.000	8.000	8.000	8.000	8.000
Octahedral	Al	0.361	0.364	0.320	0.385	0.379	0.709	0.445	0.330	0.406	0.359	0.567	0.573	0.591
M1,M2,M3	Ti	0.089	0.077	0.112	0.100	0.118	0.054	0.079	0.087	0.090	0.121	0.070	0.068	0.062
	Fe3+	0.643	0.633	0.580	0.588	0.524	0.356	0.509	0.458	0.460	0.564	0.760	0.574	0.606
	Mg	2.587	2.608	2.503	2.497	2.462	2.187	2.425	2.565	2.507	2.505	2.456	2.497	2.449
	Fe2+	1.263	1.282	1.434	1.384	1.479	1.659	1.493	1.518	1.492	1.411	1.107	1.254	1.252
	Mn	0.058	0.036	0.051	0.046	0.038	0.035	0.047	0.042	0.045	0.040	0.040	0.034	0.040
	total M1-M3	5.000	5.000	5.000	5.000	5.000	5.000	5.000	5.000	5.000	5.000	5.000	5.000	5.000
Octahedral	Ca	1.854	1.818	1.902	1.865	1.884	1.917	1.882	1.885	1.886	1.878	1.836	1.864	1.866
M4	Na	0.146	0.182	0.098	0.135	0.116	0.083	0.118	0.115	0.114	0.122	0.164	0.136	0.134
	Fe2+	0.000	0.000	0.000	0.000	0.000	0.000	0.000	0.000	0.000	0.000	0.000	0.000	0.000
	Mn	0.000	0.000	0.000	0.000	0.000	0.000	0.000	0.000	0.000	0.000	0.000	0.000	0.000
	Mg	0.000	0.000	0.000	0.000	0.000	0.000	0.000	0.000	0.000	0.000	0.000	0.000	0.000
	total M4 site	2.000	2.000	2.000	2.000	2.000	2.000	2.000	2.000	2.000	2.000	2.000	2.000	2.000
A site	Na	0.115	0.070	0.196	0.144	0.180	0.206	0.195	0.165	0.162	0.140	0.055	0.096	0.114
	K	0.045	0.037	0.052	0.049	0.053	0.057	0.056	0.038	0.047	0.049	0.051	0.045	0.054
	total A site	0.160	0.107	0.247	0.193	0.232	0.262	0.251	0.203	0.209	0.190	0.106	0.141	0.169
Mg/Mg+Fe2+		0.672	0.670	0.636	0.643	0.625	0.569	0.619	0.628	0.627	0.640	0.689	0.666	0.662

APPENDIX A: Amphibole Compositions; S81 Full Strain Transition Transitional Section

		TR1AM2	TR1AM2	TR1AM2	TR1AM1	TR1AM1	TR1AM1	TR2AM1	TR2AM1	TR2AM1	TR2AM1	TR2AM1	TR3AM1	TR3AM1
	SiO2	44.210	45.700	45.120	46.810	46.580	47.540	46.500	46.290	46.030	44.540	45.820	46.270	45.970
	Al2O3	10.730	10.790	11.090	8.470	8.490	8.590	8.350	8.430	9.230	9.680	8.720	8.460	9.560
	TiO2	0.610	0.580	0.630	0.690	0.700	0.710	0.760	0.670	0.790	0.830	0.750	0.730	0.800
	FeO	15.180	15.370	15.140	16.070	16.460	15.450	15.860	15.820	16.860	16.620	16.590	15.190	16.200
	MnO	0.330	0.260	0.280	0.330	0.400	0.350	0.300	0.310	0.380	0.340	0.380	0.340	0.390
	MgO	11.210	11.080	11.040	11.740	11.900	11.390	11.780	11.410	11.150	10.910	11.500	11.780	11.350
	CaO	11.800	11.760	11.760	11.870	11.680	11.990	11.980	11.830	11.670	11.840	11.830	11.860	11.610
	Na2O	0.850	0.820	0.850	0.910	1.010	0.970	1.020	1.000	1.110	1.090	1.100	0.830	1.080
	K2O	0.240	0.270	0.270	0.230	0.240	0.220	0.220	0.230	0.290	0.300	0.230	0.250	0.290
	Cl	0.119	0.157	0.194	0.177	0.148	0.091	0.067	0.071	0.04	0.047	0.141	0.109	0.072
	F	0	0.028	0.173	0.073	0.093	0.104	0.344	0.23	0.092	0.122	0.168	0.125	0.112
	Total	95.279	96.815	96.547	97.37	97.701	97.405	97.181	96.291	97.642	96.319	97.229	95.944	97.434
Tetrahedral	Si	6.606	6.717	6.664	6.874	6.807	6.992	6.870	6.899	6.758	6.654	6.769	6.887	6.742
	Al	1.394	1.283	1.336	1.126	1.193	1.008	1.130	1.101	1.242	1.346	1.231	1.113	1.258
	Fe3+	0.000	0.000	0.000	0.000	0.000	0.000	0.000	0.000	0.000	0.000	0.000	0.000	0.000
	total T site	8.000	8.000	8.000	8.000	8.000	8.000	8.000	8.000	8.000	8.000	8.000	8.000	8.000
Octahedral	Al	0.496	0.586	0.594	0.339	0.269	0.480	0.324	0.379	0.355	0.358	0.287	0.371	0.395
M1,M2,M3	Ti	0.069	0.064	0.070	0.076	0.077	0.079	0.084	0.075	0.087	0.093	0.083	0.082	0.088
	Fe3+	0.691	0.580	0.586	0.597	0.781	0.274	0.511	0.462	0.671	0.639	0.674	0.509	0.676
	Mg	2.497	2.428	2.431	2.570	2.593	2.497	2.595	2.535	2.440	2.430	2.533	2.614	2.482
	Fe2+	1.206	1.309	1.284	1.376	1.231	1.626	1.449	1.510	1.399	1.437	1.375	1.381	1.311
	Mn	0.042	0.032	0.035	0.041	0.050	0.044	0.038	0.039	0.047	0.043	0.048	0.043	0.048
	total M1-M3	5.000	5.000	5.000	5.000	5.000	5.000	5.000	5.000	5.000	5.000	5.000	5.000	5.000
Octahedral	Ca	1.889	1.852	1.861	1.867	1.829	1.889	1.896	1.889	1.836	1.895	1.872	1.891	1.824
M4	Na	0.111	0.148	0.139	0.133	0.171	0.111	0.104	0.111	0.164	0.105	0.128	0.109	0.176
	Fe2+	0.000	0.000	0.000	0.000	0.000	0.000	0.000	0.000	0.000	0.000	0.000	0.000	0.000
	Mn	0.000	0.000	0.000	0.000	0.000	0.000	0.000	0.000	0.000	0.000	0.000	0.000	0.000
	Mg	0.000	0.000	0.000	0.000	0.000	0.000	0.000	0.000	0.000	0.000	0.000	0.000	0.000
	total M4 site	2.000	2.000	2.000	2.000	2.000	2.000	2.000	2.000	2.000	2.000	2.000	2.000	2.000
A site	Na	0.135	0.086	0.104	0.127	0.115	0.166	0.189	0.178	0.152	0.211	0.187	0.131	0.132
	K	0.046	0.051	0.051	0.043	0.045	0.041	0.041	0.044	0.054	0.057	0.043	0.047	0.054
	total A site	0.181	0.136	0.155	0.170	0.160	0.207	0.230	0.222	0.206	0.268	0.231	0.178	0.186
Mg/Mg+Fe2+		0.674	0.650	0.654	0.651	0.678	0.606	0.642	0.627	0.636	0.628	0.648	0.654	0.654

APPENDIX A: Amphibole Compositions; S81 Full Strain Transition Transitional Section

		TR3AM1	TR3AM1	TR3AM1	TR3AM1	TR4AM1	TR4AM1	TR4AM1	TR5AM1	TR5AM1	TR5AM1	TR5AM1	TR5AM1	TR5AM1
	SiO2	45.670	44.740	44.860	47.180	45.990	44.050	46.090	47.520	46.120	48.090	48.720	49.000	46.970
	Al2O3	9.960	9.660	9.410	8.240	9.740	10.930	9.610	8.340	8.580	7.770	7.100	7.090	7.960
	TiO2	0.840	0.840	0.790	0.810	0.780	0.750	0.840	0.630	0.660	0.610	0.520	0.530	0.610
	FeO	16.140	16.260	16.220	16.230	16.030	15.830	15.840	15.060	14.950	14.380	14.180	14.820	14.460
	MnO	0.320	0.300	0.340	0.330	0.320	0.320	0.280	0.350	0.300	0.300	0.240	0.340	0.330
	MgO	11.120	11.000	11.260	12.080	11.250	10.340	11.280	12.010	11.770	12.610	12.780	12.980	12.350
	CaO	11.900	11.740	11.720	11.740	11.660	12.040	12.100	12.150	12.210	12.120	12.170	12.150	12.610
	Na2O	1.040	1.100	1.040	0.980	0.860	0.940	0.810	0.800	0.850	0.820	0.600	0.730	0.720
	K2O	0.280	0.290	0.270	0.230	0.300	0.330	0.270	0.200	0.260	0.210	0.190	0.180	0.180
	Cl	0.088	0.083	0.044	0.05	0.062	0.03	0.089	0.114	0.134	0.149	0.128	0.118	0.106
	F	0.104	0.128	0.039	0	0.029	0.087	0.002	0.095	0.328	0.231	0.182	0.283	0.042
	Total	97.462	96.141	95.993	97.87	97.021	95.647	97.211	97.269	96.162	97.29	96.81	98.221	96.338
Tetrahedral	Si	6.717	6.685	6.689	6.864	6.755	6.626	6.782	6.971	6.889	7.041	7.149	7.095	6.971
	Al	1.283	1.315	1.311	1.136	1.245	1.374	1.218	1.029	1.111	0.959	0.851	0.905	1.029
	Fe3+	0.000	0.000	0.000	0.000	0.000	0.000	0.000	0.000	0.000	0.000	0.000	0.000	0.000
	total T site	8.000	8.000	8.000	8.000	8.000	8.000	8.000	8.000	8.000	8.000	8.000	8.000	8.000
Octahedral	Al	0.444	0.386	0.343	0.276	0.441	0.564	0.449	0.413	0.399	0.382	0.377	0.304	0.363
M1,M2,M3	Ti	0.093	0.094	0.089	0.089	0.086	0.085	0.093	0.069	0.074	0.067	0.057	0.058	0.068
	Fe3+	0.554	0.608	0.694	0.704	0.660	0.421	0.487	0.393	0.359	0.367	0.326	0.478	0.278
	Mg	2.438	2.450	2.503	2.620	2.463	2.319	2.474	2.626	2.621	2.753	2.796	2.802	2.732
	Fe2+	1.432	1.424	1.329	1.271	1.309	1.570	1.463	1.455	1.508	1.394	1.414	1.317	1.517
	Mn	0.040	0.038	0.043	0.041	0.040	0.041	0.035	0.043	0.038	0.037	0.030	0.042	0.041
	total M1-M3	5.000	5.000	5.000	5.000	5.000	5.000	5.000	5.000	5.000	5.000	5.000	5.000	5.000
Octahedral	Ca	1.875	1.879	1.872	1.830	1.835	1.941	1.908	1.910	1.954	1.901	1.913	1.885	2.005
M4	Na	0.125	0.121	0.128	0.170	0.165	0.059	0.092	0.090	0.046	0.099	0.087	0.115	0.000
	Fe2+	0.000	0.000	0.000	0.000	0.000	0.000	0.000	0.000	0.000	0.000	0.000	0.000	0.000
	Mn	0.000	0.000	0.000	0.000	0.000	0.000	0.000	0.000	0.000	0.000	0.000	0.000	0.000
	Mg	0.000	0.000	0.000	0.000	0.000	0.000	0.000	0.000	0.000	0.000	0.000	0.000	0.000
	total M4 site	2.000	2.000	2.000	2.000	2.000	2.000	2.000	2.000	2.000	2.000	2.000	2.000	2.005
A site	Na	0.172	0.198	0.173	0.106	0.080	0.215	0.139	0.137	0.200	0.134	0.084	0.090	0.207
	K	0.053	0.055	0.051	0.043	0.056	0.063	0.051	0.037	0.050	0.039	0.036	0.033	0.034
	total A site	0.224	0.253	0.224	0.149	0.136	0.278	0.189	0.175	0.250	0.173	0.120	0.123	0.241
Mg/Mg+Fe2+		0.630	0.632	0.653	0.673	0.653	0.596	0.628	0.644	0.635	0.664	0.664	0.680	0.643

APPENDIX A: Amphibole Compositions; S81 Full Strain Transition Transitional Section

		TR5AM1	TR5AM1	TR5AM1	TR5AM1	TR6AM1	TR6AM1	TR6AM1	TR6AM1	TR6AM1	TR6AM1	TR7AM1	TR7AM1	TR7AM1
	SiO2	47.550	46.520	47.940	47.690	44.580	46.050	45.550	46.400	46.610	44.210	45.370	44.690	44.850
	Al2O3	8.200	8.270	8.640	8.230	9.960	8.630	9.520	9.640	9.140	12.500	10.280	10.380	10.500
	TiO2	0.610	0.620	0.750	0.710	0.800	0.760	0.910	0.790	0.840	0.410	0.790	0.840	0.860
	FeO	14.990	14.620	14.930	15.690	16.030	15.920	16.570	15.530	16.240	16.630	16.940	16.440	17.440
	MnO	0.260	0.240	0.280	0.300	0.270	0.340	0.340	0.340	0.340	0.340	0.280	0.350	0.360
	MgO	12.110	12.270	11.900	11.770	10.450	11.280	10.850	11.000	11.320	9.910	10.510	10.240	10.110
	CaO	11.620	12.270	12.280	11.610	11.700	11.670	12.000	11.890	11.670	11.950	11.730	11.920	11.460
	Na2O	0.690	0.740	0.830	0.840	1.070	0.980	1.100	0.990	0.990	0.980	1.140	1.120	1.090
	K2O	0.270	0.210	0.210	0.270	0.310	0.260	0.300	0.270	0.240	0.290	0.300	0.320	0.340
	Cl	0.103	0.102	0.105	0.04	0.103	0.115	0.118	0.146	0.194	0.231	0.149	0.128	0.118
	F	0.182	0.272	0.278	0.091	0.02	0.074	0.044	0.141	0.162	0.033	0.231	0.182	0.283
	Total	96.585	96.134	98.143	97.241	95.293	96.079	97.302	97.137	97.746	97.484	97.72	96.61	97.411
Tetrahedral	Si	6.986	6.915	6.991	6.978	6.728	6.864	6.746	6.852	6.827	6.515	6.691	6.688	6.638
	Al	1.014	1.085	1.009	1.022	1.272	1.136	1.254	1.148	1.173	1.485	1.309	1.312	1.362
	Fe3+	0.000	0.000	0.000	0.000	0.000	0.000	0.000	0.000	0.000	0.000	0.000	0.000	0.000
	total T site	8.000	8.000	8.000	8.000	8.000	8.000	8.000	8.000	8.000	8.000	8.000	8.000	8.000
Octahedral	Al	0.406	0.364	0.476	0.397	0.500	0.381	0.408	0.530	0.404	0.686	0.478	0.519	0.470
M1,M2,M3	Ti	0.067	0.069	0.082	0.078	0.091	0.085	0.101	0.088	0.093	0.045	0.088	0.095	0.096
	Fe3+	0.568	0.421	0.258	0.539	0.433	0.524	0.462	0.345	0.595	0.601	0.567	0.395	0.689
	Mg	2.652	2.719	2.587	2.567	2.351	2.507	2.396	2.422	2.472	2.177	2.311	2.285	2.231
	Fe2+	1.274	1.397	1.562	1.381	1.590	1.460	1.590	1.573	1.394	1.449	1.522	1.662	1.470
	Mn	0.032	0.030	0.035	0.037	0.035	0.043	0.043	0.043	0.042	0.042	0.035	0.044	0.045
	total M1-M3	5.000	5.000	5.000	5.000	5.000	5.000	5.000	5.000	5.000	5.000	5.000	5.000	5.000
Octahedral	Ca	1.829	1.954	1.919	1.820	1.892	1.864	1.904	1.881	1.831	1.887	1.853	1.911	1.817
M4	Na	0.171	0.046	0.081	0.180	0.108	0.136	0.096	0.119	0.169	0.113	0.147	0.089	0.183
	Fe2+	0.000	0.000	0.000	0.000	0.000	0.000	0.000	0.000	0.000	0.000	0.000	0.000	0.000
	Mn	0.000	0.000	0.000	0.000	0.000	0.000	0.000	0.000	0.000	0.000	0.000	0.000	0.000
	Mg	0.000	0.000	0.000	0.000	0.000	0.000	0.000	0.000	0.000	0.000	0.000	0.000	0.000
	total M4 site	2.000	2.000	2.000	2.000	2.000	2.000	2.000	2.000	2.000	2.000	2.000	2.000	2.000
A site	Na	0.026	0.167	0.153	0.058	0.205	0.147	0.220	0.165	0.112	0.167	0.179	0.236	0.130
	K	0.051	0.040	0.039	0.050	0.060	0.049	0.057	0.051	0.045	0.055	0.056	0.061	0.064
	total A site	0.076	0.207	0.192	0.109	0.265	0.197	0.277	0.216	0.157	0.221	0.236	0.297	0.194
Mg/Mg+Fe2+		0.675	0.661	0.623	0.650	0.597	0.632	0.601	0.606	0.639	0.600	0.603	0.579	0.603

APPENDIX A: Amphibole Compositions; S81 Full Strain Transition Transitional Section

		TR7AM1	TR7AM1	TR7AM1	TR8AM1	TR8AM1	TR8AM1	TR8AM1	TR8AM1	TR8AM1
	SiO2	46.740	46.300	44.700	45.190	44.260	45.890	47.020	46.940	44.410
	Al2O3	8.460	8.830	11.960	8.920	10.370	9.120	9.610	7.700	10.840
	TiO2	0.690	0.750	0.470	0.830	0.980	0.810	0.780	0.710	0.520
	FeO	15.800	15.760	16.150	16.120	16.860	16.370	16.170	15.840	15.340
	MnO	0.300	0.310	0.310	0.320	0.340	0.370	0.300	0.370	0.270
	MgO	11.670	11.720	9.260	11.480	10.450	11.470	11.230	12.250	10.830
	CaO	11.770	11.980	11.970	11.950	11.850	11.800	11.900	11.840	11.480
	Na2O	1.040	1.010	1.070	1.050	1.260	1.090	1.040	0.980	0.990
	K2O	0.230	0.240	0.320	0.280	0.330	0.250	0.260	0.190	0.270
	Cl	0.088	0.083	0.044	0.05	0.062	0.03	0.089	0.114	0.134
	F	0.104	0.128	0.039	0	0.029	0.087	0.002	0.095	0.328
	Total	96.892	97.111	96.293	96.19	96.791	97.287	98.401	97.029	95.412
Tetrahedral	Si	6.897	6.825	6.701	6.738	6.600	6.752	6.833	6.905	6.653
	Al	1.103	1.175	1.299	1.262	1.400	1.248	1.167	1.095	1.347
	Fe3+	0.000	0.000	0.000	0.000	0.000	0.000	0.000	0.000	0.000
	total T site	8.000	8.000	8.000	8.000	8.000	8.000	8.000	8.000	8.000
Octahedral	Al	0.369	0.360	0.814	0.305	0.422	0.334	0.479	0.240	0.567
M1,M2,M3	Ti	0.077	0.083	0.053	0.093	0.110	0.090	0.085	0.079	0.059
	Fe3+	0.518	0.531	0.162	0.597	0.546	0.656	0.469	0.650	0.639
	Mg	2.567	2.576	2.069	2.552	2.323	2.516	2.433	2.686	2.419
	Fe2+	1.432	1.412	1.862	1.413	1.557	1.358	1.496	1.299	1.283
	Mn	0.037	0.039	0.039	0.040	0.043	0.046	0.037	0.046	0.034
	total M1-M3	5.000	5.000	5.000	5.000	5.000	5.000	5.000	5.000	5.000
Octahedral	Ca	1.861	1.892	1.922	1.909	1.893	1.860	1.853	1.866	1.843
M4	Na	0.139	0.108	0.078	0.091	0.107	0.140	0.147	0.134	0.157
	Fe2+	0.000	0.000	0.000	0.000	0.000	0.000	0.000	0.000	0.000
	Mn	0.000	0.000	0.000	0.000	0.000	0.000	0.000	0.000	0.000
	Mg	0.000	0.000	0.000	0.000	0.000	0.000	0.000	0.000	0.000
	total M4 site	2.000	2.000	2.000	2.000	2.000	2.000	2.000	2.000	2.000
A site	Na	0.158	0.181	0.233	0.212	0.257	0.171	0.146	0.146	0.130
	K	0.043	0.045	0.061	0.053	0.063	0.047	0.048	0.036	0.052
	total A site	0.202	0.226	0.295	0.266	0.320	0.218	0.194	0.181	0.182
Mg/Mg+Fe2+		0.642	0.646	0.526	0.644	0.599	0.649	0.619	0.674	0.653

APPENDIX A: Amphibole Compositions; S81 Full Strain Transition Mylonitic Section

		TR1AM1	TR1AM1	TR1AM1	TR1AM1	TR1AM1	TR1AM1	TR1AM1	TR2AM1	TR2AM1	TR2AM1	TR2AM1	TR2AM1	TR2AM1
	SiO2	45.990	46.230	45.530	46.450	46.300	46.580	46.300	45.040	45.680	46.560	45.010	44.760	44.990
	Al2O3	8.490	8.070	8.560	8.900	8.660	9.030	8.600	12.720	8.700	8.170	8.920	9.530	8.950
	TiO2	0.940	0.940	0.970	0.920	0.860	0.890	0.950	0.440	0.920	0.880	0.900	0.820	0.840
	FeO	16.200	15.410	15.950	15.830	15.630	15.610	15.840	15.380	16.030	16.230	15.990	16.120	16.070
	MnO	0.310	0.350	0.330	0.280	0.310	0.360	0.330	0.290	0.300	0.290	0.310	0.310	0.330
	MgO	11.520	11.840	11.720	11.520	11.630	11.430	11.330	10.620	11.460	12.050	11.620	11.310	11.190
	CaO	11.630	11.850	11.770	11.770	11.780	11.640	11.780	11.830	11.860	11.750	11.780	11.810	11.820
	Na2O	0.920	0.860	0.990	0.990	1.000	0.930	1.040	1.090	0.960	1.010	1.020	1.070	1.040
	K2O	0.230	0.280	0.250	0.240	0.240	0.250	0.250	0.290	0.280	0.260	0.270	0.280	0.230
	Cl	0.119	0.157	0.194	0.177	0.148	0.091	0.067	0.071	0.040	0.047	0.141	0.109	0.072
	F	0.000	0.028	0.173	0.073	0.093	0.104	0.344	0.230	0.092	0.122	0.168	0.125	0.112
	Total	96.349	96.015	96.437	97.150	96.651	96.915	96.831	98.001	96.322	97.369	96.129	96.244	95.644
Tetrahedral	Si	6.818	6.886	6.769	6.840	6.853	6.858	6.874	6.557	6.797	6.829	6.714	6.672	6.756
	Al	1.182	1.114	1.231	1.160	1.147	1.142	1.126	1.443	1.203	1.171	1.286	1.328	1.244
	Fe3+	0.000	0.000	0.000	0.000	0.000	0.000	0.000	0.000	0.000	0.000	0.000	0.000	0.000
	total T site	8.000	8.000	8.000	8.000	8.000	8.000	8.000	8.000	8.000	8.000	8.000	8.000	8.000
Octahedral	Al	0.302	0.302	0.269	0.385	0.364	0.425	0.378	0.739	0.323	0.241	0.282	0.346	0.340
M1,M2,M3	Ti	0.105	0.105	0.108	0.102	0.096	0.099	0.106	0.048	0.103	0.097	0.101	0.092	0.095
	Fe3+	0.668	0.518	0.662	0.530	0.522	0.534	0.442	0.556	0.563	0.707	0.692	0.663	0.564
	Mg	2.546	2.629	2.598	2.529	2.566	2.509	2.508	2.305	2.542	2.635	2.584	2.513	2.505
	Fe2+	1.341	1.401	1.321	1.420	1.413	1.388	1.525	1.316	1.432	1.284	1.303	1.346	1.454
	Mn	0.039	0.044	0.042	0.035	0.039	0.045	0.041	0.036	0.038	0.036	0.039	0.039	0.042
	total M1-M3	5.000	5.000	5.000	5.000	5.000	5.000	5.000	5.000	5.000	5.000	5.000	5.000	5.000
Octahedral	Ca	1.847	1.891	1.875	1.857	1.868	1.836	1.874	1.845	1.891	1.846	1.883	1.886	1.902
M4	Na	0.153	0.109	0.125	0.143	0.132	0.164	0.126	0.155	0.109	0.154	0.117	0.114	0.098
	Fe2+	0.000	0.000	0.000	0.000	0.000	0.000	0.000	0.000	0.000	0.000	0.000	0.000	0.000
	Mn	0.000	0.000	0.000	0.000	0.000	0.000	0.000	0.000	0.000	0.000	0.000	0.000	0.000
	Mg	0.000	0.000	0.000	0.000	0.000	0.000	0.000	0.000	0.000	0.000	0.000	0.000	0.000
	total M4 site	2.000	2.000	2.000	2.000	2.000	2.000	2.000	2.000	2.000	2.000	2.000	2.000	2.000
A site	Na	0.112	0.139	0.160	0.140	0.155	0.102	0.173	0.153	0.168	0.134	0.178	0.195	0.205
	K	0.044	0.053	0.047	0.045	0.045	0.047	0.047	0.054	0.053	0.049	0.051	0.053	0.044
	total A site	0.155	0.193	0.208	0.185	0.201	0.149	0.220	0.207	0.221	0.182	0.229	0.249	0.249
	Mg/Mg+Fe2+	0.655	0.652	0.663	0.640	0.645	0.644	0.622	0.637	0.640	0.672	0.665	0.651	0.633

APPENDIX A: Amphibole Compositions; S81 Full Strain Transition Mylonitic Section

		TR2AM1	TR2AM1	TR3AM1	TR3AM1	TR3AM1	TR3AM1	TR3AM1	TR3AM1	17AM4.	17AM4.	17AM5.	17AM5.
	SiO2	46.210	44.610	45.040	45.870	45.130	46.260	46.200	44.610	45.480	46.620	46.700	46.360
	Al2O3	8.470	10.620	9.560	9.320	9.200	9.710	9.120	11.800	9.610	8.640	9.020	9.120
	TiO2	0.890	1.080	0.980	0.870	0.840	0.790	0.920	0.520	0.850	0.900	0.930	0.990
	FeO	15.980	16.570	15.940	16.420	16.370	15.500	15.450	16.240	16.810	15.670	16.180	16.550
	MnO	0.350	0.360	0.370	0.350	0.380	0.390	0.310	0.230	0.270	0.330	0.270	0.320
	MgO	11.430	10.330	11.120	11.580	11.300	11.240	11.300	9.860	11.770	11.620	11.550	11.420
	CaO	11.820	11.780	11.500	11.790	11.930	11.950	11.680	12.010	10.980	11.770	11.870	11.880
	Na2O	0.920	1.180	0.820	1.110	1.120	0.950	1.020	1.180	0.940	0.870	0.930	1.050
	K2O	0.260	0.330	0.260	0.250	0.260	0.250	0.300	0.350	0.280	0.230	0.250	0.300
	Cl	0.136	0.092	0.082	0.091	0.124	0.130	0.165	0.177	0.150	0.122	0.121	0.134
	F	0.020	0.259	0.122	0.154	0.173	0.049	0.047	0.000	0.061	0.000	0.165	0.000
	Total	96.486	97.211	95.794	97.805	96.827	97.219	96.512	96.977	97.201	96.772	97.986	98.124
Tetrahedral	Si	6.861	6.628	6.710	6.715	6.708	6.807	6.851	6.637	6.622	6.872	6.821	6.773
	Al	1.139	1.372	1.290	1.285	1.292	1.193	1.149	1.363	1.378	1.128	1.179	1.227
	Fe3+	0.000	0.000	0.000	0.000	0.000	0.000	0.000	0.000	0.000	0.000	0.000	0.000
	total T site	8.000	8.000	8.000	8.000	8.000	8.000	8.000	8.000	8.000	8.000	8.000	8.000
Octahedral M1,M2,M3	Al	0.343	0.487	0.388	0.323	0.320	0.491	0.445	0.706	0.272	0.374	0.373	0.343
	Ti	0.099	0.121	0.110	0.096	0.094	0.087	0.103	0.058	0.093	0.100	0.102	0.109
	Fe3+	0.523	0.491	0.725	0.710	0.613	0.441	0.438	0.306	1.176	0.545	0.577	0.595
	Mg	2.530	2.288	2.470	2.527	2.504	2.466	2.498	2.187	2.555	2.554	2.515	2.487
	Fe2+	1.461	1.568	1.261	1.301	1.422	1.466	1.478	1.715	0.871	1.387	1.400	1.427
	Mn	0.044	0.045	0.047	0.043	0.048	0.049	0.039	0.029	0.033	0.041	0.033	0.040
	total M1-M3	5.000	5.000	5.000	5.000	5.000	5.000	5.000	5.000	5.000	5.000	5.000	5.000
Octahedral M4	Ca	1.880	1.875	1.836	1.849	1.900	1.884	1.856	1.914	1.713	1.859	1.857	1.859
	Na	0.120	0.125	0.164	0.151	0.100	0.116	0.144	0.086	0.265	0.141	0.143	0.141
	Fe2+	0.000	0.000	0.000	0.000	0.000	0.000	0.000	0.000	0.000	0.000	0.000	0.000
	Mn	0.000	0.000	0.000	0.000	0.000	0.000	0.000	0.000	0.000	0.000	0.000	0.000
	Mg	0.000	0.000	0.000	0.000	0.000	0.000	0.000	0.000	0.000	0.000	0.000	0.000
	total M4 site	2.000	2.000	2.000	2.000	2.000	2.000	2.000	2.000	1.978	2.000	2.000	2.000
A site	Na	0.145	0.215	0.072	0.164	0.223	0.155	0.149	0.255	0.000	0.108	0.121	0.157
	K	0.049	0.063	0.049	0.047	0.049	0.047	0.057	0.066	0.052	0.043	0.047	0.056
	total A site	0.194	0.278	0.122	0.211	0.272	0.202	0.206	0.321	0.052	0.151	0.167	0.213
	Mg/Mg+Fe2+	0.634	0.593	0.662	0.660	0.638	0.627	0.628	0.561	0.746	0.648	0.642	0.635

APPENDIX A: Amphibole Compositions; S142 Full Strain Transition Undeformed Section

		142.4ualtr	142.4ualtr	142.4ualtr	142.4ualtr	142.4ualtr	142.4ualtr	142.4ualtr	142.4ualtr	142.4ualtr	142.4ualtr	142.4ualtr	142.4ualtr	142.4ualtr
	SiO2	46.302	46.403	46.217	47.695	47.163	46.714	46.979	47.358	48.748	48.931	48.762	48.853	49.146
	Al2O3	9.261	7.627	7.753	7.987	7.664	7.657	7.695	7.271	6.350	6.970	6.141	5.819	6.037
	TiO2	0.268	0.412	0.304	0.379	0.350	0.403	0.333	0.477	0.340	0.278	0.298	0.368	0.361
	FeO	16.700	16.289	16.016	16.066	15.743	16.155	15.883	15.843	15.566	15.100	15.141	14.995	15.626
	MnO	0.246	0.245	0.255	0.296	0.243	0.232	0.224	0.265	0.214	0.211	0.213	0.253	0.270
	MgO	11.067	11.922	11.925	11.680	11.774	11.968	11.924	12.096	12.770	11.524	12.717	13.047	12.889
	CaO	12.031	12.413	12.168	12.184	12.210	12.181	12.263	12.241	12.183	11.893	12.209	12.356	12.308
	Na2O	0.947	0.696	0.835	0.820	0.758	0.769	0.792	0.785	0.657	0.694	0.624	0.621	0.625
	K2O	0.193	0.203	0.180	0.170	0.199	0.185	0.159	0.157	0.110	0.148	0.134	0.129	0.118
	Cl	0.098	0.079	0.091	0.059	0.088	0.103	0.104	0.068	0.080	0.036	0.060	0.065	0.056
	F	0.016	0.000	0.062	0.034	0.042	0.044	0.040	0.000	0.115	0.056	0.002	0.000	0.015
	Total	97.129	96.289	95.806	97.370	96.234	96.411	96.396	96.561	97.133	95.841	96.301	96.506	97.451
Tetrahedral	Si	6.833	6.910	6.908	7.007	7.016	6.933	6.976	7.013	7.143	7.283	7.201	7.201	7.175
	Al	1.167	1.090	1.092	0.993	0.984	1.067	1.024	0.987	0.857	0.717	0.799	0.799	0.825
	Fe3+	0.000	0.000	0.000	0.000	0.000	0.000	0.000	0.000	0.000	0.000	0.000	0.000	0.000
	total T site	8.000	8.000	8.000	8.000	8.000	8.000	8.000	8.000	8.000	8.000	8.000	8.000	8.000
Octahedral M1,M2,M3	Al	0.444	0.248	0.274	0.390	0.360	0.273	0.323	0.282	0.239	0.506	0.270	0.212	0.214
	Ti	0.030	0.046	0.034	0.042	0.039	0.045	0.037	0.053	0.037	0.031	0.033	0.041	0.040
	Fe3+	0.552	0.550	0.575	0.419	0.396	0.574	0.467	0.460	0.511	0.128	0.394	0.401	0.482
	Mg	2.435	2.646	2.657	2.558	2.611	2.648	2.640	2.670	2.789	2.557	2.800	2.867	2.805
	Fe2+	1.509	1.479	1.427	1.555	1.563	1.431	1.506	1.501	1.397	1.752	1.476	1.448	1.426
	Mn	0.031	0.031	0.032	0.037	0.031	0.029	0.028	0.033	0.027	0.027	0.027	0.032	0.033
	total M1-M3	5.000	5.000	5.000	5.000	5.000	5.000	5.000	5.000	5.000	5.000	5.000	5.000	5.000
Octahedral M4	Ca	1.902	1.980	1.949	1.918	1.946	1.937	1.951	1.942	1.913	1.897	1.932	1.951	1.925
	Na	0.098	0.020	0.051	0.082	0.054	0.063	0.049	0.058	0.087	0.103	0.068	0.049	0.075
	Fe2+	0.000	0.000	0.000	0.000	0.000	0.000	0.000	0.000	0.000	0.000	0.000	0.000	0.000
	Mn	0.000	0.000	0.000	0.000	0.000	0.000	0.000	0.000	0.000	0.000	0.000	0.000	0.000
	Mg	0.000	0.000	0.000	0.000	0.000	0.000	0.000	0.000	0.000	0.000	0.000	0.000	0.000
	total M4 site	2.000	2.000	2.000	2.000	2.000	2.000	2.000	2.000	2.000	2.000	2.000	2.000	2.000
A site	Na	0.173	0.181	0.191	0.151	0.165	0.158	0.179	0.167	0.099	0.097	0.111	0.129	0.102
	K	0.036	0.039	0.034	0.032	0.038	0.035	0.030	0.030	0.021	0.028	0.025	0.024	0.022
	total A site	0.210	0.220	0.225	0.183	0.203	0.193	0.209	0.197	0.120	0.125	0.136	0.153	0.124
	Mg/Fe2+ + Mg	0.617	0.642	0.651	0.622	0.626	0.649	0.637	0.640	0.666	0.593	0.655	0.664	0.663

APPENDIX A: Amphibole Compositions; S142 Full Strain Transition Undeformed Section

		142.4ualtr	142.4ualtr	142.4ualtr	142.4ualtr	142.4ua8tr	142.4ua8tr	142.4ua8tr	142.4ua8tr	142.4ua8tr	142.4ua8tr	142.4ua8tr	142.4ua8tr	142.4ua8tr
	SiO2	47.500	47.073	48.637	46.841	43.983	46.685	49.311	47.499	44.504	44.446	43.810	43.913	44.039
	Al2O3	7.414	7.607	7.117	7.819	9.153	5.890	3.389	5.454	8.990	7.404	7.797	7.912	7.926
	TiO2	0.363	0.425	0.521	0.446	0.500	0.414	0.165	0.418	0.333	0.568	0.604	0.683	0.658
	FeO	15.644	15.715	15.806	16.144	17.282	15.631	14.691	15.897	16.477	17.014	17.432	17.182	17.524
	MnO	0.255	0.224	0.297	0.270	0.305	0.321	0.271	0.309	0.196	0.284	0.340	0.324	0.312
	MgO	12.227	12.066	12.255	11.711	10.850	12.472	14.279	13.278	10.929	11.565	11.214	11.092	11.222
	CaO	12.442	12.160	12.552	12.086	11.642	12.064	12.321	11.958	12.043	11.906	11.729	11.744	11.653
	Na2O	0.681	0.752	0.742	0.739	0.910	0.729	0.375	0.662	0.929	0.783	0.982	0.979	0.981
	K2O	0.160	0.180	0.156	0.199	0.242	0.156	0.102	0.136	0.191	0.216	0.246	0.211	0.233
	Cl	0.065	0.090	0.068	0.064	0.108	0.077	0.017	0.093	0.109	0.094	0.069	0.110	0.092
	F	0.026	0.039	0.036	0.052	0.000	0.044	0.000	0.000	0.103	0.031	0.026	0.045	0.072
	Total	96.777	96.331	98.187	96.371	94.975	94.483	94.921	95.704	94.804	94.311	94.249	94.195	94.712
Tetrahedral	Si	7.014	6.980	7.092	6.953	6.646	7.067	7.349	7.050	6.760	6.773	6.697	6.722	6.694
	Al	0.986	1.020	0.908	1.047	1.354	0.933	0.595	0.950	1.240	1.227	1.303	1.278	1.306
	Fe3+	0.000	0.000	0.000	0.000	0.000	0.000	0.056	0.000	0.000	0.000	0.000	0.000	0.000
	total T site	8.000	8.000	8.000	8.000	8.000	8.000	8.000	8.000	8.000	8.000	8.000	8.000	8.000
Octahedral M1,M2,M3	Al	0.304	0.309	0.315	0.321	0.276	0.118	0.000	0.004	0.369	0.103	0.102	0.149	0.114
	Ti	0.040	0.047	0.057	0.050	0.057	0.047	0.018	0.047	0.038	0.065	0.069	0.079	0.075
	Fe3+	0.439	0.503	0.318	0.532	0.881	0.563	0.608	0.834	0.565	0.833	0.880	0.789	0.912
	Mg	2.692	2.667	2.664	2.591	2.444	2.815	3.172	2.938	2.475	2.627	2.556	2.531	2.543
	Fe2+	1.493	1.445	1.609	1.472	1.303	1.416	1.201	1.139	1.528	1.335	1.348	1.411	1.316
	Mn	0.032	0.028	0.037	0.034	0.039	0.041	0.000	0.039	0.025	0.037	0.044	0.042	0.040
	total M1-M3	5.000	5.000	5.000	5.000	5.000	5.000	5.000	5.000	5.000	5.000	5.000	5.000	5.000
Octahedral M4	Ca	1.968	1.932	1.961	1.922	1.885	1.957	1.967	1.902	1.960	1.944	1.921	1.926	1.898
	Na	0.032	0.068	0.039	0.078	0.115	0.043	0.000	0.098	0.040	0.056	0.079	0.074	0.102
	Fe2+	0.000	0.000	0.000	0.000	0.000	0.000	0.022	0.000	0.000	0.000	0.000	0.000	0.000
	Mn	0.000	0.000	0.000	0.000	0.000	0.000	0.034	0.000	0.000	0.000	0.000	0.000	0.000
	Mg	0.000	0.000	0.000	0.000	0.000	0.000	0.000	0.000	0.000	0.000	0.000	0.000	0.000
	total M4 site	2.000	2.000	2.000	2.000	2.000	2.000	2.023	2.000	2.000	2.000	2.000	2.000	2.000
A site	Na	0.163	0.148	0.171	0.135	0.151	0.171	0.108	0.092	0.233	0.175	0.212	0.217	0.187
	K	0.030	0.034	0.029	0.038	0.047	0.030	0.019	0.026	0.037	0.042	0.048	0.041	0.045
	total A site	0.194	0.182	0.200	0.172	0.198	0.201	0.128	0.118	0.270	0.217	0.260	0.258	0.232
	Mg/Fe2+ + Mg	0.643	0.649	0.623	0.638	0.652	0.665	0.722	0.721	0.618	0.663	0.655	0.642	0.659

APPENDIX A: Amphibole Compositions; S142 Full Strain Transition Undeformed Section

		142.4ua8tr	142.4ua2tr	142.4ua2tr	142.4ua2tr
	SiO2	43.754	43.569	45.357	50.656
	Al2O3	7.950	10.373	7.545	4.127
	TiO2	0.688	0.355	0.588	0.296
	FeO	17.192	17.140	17.005	15.281
	MnO	0.223	0.208	0.272	0.310
	MgO	11.322	10.356	11.470	13.772
	CaO	11.742	12.046	11.901	11.938
	Na2O	0.929	1.077	0.840	0.514
	K2O	0.252	0.221	0.229	0.046
	Cl	0.080	0.093	0.080	0.040
	F	0.000	0.000	0.000	0.060
	Total	94.132	95.438	95.287	97.040
Tetrahedral	Si	6.685	6.585	6.837	7.373
	Al	1.315	1.415	1.163	0.627
	Fe3+	0.000	0.000	0.000	0.000
	total T site	8.000	8.000	8.000	8.000
Octahedral	Al	0.117	0.433	0.177	0.081
M1,M2,M3	Ti	0.079	0.040	0.067	0.032
	Fe3+	0.872	0.641	0.719	0.604
	Mg	2.579	2.333	2.577	2.988
	Fe2+	1.325	1.525	1.425	1.256
	Mn	0.029	0.027	0.035	0.038
	total M1-M3	5.000	5.000	5.000	5.000
Octahedral	Ca	1.922	1.951	1.922	1.862
M4	Na	0.078	0.049	0.078	0.138
	Fe2+	0.000	0.000	0.000	0.000
	Mn	0.000	0.000	0.000	0.000
	Mg	0.000	0.000	0.000	0.000
	total M4 site	2.000	2.000	2.000	2.000
A site	Na	0.197	0.266	0.168	0.007
	K	0.049	0.043	0.044	0.009
	total A site	0.246	0.309	0.212	0.015
	Mg/Fe2+ + Mg	0.661	0.605	0.644	0.704

APPENDIX A: Amphibole Compositions; S142 Full Strain Transition Transitional Section

		142.2ta2tr	142.2ta2tr	142.2ta2tr	142.2ta2tr	142.2ta2tr	142.2ta6tr	142.2ta6tr	142.2ta6tr	142.2ta6tr	142.2ta1.1	142.2ta1.2	142.2ta1.3	142.2ta1.4
	SiO2	46.514	46.232	45.691	46.104	45.783	45.397	46.410	46.173	47.069	47.903	47.134	47.193	46.470
	Al2O3	7.790	8.181	8.556	8.078	8.072	8.248	8.050	8.188	8.037	8.408	8.105	7.983	8.279
	TiO2	0.510	0.634	0.556	0.567	0.564	1.402	1.286	0.616	0.486	0.358	0.430	0.508	0.518
	FeO	16.901	17.274	17.279	17.565	17.687	16.931	16.993	16.488	16.239	16.235	15.959	16.585	16.649
	MnO	0.232	0.249	0.242	0.282	0.296	0.325	0.249	0.252	0.254	0.320	0.169	0.261	0.195
	MgO	11.745	11.295	11.185	11.459	11.374	11.006	11.559	11.761	12.022	11.912	11.717	11.801	11.604
	CaO	12.100	11.900	12.155	12.029	11.998	12.126	12.087	12.283	12.217	12.105	12.231	12.166	12.014
	Na2O	0.800	1.071	0.936	0.973	0.944	0.804	0.806	0.846	0.794	0.773	0.704	0.870	0.850
	K2O	0.200	0.224	0.247	0.229	0.245	0.188	0.181	0.191	0.196	0.179	0.169	0.237	0.217
	Cl	0.083	0.130	0.107	0.117	0.119	0.060	0.105	0.065	0.121	0.083	0.089	0.112	0.088
	F	0.013	0.013	0.078	0.000	0.000	0.030	0.008	0.017	0.078	0.000	0.024	0.090	0.000
	Total	96.888	97.203	97.032	97.403	97.082	96.517	97.734	96.880	97.513	98.276	96.731	97.806	96.884
Tetrahedral	Si	6.878	6.842	6.787	6.806	6.785	6.782	6.816	6.835	6.904	6.943	6.966	6.919	6.865
	Al	1.122	1.158	1.213	1.194	1.215	1.218	1.184	1.165	1.096	1.057	1.034	1.081	1.135
	Fe3+	0.000	0.000	0.000	0.000	0.000	0.000	0.000	0.000	0.000	0.000	0.000	0.000	0.000
	total T site	8.000	8.000	8.000	8.000	8.000	8.000	8.000	8.000	8.000	8.000	8.000	8.000	8.000
Octahedral	Al	0.235	0.269	0.284	0.211	0.195	0.235	0.209	0.263	0.294	0.380	0.377	0.299	0.306
M1,M2,M3	Ti	0.057	0.071	0.062	0.063	0.063	0.158	0.142	0.069	0.054	0.039	0.048	0.056	0.058
	Fe3+	0.673	0.625	0.620	0.730	0.766	0.517	0.624	0.590	0.592	0.589	0.455	0.556	0.627
	Mg	2.589	2.492	2.477	2.522	2.513	2.451	2.531	2.595	2.629	2.574	2.581	2.579	2.555
	Fe2+	1.417	1.512	1.527	1.439	1.426	1.598	1.463	1.452	1.400	1.379	1.518	1.477	1.430
	Mn	0.029	0.031	0.030	0.035	0.037	0.041	0.031	0.032	0.032	0.039	0.021	0.032	0.024
	total M1-M3	5.000	5.000	5.000	5.000	5.000	5.000	5.000	5.000	5.000	5.000	5.000	5.000	5.000
Octahedral	Ca	1.917	1.887	1.934	1.903	1.905	1.941	1.902	1.948	1.920	1.880	1.937	1.911	1.901
M4	Na	0.083	0.113	0.066	0.097	0.095	0.059	0.098	0.052	0.080	0.120	0.063	0.089	0.099
	Fe2+	0.000	0.000	0.000	0.000	0.000	0.000	0.000	0.000	0.000	0.000	0.000	0.000	0.000
	Mn	0.000	0.000	0.000	0.000	0.000	0.000	0.000	0.000	0.000	0.000	0.000	0.000	0.000
	Mg	0.000	0.000	0.000	0.000	0.000	0.000	0.000	0.000	0.000	0.000	0.000	0.000	0.000
	total M4 site	2.000	2.000	2.000	2.000	2.000	2.000	2.000	2.000	2.000	2.000	2.000	2.000	2.000
A site	Na	0.146	0.194	0.204	0.181	0.176	0.174	0.131	0.191	0.146	0.097	0.138	0.158	0.145
	K	0.038	0.042	0.047	0.043	0.046	0.036	0.034	0.036	0.037	0.033	0.032	0.044	0.041
	total A site	0.184	0.236	0.251	0.224	0.223	0.210	0.165	0.227	0.183	0.130	0.170	0.203	0.186
	Mg/Fe2+ + Mg	0.646	0.622	0.619	0.637	0.638	0.605	0.634	0.641	0.652	0.651	0.630	0.636	0.641

APPENDIX A: Amphibole Compositions; S142 Full Strain Transition Transitional Section

		142.2ta1.5	142.2ta1.6	142.2ta5tr	142.2ta5tr	142.2ta5tr	142.2ta5tr	142.2ta5tr	142.2ta3tr	142.2ta3tr	142.3ta2tr	142.3ta2tr	142.3ta2tr	142.3ta2tr
	SiO2	46.752	47.553	46.823	46.696	50.850	49.085	46.871	44.653	42.520	45.676	46.311	47.073	47.338
	Al2O3	8.512	8.564	7.814	7.747	4.218	6.700	8.213	11.991	11.064	9.676	8.475	8.099	8.012
	TiO2	0.389	0.463	0.512	0.530	0.274	0.422	0.527	0.307	0.940	0.755	0.704	0.758	0.676
	FeO	16.182	16.419	16.618	17.134	15.899	16.121	16.892	17.697	18.444	17.675	17.503	17.102	17.298
	MnO	0.234	0.210	0.235	0.238	0.361	0.292	0.281	0.292	0.338	0.243	0.277	0.262	0.274
	MgO	11.679	11.527	11.947	11.607	13.991	12.245	11.156	9.543	9.282	10.472	11.168	11.486	11.480
	CaO	12.277	12.105	12.092	12.153	12.434	12.178	12.086	12.111	11.819	12.079	11.975	11.851	11.807
	Na2O	0.809	0.851	0.868	0.870	0.473	0.713	0.838	1.239	1.209	1.003	0.941	0.926	0.924
	K2O	0.237	0.232	0.192	0.193	0.070	0.153	0.225	0.255	0.386	0.300	0.201	0.220	0.210
	Cl	0.110	0.119	0.093	0.082	0.107	0.056	0.057	0.100	0.140	0.156	0.109	0.107	0.120
	F	0.000	0.036	0.064	0.107	0.028	0.046	0.030	0.028	0.000	0.000	0.000	0.049	0.000
	Total	97.181	98.079	97.258	97.357	98.705	98.011	97.176	98.216	96.142	98.035	97.664	97.933	98.139
Tetrahedral	Si	6.889	6.939	6.892	6.894	7.306	7.147	6.929	6.575	6.441	6.729	6.814	6.889	6.907
	Al	1.111	1.061	1.108	1.106	0.694	0.853	1.071	1.425	1.559	1.271	1.186	1.111	1.093
	Fe3+	0.000	0.000	0.000	0.000	0.000	0.000	0.000	0.000	0.000	0.000	0.000	0.000	0.000
	total T site	8.000	8.000	8.000	8.000	8.000	8.000	8.000	8.000	8.000	8.000	8.000	8.000	8.000
Octahedral M1,M2,M3	Al	0.368	0.412	0.247	0.242	0.020	0.297	0.360	0.656	0.417	0.409	0.284	0.285	0.284
	Ti	0.043	0.051	0.057	0.059	0.030	0.046	0.059	0.034	0.107	0.084	0.078	0.083	0.074
	Fe3+	0.504	0.478	0.650	0.617	0.643	0.434	0.484	0.479	0.661	0.539	0.664	0.639	0.669
	Mg	2.566	2.508	2.621	2.554	2.997	2.658	2.458	2.095	2.096	2.300	2.450	2.506	2.497
	Fe2+	1.490	1.526	1.395	1.498	1.267	1.529	1.605	1.701	1.675	1.638	1.490	1.454	1.442
	Mn	0.029	0.026	0.029	0.030	0.044	0.036	0.035	0.036	0.043	0.030	0.035	0.032	0.034
	total M1-M3	5.000	5.000	5.000	5.000	5.000	5.000	5.000	5.000	5.000	5.000	5.000	5.000	5.000
Octahedral M4	Ca	1.938	1.893	1.907	1.922	1.914	1.900	1.914	1.911	1.918	1.907	1.888	1.858	1.846
	Na	0.062	0.107	0.093	0.078	0.086	0.100	0.086	0.089	0.082	0.093	0.112	0.142	0.154
	Fe2+	0.000	0.000	0.000	0.000	0.000	0.000	0.000	0.000	0.000	0.000	0.000	0.000	0.000
	Mn	0.000	0.000	0.000	0.000	0.000	0.000	0.000	0.000	0.000	0.000	0.000	0.000	0.000
	Mg	0.000	0.000	0.000	0.000	0.000	0.000	0.000	0.000	0.000	0.000	0.000	0.000	0.000
	total M4 site	2.000	2.000	2.000	2.000	2.000	2.000	2.000	2.000	2.000	2.000	2.000	2.000	2.000
A site	Na	0.170	0.133	0.155	0.171	0.046	0.101	0.154	0.264	0.273	0.193	0.156	0.121	0.107
	K	0.045	0.043	0.036	0.036	0.013	0.028	0.042	0.048	0.075	0.056	0.038	0.041	0.039
	total A site	0.214	0.177	0.191	0.208	0.059	0.130	0.197	0.312	0.348	0.249	0.194	0.162	0.146
	Mg/Fe2+ + Mg	0.633	0.622	0.653	0.630	0.703	0.635	0.605	0.552	0.556	0.584	0.622	0.633	0.634

APPENDIX A: Amphibole Compositions; S142 Full Strain Transition Transitional Section

		142.3ta2tr	142.3ta5tr	142.3ta5tr	142.3ta5tr	142.3ta5tr	142.3ta5tr	142.3ta7tr	142.3ta7tr	142.3ta7tr	142.3ta7tr	142.3ta7tr	142.3ta1.1	142.3ta1.2
	SiO2	46.223	47.439	47.409	46.038	46.069	46.550	45.805	46.001	46.728	48.471	45.787	42.964	46.662
	Al2O3	7.820	8.256	8.174	8.503	8.424	7.739	8.787	8.083	8.043	6.924	8.891	12.593	8.757
	TiO2	0.702	0.612	0.639	0.691	0.659	0.634	0.725	0.608	0.567	0.525	0.712	0.385	0.697
	FeO	17.264	17.457	17.482	17.387	17.584	17.382	17.969	17.694	16.875	16.872	17.320	18.391	17.533
	MnO	0.235	0.221	0.257	0.227	0.240	0.295	0.371	0.310	0.266	0.331	0.300	0.264	0.241
	MgO	11.339	11.348	11.408	11.134	11.241	11.545	10.988	11.154	11.370	12.177	10.939	8.775	11.181
	CaO	11.979	12.060	12.234	12.079	12.141	12.085	12.036	12.027	12.013	12.125	12.106	11.681	12.022
	Na2O	0.920	0.994	0.929	0.989	0.971	0.839	0.996	0.909	0.866	0.812	0.898	1.241	0.922
	K2O	0.253	0.235	0.223	0.252	0.259	0.247	0.296	0.209	0.185	0.175	0.269	0.369	0.262
	Cl	0.117	0.126	0.105	0.118	0.101	0.099	0.110	0.132	0.113	0.086	0.114	0.210	0.131
	F	0.000	0.036	0.059	0.000	0.000	0.048	0.000	0.000	0.000	0.000	0.000	0.051	0.000
	Total	96.852	98.784	98.919	97.418	97.689	97.463	98.083	97.127	97.026	98.498	97.336	96.924	98.408
Tetrahedral	Si	6.867	6.903	6.896	6.808	6.793	6.865	6.734	6.821	6.909	7.035	6.776	6.436	6.813
	Al	1.133	1.097	1.104	1.192	1.207	1.135	1.266	1.179	1.091	0.965	1.224	1.564	1.187
	Fe3+	0.000	0.000	0.000	0.000	0.000	0.000	0.000	0.000	0.000	0.000	0.000	0.000	0.000
	total T site	8.000	8.000	8.000	8.000	8.000	8.000	8.000	8.000	8.000	8.000	8.000	8.000	8.000
Octahedral M1,M2,M3	Al	0.236	0.319	0.298	0.290	0.257	0.211	0.256	0.234	0.311	0.219	0.326	0.659	0.319
	Ti	0.078	0.067	0.070	0.077	0.073	0.070	0.080	0.068	0.063	0.057	0.079	0.043	0.077
	Fe3+	0.614	0.558	0.549	0.590	0.640	0.678	0.718	0.688	0.565	0.599	0.592	0.637	0.644
	Mg	2.511	2.462	2.474	2.455	2.471	2.538	2.408	2.466	2.506	2.635	2.413	1.960	2.434
	Fe2+	1.531	1.566	1.578	1.561	1.528	1.466	1.491	1.507	1.522	1.449	1.551	1.667	1.497
	Mn	0.030	0.027	0.032	0.028	0.030	0.037	0.046	0.039	0.033	0.041	0.038	0.033	0.030
	total M1-M3	5.000	5.000	5.000	5.000	5.000	5.000	5.000	5.000	5.000	5.000	5.000	5.000	5.000
Octahedral M4	Ca	1.907	1.880	1.907	1.914	1.918	1.910	1.896	1.911	1.903	1.885	1.919	1.875	1.881
	Na	0.093	0.120	0.093	0.086	0.082	0.090	0.104	0.089	0.097	0.115	0.081	0.125	0.119
	Fe2+	0.000	0.000	0.000	0.000	0.000	0.000	0.000	0.000	0.000	0.000	0.000	0.000	0.000
	Mn	0.000	0.000	0.000	0.000	0.000	0.000	0.000	0.000	0.000	0.000	0.000	0.000	0.000
	Mg	0.000	0.000	0.000	0.000	0.000	0.000	0.000	0.000	0.000	0.000	0.000	0.000	0.000
	total M4 site	2.000	2.000	2.000	2.000	2.000	2.000	2.000	2.000	2.000	2.000	2.000	2.000	2.000
A site	Na	0.172	0.161	0.169	0.197	0.196	0.150	0.180	0.172	0.151	0.114	0.177	0.235	0.142
	K	0.048	0.044	0.041	0.048	0.049	0.046	0.056	0.040	0.035	0.032	0.051	0.071	0.049
	total A site	0.220	0.204	0.210	0.245	0.245	0.196	0.235	0.212	0.186	0.146	0.228	0.306	0.190
	Mg/Fe2+ + Mg	0.621	0.611	0.611	0.611	0.618	0.634	0.618	0.621	0.622	0.645	0.609	0.540	0.619

APPENDIX A: Amphibole Compositions; S142 Full Strain Transition Transitional Section

		142.3ta1.3	142.3ta1.4	142.3ta1.5	142.3ta1.6	142.3ta1.7	142.3ta1.8	142.3ta1.9	142.3ta1.10
	SiO2	46.303	48.713	46.568	47.416	50.278	46.853	47.917	49.493
	Al2O3	8.448	5.265	7.946	6.225	5.001	7.562	7.697	5.998
	TiO2	0.671	0.343	0.422	0.389	0.286	0.444	0.513	0.428
	FeO	16.963	15.542	16.521	16.456	15.534	16.084	15.956	15.958
	MnO	0.290	0.333	0.202	0.231	0.233	0.308	0.241	0.351
	MgO	11.229	13.191	11.607	12.153	13.129	11.890	11.794	12.655
	CaO	12.202	12.130	12.104	11.920	12.229	12.329	12.344	12.196
	Na2O	0.891	0.584	0.812	0.711	0.512	0.745	0.803	0.546
	K2O	0.236	0.114	0.188	0.152	0.075	0.171	0.157	0.121
	Cl	0.122	0.054	0.098	0.069	0.048	0.067	0.085	0.079
	F	0.037	0.069	0.000	0.000	0.000	0.000	0.003	0.005
	Total	97.392	96.338	96.468	95.722	97.325	96.453	97.510	97.830
Tetrahedral	Si	6.845	7.186	6.915	7.075	7.332	6.958	7.038	7.198
	Al	1.155	0.814	1.085	0.925	0.668	1.042	0.962	0.802
	Fe3+	0.000	0.000	0.000	0.000	0.000	0.000	0.000	0.000
	total T site	8.000	8.000	8.000	8.000	8.000	8.000	8.000	8.000
Octahedral	Al	0.317	0.102	0.306	0.170	0.191	0.282	0.371	0.226
M1,M2,M3	Ti	0.075	0.038	0.047	0.044	0.031	0.050	0.057	0.047
	Fe3+	0.523	0.613	0.563	0.621	0.434	0.491	0.334	0.506
	Mg	2.475	2.901	2.570	2.703	2.854	2.632	2.583	2.744
	Fe2+	1.574	1.305	1.489	1.432	1.460	1.507	1.626	1.435
	Mn	0.036	0.042	0.025	0.029	0.029	0.039	0.030	0.043
	total M1-M3	5.000	5.000	5.000	5.000	5.000	5.000	5.000	5.000
Octahedral	Ca	1.933	1.917	1.926	1.906	1.911	1.962	1.943	1.900
M4	Na	0.067	0.083	0.074	0.094	0.089	0.038	0.057	0.100
	Fe2+	0.000	0.000	0.000	0.000	0.000	0.000	0.000	0.000
	Mn	0.000	0.000	0.000	0.000	0.000	0.000	0.000	0.000
	Mg	0.000	0.000	0.000	0.000	0.000	0.000	0.000	0.000
	total M4 site	2.000	2.000	2.000	2.000	2.000	2.000	2.000	2.000
A site	Na	0.188	0.084	0.160	0.111	0.055	0.176	0.171	0.054
	K	0.045	0.021	0.036	0.029	0.014	0.032	0.029	0.022
	total A site	0.233	0.106	0.195	0.140	0.069	0.209	0.201	0.077
	Mg/Fe2+ + Mg	0.611	0.690	0.633	0.654	0.662	0.636	0.614	0.657

APPENDIX A: Amphibole Compositions; S142 Full Strain Transition Mylonitic Section

		142.3m9tr	142.3m9tr	142.3m9tr	142.3m9tr	142.3m9tr	142.3ma8tr	142.3ma8tr	142.3ma7tr	142.3ma7tr	142.3ma7tr	142.3ma7tr	142.3ma7tr	142.3ma1.1
	SiO2	46.868	45.945	43.641	42.795	39.871	44.205	41.801	46.059	45.580	45.784	46.807	47.196	49.582
	Al2O3	8.569	8.923	10.888	12.472	15.899	11.683	14.647	8.601	8.376	8.485	7.879	8.152	6.472
	TiO2	0.657	0.701	0.833	0.503	0.397	0.348	0.406	0.686	0.717	0.599	0.606	0.637	0.418
	FeO	17.282	17.055	17.769	17.955	19.428	17.926	19.003	17.070	17.352	17.376	17.486	17.356	16.473
	MnO	0.270	0.292	0.292	0.292	0.228	0.268	0.291	0.294	0.252	0.319	0.298	0.281	0.243
	MgO	11.293	11.193	10.016	9.375	6.850	9.523	7.876	11.321	11.150	11.164	11.235	11.292	12.567
	CaO	12.013	12.082	12.106	12.011	12.101	12.188	12.062	11.926	12.056	12.192	11.938	11.999	12.208
	Na2O	1.000	0.844	1.068	1.128	1.451	1.089	1.353	0.894	0.938	1.013	0.937	0.891	0.697
	K2O	0.240	0.265	0.343	0.349	0.501	0.301	0.508	0.256	0.244	0.257	0.233	0.255	0.177
	Cl	0.115	0.081	0.167	0.177	0.132	0.106	0.270	0.098	0.103	0.084	0.083	0.104	0.105
	F	0.000	0.062	0.031	0.044	0.000	0.000	0.000	0.017	0.056	0.013	0.051	0.046	0.000
	Total	98.307	97.443	97.154	97.101	96.858	97.637	98.217	97.222	96.824	97.286	97.553	98.209	98.942
Tetrahedral	Si	6.848	6.773	6.511	6.387	6.058	6.556	6.228	6.795	6.784	6.788	6.901	6.904	7.143
	Al	1.152	1.227	1.489	1.613	1.942	1.444	1.772	1.205	1.216	1.212	1.099	1.096	0.857
	Fe3+	0.000	0.000	0.000	0.000	0.000	0.000	0.000	0.000	0.000	0.000	0.000	0.000	0.000
	total T site	8.000	8.000	8.000	8.000	8.000	8.000	8.000	8.000	8.000	8.000	8.000	8.000	8.000
Octahedral M1,M2,M3	Al	0.323	0.323	0.425	0.580	0.905	0.598	0.800	0.291	0.254	0.271	0.270	0.309	0.242
	Ti	0.072	0.078	0.093	0.056	0.045	0.039	0.045	0.076	0.080	0.067	0.067	0.070	0.045
	Fe3+	0.596	0.640	0.633	0.687	0.482	0.524	0.542	0.687	0.639	0.594	0.611	0.585	0.529
	Mg	2.460	2.460	2.228	2.086	1.552	2.106	1.749	2.490	2.474	2.468	2.469	2.462	2.699
	Fe2+	1.516	1.462	1.584	1.554	1.987	1.700	1.826	1.419	1.521	1.561	1.545	1.538	1.455
	Mn	0.033	0.036	0.037	0.037	0.029	0.034	0.037	0.037	0.032	0.040	0.037	0.035	0.030
	total M1-M3	5.000	5.000	5.000	5.000	5.000	5.000	5.000	5.000	5.000	5.000	5.000	5.000	5.000
Octahedral M4	Ca	1.880	1.908	1.935	1.920	1.970	1.937	1.926	1.885	1.923	1.937	1.886	1.881	1.884
	Na	0.120	0.092	0.065	0.080	0.030	0.063	0.074	0.115	0.077	0.063	0.114	0.119	0.116
	Fe2+	0.000	0.000	0.000	0.000	0.000	0.000	0.000	0.000	0.000	0.000	0.000	0.000	0.000
	Mn	0.000	0.000	0.000	0.000	0.000	0.000	0.000	0.000	0.000	0.000	0.000	0.000	0.000
	Mg	0.000	0.000	0.000	0.000	0.000	0.000	0.000	0.000	0.000	0.000	0.000	0.000	0.000
	total M4 site	2.000	2.000	2.000	2.000	2.000	2.000	2.000	2.000	2.000	2.000	2.000	2.000	2.000
A site	Na	0.164	0.150	0.244	0.247	0.397	0.250	0.316	0.141	0.193	0.228	0.154	0.133	0.079
	K	0.045	0.050	0.065	0.066	0.097	0.057	0.097	0.048	0.046	0.049	0.044	0.048	0.033
	total A site	0.209	0.199	0.309	0.313	0.495	0.307	0.413	0.189	0.240	0.277	0.197	0.181	0.111
	Mg/Fe2+ + Mg	0.619	0.627	0.584	0.573	0.438	0.553	0.489	0.637	0.619	0.613	0.615	0.616	0.650

APPENDIX A: Amphibole Compositions; S142 Full Strain Transition Mylonitic Section

		142.3ma1.2	142.3ma1.3	142.3ma1.4	142.3ma1.5	142.3ma1.6	142.3ma1.7	142.3ma1.8	142.3ma1.9	142.3ma1.10	142.3ma1.11	142.3ma1.12	142.3ma1.13	142.3ma1.14
	SiO2	48.994	48.932	46.692	51.970	48.287	47.479	45.560	47.347	47.936	47.216	49.788	47.048	46.736
	Al2O3	6.483	6.589	8.053	3.659	6.149	8.066	8.106	7.753	7.806	7.893	7.465	8.163	7.986
	TiO2	0.261	0.264	0.642	0.125	0.474	0.558	0.689	0.616	0.633	0.517	0.569	0.625	0.530
	FeO	15.732	15.825	16.934	14.298	16.079	16.108	16.892	16.368	16.261	15.875	16.093	16.613	16.643
	MnO	0.248	0.262	0.253	0.243	0.279	0.227	0.296	0.288	0.256	0.324	0.251	0.224	0.253
	MgO	12.857	12.345	11.683	14.335	12.528	11.166	11.413	11.902	11.447	12.012	11.783	11.690	11.658
	CaO	12.512	12.346	12.082	12.540	12.371	11.616	12.174	12.281	12.043	12.235	12.006	12.243	12.250
	Na2O	0.605	0.609	0.854	0.348	0.663	0.856	0.818	0.716	0.816	0.773	0.698	0.874	0.776
	K2O	0.110	0.124	0.200	0.055	0.182	0.234	0.225	0.233	0.232	0.210	0.168	0.191	0.171
	Cl	0.082	0.079	0.086	0.028	0.095	0.064	0.090	0.122	0.116	0.090	0.096	0.107	0.092
	F	0.000	0.000	0.000	0.029	0.024	0.000	0.029	0.112	0.000	0.049	0.007	0.000	0.011
	Total	97.884	97.375	97.479	97.630	97.131	96.374	96.292	97.738	97.546	97.194	98.924	97.778	97.106
Tetrahedral	Si	7.127	7.167	6.862	7.514	7.113	7.037	6.806	6.945	7.042	6.946	7.172	6.899	6.900
	Al	0.873	0.833	1.138	0.486	0.887	0.963	1.194	1.055	0.958	1.054	0.828	1.101	1.100
	Fe3+	0.000	0.000	0.000	0.000	0.000	0.000	0.000	0.000	0.000	0.000	0.000	0.000	0.000
	total T site	8.000	8.000	8.000	8.000	8.000	8.000	8.000	8.000	8.000	8.000	8.000	8.000	8.000
Octahedral M1,M2,M3	Al	0.239	0.304	0.257	0.138	0.181	0.446	0.233	0.286	0.394	0.315	0.439	0.310	0.289
	Ti	0.029	0.029	0.071	0.014	0.053	0.062	0.077	0.068	0.070	0.057	0.062	0.069	0.059
	Fe3+	0.486	0.399	0.654	0.328	0.473	0.414	0.629	0.526	0.358	0.508	0.335	0.521	0.564
	Mg	2.788	2.696	2.560	3.090	2.751	2.467	2.542	2.603	2.507	2.634	2.530	2.556	2.566
	Fe2+	1.428	1.539	1.427	1.401	1.508	1.583	1.481	1.482	1.640	1.446	1.604	1.516	1.491
	Mn	0.031	0.033	0.031	0.030	0.035	0.028	0.037	0.036	0.032	0.040	0.031	0.028	0.032
	total M1-M3	5.000	5.000	5.000	5.000	5.000	5.000	5.000	5.000	5.000	5.000	5.000	5.000	5.000
Octahedral M4	Ca	1.950	1.937	1.902	1.943	1.953	1.845	1.949	1.930	1.896	1.929	1.853	1.924	1.938
	Na	0.050	0.063	0.098	0.057	0.047	0.155	0.051	0.070	0.104	0.071	0.147	0.076	0.062
	Fe2+	0.000	0.000	0.000	0.000	0.000	0.000	0.000	0.000	0.000	0.000	0.000	0.000	0.000
	Mn	0.000	0.000	0.000	0.000	0.000	0.000	0.000	0.000	0.000	0.000	0.000	0.000	0.000
	Mg	0.000	0.000	0.000	0.000	0.000	0.000	0.000	0.000	0.000	0.000	0.000	0.000	0.000
	total M4 site	2.000	2.000	2.000	2.000	2.000	2.000	2.000	2.000	2.000	2.000	2.000	2.000	2.000
A site	Na	0.121	0.110	0.146	0.040	0.142	0.091	0.185	0.134	0.128	0.149	0.048	0.172	0.160
	K	0.020	0.023	0.037	0.010	0.034	0.044	0.043	0.044	0.043	0.039	0.031	0.036	0.032
	total A site	0.141	0.134	0.183	0.050	0.176	0.135	0.228	0.177	0.171	0.188	0.079	0.208	0.192
	Mg/Fe2+ + Mg	0.661	0.637	0.642	0.688	0.646	0.609	0.632	0.637	0.605	0.646	0.612	0.628	0.633

APPENDIX A: Amphibole Compositions; S142 F

		142.3ma1.15	142.3ma1.16
	SiO2	47.519	47.046
	Al2O3	8.266	8.335
	TiO2	0.525	0.676
	FeO	16.384	17.012
	MnO	0.222	0.288
	MgO	11.535	11.091
	CaO	12.267	12.193
	Na2O	0.712	0.853
	K2O	0.169	0.269
	Cl	0.089	0.094
	F	0.000	0.000
	Total	97.688	97.857
Tetrahedral	Si	6.961	6.920
	Al	1.039	1.080
	Fe3+	0.000	0.000
	total T site	8.000	8.000
Octahedral	Al	0.388	0.365
M1,M2,M3	Ti	0.058	0.075
	Fe3+	0.450	0.429
	Mg	2.519	2.432
	Fe2+	1.557	1.664
	Mn	0.028	0.036
	total M1-M3	5.000	5.000
Octahedral	Ca	1.925	1.922
M4	Na	0.075	0.078
	Fe2+	0.000	0.000
	Mn	0.000	0.000
	Mg	0.000	0.000
	total M4 site	2.000	2.000
A site	Na	0.128	0.165
	K	0.032	0.050
	total A site	0.159	0.215
	Mg/Fe2+ + Mg	0.618	0.594

APPENDIX A: Amphibole Compositions; S75 Mylonitic Amphibolite

		AMTR1.1	AMTR1.2	AMTR1.3	AMTR1.4	AMTR1.5	AMTR1.6	AMTR1.7	AMTR1.8	AM7R1.9	AMTR1.10	AMTR2.1	AMTR2.2	AMTR2.3
	SiO2	45.342	45.579	42.893	42.995	44.263	42.988	46.758	44.245	43.192	43.334	44.061	44.765	44.206
	Al2O3	9.887	9.423	10.977	11.243	9.738	11.159	7.780	11.557	13.431	14.013	12.734	11.438	11.082
	TiO2	0.990	1.034	1.123	1.051	0.770	0.819	0.489	0.410	0.259	0.379	0.518	0.633	1.073
	FeO	18.474	18.419	19.063	19.043	17.608	17.897	16.950	18.224	18.807	18.547	17.751	17.610	17.841
	MnO	0.226	0.277	0.250	0.381	0.204	0.244	0.211	0.225	0.241	0.219	0.235	0.235	0.241
	MgO	10.147	10.439	9.494	9.453	10.555	9.996	7.338	10.043	8.669	8.265	8.806	9.879	9.850
	CaO	11.573	11.605	11.907	11.759	11.702	11.537	12.002	11.506	11.840	11.974	10.876	11.375	11.766
	Na2O	1.040	1.119	1.197	1.278	0.956	1.034	0.428	1.222	1.147	1.271	1.179	1.049	0.995
	K2O	0.408	0.381	0.478	0.454	0.396	0.459	0.298	0.338	0.380	0.414	0.408	0.404	0.474
	Cl	0.103	0.102	0.105	0.040	0.103	0.115	0.118	0.146	0.194	0.231	0.136	0.092	0.082
	F	0.182	0.272	0.278	0.091	0.020	0.074	0.044	0.141	0.162	0.033	0.020	0.259	0.122
	Total	98.371	98.651	97.764	97.788	96.316	96.322	92.416	98.057	98.321	98.681	96.724	97.737	97.733
Tetrahedral	Si	6.660	6.683	6.411	6.397	6.618	6.436	7.450	6.494	6.375	6.391	6.537	6.585	6.539
	Al	1.340	1.317	1.589	1.603	1.382	1.564	0.550	1.506	1.625	1.609	1.463	1.415	1.461
	Fe3+	0.000	0.000	0.000	0.000	0.000	0.000	0.000	0.000	0.000	0.000	0.000	0.000	0.000
	total T site	8.000	8.000	8.000	8.000	8.000	8.000	8.000	8.000	8.000	8.000	8.000	8.000	8.000
Octahedral M1,M2,M3	Al	0.371	0.311	0.344	0.368	0.334	0.405	0.911	0.493	0.712	0.826	0.763	0.568	0.471
	Ti	0.109	0.114	0.126	0.118	0.087	0.092	0.059	0.045	0.029	0.042	0.058	0.070	0.119
	Fe3+	0.735	0.742	0.742	0.796	0.774	0.885	0.000	0.894	0.710	0.474	0.711	0.747	0.646
	Mg	2.222	2.282	2.115	2.097	2.352	2.231	1.743	2.197	1.908	1.817	1.947	2.166	2.172
	Fe2+	1.534	1.516	1.641	1.573	1.428	1.356	2.287	1.343	1.612	1.814	1.491	1.420	1.561
	Mn	0.028	0.034	0.032	0.048	0.026	0.031	0.000	0.028	0.030	0.027	0.030	0.029	0.030
	total M1-M3	5.000	5.000	5.000	5.000	5.000	5.000	5.000	5.000	5.000	5.000	5.000	5.000	5.000
Octahedral M4	Ca	1.821	1.823	1.907	1.874	1.874	1.851	2.049	1.809	1.872	1.892	1.729	1.793	1.865
	Na	0.179	0.177	0.093	0.126	0.126	0.149	0.000	0.191	0.128	0.108	0.271	0.207	0.135
	Fe2+	0.000	0.000	0.000	0.000	0.000	0.000	0.741	0.000	0.000	0.000	0.000	0.000	0.000
	Mn	0.000	0.000	0.000	0.000	0.000	0.000	0.029	0.000	0.000	0.000	0.000	0.000	0.000
	Mg	0.000	0.000	0.000	0.000	0.000	0.000	0.000	0.000	0.000	0.000	0.000	0.000	0.000
	total M4 site	2.000	2.000	2.000	2.000	2.000	2.000	2.818	2.000	2.000	2.000	2.000	2.000	2.000
A site	Na	0.117	0.141	0.254	0.243	0.152	0.151	0.132	0.157	0.201	0.255	0.068	0.092	0.150
	K	0.076	0.071	0.091	0.086	0.076	0.088	0.061	0.063	0.072	0.078	0.077	0.076	0.089
	total A site	0.194	0.213	0.345	0.329	0.227	0.239	0.193	0.220	0.272	0.333	0.145	0.168	0.240
	Mg/Mg+Fe2+	0.592	0.601	0.563	0.571	0.622	0.622	0.365	0.621	0.542	0.500	0.566	0.604	0.582

APPENDIX A: Amphibole Compositions; S75 Mylonitic Amphibolite

		AMTR2.4	AMTR2.5	AMTR2.6	AMTR3.1	AMTR3.2	AMTR3.3	AMTR3.4	AMTR3.5	AMTR3.6	AMTR1.1	AMTR1.3	AMTR1.4	AMTR1.5
	SiO2	44.560	44.703	45.312	44.126	43.505	44.069	44.385	42.981	43.306	45.589	44.461	46.067	45.587
	Al2O3	10.279	10.848	10.524	10.426	11.460	11.003	10.898	10.927	11.237	9.629	9.191	8.738	9.047
	TiO2	0.948	1.099	0.986	0.916	0.999	1.162	1.119	1.017	1.270	0.829	0.614	0.513	0.526
	FeO	17.730	17.861	17.273	18.681	17.957	18.858	18.031	18.346	18.701	17.469	17.915	17.690	17.837
	MnO	0.241	0.241	0.260	0.293	0.333	0.220	0.327	0.247	0.220	0.220	0.223	0.263	0.254
	MgO	10.117	9.858	10.234	9.890	9.223	9.426	9.487	9.713	9.348	10.516	10.780	10.780	10.911
	CaO	11.627	11.712	11.535	11.821	11.708	11.506	11.592	11.639	11.690	11.784	11.699	11.079	11.734
	Na2O	0.965	0.993	0.936	1.244	1.210	1.215	1.132	1.143	1.159	0.987	1.008	1.067	1.005
	K2O	0.459	0.450	0.398	0.441	0.514	0.469	0.456	0.449	0.484	0.350	0.329	0.339	0.296
	Cl	0.182	0.107	0.171	0.134	0.089	0.099	0.096	0.194	0.165	0.184	0.183	0.117	0.096
	F	1.976	0.142	0.242	0.119	0.095	0.101	0.118	0.717	0.132	0.003	0.050	0.000	0.000
	Total	99.085	98.013	97.871	98.091	97.091	98.126	97.639	97.373	97.712	97.559	96.454	96.652	97.291
Tetrahedral	Si	6.620	6.593	6.665	6.540	6.515	6.516	6.589	6.448	6.451	6.732	6.644	6.818	6.731
	Al	1.380	1.407	1.335	1.460	1.485	1.484	1.411	1.552	1.549	1.268	1.356	1.182	1.269
	Fe3+	0.000	0.000	0.000	0.000	0.000	0.000	0.000	0.000	0.000	0.000	0.000	0.000	0.000
	total T site	8.000	8.000	8.000	8.000	8.000	8.000	8.000	8.000	8.000	8.000	8.000	8.000	8.000
Octahedral M1,M2,M3	Al	0.420	0.478	0.490	0.361	0.538	0.434	0.496	0.380	0.424	0.408	0.263	0.342	0.306
	Ti	0.106	0.122	0.109	0.102	0.112	0.129	0.125	0.115	0.142	0.092	0.069	0.057	0.058
	Fe3+	0.681	0.616	0.649	0.701	0.516	0.709	0.566	0.783	0.682	0.598	0.855	0.842	0.790
	Mg	2.241	2.167	2.244	2.185	2.059	2.078	2.100	2.172	2.076	2.315	2.401	2.378	2.402
	Fe2+	1.522	1.587	1.475	1.615	1.733	1.622	1.673	1.519	1.648	1.559	1.384	1.348	1.412
	Mn	0.030	0.030	0.032	0.037	0.042	0.028	0.041	0.031	0.028	0.028	0.028	0.033	0.032
	total M1-M3	5.000	5.000	5.000	5.000	5.000	5.000	5.000	5.000	5.000	5.000	5.000	5.000	5.000
Octahedral M4	Ca	1.851	1.851	1.818	1.877	1.878	1.823	1.844	1.871	1.866	1.864	1.873	1.757	1.856
	Na	0.149	0.149	0.182	0.123	0.122	0.177	0.156	0.129	0.134	0.136	0.127	0.243	0.144
	Fe2+	0.000	0.000	0.000	0.000	0.000	0.000	0.000	0.000	0.000	0.000	0.000	0.000	0.000
	Mn	0.000	0.000	0.000	0.000	0.000	0.000	0.000	0.000	0.000	0.000	0.000	0.000	0.000
	Mg	0.000	0.000	0.000	0.000	0.000	0.000	0.000	0.000	0.000	0.000	0.000	0.000	0.000
	total M4 site	2.000	2.000	2.000	2.000	2.000	2.000	2.000	2.000	2.000	2.000	2.000	2.000	2.000
A site	Na	0.129	0.135	0.085	0.235	0.230	0.171	0.169	0.203	0.200	0.147	0.165	0.063	0.144
	K	0.087	0.085	0.075	0.083	0.098	0.088	0.086	0.086	0.092	0.066	0.063	0.064	0.056
	total A site	0.216	0.219	0.160	0.318	0.328	0.260	0.256	0.289	0.292	0.213	0.228	0.127	0.200
	Mg/Mg+Fe2+	0.596	0.577	0.603	0.575	0.543	0.562	0.557	0.589	0.557	0.598	0.634	0.638	0.630

APPENDIX A: Amphibole Compositions; S75 Mylonitic Amphibolite

		AMTR1.6	AMTR1.7	AMTR1.8	AMTR1.9	AMTR1.10	AMTR2.1	AMTR2.2	AMTR21.1	AMTR3.1	AMTR3.2	AMTR3.3	AMTR3.4	AMTR3.5
	SiO2	46.384	46.694	45.768	43.416	45.037	43.487	46.466	44.086	46.290	45.434	45.668	45.966	44.441
	Al2O3	9.160	8.882	8.989	10.245	9.976	11.374	9.981	10.542	9.141	9.521	9.175	8.915	9.283
	TiO2	0.608	0.564	0.829	0.785	0.943	0.924	0.684	0.948	0.634	0.652	0.679	0.772	0.673
	FeO	17.569	17.856	17.548	17.083	18.590	17.749	17.744	17.804	16.792	14.481	17.461	16.985	17.821
	MnO	0.238	0.232	0.300	0.272	0.242	0.211	0.269	0.318	0.322	0.254	0.254	0.349	0.297
	MgO	11.024	10.884	10.749	10.321	10.547	9.407	10.333	9.787	10.938	10.956	10.840	10.971	10.495
	CaO	11.566	11.570	11.615	11.494	11.489	11.939	11.397	11.685	11.800	11.223	11.849	11.668	11.657
	Na2O	0.906	1.060	1.012	0.948	1.029	1.059	0.994	0.977	0.926	0.926	0.996	0.977	1.018
	K2O	0.311	0.322	0.333	0.362	0.379	0.435	0.386	0.415	0.304	0.290	0.348	0.339	0.367
	Cl	0.119	0.157	0.194	0.177	0.148	0.091	0.067	0.071	0.040	0.047	0.141	0.109	0.072
	F	0.000	0.028	0.173	0.073	0.093	0.104	0.344	0.230	0.092	0.122	0.168	0.125	0.112
	Total	97.885	98.250	97.508	95.177	98.471	96.780	98.664	96.863	97.279	93.906	97.578	97.175	96.236
Tetrahedral	Si	6.778	6.825	6.766	6.564	6.580	6.526	6.771	6.590	6.826	6.884	6.749	6.798	6.664
	Al	1.222	1.175	1.234	1.436	1.420	1.474	1.229	1.410	1.174	1.116	1.251	1.202	1.336
	Fe3+	0.000	0.000	0.000	0.000	0.000	0.000	0.000	0.000	0.000	0.000	0.000	0.000	0.000
	total T site	8.000	8.000	8.000	8.000	8.000	8.000	8.000	8.000	8.000	8.000	8.000	8.000	8.000
Octahedral	Al	0.355	0.355	0.332	0.390	0.298	0.537	0.485	0.447	0.414	0.584	0.347	0.351	0.305
M1,M2,M3	Ti	0.067	0.062	0.092	0.089	0.104	0.104	0.075	0.107	0.070	0.074	0.075	0.086	0.076
	Fe3+	0.797	0.712	0.685	0.796	0.956	0.498	0.683	0.646	0.569	0.412	0.651	0.638	0.767
	Mg	2.401	2.372	2.369	2.326	2.297	2.104	2.245	2.181	2.404	2.475	2.388	2.419	2.346
	Fe2+	1.350	1.471	1.484	1.364	1.316	1.729	1.479	1.580	1.502	1.423	1.507	1.463	1.468
	Mn	0.030	0.029	0.038	0.035	0.030	0.027	0.033	0.040	0.040	0.033	0.032	0.044	0.038
	total M1-M3	5.000	5.000	5.000	5.000	5.000	5.000	5.000	5.000	5.000	5.000	5.000	5.000	5.000
Octahedral	Ca	1.811	1.812	1.840	1.862	1.799	1.920	1.779	1.871	1.864	1.822	1.876	1.849	1.873
M4	Na	0.189	0.188	0.160	0.138	0.201	0.080	0.221	0.129	0.136	0.178	0.124	0.151	0.127
	Fe2+	0.000	0.000	0.000	0.000	0.000	0.000	0.000	0.000	0.000	0.000	0.000	0.000	0.000
	Mn	0.000	0.000	0.000	0.000	0.000	0.000	0.000	0.000	0.000	0.000	0.000	0.000	0.000
	Mg	0.000	0.000	0.000	0.000	0.000	0.000	0.000	0.000	0.000	0.000	0.000	0.000	0.000
	total M4 site	2.000	2.000	2.000	2.000	2.000	2.000	2.000	2.000	2.000	2.000	2.000	2.000	2.000
A site	Na	0.067	0.112	0.130	0.140	0.090	0.228	0.060	0.154	0.129	0.094	0.161	0.129	0.169
	K	0.058	0.060	0.063	0.070	0.071	0.083	0.072	0.079	0.057	0.056	0.066	0.064	0.070
	total A site	0.125	0.172	0.193	0.210	0.160	0.311	0.132	0.234	0.186	0.150	0.227	0.193	0.239
	Mg/Mg+Fe2+	0.640	0.617	0.615	0.630	0.636	0.549	0.603	0.580	0.615	0.635	0.613	0.623	0.615

APPENDIX A: Amphibole Compositions; S75 Mylonitic Amphibolite

		AMTR3.6	AMTR2	AMTR3.1	AMTR3.2	AMTR3.3	AMTR3.4	AMTR3.5	AMTR4.1	AMTR4.2	AMTR4.3	AMTR4.4	AMTR4.5	AMTR4.6
	SiO2	45.134	45.520	45.764	45.809	46.063	44.090	47.215	50.778	45.644	45.020	46.049	44.840	44.452
	Al2O3	9.559	10.182	8.922	9.599	9.909	11.890	8.123	8.897	9.465	10.029	10.599	10.571	10.475
	TiO2	0.734	1.003	0.678	0.641	0.488	0.394	0.260	0.630	0.735	0.521	0.298	0.413	0.603
	FeO	17.684	16.801	17.468	17.178	17.239	18.112	18.007	15.535	17.459	16.466	16.812	16.706	16.253
	MnO	0.269	0.251	0.205	0.254	0.294	0.177	0.147	0.246	0.269	0.221	0.236	0.224	0.230
	MgO	10.747	10.219	10.804	10.827	10.542	9.363	10.742	8.881	10.579	10.325	10.496	10.143	9.963
	CaO	11.604	11.689	11.765	11.946	11.961	11.728	12.199	9.818	11.517	11.442	11.602	11.545	11.505
	Na2O	1.054	0.944	0.856	0.954	0.934	1.102	0.695	0.953	1.018	0.877	1.000	0.947	0.971
	K2O	0.332	0.369	0.340	0.369	0.309	0.368	0.229	0.277	0.374	0.346	0.300	0.339	0.338
	Cl	0.089	0.119	0.078	0.104	0.096	0.087	0.125	0.074	0.068	0.069	0.106	0.110	0.061
	F	0.123	0.186	0.078	0.184	0.251	0.292	0.278	0.091	0.074	0.061	0.059	0.259	0.003
	Total	97.328	97.283	96.957	97.865	98.088	97.602	98.020	96.180	97.204	95.375	97.558	96.096	94.853
Tetrahedral	Si	6.668	6.742	6.785	6.742	6.767	6.539	6.961	7.486	6.747	6.760	6.751	6.709	6.728
	Al	1.332	1.258	1.215	1.258	1.233	1.461	1.039	0.514	1.253	1.240	1.249	1.291	1.272
	Fe3+	0.000	0.000	0.000	0.000	0.000	0.000	0.000	0.000	0.000	0.000	0.000	0.000	0.000
	total T site	8.000	8.000	8.000	8.000	8.000	8.000	8.000	8.000	8.000	8.000	8.000	8.000	8.000
Octahedral M1,M2,M3	Al	0.333	0.519	0.345	0.407	0.483	0.617	0.372	1.032	0.395	0.534	0.583	0.573	0.597
	Ti	0.082	0.112	0.076	0.071	0.054	0.044	0.029	0.070	0.082	0.059	0.033	0.046	0.069
	Fe3+	0.798	0.465	0.671	0.599	0.553	0.642	0.514	0.000	0.684	0.585	0.615	0.585	0.456
	Mg	2.367	2.256	2.388	2.376	2.309	2.070	2.361	1.952	2.331	2.311	2.294	2.262	2.248
	Fe2+	1.387	1.616	1.495	1.515	1.565	1.604	1.706	1.946	1.474	1.482	1.446	1.505	1.601
	Mn	0.034	0.032	0.026	0.032	0.037	0.022	0.018	0.000	0.034	0.028	0.029	0.028	0.029
	total M1-M3	5.000	5.000	5.000	5.000	5.000	5.000	5.000	5.000	5.000	5.000	5.000	5.000	5.000
Octahedral M4	Ca	1.837	1.855	1.869	1.884	1.883	1.864	1.927	1.551	1.824	1.841	1.822	1.851	1.866
	Na	0.163	0.145	0.131	0.116	0.117	0.136	0.073	0.272	0.176	0.159	0.178	0.149	0.134
	Fe2+	0.000	0.000	0.000	0.000	0.000	0.000	0.000	0.054	0.000	0.000	0.000	0.000	0.000
	Mn	0.000	0.000	0.000	0.000	0.000	0.000	0.000	0.031	0.000	0.000	0.000	0.000	0.000
	Mg	0.000	0.000	0.000	0.000	0.000	0.000	0.000	0.000	0.000	0.000	0.000	0.000	0.000
	total M4 site	2.000	2.000	2.000	2.000	2.000	2.000	2.000	1.908	2.000	2.000	2.000	2.000	2.000
A site	Na	0.139	0.126	0.115	0.156	0.149	0.180	0.126	0.000	0.116	0.096	0.107	0.125	0.151
	K	0.063	0.070	0.064	0.069	0.058	0.070	0.043	0.052	0.071	0.066	0.056	0.065	0.065
	total A site	0.201	0.195	0.179	0.225	0.207	0.250	0.169	0.052	0.186	0.162	0.163	0.190	0.216
	Mg/Mg+Fe2+	0.631	0.583	0.615	0.611	0.596	0.563	0.581	0.494	0.613	0.609	0.613	0.600	0.584

APPENDIX A: Amphibole Compositions; S75 Mylonitic Amphibolite

		AMTR1.1	AMTR1.2	AMTR1.3	AMTR3.1	AMTR3.2	AMTR3.3	AMTR4.1	AMTR4.2	AMTR4.3	AMTR4.4	AMTR4.5	AMTR4.6	AMTR4.7
	SiO2	44.157	44.215	47.489	43.604	44.353	45.448	44.614	44.952	56.811	44.460	44.232	44.099	48.943
	Al2O3	10.724	11.397	10.067	10.817	10.657	10.793	10.323	9.966	8.372	9.394	10.018	10.137	8.249
	TiO2	0.905	0.892	0.527	0.879	1.197	0.596	0.836	1.709	0.447	2.183	0.886	0.982	0.395
	FeO	17.612	18.169	16.703	17.069	18.352	17.176	17.449	17.416	14.149	16.504	17.827	16.499	15.362
	MnO	0.263	0.235	0.187	0.263	0.242	0.168	0.245	0.233	0.157	0.242	0.257	0.214	0.163
	MgO	9.809	9.500	9.763	10.094	9.831	9.739	10.253	10.122	7.730	10.031	10.104	9.891	10.292
	CaO	11.856	11.651	11.471	11.904	11.661	11.693	11.886	11.931	9.446	12.421	11.952	11.711	11.281
	Na2O	1.051	1.090	1.017	1.078	0.967	1.009	0.921	0.989	0.802	0.796	1.033	1.076	0.767
	K2O	0.402	0.415	0.384	0.432	0.441	0.387	0.414	0.390	0.289	0.337	0.402	0.428	0.264
	Cl	0.088	0.083	0.044	0.050	0.062	0.030	0.089	0.114	0.134	0.149	0.128	0.118	0.106
	F	0.104	0.128	0.039	0.000	0.029	0.087	0.002	0.095	0.328	0.231	0.182	0.283	0.042
	Total	96.971	97.774	97.690	96.189	97.791	97.127	97.032	97.916	98.664	96.746	97.020	95.436	95.864
Tetrahedral	Si	6.594	6.541	6.981	6.549	6.551	6.741	6.629	6.653	8.160	6.710	6.617	6.704	7.289
	Al	1.406	1.459	1.019	1.451	1.449	1.259	1.371	1.347	0.000	1.290	1.383	1.296	0.711
	Fe3+	0.000	0.000	0.000	0.000	0.000	0.000	0.000	0.000	0.000	0.000	0.000	0.000	0.000
	total T site	8.000	8.000	8.000	8.000	8.000	8.000	8.000	8.000	8.160	8.000	8.000	8.000	8.000
Octahedral M1,M2,M3	Al	0.482	0.528	0.725	0.463	0.406	0.628	0.436	0.392	1.417	0.381	0.384	0.521	0.737
	Ti	0.102	0.099	0.058	0.099	0.133	0.066	0.093	0.190	0.048	0.248	0.100	0.112	0.044
	Fe3+	0.545	0.648	0.201	0.561	0.727	0.417	0.620	0.433	0.000	0.098	0.592	0.335	0.014
	Mg	2.184	2.095	2.140	2.260	2.164	2.154	2.271	2.233	1.655	2.257	2.254	2.242	2.285
	Fe2+	1.654	1.600	1.852	1.583	1.539	1.713	1.548	1.722	1.879	1.985	1.639	1.763	1.899
	Mn	0.033	0.029	0.023	0.033	0.030	0.021	0.031	0.029	0.000	0.031	0.033	0.028	0.021
	total M1-M3	5.000	5.000	5.000	5.000	5.000	5.000	5.000	5.000	5.000	5.000	5.000	5.000	5.000
Octahedral M4	Ca	1.897	1.847	1.807	1.916	1.845	1.858	1.892	1.892	1.454	2.009	1.916	1.908	1.800
	Na	0.103	0.153	0.193	0.084	0.155	0.142	0.108	0.108	0.000	0.000	0.084	0.092	0.200
	Fe2+	0.000	0.000	0.000	0.000	0.000	0.000	0.000	0.000	0.839	0.000	0.000	0.000	0.000
	Mn	0.000	0.000	0.000	0.000	0.000	0.000	0.000	0.000	0.019	0.000	0.000	0.000	0.000
	Mg	0.000	0.000	0.000	0.000	0.000	0.000	0.000	0.000	0.000	0.000	0.000	0.000	0.000
	total M4 site	2.000	2.000	2.000	2.000	2.000	2.000	2.000	2.000	2.311	2.009	2.000	2.000	2.000
A site	Na	0.201	0.159	0.097	0.230	0.122	0.149	0.157	0.176	0.223	0.233	0.215	0.225	0.021
	K	0.077	0.078	0.072	0.083	0.083	0.073	0.078	0.074	0.053	0.065	0.077	0.083	0.050
	total A site	0.278	0.238	0.169	0.312	0.205	0.222	0.236	0.250	0.276	0.298	0.292	0.308	0.072
	Mg/Mg+Fe2+	0.569	0.567	0.536	0.588	0.584	0.557	0.595	0.565	0.379	0.532	0.579	0.560	0.546

APPENDIX A: Amphibole Compositions; S75 Mylonitic Amphibolite

		AMTR4.8	AMTR4.9	AMTR6.1	AMTR6.2	AMTR6.3	AMTR6.4	AMTR6.5	AMTR6.6
	SiO2	45.533	43.793	48.062	44.871	45.486	45.421	45.133	45.642
	Al2O3	10.033	9.759	10.196	9.570	9.717	9.598	10.211	9.154
	TiO2	0.912	0.897	0.846	0.691	0.951	0.893	0.818	0.344
	FeO	16.668	15.504	15.474	17.579	17.079	17.632	17.166	16.056
	MnO	0.297	0.258	0.298	0.279	0.242	0.263	0.270	0.261
	MgO	9.932	9.847	9.171	10.525	14.450	10.561	10.214	11.669
	CaO	11.814	11.486	10.636	11.704	11.546	11.625	11.727	11.587
	Na2O	0.985	0.851	0.947	0.973	1.026	0.960	0.925	0.807
	K2O	0.414	0.393	0.337	0.337	0.365	0.373	0.386	0.260
	Cl	0.136	0.092	0.082	0.091	0.124	0.130	0.165	0.177
	F	0.020	0.259	0.122	0.154	0.173	0.049	0.047	0.000
	Total	96.743	93.139	96.171	96.773	101.158	97.506	97.059	95.958
Tetrahedral	Si	6.801	6.791	7.134	6.682	6.312	6.701	6.698	6.763
	Al	1.199	1.209	0.866	1.318	1.589	1.299	1.302	1.237
	Fe3+	0.000	0.000	0.000	0.000	0.099	0.000	0.000	0.000
	total T site	8.000	8.000	8.000	8.000	8.000	8.000	8.000	8.000
Octahedral	Al	0.567	0.575	0.918	0.362	0.000	0.370	0.484	0.362
M1,M2,M3	Ti	0.102	0.105	0.094	0.077	0.099	0.099	0.091	0.038
	Fe3+	0.283	0.275	0.040	0.721	1.815	0.711	0.566	0.838
	Mg	2.211	2.276	2.029	2.337	2.989	2.323	2.260	2.578
	Fe2+	1.799	1.736	1.881	1.468	0.097	1.464	1.564	1.151
	Mn	0.038	0.034	0.038	0.035	0.000	0.033	0.034	0.033
	total M1-M3	5.000	5.000	5.000	5.000	5.000	5.000	5.000	5.000
Octahedral	Ca	1.891	1.908	1.691	1.867	1.717	1.837	1.865	1.840
M4	Na	0.109	0.092	0.273	0.133	0.184	0.163	0.135	0.160
	Fe2+	0.000	0.000	0.000	0.000	0.070	0.000	0.000	0.000
	Mn	0.000	0.000	0.000	0.000	0.028	0.000	0.000	0.000
	Mg	0.000	0.000	0.000	0.000	0.000	0.000	0.000	0.000
	total M4 site	2.000	2.000	1.964	2.000	2.000	2.000	2.000	2.000
A site	Na	0.176	0.164	0.000	0.149	0.092	0.112	0.131	0.072
	K	0.079	0.078	0.064	0.064	0.065	0.070	0.073	0.049
	total A site	0.254	0.242	0.064	0.213	0.156	0.182	0.204	0.121
	Mg/Mg+Fe2+	0.551	0.567	0.519	0.614	0.947	0.613	0.591	0.691

APPENDIX A: Amphibole Compositions; S895a Mylonitic Amphibolite

		895.5a1.1	895.5a1.2	895.5a1.3	895.5a1.4	895.5a1.5	895.5a1.6	895.5a2.1	895.5a2.2	895.5a2.3	895.5a2.4	895.5a2.5	895.6a1.1	895.6a1.2
	SiO2	49.338	45.525	44.151	45.178	45.781	48.349	45.260	46.217	48.133	45.840	46.233	50.128	48.777
	Al2O3	6.421	8.601	10.397	10.246	9.408	7.065	10.122	8.330	7.905	8.012	8.216	5.416	6.965
	TiO2	0.447	0.712	0.955	0.818	0.837	0.573	0.823	0.734	0.601	0.742	0.624	0.254	0.384
	FeO	15.493	17.163	18.196	18.449	17.657	16.687	17.908	17.288	16.419	16.877	16.780	14.714	15.839
	MnO	0.197	0.248	0.244	0.269	0.251	0.255	0.275	0.244	0.235	0.215	0.255	0.240	0.279
	MgO	12.785	11.322	10.263	10.312	10.752	12.428	10.370	11.513	11.864	11.789	11.691	13.521	12.501
	CaO	12.621	12.095	12.066	12.342	12.216	12.261	12.030	12.299	12.402	12.368	12.298	12.572	12.669
	Na2O	0.599	1.011	1.180	1.089	0.954	0.752	1.037	0.957	0.693	0.867	0.837	0.497	0.685
	K2O	0.154	0.219	0.314	0.302	0.274	0.165	0.310	0.239	0.218	0.252	0.246	0.098	0.170
	Cl	0.121	0.140	0.199	0.192	0.187	0.100	0.187	0.138	0.136	0.173	0.125	0.058	0.089
	F	0.028	0.053	0.053	0.000	0.012	0.047	0.000	0.020	0.050	0.000	0.000	0.057	0.076
	Total	98.204	97.089	98.018	99.197	98.329	98.682	98.322	97.979	98.656	97.135	97.305	97.555	98.434
Tetrahedral	Si	7.172	6.753	6.534	6.607	6.724	6.999	6.650	6.796	6.990	6.794	6.825	7.292	7.093
	Al	0.828	1.247	1.466	1.393	1.276	1.001	1.350	1.204	1.010	1.206	1.175	0.708	0.907
	Fe3+	0.000	0.000	0.000	0.000	0.000	0.000	0.000	0.000	0.000	0.000	0.000	0.000	0.000
	total T site	8.000	8.000	8.000	8.000	8.000	8.000	8.000	8.000	8.000	8.000	8.000	8.000	8.000
Octahedral M1,M2,M3	Al	0.273	0.257	0.347	0.372	0.353	0.204	0.403	0.239	0.343	0.194	0.254	0.221	0.287
	Ti	0.049	0.079	0.106	0.090	0.092	0.062	0.091	0.081	0.066	0.083	0.069	0.028	0.042
	Fe3+	0.328	0.655	0.683	0.608	0.570	0.627	0.624	0.610	0.441	0.622	0.606	0.355	0.363
	Mg	2.771	2.504	2.264	2.248	2.354	2.682	2.271	2.524	2.568	2.605	2.573	2.932	2.710
	Fe2+	1.555	1.474	1.569	1.648	1.599	1.393	1.577	1.515	1.553	1.470	1.466	1.435	1.564
	Mn	0.024	0.031	0.031	0.033	0.031	0.031	0.034	0.030	0.029	0.027	0.032	0.030	0.034
	total M1-M3	5.000	5.000	5.000	5.000	5.000	5.000	5.000	5.000	5.000	5.000	5.000	5.000	5.000
Octahedral M4	Ca	1.966	1.922	1.913	1.934	1.922	1.902	1.894	1.938	1.930	1.964	1.945	1.959	1.974
	Na	0.034	0.078	0.087	0.066	0.078	0.098	0.106	0.062	0.070	0.036	0.055	0.041	0.026
	Fe2+	0.000	0.000	0.000	0.000	0.000	0.000	0.000	0.000	0.000	0.000	0.000	0.000	0.000
	Mn	0.000	0.000	0.000	0.000	0.000	0.000	0.000	0.000	0.000	0.000	0.000	0.000	0.000
	Mg	0.000	0.000	0.000	0.000	0.000	0.000	0.000	0.000	0.000	0.000	0.000	0.000	0.000
	total M4 site	2.000	2.000	2.000	2.000	2.000	2.000	2.000	2.000	2.000	2.000	2.000	2.000	2.000
A site	Na	0.135	0.213	0.252	0.242	0.194	0.113	0.189	0.210	0.125	0.213	0.185	0.100	0.167
	K	0.029	0.041	0.059	0.056	0.051	0.030	0.058	0.045	0.040	0.048	0.046	0.018	0.032
	total A site	0.163	0.254	0.311	0.299	0.245	0.143	0.247	0.255	0.165	0.261	0.231	0.118	0.199
	Mg/Mg+Fe2+	0.640	0.629	0.591	0.577	0.595	0.658	0.590	0.625	0.623	0.639	0.637	0.671	0.634

APPENDIX A: Amphibole Compositions; S895a Mylonitic Amphibolite

		895.6a1.3	895.6a1.4	895.6a1.5	895.6a1.6	895.6a1.7	895.6a1.8	895.6a2.1	895.6a2.2	895.6a2.3	895.6a2tr	895.6a2tr	895.6a2tr	895.6a2tr
	SiO2	47.938	47.495	48.343	46.866	48.097	48.817	48.430	53.611	51.098	54.325	51.938	48.602	50.173
	Al2O3	8.059	8.299	7.893	8.612	7.531	6.922	7.267	2.481	4.093	1.907	3.226	6.815	5.333
	TiO2	0.400	0.407	0.357	0.393	0.435	0.353	0.333	0.079	0.089	0.073	0.061	0.172	0.169
	FeO	16.453	16.484	16.350	16.896	16.117	16.088	15.936	13.321	14.525	12.692	14.002	15.501	14.702
	MnO	0.207	0.302	0.261	0.242	0.234	0.199	0.195	0.202	0.214	0.205	0.205	0.207	0.152
	MgO	11.846	11.758	11.987	11.572	11.965	12.564	12.378	15.212	14.256	15.473	14.789	12.747	13.956
	CaO	12.345	12.309	12.352	12.111	12.364	12.348	12.431	12.776	12.531	12.788	12.918	12.514	12.516
	Na2O	0.831	0.869	0.765	0.986	0.844	0.663	0.713	0.201	0.343	0.197	0.291	0.602	0.469
	K2O	0.166	0.175	0.213	0.219	0.192	0.162	0.164	0.035	0.082	0.011	0.051	0.132	0.112
	Cl	0.132	0.116	0.124	0.140	0.121	0.114	0.106	0.024	0.051	0.019	0.039	0.060	0.067
	F	0.060	0.000	0.005	0.009	0.056	0.083	0.000	0.018	0.062	0.000	0.011	0.061	0.000
	Total	98.437	98.214	98.650	98.046	97.956	98.313	97.953	97.960	97.344	97.690	97.531	97.413	97.649
Tetrahedral	Si	6.976	6.926	7.008	6.853	7.040	7.083	7.059	7.694	7.416	7.805	7.526	7.107	7.262
	Al	1.024	1.074	0.992	1.147	0.960	0.917	0.941	0.306	0.584	0.195	0.474	0.893	0.738
	Fe3+	0.000	0.000	0.000	0.000	0.000	0.000	0.000	0.000	0.000	0.000	0.000	0.000	0.000
	total T site	8.000	8.000	8.000	8.000	8.000	8.000	8.000	8.000	8.000	8.000	8.000	8.000	8.000
Octahedral M1,M2,M3	Al	0.358	0.352	0.356	0.338	0.339	0.267	0.307	0.114	0.116	0.128	0.077	0.281	0.172
	Ti	0.044	0.045	0.039	0.043	0.048	0.039	0.037	0.009	0.010	0.008	0.007	0.019	0.018
	Fe3+	0.463	0.509	0.466	0.607	0.371	0.517	0.446	0.184	0.439	0.057	0.282	0.458	0.495
	Mg	2.570	2.556	2.590	2.523	2.611	2.718	2.690	3.255	3.085	3.314	3.195	2.779	3.011
	Fe2+	1.539	1.501	1.516	1.460	1.602	1.436	1.496	1.415	1.324	1.468	1.415	1.438	1.285
	Mn	0.026	0.037	0.032	0.030	0.029	0.024	0.024	0.025	0.026	0.025	0.025	0.026	0.019
	total M1-M3	5.000	5.000	5.000	5.000	5.000	5.000	5.000	5.000	5.000	5.000	5.000	5.000	5.000
Octahedral M4	Ca	1.925	1.923	1.918	1.898	1.939	1.920	1.941	1.964	1.949	1.969	2.006	1.961	1.941
	Na	0.075	0.077	0.082	0.102	0.061	0.080	0.059	0.036	0.051	0.031	0.000	0.039	0.059
	Fe2+	0.000	0.000	0.000	0.000	0.000	0.000	0.000	0.000	0.000	0.000	0.000	0.000	0.000
	Mn	0.000	0.000	0.000	0.000	0.000	0.000	0.000	0.000	0.000	0.000	0.000	0.000	0.000
	Mg	0.000	0.000	0.000	0.000	0.000	0.000	0.000	0.000	0.000	0.000	0.000	0.000	0.000
	total M4 site	2.000	2.000	2.000	2.000	2.000	2.000	2.000	2.000	2.000	2.000	2.006	2.000	2.000
A site	Na	0.159	0.169	0.133	0.177	0.179	0.106	0.143	0.020	0.045	0.023	0.082	0.131	0.073
	K	0.031	0.033	0.039	0.041	0.036	0.030	0.030	0.006	0.015	0.002	0.009	0.025	0.021
	total A site	0.190	0.201	0.173	0.218	0.214	0.136	0.173	0.027	0.060	0.025	0.091	0.156	0.093
	Mg/Mg+Fe2+	0.625	0.630	0.631	0.633	0.620	0.654	0.643	0.697	0.700	0.693	0.693	0.659	0.701

APPENDIX A: Amphibole Compositions; S895a Mylonitic Amphibolite

		895.6a2tr	895.6a2tr	895.6a2tr	895.6a2tr	895.6a2tr	895.6a2tr
	SiO2	54.065	47.682	49.186	49.211	56.105	56.039
	Al2O3	5.396	7.570	7.214	6.870	1.842	1.471
	TiO2	0.228	0.459	0.204	0.217	0.007	0.009
	FeO	13.561	16.088	15.800	15.163	12.052	12.211
	MnO	0.194	0.248	0.252	0.173	0.260	0.221
	MgO	11.501	12.236	12.516	12.594	14.435	15.288
	CaO	11.244	12.481	12.583	12.338	11.980	12.229
	Na2O	0.559	0.689	0.676	0.686	0.169	0.117
	K2O	0.144	0.186	0.146	0.136	0.016	0.040
	Cl	0.055	0.124	0.058	0.092	0.006	0.018
	F	0.021	0.000	0.000	0.090	0.032	0.000
	Total	96.968	97.763	98.635	97.570	96.904	97.643
Tetrahedral	Si	7.875	6.976	7.110	7.182	8.095	8.008
	Al	0.125	1.024	0.890	0.818	0.000	0.000
	Fe3+	0.000	0.000	0.000	0.000	0.000	0.000
	total T site	8.000	8.000	8.000	8.000	8.095	8.008
Octahedral	Al	0.802	0.282	0.340	0.364	0.313	0.248
M1,M2,M3	Ti	0.025	0.051	0.022	0.024	0.001	0.001
	Fe3+	0.000	0.498	0.391	0.328	0.000	0.000
	Mg	2.497	2.669	2.697	2.740	3.105	3.257
	Fe2+	1.676	1.470	1.519	1.523	1.581	1.494
	Mn	0.000	0.031	0.031	0.021	0.000	0.000
	total M1-M3	5.000	5.000	5.000	5.000	5.000	5.000
Octahedral	Ca	1.755	1.956	1.949	1.929	1.852	1.872
M4	Na	0.000	0.044	0.051	0.071	0.000	0.032
	Fe2+	0.397	0.000	0.000	0.000	0.132	0.016
	Mn	0.024	0.000	0.000	0.000	0.032	0.027
	Mg	0.000	0.000	0.000	0.000	0.000	0.000
	total M4 site	2.176	2.000	2.000	2.000	2.016	1.947
A site	Na	0.158	0.152	0.138	0.123	0.047	0.000
	K	0.027	0.035	0.027	0.025	0.003	0.007
	total A site	0.185	0.187	0.165	0.149	0.050	0.007
	Mg/Mg+Fe2+	0.546	0.645	0.640	0.643	0.644	0.683

APPENDIX A: Amphibole Compositions; S910a Mylonitic Amphibolite

		910a.2a2.1	910a.2a2.2	910a.2a2.3	910a.2a2.4	910a.2a2.5	910a.2a4.1	910a.2a4.2	910a.2a4.3	910a.2a4.4	910a.2a1.1	910a.2a1.2	910a.2a1.3	910a.2a1.4
	SiO2	43.727	44.069	45.740	46.456	46.513	44.667	45.351	44.129	44.598	45.018	44.049	44.406	44.473
	Al2O3	10.997	10.798	10.249	9.622	9.799	10.991	10.487	10.863	11.109	10.178	11.206	10.932	10.782
	TiO2	0.813	0.907	0.867	0.766	0.705	1.051	0.980	1.013	0.978	0.858	0.942	0.841	0.931
	FeO	18.709	18.646	18.124	17.639	17.134	18.627	18.344	18.513	17.748	18.486	18.594	18.337	18.368
	MnO	0.229	0.276	0.255	0.228	0.197	0.260	0.313	0.192	0.204	0.222	0.187	0.166	0.269
	MgO	9.641	9.916	10.510	10.750	11.013	9.718	9.771	9.697	9.863	10.018	9.725	9.887	10.011
	CaO	11.958	11.833	12.144	11.954	12.111	11.912	11.765	11.905	12.005	11.775	11.838	11.973	11.855
	Na2O	1.279	1.205	1.115	1.080	0.950	1.258	1.297	1.274	1.060	1.175	1.344	1.225	1.166
	K2O	0.384	0.379	0.330	0.292	0.309	0.406	0.347	0.395	0.409	0.387	0.446	0.409	0.440
	Cl	0.229	0.232	0.193	0.200	0.165	0.266	0.247	0.273	0.246	0.269	0.298	0.278	0.249
	F	0.000	0.019	0.020	0.056	0.000	0.000	0.000	0.023	0.000	0.002	0.013	0.064	0.000
	Total	97.966	98.280	99.547	99.043	98.896	99.156	98.902	98.277	98.220	98.388	98.642	98.518	98.544
Tetrahedral	Si	6.496	6.504	6.643	6.760	6.756	6.547	6.653	6.534	6.578	6.632	6.495	6.550	6.541
	Al	1.504	1.496	1.357	1.240	1.244	1.453	1.347	1.466	1.422	1.368	1.505	1.450	1.459
	Fe3+	0.000	0.000	0.000	0.000	0.000	0.000	0.000	0.000	0.000	0.000	0.000	0.000	0.000
	total T site	8.000	8.000	8.000	8.000	8.000	8.000	8.000	8.000	8.000	8.000	8.000	8.000	8.000
Octahedral M1,M2,M3	Al	0.421	0.382	0.397	0.410	0.433	0.445	0.466	0.430	0.508	0.399	0.442	0.450	0.409
	Ti	0.091	0.101	0.095	0.084	0.077	0.116	0.108	0.113	0.108	0.095	0.104	0.093	0.103
	Fe3+	0.654	0.755	0.616	0.577	0.563	0.602	0.533	0.592	0.523	0.653	0.646	0.602	0.693
	Mg	2.135	2.182	2.275	2.332	2.385	2.123	2.137	2.141	2.169	2.200	2.138	2.174	2.195
	Fe2+	1.670	1.547	1.585	1.570	1.518	1.682	1.717	1.700	1.666	1.625	1.646	1.660	1.566
	Mn	0.029	0.035	0.031	0.028	0.024	0.032	0.039	0.024	0.025	0.028	0.023	0.021	0.034
	total M1-M3	5.000	5.000	5.000	5.000	5.000	5.000	5.000	5.000	5.000	5.000	5.000	5.000	5.000
Octahedral M4	Ca	1.903	1.871	1.890	1.864	1.885	1.871	1.849	1.889	1.897	1.859	1.870	1.892	1.868
	Na	0.097	0.129	0.110	0.136	0.115	0.129	0.151	0.111	0.103	0.141	0.130	0.108	0.132
	Fe2+	0.000	0.000	0.000	0.000	0.000	0.000	0.000	0.000	0.000	0.000	0.000	0.000	0.000
	Mn	0.000	0.000	0.000	0.000	0.000	0.000	0.000	0.000	0.000	0.000	0.000	0.000	0.000
	Mg	0.000	0.000	0.000	0.000	0.000	0.000	0.000	0.000	0.000	0.000	0.000	0.000	0.000
	total M4 site	2.000	2.000	2.000	2.000	2.000	2.000	2.000	2.000	2.000	2.000	2.000	2.000	2.000
A site	Na	0.272	0.216	0.204	0.168	0.152	0.228	0.218	0.254	0.200	0.194	0.254	0.242	0.201
	K	0.073	0.071	0.061	0.054	0.057	0.076	0.065	0.075	0.077	0.073	0.084	0.077	0.083
	total A site	0.344	0.287	0.265	0.223	0.209	0.304	0.283	0.329	0.277	0.267	0.338	0.319	0.283
	Mg/Mg+Fe2+	0.561	0.585	0.589	0.598	0.611	0.558	0.554	0.557	0.566	0.575	0.565	0.567	0.584

APPENDIX A: Amphibole Compositions; S910a My

		910a.2a1.5
	SiO2	43.109
	Al2O3	11.712
	TiO2	0.974
	FeO	18.689
	MnO	0.282
	MgO	9.336
	CaO	12.098
	Na2O	1.352
	K2O	0.437
	Cl	0.334
	F	0.000
	Total	98.323
Tetrahedral	Si	6.410
	Al	1.590
	Fe3+	0.000
	total T site	8.000
Octahedral	Al	0.462
M1,M2,M3	Ti	0.109
	Fe3+	0.583
	Mg	2.069
	Fe2+	1.741
	Mn	0.036
	total M1-M3	5.000
Octahedral	Ca	1.927
M4	Na	0.073
	Fe2+	0.000
	Mn	0.000
	Mg	0.000
	total M4 site	2.000
A site	Na	0.317
	K	0.083
	total A site	0.400
	Mg/Mg+Fe2+	0.543

APPENDIX A: Amphibole Compositions; S141 Mylonitic Amphibolite

		141.3a5tr	141.3a5tr	141.3a5tr	141.3a5tr	141.3a5tr	141.3a3tr	141.3a3tr	141.3a3tr	141.3a3tr	141.3a3tr	141.3a3tr	141.3a3tr	141.3a3tr
	SiO2	47.203	46.731	45.765	45.562	46.858	46.683	47.642	47.890	50.082	50.547	51.490	50.382	50.913
	Al2O3	7.770	8.052	8.166	8.261	8.478	8.239	7.778	6.055	4.944	4.458	4.624	4.439	4.440
	TiO2	0.594	0.635	0.613	0.632	0.743	0.726	0.613	0.500	0.445	0.252	0.354	0.308	0.339
	FeO	17.437	17.586	18.005	17.635	17.656	17.041	17.186	16.193	15.274	15.027	14.929	14.787	14.601
	MnO	0.248	0.228	0.268	0.254	0.277	0.242	0.270	0.341	0.275	0.333	0.362	0.298	0.271
	MgO	11.418	11.329	11.316	11.319	11.424	11.413	11.769	12.841	13.851	13.882	14.053	14.079	13.919
	CaO	12.172	11.871	11.917	11.773	11.943	12.376	12.206	12.007	12.240	12.283	12.380	12.378	12.218
	Na2O	0.912	0.873	1.004	1.044	1.020	0.856	0.777	0.634	0.526	0.464	0.467	0.452	0.390
	K2O	0.230	0.197	0.225	0.239	0.262	0.239	0.214	0.133	0.115	0.106	0.086	0.076	0.079
	Cl	0.091	0.099	0.123	0.116	0.099	0.111	0.108	0.097	0.063	0.037	0.054	0.062	0.051
	F	0.000	0.000	0.016	0.027	0.000	0.028	0.028	0.018	0.007	0.011	0.063	0.111	0.040
	Total	98.075	97.601	97.418	96.862	98.760	97.954	98.591	96.709	97.822	97.400	98.862	97.372	97.261
Tetrahedral	Si	6.924	6.865	6.760	6.761	6.811	6.864	6.927	7.045	7.242	7.339	7.360	7.322	7.388
	Al	1.076	1.135	1.240	1.239	1.189	1.136	1.073	0.955	0.758	0.661	0.640	0.678	0.612
	Fe3+	0.000	0.000	0.000	0.000	0.000	0.000	0.000	0.000	0.000	0.000	0.000	0.000	0.000
	total T site	8.000	8.000	8.000	8.000	8.000	8.000	8.000	8.000	8.000	8.000	8.000	8.000	8.000
Octahedral	Al	0.268	0.260	0.182	0.205	0.263	0.292	0.259	0.094	0.085	0.102	0.139	0.082	0.147
M1,M2,M3	Ti	0.066	0.070	0.068	0.071	0.081	0.080	0.067	0.055	0.048	0.028	0.038	0.034	0.037
	Fe3+	0.549	0.712	0.819	0.804	0.708	0.494	0.619	0.760	0.615	0.532	0.488	0.532	0.468
	Mg	2.497	2.481	2.492	2.504	2.475	2.502	2.551	2.816	2.986	3.005	2.995	3.050	3.011
	Fe2+	1.591	1.449	1.405	1.384	1.438	1.601	1.471	1.232	1.232	1.293	1.297	1.265	1.304
	Mn	0.031	0.028	0.034	0.032	0.034	0.030	0.033	0.042	0.034	0.041	0.044	0.037	0.033
	total M1-M3	5.000	5.000	5.000	5.000	5.000	5.000	5.000	5.000	5.000	5.000	5.000	5.000	5.000
Octahedral	Ca	1.913	1.869	1.886	1.872	1.860	1.950	1.901	1.892	1.896	1.911	1.896	1.927	1.899
M4	Na	0.087	0.131	0.114	0.128	0.140	0.050	0.099	0.108	0.104	0.089	0.104	0.073	0.101
	Fe2+	0.000	0.000	0.000	0.000	0.000	0.000	0.000	0.000	0.000	0.000	0.000	0.000	0.000
	Mn	0.000	0.000	0.000	0.000	0.000	0.000	0.000	0.000	0.000	0.000	0.000	0.000	0.000
	Mg	0.000	0.000	0.000	0.000	0.000	0.000	0.000	0.000	0.000	0.000	0.000	0.000	0.000
	total M4 site	2.000	2.000	2.000	2.000	2.000	2.000	2.000	2.000	2.000	2.000	2.000	2.000	2.000
A site	Na	0.172	0.117	0.174	0.172	0.147	0.194	0.120	0.073	0.044	0.041	0.025	0.055	0.009
	K	0.043	0.037	0.042	0.045	0.049	0.045	0.040	0.025	0.021	0.020	0.016	0.014	0.015
	total A site	0.215	0.154	0.216	0.217	0.196	0.239	0.160	0.098	0.065	0.061	0.041	0.069	0.024
	Mg/Mg+Fe2+	0.611	0.631	0.639	0.644	0.632	0.610	0.634	0.696	0.708	0.699	0.698	0.707	0.698

APPENDIX A: Amphibole Compositions; S141 Mylonitic Amphibolite

		141.3a3tr	141.3a3tr	141.3a3tr	141.3a3tr	141.3a3tr	141.3a3tr	141.3a3tr	141.3a3tr	141.3a3tr	141.3a3tr	141.3a3tr	141.3a3tr	141.3a2tr
	SiO2	52.648	50.981	45.936	46.464	45.521	46.000	46.365	45.150	45.080	46.853	45.152	46.231	46.492
	Al2O3	4.659	5.730	8.454	8.833	8.997	9.225	9.082	8.439	8.349	8.271	8.146	8.417	7.844
	TiO2	0.185	0.392	0.558	0.640	0.830	0.832	0.791	0.776	0.771	0.821	0.854	0.782	0.659
	FeO	14.176	14.885	16.557	16.887	17.658	17.795	17.503	17.788	17.761	17.614	17.613	17.011	16.920
	MnO	0.223	0.293	0.237	0.281	0.326	0.265	0.256	0.250	0.286	0.287	0.299	0.221	0.358
	MgO	13.272	12.544	11.514	11.212	10.538	10.497	10.768	11.016	10.955	10.722	11.103	11.462	11.613
	CaO	11.816	11.711	12.111	12.133	11.999	11.920	11.875	11.663	12.016	11.940	11.950	11.994	11.806
	Na2O	0.444	0.538	0.853	0.937	0.995	1.050	0.972	0.956	0.952	1.078	0.893	0.889	0.934
	K2O	0.069	0.119	0.215	0.235	0.243	0.292	0.264	0.249	0.235	0.254	0.219	0.212	0.237
	Cl	0.047	0.053	0.095	0.103	0.124	0.135	0.108	0.110	0.088	0.114	0.116	0.123	0.090
	F	0.000	0.075	0.000	0.000	0.000	0.075	0.092	0.063	0.000	0.037	0.034	0.018	0.022
	Total	97.539	97.321	96.530	97.725	97.231	98.086	98.076	96.460	96.493	97.991	96.379	97.360	96.975
Tetrahedral	Si	7.596	7.411	6.822	6.831	6.763	6.776	6.805	6.732	6.742	6.908	6.752	6.811	6.868
	Al	0.404	0.589	1.178	1.169	1.237	1.224	1.195	1.268	1.258	1.092	1.248	1.189	1.132
	Fe3+	0.000	0.000	0.000	0.000	0.000	0.000	0.000	0.000	0.000	0.000	0.000	0.000	0.000
	total T site	8.000	8.000	8.000	8.000	8.000	8.000	8.000	8.000	8.000	8.000	8.000	8.000	8.000
Octahedral	Al	0.388	0.393	0.302	0.361	0.338	0.378	0.376	0.215	0.213	0.345	0.188	0.273	0.234
M1,M2,M3	Ti	0.020	0.043	0.062	0.071	0.093	0.092	0.087	0.087	0.087	0.091	0.096	0.087	0.073
	Fe3+	0.187	0.288	0.610	0.534	0.561	0.545	0.583	0.829	0.700	0.437	0.737	0.663	0.702
	Mg	2.854	2.718	2.549	2.457	2.334	2.305	2.356	2.449	2.442	2.357	2.475	2.517	2.558
	Fe2+	1.524	1.521	1.446	1.542	1.633	1.647	1.566	1.389	1.521	1.734	1.465	1.433	1.389
	Mn	0.027	0.036	0.030	0.035	0.041	0.033	0.032	0.032	0.036	0.036	0.038	0.028	0.045
	total M1-M3	5.000	5.000	5.000	5.000	5.000	5.000	5.000	5.000	5.000	5.000	5.000	5.000	5.000
Octahedral	Ca	1.826	1.824	1.927	1.911	1.910	1.881	1.867	1.863	1.925	1.886	1.915	1.893	1.869
M4	Na	0.124	0.152	0.073	0.089	0.090	0.119	0.133	0.137	0.075	0.114	0.085	0.107	0.131
	Fe2+	0.000	0.000	0.000	0.000	0.000	0.000	0.000	0.000	0.000	0.000	0.000	0.000	0.000
	Mn	0.000	0.000	0.000	0.000	0.000	0.000	0.000	0.000	0.000	0.000	0.000	0.000	0.000
	Mg	0.000	0.000	0.000	0.000	0.000	0.000	0.000	0.000	0.000	0.000	0.000	0.000	0.000
	total M4 site	1.951	1.976	2.000	2.000	2.000	2.000	2.000	2.000	2.000	2.000	2.000	2.000	2.000
A site	Na	0.000	0.000	0.173	0.178	0.197	0.181	0.144	0.140	0.201	0.194	0.174	0.147	0.136
	K	0.013	0.022	0.041	0.044	0.046	0.055	0.049	0.047	0.045	0.048	0.042	0.040	0.045
	total A site	0.013	0.022	0.214	0.222	0.243	0.236	0.193	0.187	0.246	0.242	0.215	0.187	0.181
	Mg/Mg+Fe2+	0.652	0.641	0.638	0.614	0.588	0.583	0.601	0.638	0.616	0.576	0.628	0.637	0.648

APPENDIX A: Amphibole Compositions; S141 Mylonitic Amphibolite

		141.3a2tr	141.3a2tr	141.3a2tr	141.3a2tr	141.4a6tr	141.4a6tr	141.4a6tr	141.4a6tr	141.4a6tr	141.4a2tr	141.4a2tr	141.4a2tr
	SiO2	47.627	45.292	45.040	45.949	46.780	45.009	46.655	46.513	46.724	47.017	44.753	49.189
	Al2O3	7.872	8.248	8.230	9.008	7.876	8.026	8.133	8.166	7.830	8.043	8.052	5.409
	TiO2	0.596	0.643	0.647	0.816	0.651	0.599	0.623	0.587	0.694	0.662	0.658	0.371
	FeO	17.464	17.458	17.590	17.627	17.037	17.427	17.227	17.344	17.084	17.372	17.263	15.741
	MnO	0.295	0.261	0.245	0.291	0.209	0.280	0.250	0.238	0.251	0.265	0.295	0.261
	MgO	11.610	11.175	11.087	10.791	11.711	11.399	10.730	11.309	11.426	11.072	11.001	13.146
	CaO	12.063	12.313	11.930	11.916	12.036	12.071	11.533	11.944	11.920	11.925	11.721	12.156
	Na2O	0.848	0.930	0.986	1.015	0.939	0.967	0.999	0.959	0.999	1.066	1.069	0.638
	K2O	0.202	0.220	0.212	0.297	0.220	0.221	0.235	0.244	0.230	0.237	0.218	0.118
	Cl	0.119	0.113	0.104	0.148	0.088	0.071	0.117	0.097	0.113	0.092	0.122	0.043
	F	0.007	0.000	0.028	0.060	0.000	0.069	0.077	0.019	0.013	0.066	0.000	0.047
	Total	98.703	96.653	96.099	97.918	97.547	96.139	96.579	97.420	97.284	97.817	95.152	97.119
Tetrahedral	Si	6.917	6.770	6.756	6.768	6.877	6.747	6.946	6.860	6.902	6.926	6.779	7.199
	Al	1.083	1.230	1.244	1.232	1.123	1.253	1.054	1.140	1.098	1.074	1.221	0.801
	Fe3+	0.000	0.000	0.000	0.000	0.000	0.000	0.000	0.000	0.000	0.000	0.000	0.000
	total T site	8.000	8.000	8.000	8.000	8.000	8.000	8.000	8.000	8.000	8.000	8.000	8.000
Octahedral	Al	0.264	0.223	0.210	0.332	0.241	0.165	0.373	0.279	0.265	0.322	0.216	0.132
M1,M2,M3	Ti	0.065	0.072	0.073	0.090	0.072	0.068	0.070	0.065	0.077	0.073	0.075	0.041
	Fe3+	0.659	0.608	0.726	0.612	0.638	0.752	0.530	0.635	0.577	0.492	0.694	0.572
	Mg	2.514	2.490	2.479	2.370	2.566	2.547	2.381	2.486	2.516	2.431	2.484	2.868
	Fe2+	1.462	1.574	1.480	1.560	1.456	1.432	1.615	1.504	1.534	1.648	1.492	1.355
	Mn	0.036	0.033	0.031	0.036	0.026	0.036	0.032	0.030	0.031	0.033	0.038	0.032
	total M1-M3	5.000	5.000	5.000	5.000	5.000	5.000	5.000	5.000	5.000	5.000	5.000	5.000
Octahedral	Ca	1.877	1.972	1.917	1.881	1.896	1.939	1.840	1.887	1.887	1.882	1.902	1.906
M4	Na	0.123	0.028	0.083	0.119	0.104	0.061	0.160	0.113	0.113	0.118	0.098	0.094
	Fe2+	0.000	0.000	0.000	0.000	0.000	0.000	0.000	0.000	0.000	0.000	0.000	0.000
	Mn	0.000	0.000	0.000	0.000	0.000	0.000	0.000	0.000	0.000	0.000	0.000	0.000
	Mg	0.000	0.000	0.000	0.000	0.000	0.000	0.000	0.000	0.000	0.000	0.000	0.000
	total M4 site	2.000	2.000	2.000	2.000	2.000	2.000	2.000	2.000	2.000	2.000	2.000	2.000
A site	Na	0.116	0.241	0.204	0.170	0.163	0.220	0.128	0.162	0.173	0.187	0.216	0.087
	K	0.037	0.042	0.041	0.056	0.041	0.042	0.045	0.046	0.043	0.045	0.042	0.022
	total A site	0.153	0.283	0.244	0.226	0.205	0.262	0.173	0.208	0.216	0.231	0.258	0.109
	Mg/Mg+Fe2+	0.632	0.613	0.626	0.603	0.638	0.640	0.596	0.623	0.621	0.596	0.625	0.679

APPENDIX A: Amphibole Compositions; S141 Mylonitic Amphibolite

		141.4a7	141.4a7	141.4a7	141.4a7	141.4a7	141.4a7	141.4a7	141.4a7	141.4a7	141.4a7	141.4a7	141.4a7	141.4a7
	SiO2	47.382	49.772	49.516	50.188	48.614	46.569	46.347	46.765	46.543	46.192	46.824	46.528	47.688
	Al2O3	7.179	5.905	5.356	5.476	5.964	7.773	7.947	8.108	8.066	8.071	7.901	7.833	8.429
	TiO2	0.576	0.359	0.338	0.377	0.381	0.521	0.709	0.652	0.775	0.676	0.733	0.724	0.620
	FeO	16.916	16.235	16.219	16.007	16.375	17.292	17.285	17.616	17.326	17.622	17.518	17.633	17.134
	MnO	0.288	0.249	0.314	0.343	0.216	0.206	0.267	0.293	0.177	0.270	0.232	0.316	0.249
	MgO	11.721	12.738	13.123	13.203	12.760	11.583	11.490	11.453	11.479	11.471	11.778	11.619	11.146
	CaO	11.898	12.081	12.221	12.173	12.171	11.845	12.122	12.015	11.969	11.987	11.987	12.023	11.750
	Na2O	0.855	0.724	0.550	0.653	0.714	0.914	0.999	0.940	0.979	0.973	0.994	0.936	0.921
	K2O	0.177	0.152	0.129	0.112	0.137	0.242	0.217	0.225	0.241	0.243	0.215	0.225	0.236
	Cl	0.109	0.099	0.075	0.059	0.058	0.073	0.114	0.120	0.113	0.100	0.112	0.103	0.133
	F	0.000	0.057	0.079	0.032	0.000	0.000	0.034	0.000	0.000	0.039	0.045	0.000	0.006
	Total	97.101	98.371	97.920	98.623	97.390	97.018	97.531	98.187	97.668	97.644	98.339	97.940	98.312
Tetrahedral	Si	6.989	7.207	7.194	7.227	7.115	6.878	6.842	6.841	6.846	6.802	6.832	6.824	6.947
	Al	1.011	0.793	0.806	0.773	0.885	1.122	1.158	1.159	1.154	1.198	1.168	1.176	1.053
	Fe3+	0.000	0.000	0.000	0.000	0.000	0.000	0.000	0.000	0.000	0.000	0.000	0.000	0.000
	total T site	8.000	8.000	8.000	8.000	8.000	8.000	8.000	8.000	8.000	8.000	8.000	8.000	8.000
Octahedral	Al	0.236	0.215	0.111	0.156	0.143	0.231	0.225	0.239	0.244	0.203	0.191	0.178	0.394
M1,M2,M3	Ti	0.064	0.039	0.037	0.041	0.042	0.058	0.079	0.072	0.086	0.075	0.080	0.080	0.068
	Fe3+	0.609	0.520	0.637	0.577	0.613	0.720	0.614	0.701	0.642	0.739	0.746	0.752	0.552
	Mg	2.577	2.750	2.842	2.834	2.784	2.550	2.529	2.498	2.517	2.518	2.562	2.540	2.420
	Fe2+	1.477	1.446	1.334	1.350	1.391	1.415	1.521	1.454	1.489	1.431	1.391	1.411	1.535
	Mn	0.036	0.031	0.039	0.042	0.027	0.026	0.033	0.036	0.022	0.034	0.029	0.039	0.031
	total M1-M3	5.000	5.000	5.000	5.000	5.000	5.000	5.000	5.000	5.000	5.000	5.000	5.000	5.000
Octahedral	Ca	1.880	1.874	1.902	1.878	1.908	1.874	1.917	1.883	1.886	1.891	1.874	1.889	1.834
M4	Na	0.120	0.126	0.098	0.122	0.092	0.126	0.083	0.117	0.114	0.109	0.126	0.111	0.166
	Fe2+	0.000	0.000	0.000	0.000	0.000	0.000	0.000	0.000	0.000	0.000	0.000	0.000	0.000
	Mn	0.000	0.000	0.000	0.000	0.000	0.000	0.000	0.000	0.000	0.000	0.000	0.000	0.000
	Mg	0.000	0.000	0.000	0.000	0.000	0.000	0.000	0.000	0.000	0.000	0.000	0.000	0.000
	total M4 site	2.000	2.000	2.000	2.000	2.000	2.000	2.000	2.000	2.000	2.000	2.000	2.000	2.000
A site	Na	0.125	0.078	0.057	0.060	0.111	0.136	0.203	0.150	0.165	0.169	0.155	0.155	0.094
	K	0.033	0.028	0.024	0.021	0.026	0.046	0.041	0.042	0.045	0.046	0.040	0.042	0.044
	total A site	0.158	0.106	0.081	0.081	0.137	0.182	0.244	0.192	0.211	0.215	0.195	0.198	0.138
	Mg/Mg+Fe2+	0.636	0.655	0.681	0.677	0.667	0.643	0.625	0.632	0.628	0.638	0.648	0.643	0.612

APPENDIX A: Amphibole Compositions; S141 Mylonitic Amphibolite

		141.4a7	141.4a7	141.4a7	141.4a7	141.4a7	141.4a7	141.4a7	141.4a8	141.4a8	141.4a8	141.4a8	141.4a8	141.4a8
	SiO2	45.500	46.587	46.698	46.180	46.678	47.218	48.539	45.101	47.379	46.526	47.048	47.047	46.388
	Al2O3	8.234	8.286	8.222	8.309	8.163	7.632	7.073	8.370	7.842	7.873	7.817	7.892	7.954
	TiO2	0.302	0.755	0.733	0.654	0.679	0.599	0.561	0.558	0.673	0.732	0.681	0.697	0.679
	FeO	15.841	17.150	17.468	17.069	17.182	16.656	16.747	17.943	17.206	17.573	17.131	17.196	17.872
	MnO	0.268	0.290	0.227	0.263	0.265	0.252	0.273	0.254	0.283	0.283	0.216	0.274	0.320
	MgO	11.859	11.602	11.039	11.108	11.391	11.801	12.059	11.352	11.584	11.208	11.632	11.451	11.344
	CaO	11.673	11.904	11.954	11.816	12.015	11.950	12.165	10.918	12.242	12.113	12.045	12.170	11.962
	Na2O	0.703	0.876	0.914	0.881	0.952	0.869	0.830	0.849	0.873	0.880	0.911	0.926	1.025
	K2O	0.247	0.235	0.222	0.253	0.296	0.245	0.214	0.214	0.233	0.253	0.230	0.232	0.255
	Cl	0.121	0.091	0.129	0.113	0.094	0.095	0.083	0.117	0.148	0.113	0.125	0.120	0.116
	F	0.000	0.000	0.000	0.000	0.032	0.032	0.023	0.095	0.044	0.000	0.000	0.140	0.029
	Total	94.748	97.776	97.606	96.646	97.747	97.349	98.567	95.771	98.507	97.554	97.836	98.145	97.944
Tetrahedral	Si	6.831	6.820	6.883	6.859	6.866	6.944	7.050	6.698	6.919	6.873	6.901	6.906	6.822
	Al	1.169	1.180	1.117	1.141	1.134	1.056	0.950	1.302	1.081	1.127	1.099	1.094	1.178
	Fe3+	0.000	0.000	0.000	0.000	0.000	0.000	0.000	0.000	0.000	0.000	0.000	0.000	0.000
	total T site	8.000	8.000	8.000	8.000	8.000	8.000	8.000	8.000	8.000	8.000	8.000	8.000	8.000
Octahedral	Al	0.288	0.249	0.312	0.314	0.281	0.267	0.260	0.164	0.268	0.244	0.253	0.272	0.200
M1,M2,M3	Ti	0.034	0.083	0.081	0.073	0.075	0.066	0.061	0.062	0.074	0.081	0.075	0.077	0.075
	Fe3+	0.804	0.738	0.564	0.618	0.590	0.597	0.508	1.253	0.544	0.586	0.607	0.532	0.718
	Mg	2.654	2.532	2.426	2.460	2.498	2.587	2.611	2.513	2.522	2.468	2.544	2.506	2.487
	Fe2+	1.185	1.362	1.589	1.502	1.524	1.451	1.526	0.975	1.557	1.585	1.494	1.579	1.480
	Mn	0.034	0.036	0.028	0.033	0.033	0.031	0.034	0.032	0.035	0.035	0.027	0.034	0.040
	total M1-M3	5.000	5.000	5.000	5.000	5.000	5.000	5.000	5.000	5.000	5.000	5.000	5.000	5.000
Octahedral	Ca	1.878	1.867	1.888	1.880	1.893	1.883	1.893	1.737	1.915	1.917	1.893	1.914	1.885
M4	Na	0.122	0.133	0.112	0.120	0.107	0.117	0.107	0.244	0.085	0.083	0.107	0.086	0.115
	Fe2+	0.000	0.000	0.000	0.000	0.000	0.000	0.000	0.000	0.000	0.000	0.000	0.000	0.000
	Mn	0.000	0.000	0.000	0.000	0.000	0.000	0.000	0.000	0.000	0.000	0.000	0.000	0.000
	Mg	0.000	0.000	0.000	0.000	0.000	0.000	0.000	0.000	0.000	0.000	0.000	0.000	0.000
	total M4 site	2.000	2.000	2.000	2.000	2.000	2.000	2.000	1.982	2.000	2.000	2.000	2.000	2.000
A site	Na	0.082	0.116	0.149	0.134	0.165	0.131	0.127	0.000	0.162	0.169	0.152	0.178	0.177
	K	0.047	0.044	0.042	0.048	0.056	0.046	0.040	0.041	0.043	0.048	0.043	0.043	0.048
	total A site	0.130	0.160	0.191	0.182	0.220	0.177	0.166	0.041	0.206	0.217	0.195	0.221	0.225
	Mg/Mg+Fe2+	0.691	0.650	0.604	0.621	0.621	0.641	0.631	0.720	0.618	0.609	0.630	0.614	0.627

APPENDIX A: Amphibole Compositions; S141 Mylonitic Amphibolite

		141.4a8	141.4a8	141.4a8	141.4a8	141.4a8	141.4a8	141.4a8	141.4a8	141.4a8	141.4a8	141.4a8	141.4a8	141.4a8
	SiO2	46.124	47.775	46.117	45.596	46.718	46.568	46.468	47.025	47.034	47.707	48.823	49.894	49.058
	Al2O3	7.887	7.309	7.697	8.707	8.692	8.749	8.526	8.412	8.291	7.942	7.462	6.327	5.829
	TiO2	0.670	0.645	0.627	0.618	0.415	0.450	0.451	0.449	0.604	0.553	0.432	0.506	0.368
	FeO	17.421	17.341	16.914	16.598	16.216	16.211	16.560	16.146	16.092	16.151	15.766	15.477	15.376
	MnO	0.194	0.308	0.290	0.222	0.209	0.198	0.214	0.184	0.240	0.236	0.274	0.239	0.257
	MgO	11.296	11.691	11.490	11.122	11.349	11.586	11.495	11.609	11.863	11.780	12.295	12.767	12.875
	CaO	11.997	12.089	11.739	11.270	12.379	12.218	12.139	12.234	12.192	12.058	12.330	12.257	12.209
	Na2O	0.926	0.939	0.866	0.854	0.816	0.853	0.908	0.716	0.715	0.861	0.808	0.673	0.573
	K2O	0.221	0.204	0.211	0.257	0.212	0.190	0.202	0.217	0.187	0.241	0.181	0.148	0.147
	Cl	0.101	0.082	0.089	0.125	0.087	0.098	0.098	0.098	0.093	0.081	0.085	0.070	0.080
	F	0.115	0.045	0.144	0.043	0.066	0.056	0.009	0.088	0.026	0.026	0.073	0.017	0.000
	Total	96.952	98.428	96.184	95.412	97.159	97.177	97.070	97.178	97.337	97.636	98.529	98.375	96.772
Tetrahedral	Si	6.853	6.973	6.877	6.815	6.907	6.863	6.863	6.928	6.901	6.988	7.077	7.214	7.208
	Al	1.147	1.027	1.123	1.185	1.093	1.137	1.137	1.072	1.099	1.012	0.923	0.786	0.792
	Fe3+	0.000	0.000	0.000	0.000	0.000	0.000	0.000	0.000	0.000	0.000	0.000	0.000	0.000
	total T site	8.000	8.000	8.000	8.000	8.000	8.000	8.000	8.000	8.000	8.000	8.000	8.000	8.000
Octahedral	Al	0.234	0.231	0.230	0.349	0.421	0.382	0.347	0.388	0.334	0.359	0.351	0.292	0.218
M1,M2,M3	Ti	0.075	0.071	0.070	0.069	0.046	0.050	0.050	0.050	0.067	0.061	0.047	0.055	0.041
	Fe3+	0.635	0.570	0.711	0.790	0.384	0.518	0.550	0.477	0.560	0.457	0.387	0.370	0.458
	Mg	2.502	2.544	2.554	2.478	2.501	2.545	2.531	2.550	2.595	2.572	2.657	2.752	2.820
	Fe2+	1.530	1.547	1.398	1.285	1.621	1.480	1.495	1.512	1.414	1.522	1.524	1.502	1.432
	Mn	0.024	0.038	0.037	0.028	0.026	0.025	0.027	0.023	0.030	0.029	0.034	0.029	0.032
	total M1-M3	5.000	5.000	5.000	5.000	5.000	5.000	5.000	5.000	5.000	5.000	5.000	5.000	5.000
Octahedral	Ca	1.910	1.891	1.876	1.805	1.961	1.929	1.921	1.931	1.917	1.892	1.915	1.899	1.922
M4	Na	0.090	0.109	0.124	0.195	0.039	0.071	0.079	0.069	0.083	0.108	0.085	0.101	0.078
	Fe2+	0.000	0.000	0.000	0.000	0.000	0.000	0.000	0.000	0.000	0.000	0.000	0.000	0.000
	Mn	0.000	0.000	0.000	0.000	0.000	0.000	0.000	0.000	0.000	0.000	0.000	0.000	0.000
	Mg	0.000	0.000	0.000	0.000	0.000	0.000	0.000	0.000	0.000	0.000	0.000	0.000	0.000
	total M4 site	2.000	2.000	2.000	2.000	2.000	2.000	2.000	2.000	2.000	2.000	2.000	2.000	2.000
A site	Na	0.177	0.156	0.126	0.052	0.195	0.173	0.181	0.136	0.120	0.137	0.142	0.087	0.085
	K	0.042	0.038	0.040	0.049	0.040	0.036	0.038	0.041	0.035	0.045	0.033	0.027	0.028
	total A site	0.218	0.194	0.166	0.101	0.235	0.209	0.219	0.176	0.155	0.182	0.175	0.115	0.113
	Mg/Mg+Fe2+	0.621	0.622	0.646	0.659	0.607	0.632	0.629	0.628	0.647	0.628	0.636	0.647	0.663

APPENDIX A: Amphibole Compositions; S141 Mylonitic Amphibolite

		141.3a4tr	141.3a4tr	141.3a4tr	141.3a4tr	141.3a4tr	141.3a4tr	141.3a4tr	141.3a4tr	141.3a4tr	141.3a4tr	141.3a4tr	141.3a4tr	141.3a4tr
	SiO2	47.569	47.173	46.854	46.988	47.346	49.348	50.015	50.707	50.784	50.808	53.960	50.227	48.087
	Al2O3	7.862	8.072	8.178	8.026	7.493	6.046	5.046	4.413	4.001	3.885	4.840	5.262	7.033
	TiO2	0.633	0.688	0.750	0.656	0.549	0.446	0.332	0.283	0.253	0.272	0.321	0.413	0.529
	FeO	17.000	17.703	17.402	17.604	17.410	16.389	16.149	15.563	15.660	15.397	15.088	15.677	16.834
	MnO	0.324	0.235	0.261	0.344	0.243	0.334	0.290	0.355	0.286	0.323	0.289	0.296	0.244
	MgO	11.798	11.428	11.396	11.366	11.574	12.648	13.486	13.657	14.009	14.255	12.758	13.382	12.141
	CaO	12.152	12.099	12.006	12.138	12.136	11.919	11.987	12.002	12.222	12.085	11.360	12.296	12.227
	Na2O	0.875	0.925	0.999	0.912	0.837	0.762	0.582	0.512	0.427	0.504	0.493	0.616	0.744
	K2O	0.228	0.263	0.243	0.214	0.194	0.154	0.104	0.079	0.072	0.048	0.093	0.114	0.188
	Cl	0.102	0.114	0.118	0.101	0.128	0.120	0.080	0.096	0.066	0.079	0.066	0.054	0.056
	F	0.033	0.000	0.104	0.045	0.045	0.069	0.033	0.000	0.056	0.040	0.098	0.119	0.155
	Total	98.576	98.700	98.311	98.394	97.955	98.235	98.104	97.667	97.836	97.696	99.366	98.456	98.238
Tetrahedral	Si	6.918	6.872	6.858	6.871	6.946	7.156	7.219	7.341	7.343	7.340	7.642	7.251	7.012
	Al	1.082	1.128	1.142	1.129	1.054	0.844	0.781	0.659	0.657	0.660	0.358	0.749	0.988
	Fe3+	0.000	0.000	0.000	0.000	0.000	0.000	0.000	0.000	0.000	0.000	0.000	0.000	0.000
	total T site	8.000	8.000	8.000	8.000	8.000	8.000	8.000	8.000	8.000	8.000	8.000	8.000	8.000
Octahedral M1,M2,M3	Al	0.265	0.257	0.268	0.255	0.242	0.189	0.077	0.094	0.024	0.001	0.450	0.146	0.220
	Ti	0.069	0.075	0.083	0.072	0.061	0.049	0.036	0.031	0.028	0.030	0.034	0.045	0.058
	Fe3+	0.602	0.634	0.614	0.628	0.601	0.612	0.742	0.622	0.658	0.709	0.239	0.516	0.587
	Mg	2.558	2.482	2.487	2.478	2.531	2.734	2.902	2.947	3.020	3.070	2.694	2.880	2.639
	Fe2+	1.465	1.523	1.516	1.525	1.535	1.375	1.207	1.262	1.235	1.151	1.548	1.377	1.466
	Mn	0.040	0.029	0.032	0.043	0.030	0.041	0.035	0.044	0.035	0.040	0.035	0.036	0.030
	total M1-M3	5.000	5.000	5.000	5.000	5.000	5.000	5.000	5.000	5.000	5.000	5.000	5.000	5.000
Octahedral M4	Ca	1.893	1.888	1.883	1.902	1.908	1.852	1.854	1.862	1.893	1.870	1.724	1.902	1.910
	Na	0.107	0.112	0.117	0.098	0.092	0.148	0.146	0.138	0.107	0.130	0.135	0.098	0.090
	Fe2+	0.000	0.000	0.000	0.000	0.000	0.000	0.000	0.000	0.000	0.000	0.000	0.000	0.000
	Mn	0.000	0.000	0.000	0.000	0.000	0.000	0.000	0.000	0.000	0.000	0.000	0.000	0.000
	Mg	0.000	0.000	0.000	0.000	0.000	0.000	0.000	0.000	0.000	0.000	0.000	0.000	0.000
	total M4 site	2.000	2.000	2.000	2.000	2.000	2.000	2.000	2.000	2.000	2.000	1.859	2.000	2.000
A site	Na	0.140	0.150	0.166	0.160	0.146	0.066	0.017	0.005	0.013	0.012	0.000	0.074	0.120
	K	0.042	0.049	0.045	0.040	0.036	0.028	0.019	0.015	0.013	0.009	0.017	0.021	0.035
	total A site	0.182	0.198	0.212	0.200	0.182	0.094	0.036	0.020	0.026	0.020	0.017	0.095	0.155
	Mg/Mg+Fe2+	0.636	0.620	0.621	0.619	0.623	0.665	0.706	0.700	0.710	0.727	0.635	0.677	0.643

APPENDIX A: Amphibole Compositions; S141 Mylonitic Amphibolite

		141.3a4tr	141.3a4tr	141.3a4tr	141.3a4tr	141.3a4tr	141.3a1.1	141.3a1.2	141.3a1.3	141.3a1.4	141.3a1.5	141.3a1.6	141.3a1.7	141.4a1tr
	SiO2	46.976	46.770	47.731	44.946	44.067	47.188	47.223	46.735	47.483	46.738	47.161	48.762	43.672
	Al2O3	7.968	8.048	8.071	9.837	11.386	8.479	8.151	8.297	7.895	8.598	7.482	6.547	11.315
	TiO2	0.617	0.671	0.737	0.844	0.712	0.702	0.564	0.620	0.582	0.500	0.631	0.431	0.442
	FeO	17.132	17.259	17.233	17.949	18.118	16.607	16.297	16.569	16.256	16.374	16.569	15.940	17.767
	MnO	0.300	0.248	0.318	0.267	0.261	0.213	0.259	0.303	0.214	0.258	0.312	0.265	0.237
	MgO	11.699	11.372	11.573	10.397	9.668	11.349	11.800	11.640	11.745	11.494	11.882	12.686	9.940
	CaO	12.142	12.078	11.933	12.188	11.948	12.121	12.273	11.949	12.298	11.741	11.975	12.187	11.813
	Na2O	0.955	0.944	0.868	0.991	1.204	0.897	0.749	0.813	0.837	0.808	0.736	0.718	1.153
	K2O	0.208	0.223	0.254	0.368	0.363	0.242	0.176	0.208	0.221	0.195	0.173	0.151	0.309
	Cl	0.048	0.080	0.103	0.105	0.108	0.142	0.198	0.100	0.112	0.117	0.089	0.107	0.094
	F	0.041	0.000	0.000	0.041	0.044	0.000	0.037	0.049	0.001	0.000	0.000	0.048	0.024
	Total	98.086	97.693	98.821	97.933	97.879	97.940	97.727	97.283	97.644	96.823	97.010	97.842	96.766
Tetrahedral	Si	6.873	6.881	6.915	6.647	6.524	6.916	6.922	6.869	6.974	6.881	6.944	7.101	6.509
	Al	1.127	1.119	1.085	1.353	1.476	1.084	1.078	1.131	1.026	1.119	1.056	0.899	1.491
	Fe3+	0.000	0.000	0.000	0.000	0.000	0.000	0.000	0.000	0.000	0.000	0.000	0.000	0.000
	total T site	8.000	8.000	8.000	8.000	8.000	8.000	8.000	8.000	8.000	8.000	8.000	8.000	8.000
Octahedral M1,M2,M3	Al	0.247	0.277	0.293	0.361	0.511	0.381	0.330	0.307	0.341	0.373	0.243	0.225	0.497
	Ti	0.068	0.074	0.080	0.094	0.079	0.077	0.062	0.069	0.064	0.055	0.070	0.047	0.050
	Fe3+	0.628	0.574	0.636	0.589	0.602	0.441	0.524	0.653	0.406	0.663	0.652	0.546	0.729
	Mg	2.552	2.494	2.500	2.292	2.134	2.480	2.578	2.551	2.572	2.523	2.608	2.754	2.209
	Fe2+	1.468	1.549	1.452	1.631	1.642	1.594	1.474	1.384	1.590	1.353	1.388	1.395	1.485
	Mn	0.037	0.031	0.039	0.033	0.033	0.026	0.032	0.038	0.027	0.032	0.039	0.033	0.030
	total M1-M3	5.000	5.000	5.000	5.000	5.000	5.000	5.000	5.000	5.000	5.000	5.000	5.000	5.000
Octahedral M4	Ca	1.903	1.904	1.852	1.931	1.895	1.903	1.927	1.882	1.935	1.852	1.889	1.902	1.887
	Na	0.097	0.096	0.148	0.069	0.105	0.097	0.073	0.118	0.065	0.148	0.111	0.098	0.113
	Fe2+	0.000	0.000	0.000	0.000	0.000	0.000	0.000	0.000	0.000	0.000	0.000	0.000	0.000
	Mn	0.000	0.000	0.000	0.000	0.000	0.000	0.000	0.000	0.000	0.000	0.000	0.000	0.000
	Mg	0.000	0.000	0.000	0.000	0.000	0.000	0.000	0.000	0.000	0.000	0.000	0.000	0.000
	total M4 site	2.000	2.000	2.000	2.000	2.000	2.000	2.000	2.000	2.000	2.000	2.000	2.000	2.000
A site	Na	0.174	0.173	0.096	0.215	0.241	0.158	0.140	0.113	0.174	0.083	0.099	0.104	0.220
	K	0.039	0.042	0.047	0.069	0.069	0.045	0.033	0.039	0.041	0.037	0.032	0.028	0.059
	total A site	0.213	0.215	0.143	0.285	0.309	0.204	0.173	0.152	0.215	0.119	0.132	0.132	0.278
	Mg/Mg+Fe2+	0.635	0.617	0.633	0.584	0.565	0.609	0.636	0.648	0.618	0.651	0.653	0.664	0.598

APPENDIX A: Amphibole Compositions; S141 Mylonitic Amphibolite

		141.4a3tr	141.4a3tr	141.4a3tr	141.4a3tr	141.4a3tr	141.4a3tr	141.4a3tr	141.4a3tr	141.4a3tr	141.4a3tr	141.4a3tr	141.4a3tr	141.4a3tr
	SiO2	47.452	46.222	47.900	47.820	47.803	48.017	47.753	46.854	47.483	46.524	46.227	47.350	47.051
	Al2O3	7.797	7.972	6.858	7.343	7.407	7.939	8.262	8.235	6.755	8.556	9.810	8.773	8.060
	TiO2	0.625	0.619	0.602	0.454	0.550	0.565	0.530	0.538	0.537	0.374	0.335	0.305	0.619
	FeO	17.110	17.310	16.924	15.516	15.965	16.178	16.215	16.807	16.418	16.470	16.771	16.450	16.950
	MnO	0.267	0.284	0.345	0.265	0.215	0.237	0.211	0.163	0.241	0.225	0.238	0.256	0.303
	MgO	11.481	11.110	12.095	12.236	12.039	11.636	11.778	11.534	12.033	11.261	10.646	10.979	11.565
	CaO	12.065	12.090	12.084	12.180	12.154	12.253	12.399	12.207	12.176	12.312	12.529	12.102	12.083
	Na2O	0.887	0.889	0.808	0.718	0.802	0.737	0.697	0.788	0.788	0.783	0.851	0.810	0.867
	K2O	0.243	0.252	0.221	0.182	0.182	0.168	0.199	0.235	0.182	0.206	0.203	0.183	0.233
	Cl	0.114	0.143	0.086	0.063	0.096	0.104	0.064	0.101	0.092	0.083	0.112	0.112	0.118
	F	0.060	0.000	0.044	0.000	0.051	0.000	0.000	0.042	0.059	0.032	0.068	0.056	0.021
	Total	98.101	96.891	97.967	96.777	97.264	97.834	98.108	97.504	96.764	96.826	97.790	97.376	97.870
Tetrahedral	Si	6.950	6.878	7.004	7.044	7.028	7.024	6.961	6.894	7.037	6.901	6.818	6.974	6.897
	Al	1.050	1.122	0.996	0.956	0.972	0.976	1.039	1.106	0.963	1.099	1.182	1.026	1.103
	Fe3+	0.000	0.000	0.000	0.000	0.000	0.000	0.000	0.000	0.000	0.000	0.000	0.000	0.000
	total T site	8.000	8.000	8.000	8.000	8.000	8.000	8.000	8.000	8.000	8.000	8.000	8.000	8.000
Octahedral M1,M2,M3	Al	0.296	0.276	0.185	0.318	0.311	0.392	0.380	0.322	0.217	0.397	0.524	0.497	0.289
	Ti	0.069	0.069	0.066	0.050	0.061	0.062	0.058	0.060	0.060	0.042	0.037	0.034	0.068
	Fe3+	0.533	0.548	0.622	0.454	0.448	0.379	0.437	0.547	0.499	0.441	0.342	0.376	0.592
	Mg	2.507	2.465	2.636	2.687	2.639	2.537	2.559	2.530	2.658	2.490	2.341	2.411	2.527
	Fe2+	1.563	1.606	1.447	1.458	1.515	1.600	1.540	1.521	1.536	1.602	1.726	1.651	1.485
	Mn	0.033	0.036	0.043	0.033	0.027	0.029	0.026	0.020	0.030	0.028	0.030	0.032	0.038
	total M1-M3	5.000	5.000	5.000	5.000	5.000	5.000	5.000	5.000	5.000	5.000	5.000	5.000	5.000
Octahedral M4	Ca	1.893	1.928	1.893	1.922	1.914	1.920	1.936	1.924	1.933	1.957	1.980	1.910	1.898
	Na	0.107	0.072	0.107	0.078	0.086	0.080	0.064	0.076	0.067	0.043	0.020	0.090	0.102
	Fe2+	0.000	0.000	0.000	0.000	0.000	0.000	0.000	0.000	0.000	0.000	0.000	0.000	0.000
	Mn	0.000	0.000	0.000	0.000	0.000	0.000	0.000	0.000	0.000	0.000	0.000	0.000	0.000
	Mg	0.000	0.000	0.000	0.000	0.000	0.000	0.000	0.000	0.000	0.000	0.000	0.000	0.000
	total M4 site	2.000	2.000	2.000	2.000	2.000	2.000	2.000	2.000	2.000	2.000	2.000	2.000	2.000
A site	Na	0.145	0.184	0.122	0.127	0.143	0.129	0.133	0.149	0.160	0.182	0.223	0.141	0.144
	K	0.045	0.048	0.041	0.034	0.034	0.031	0.037	0.044	0.034	0.039	0.038	0.034	0.044
	total A site	0.191	0.232	0.163	0.161	0.177	0.161	0.170	0.193	0.194	0.221	0.262	0.176	0.188
	Mg/Mg+Fe2+	0.616	0.605	0.646	0.648	0.635	0.613	0.624	0.625	0.634	0.609	0.576	0.594	0.630

APPENDIX A: Amphibole Compositions; S141 Mylonitic Amphibolite

		141.4a3tr	141.4a3tr	141.4a3tr	141.4a3tr	141.4a3tr	141.4a3tr	141.4a3tr	141.4a5tr	141.4a5tr	141.4a5tr	141.4a5tr	141.4a5tr
	SiO2	47.014	48.110	47.585	44.788	47.914	47.795	46.918	47.826	49.384	48.438	50.194	49.818
	Al2O3	8.517	7.563	8.317	9.683	8.543	8.096	7.772	7.775	6.387	7.093	5.443	5.383
	TiO2	0.365	0.434	0.502	0.334	0.425	0.556	0.499	0.612	0.546	0.693	0.360	0.407
	FeO	16.204	15.991	16.220	16.702	16.285	16.424	16.111	17.045	16.218	16.753	15.811	15.772
	MnO	0.192	0.256	0.281	0.274	0.226	0.263	0.226	0.278	0.303	0.306	0.313	0.243
	MgO	11.558	12.093	11.504	10.519	11.357	11.611	11.715	11.885	12.439	12.200	12.769	13.018
	CaO	12.193	12.142	12.020	11.702	12.037	12.048	11.966	11.811	12.183	12.071	11.947	12.097
	Na2O	0.784	0.746	0.787	1.073	0.832	0.784	0.778	0.879	0.765	0.884	0.674	0.564
	K2O	0.181	0.160	0.212	0.234	0.166	0.230	0.185	0.220	0.171	0.163	0.123	0.129
	Cl	0.078	0.097	0.076	0.109	0.087	0.102	0.094	0.107	0.066	0.078	0.062	0.065
	F	0.094	0.000	0.011	0.089	0.013	0.018	0.028	0.020	0.039	0.049	0.071	0.000
	Total	97.180	97.592	97.515	95.507	97.885	97.927	96.292	98.458	98.501	98.728	97.767	97.496
Tetrahedral	Si	6.924	7.030	6.973	6.744	6.995	6.980	6.964	6.935	7.158	7.014	7.299	7.255
	Al	1.076	0.970	1.027	1.256	1.005	1.020	1.036	1.065	0.842	0.986	0.701	0.745
	Fe3+	0.000	0.000	0.000	0.000	0.000	0.000	0.000	0.000	0.000	0.000	0.000	0.000
	total T site	8.000	8.000	8.000	8.000	8.000	8.000	8.000	8.000	8.000	8.000	8.000	8.000
Octahedral	Al	0.402	0.332	0.409	0.463	0.465	0.373	0.324	0.263	0.249	0.225	0.231	0.179
M1,M2,M3	Ti	0.040	0.048	0.055	0.038	0.047	0.061	0.056	0.067	0.060	0.075	0.039	0.045
	Fe3+	0.487	0.499	0.470	0.583	0.414	0.490	0.536	0.711	0.443	0.587	0.456	0.520
	Mg	2.538	2.634	2.513	2.361	2.472	2.528	2.592	2.569	2.688	2.634	2.768	2.826
	Fe2+	1.509	1.455	1.518	1.520	1.574	1.515	1.464	1.356	1.523	1.442	1.467	1.401
	Mn	0.024	0.032	0.035	0.035	0.028	0.033	0.028	0.034	0.037	0.038	0.039	0.030
	total M1-M3	5.000	5.000	5.000	5.000	5.000	5.000	5.000	5.000	5.000	5.000	5.000	5.000
Octahedral	Ca	1.924	1.901	1.887	1.888	1.883	1.885	1.903	1.835	1.892	1.873	1.861	1.887
M4	Na	0.076	0.099	0.113	0.112	0.117	0.115	0.097	0.165	0.108	0.127	0.139	0.113
	Fe2+	0.000	0.000	0.000	0.000	0.000	0.000	0.000	0.000	0.000	0.000	0.000	0.000
	Mn	0.000	0.000	0.000	0.000	0.000	0.000	0.000	0.000	0.000	0.000	0.000	0.000
	Mg	0.000	0.000	0.000	0.000	0.000	0.000	0.000	0.000	0.000	0.000	0.000	0.000
	total M4 site	2.000	2.000	2.000	2.000	2.000	2.000	2.000	2.000	2.000	2.000	2.000	2.000
A site	Na	0.148	0.112	0.111	0.201	0.118	0.107	0.127	0.082	0.107	0.121	0.051	0.047
	K	0.034	0.030	0.040	0.045	0.031	0.043	0.035	0.041	0.032	0.030	0.023	0.024
	total A site	0.182	0.142	0.150	0.246	0.149	0.150	0.162	0.123	0.139	0.151	0.074	0.071
	Mg/Mg+Fe2+	0.627	0.644	0.623	0.608	0.611	0.625	0.639	0.655	0.638	0.646	0.654	0.669

APPENDIX A: Amphibole Compositions; S899 Mylonitic Amphibolite

		899.1altr	899.1altr	899.1altr	899.1altr	899.1altrl	899.1altrl	899.1altrl	899.1altrl	899.1altrl	899.1a2.1	899.1a2.2	899.1a2.3	899.1a2.4
	SiO2	46.747	45.338	45.643	47.278	44.643	43.976	43.436	43.218	45.542	47.711	46.673	51.252	51.267
	Al2O3	7.843	8.632	8.775	8.026	9.609	10.083	10.480	10.825	9.342	7.477	7.595	10.249	3.411
	TiO2	0.534	0.554	0.688	0.535	0.760	0.735	0.692	0.775	0.692	0.525	0.370	0.068	0.079
	FeO	15.964	16.556	16.638	16.133	17.171	17.358	17.364	17.877	16.652	16.134	16.057	10.520	12.759
	MnO	0.173	0.279	0.190	0.206	0.201	0.171	0.252	0.287	0.286	0.220	0.165	0.230	0.193
	MgO	11.597	11.011	10.562	11.580	10.280	9.976	9.646	9.466	10.518	11.666	11.711	10.596	14.300
	CaO	12.174	11.931	12.024	12.092	11.858	11.745	11.863	12.023	11.823	11.924	11.864	11.671	12.579
	Na2O	0.741	0.801	0.956	0.810	0.976	1.171	1.113	1.147	0.973	0.737	0.777	2.123	0.273
	K2O	0.208	0.249	0.288	0.232	0.286	0.305	0.330	0.275	0.278	0.221	0.186	0.316	0.046
	Cl	0.138	0.168	0.186	0.184	0.198	0.234	0.275	0.282	0.215	0.136	0.155	0.027	0.020
	F	0.000	0.000	0.000	0.092	0.000	0.000	0.002	0.000	0.029	0.002	0.036	0.034	0.000
	Total	96.119	95.519	95.950	97.168	95.982	95.754	95.453	96.175	96.350	96.753	95.589	97.086	94.927
Tetrahedral	Si	6.971	6.820	6.874	6.979	6.718	6.652	6.610	6.543	6.811	7.049	6.980	7.557	7.617
	Al	1.029	1.180	1.126	1.021	1.282	1.348	1.390	1.457	1.189	0.951	1.020	0.443	0.383
	Fe3+	0.000	0.000	0.000	0.000	0.000	0.000	0.000	0.000	0.000	0.000	0.000	0.000	0.000
	total T site	8.000	8.000	8.000	8.000	8.000	8.000	8.000	8.000	8.000	8.000	8.000	8.000	8.000
Octahedral M1,M2,M3	Al	0.349	0.350	0.431	0.375	0.422	0.449	0.490	0.475	0.458	0.351	0.318	1.338	0.214
	Ti	0.060	0.063	0.078	0.059	0.086	0.084	0.079	0.088	0.078	0.058	0.042	0.008	0.009
	Fe3+	0.416	0.578	0.325	0.427	0.526	0.523	0.480	0.515	0.451	0.455	0.556	0.000	0.059
	Mg	2.578	2.469	2.371	2.548	2.306	2.250	2.188	2.137	2.345	2.570	2.611	2.329	3.167
	Fe2+	1.575	1.505	1.771	1.564	1.635	1.673	1.730	1.749	1.632	1.538	1.452	1.326	1.526
	Mn	0.022	0.036	0.024	0.026	0.026	0.022	0.032	0.037	0.036	0.028	0.021	0.000	0.024
	total M1-M3	5.000	5.000	5.000	5.000	5.000	5.000	5.000	5.000	5.000	5.000	5.000	5.000	5.000
Octahedral M4	Ca	1.945	1.923	1.940	1.912	1.912	1.903	1.934	1.950	1.895	1.888	1.901	1.844	2.002
	Na	0.055	0.077	0.060	0.088	0.088	0.097	0.066	0.050	0.105	0.112	0.099	0.000	0.000
	Fe2+	0.000	0.000	0.000	0.000	0.000	0.000	0.000	0.000	0.000	0.000	0.000	1.234	0.000
	Mn	0.000	0.000	0.000	0.000	0.000	0.000	0.000	0.000	0.000	0.000	0.000	0.029	0.000
	Mg	0.000	0.000	0.000	0.000	0.000	0.000	0.000	0.000	0.000	0.000	0.000	0.000	0.000
	total M4 site	2.000	2.000	2.000	2.000	2.000	2.000	2.000	2.000	2.000	2.000	2.000	3.107	2.002
A site	Na	0.159	0.156	0.219	0.144	0.196	0.247	0.263	0.287	0.177	0.099	0.126	0.607	0.079
	K	0.040	0.048	0.055	0.044	0.055	0.059	0.064	0.053	0.053	0.042	0.035	0.059	0.009
	total A site	0.199	0.204	0.275	0.188	0.251	0.306	0.327	0.340	0.230	0.140	0.162	0.666	0.087
	Mg/(Mg+Fe2+)	0.861	0.810	0.880	0.856	0.814	0.811	0.820	0.806	0.839	0.850	0.824	2.185	0.982

APPENDIX A: Amphibole Compositions; S899 Mylonitic Amp

		899.1a2.5	899.1a3tr	899.1a3tr	899.1a3tr	899.1a3tr	899.1a3tr
	SiO2	54.881	43.585	43.515	45.113	45.175	44.739
	Al2O3	3.518	10.459	11.249	9.442	8.773	9.755
	TiO2	0.075	0.929	0.676	0.848	0.784	0.976
	FeO	12.362	17.590	17.022	17.048	17.063	17.217
	MnO	0.271	0.235	0.233	0.247	0.229	0.255
	MgO	13.411	9.803	9.431	10.216	10.319	9.933
	CaO	11.304	11.828	11.607	11.634	11.629	11.756
	Na2O	0.305	1.125	1.162	1.037	0.972	0.946
	K2O	0.075	0.345	0.336	0.290	0.269	0.326
	Cl	0.025	0.000	0.000	0.011	0.262	0.220
	F	0.029	0.000	0.021	0.044	0.014	0.000
	Total	96.256	95.899	95.252	95.930	95.489	96.123
Tetrahedral	Si	7.959	6.578	6.595	6.774	6.833	6.732
	Al	0.041	1.422	1.405	1.226	1.167	1.268
	Fe3+	0.000	0.000	0.000	0.000	0.000	0.000
	total T site	8.000	8.000	8.000	8.000	8.000	8.000
Octahedral	Al	0.560	0.439	0.605	0.445	0.397	0.462
M1,M2,M3	Ti	0.008	0.105	0.077	0.096	0.089	0.110
	Fe3+	0.000	0.551	0.470	0.488	0.487	0.455
	Mg	2.899	2.206	2.131	2.287	2.327	2.228
	Fe2+	1.533	1.669	1.688	1.653	1.672	1.711
	Mn	0.000	0.030	0.030	0.031	0.029	0.033
	total M1-M3	5.000	5.000	5.000	5.000	5.000	5.000
Octahedral	Ca	1.756	1.913	1.885	1.872	1.884	1.895
M4	Na	0.086	0.087	0.115	0.128	0.116	0.105
	Fe2+	0.114	0.000	0.000	0.000	0.000	0.000
	Mn	0.033	0.000	0.000	0.000	0.000	0.000
	Mg	0.000	0.000	0.000	0.000	0.000	0.000
	total M4 site	1.990	2.000	2.000	2.000	2.000	2.000
A site	Na	0.000	0.242	0.226	0.174	0.170	0.171
	K	0.014	0.066	0.065	0.056	0.052	0.063
	total A site	0.014	0.308	0.291	0.229	0.221	0.234
	Mg/(Mg+Fe2+)	1.054	0.800	0.819	0.824	0.827	0.830

APPENDIX A: Amphibole Compositions; S898 Mylonitic Amphibolite

		898.1altr	898.1altr	898.1altr	898.1altr	898.1altr	898.1altr	898.1altr	898.1altr	898.1altr	898.1altr	898.1a2tr	898.1a2tr	898.1a2tr
	SiO2	44.170	43.597	43.197	43.304	42.857	43.590	43.633	45.427	44.926	43.413	46.780	46.568	45.969
	Al2O3	10.986	11.620	12.190	11.582	11.682	10.951	10.216	10.188	10.498	11.974	8.451	8.778	8.714
	TiO2	0.661	0.690	0.717	0.709	0.721	0.726	0.569	0.502	0.608	0.789	0.446	0.439	0.520
	FeO	19.118	19.509	19.540	19.393	19.574	19.370	19.130	18.240	18.653	18.977	18.141	17.647	18.257
	MnO	0.241	0.284	0.260	0.296	0.351	0.254	0.235	0.243	0.215	0.179	0.309	0.265	0.283
	MgO	9.359	9.041	8.619	8.660	8.598	9.128	9.391	10.078	9.741	8.789	10.872	10.807	10.543
	CaO	11.834	11.869	11.846	11.783	11.857	11.941	11.631	12.100	12.082	11.536	11.817	12.046	11.740
	Na2O	1.198	1.226	1.376	1.255	1.321	1.232	1.030	1.003	1.149	1.344	0.979	1.009	1.013
	K2O	0.375	0.432	0.450	0.422	0.403	0.406	0.327	0.266	0.344	0.457	0.229	0.230	0.251
	Cl	0.383	0.409	0.420	0.436	0.370	0.349	0.260	0.225	0.251	0.364	0.245	0.228	0.240
	F	0.060	0.032	0.094	0.027	0.083	0.062	0.077	0.009	0.044	0.000	0.028	0.009	0.077
	Total	98.385	98.709	98.709	97.867	97.817	98.009	96.499	98.281	98.511	97.822	98.297	98.026	97.607
Tetrahedral	Si	6.543	6.452	6.417	6.481	6.430	6.509	6.573	6.688	6.632	6.469	6.855	6.853	6.802
	Al	1.457	1.548	1.583	1.519	1.570	1.491	1.427	1.312	1.368	1.531	1.145	1.147	1.198
	Fe3+	0.000	0.000	0.000	0.000	0.000	0.000	0.000	0.000	0.000	0.000	0.000	0.000	0.000
	total T site	8.000	8.000	8.000	8.000	8.000	8.000	8.000	8.000	8.000	8.000	8.000	8.000	8.000
Octahedral	Al	0.461	0.479	0.551	0.523	0.495	0.436	0.387	0.456	0.459	0.572	0.314	0.376	0.322
M1,M2,M3	Ti	0.074	0.077	0.080	0.080	0.081	0.082	0.064	0.056	0.067	0.088	0.049	0.049	0.058
	Fe3+	0.677	0.719	0.620	0.613	0.639	0.638	0.793	0.590	0.558	0.624	0.701	0.544	0.700
	Mg	2.067	1.995	1.909	1.932	1.923	2.032	2.109	2.212	2.144	1.952	2.375	2.371	2.326
	Fe2+	1.691	1.696	1.808	1.814	1.817	1.781	1.617	1.655	1.745	1.741	1.522	1.628	1.559
	Mn	0.030	0.036	0.033	0.038	0.045	0.032	0.030	0.030	0.027	0.023	0.038	0.033	0.035
	total M1-M3	5.000	5.000	5.000	5.000	5.000	5.000	5.000	5.000	5.000	5.000	5.000	5.000	5.000
Octahedral	Ca	1.878	1.882	1.885	1.889	1.906	1.910	1.877	1.909	1.911	1.842	1.855	1.899	1.861
M4	Na	0.122	0.118	0.115	0.111	0.094	0.090	0.123	0.091	0.089	0.158	0.145	0.101	0.139
	Fe2+	0.000	0.000	0.000	0.000	0.000	0.000	0.000	0.000	0.000	0.000	0.000	0.000	0.000
	Mn	0.000	0.000	0.000	0.000	0.000	0.000	0.000	0.000	0.000	0.000	0.000	0.000	0.000
	Mg	0.000	0.000	0.000	0.000	0.000	0.000	0.000	0.000	0.000	0.000	0.000	0.000	0.000
	total M4 site	2.000	2.000	2.000	2.000	2.000	2.000	2.000	2.000	2.000	2.000	2.000	2.000	2.000
A site	Na	0.222	0.234	0.282	0.253	0.290	0.267	0.178	0.195	0.240	0.230	0.133	0.187	0.152
	K	0.071	0.082	0.085	0.081	0.077	0.077	0.063	0.050	0.065	0.087	0.043	0.043	0.047
	total A site	0.293	0.315	0.367	0.334	0.367	0.344	0.241	0.245	0.305	0.317	0.176	0.230	0.199
	Mg/Fe2+ + Mg	0.550	0.541	0.514	0.516	0.514	0.533	0.566	0.572	0.551	0.529	0.609	0.593	0.599

APPENDIX A: Amphibole Compositions; S898 Mylonitic Amphibolite

		898.1a2tr	898.1a2tr	898.1a2tr	898.1a2tr	898.1a2tr	898.1a2tr	898.1a2tr	898.1a4.1	898.1a4.2	898.1a4.3	898.1a5.1	898.1a5.2	898.1a6.1
	SiO2	45.494	45.303	44.117	43.523	44.109	46.777	44.019	44.213	43.453	45.015	45.363	41.960	45.638
	Al2O3	8.922	9.569	10.953	11.379	10.495	9.154	11.655	9.903	12.927	9.444	9.433	14.641	10.226
	TiO2	0.436	0.473	0.575	0.650	0.593	0.469	0.567	0.479	0.440	0.557	0.537	0.354	0.461
	FeO	19.370	18.484	18.982	19.246	18.960	17.784	19.461	19.028	19.040	19.009	18.827	18.992	18.460
	MnO	0.341	0.308	0.311	0.306	0.247	0.335	0.298	0.281	0.206	0.324	0.279	0.296	0.300
	MgO	10.449	10.137	9.492	9.014	9.434	10.465	8.994	9.424	8.275	9.999	10.073	7.338	10.016
	CaO	11.698	12.007	11.993	11.808	11.937	12.016	12.166	11.656	11.943	11.710	11.860	11.779	11.848
	Na2O	1.054	0.977	1.112	1.254	1.206	0.985	1.217	1.273	1.256	1.160	1.073	1.391	1.081
	K2O	0.230	0.244	0.344	0.387	0.330	0.244	0.369	0.296	0.350	0.257	0.276	0.401	0.286
	Cl	0.220	0.256	0.221	0.409	0.363	0.238	0.316	0.335	0.283	0.284	0.292	0.231	0.248
	F	0.015	0.044	0.000	0.037	0.000	0.000	0.056	0.062	0.000	0.087	0.080	0.041	0.000
	Total	98.229	97.802	98.100	98.013	97.674	98.467	99.118	96.950	98.173	97.846	98.093	97.424	98.564
Tetrahedral	Si	6.690	6.710	6.536	6.487	6.587	6.858	6.494	6.649	6.459	6.677	6.710	6.302	6.692
	Al	1.310	1.290	1.464	1.513	1.413	1.142	1.506	1.351	1.541	1.323	1.290	1.698	1.308
	Fe3+	0.000	0.000	0.000	0.000	0.000	0.000	0.000	0.000	0.000	0.000	0.000	0.000	0.000
	total T site	8.000	8.000	8.000	8.000	8.000	8.000	8.000	8.000	8.000	8.000	8.000	8.000	8.000
Octahedral M1,M2,M3	Al	0.236	0.381	0.449	0.486	0.434	0.439	0.521	0.404	0.724	0.328	0.355	0.894	0.459
	Ti	0.048	0.053	0.064	0.073	0.067	0.052	0.063	0.054	0.049	0.062	0.060	0.040	0.051
	Fe3+	0.947	0.666	0.695	0.673	0.614	0.499	0.596	0.654	0.485	0.766	0.696	0.451	0.664
	Mg	2.291	2.238	2.096	2.003	2.100	2.287	1.978	2.113	1.834	2.211	2.221	1.643	2.189
	Fe2+	1.435	1.624	1.657	1.726	1.754	1.681	1.805	1.739	1.881	1.592	1.633	1.934	1.599
	Mn	0.042	0.039	0.039	0.039	0.031	0.042	0.037	0.036	0.026	0.041	0.035	0.038	0.037
	total M1-M3	5.000	5.000	5.000	5.000	5.000	5.000	5.000	5.000	5.000	5.000	5.000	5.000	5.000
Octahedral M4	Ca	1.843	1.905	1.904	1.886	1.910	1.887	1.923	1.878	1.902	1.861	1.880	1.895	1.861
	Na	0.157	0.095	0.096	0.114	0.090	0.113	0.077	0.122	0.098	0.139	0.120	0.105	0.139
	Fe2+	0.000	0.000	0.000	0.000	0.000	0.000	0.000	0.000	0.000	0.000	0.000	0.000	0.000
	Mn	0.000	0.000	0.000	0.000	0.000	0.000	0.000	0.000	0.000	0.000	0.000	0.000	0.000
	Mg	0.000	0.000	0.000	0.000	0.000	0.000	0.000	0.000	0.000	0.000	0.000	0.000	0.000
	total M4 site	2.000	2.000	2.000	2.000	2.000	2.000	2.000	2.000	2.000	2.000	2.000	2.000	2.000
A site	Na	0.144	0.186	0.223	0.248	0.259	0.167	0.271	0.249	0.264	0.195	0.187	0.301	0.169
	K	0.043	0.046	0.065	0.074	0.063	0.046	0.069	0.057	0.066	0.049	0.052	0.077	0.053
	total A site	0.187	0.232	0.288	0.322	0.322	0.213	0.341	0.306	0.331	0.243	0.240	0.377	0.222
	Mg/Fe2+ + Mg	0.615	0.580	0.559	0.537	0.545	0.576	0.523	0.549	0.494	0.581	0.576	0.459	0.578

APPENDIX A: Amphibole Compositions; S898 Mylonitic Amphibolite

		898.1a6.2	898.1a6.3	898.1a7.1	898.1a7.2	898.1a8.1	898.1a8.2	898.1a8.3	898.1a8.4	898.5a3.1	898.5a3.2	898.5a3.3	898.5a3.4	898.5a4.1
	SiO2	45.059	45.288	44.859	43.226	43.767	42.912	42.715	63.420	42.137	42.678	43.160	43.928	45.720
	Al2O3	9.451	10.075	10.589	11.954	12.946	12.055	13.053	22.564	12.364	12.096	11.954	11.417	17.577
	TiO2	0.505	0.461	0.474	0.776	0.395	0.836	0.389	0.000	0.635	0.656	0.658	0.614	0.225
	FeO	18.425	18.591	18.604	20.225	18.967	19.552	19.268	0.355	20.851	20.668	20.056	19.437	14.392
	MnO	0.345	0.266	0.314	0.282	0.250	0.277	0.295	0.018	0.345	0.257	0.251	0.304	0.281
	MgO	10.385	9.879	9.777	8.506	8.337	8.253	8.358	0.007	8.180	8.276	8.317	8.820	5.072
	CaO	11.848	11.897	11.804	11.978	11.856	11.610	11.910	3.948	11.632	11.800	11.972	11.330	10.152
	Na2O	1.105	1.100	1.055	1.431	1.214	1.368	1.273	9.415	1.470	1.342	1.291	1.333	3.664
	K2O	0.255	0.239	0.309	0.403	0.351	0.403	0.369	0.066	0.536	0.421	0.417	0.395	0.348
	Cl	0.289	0.262	0.183	0.400	0.186	0.412	0.169	0.000	0.473	0.487	0.382	0.358	0.143
	F	0.028	0.011	0.000	0.016	0.037	0.000	0.000	0.000	0.013	0.066	0.000	0.047	0.000
	Total	97.695	98.069	97.968	99.197	98.306	97.678	97.799	99.793	98.636	98.747	98.458	97.983	97.574
Tetrahedral	Si	6.675	6.690	6.620	6.405	6.479	6.439	6.367	9.127	6.288	6.358	6.440	6.526	6.876
	Al	1.325	1.310	1.380	1.595	1.521	1.561	1.633	0.000	1.712	1.642	1.560	1.474	1.124
	Fe3+	0.000	0.000	0.000	0.000	0.000	0.000	0.000	0.000	0.000	0.000	0.000	0.000	0.000
	total T site	8.000	8.000	8.000	8.000	8.000	8.000	8.000	9.127	8.000	8.000	8.000	8.000	8.000
Octahedral	Al	0.325	0.444	0.461	0.493	0.737	0.571	0.660	3.827	0.463	0.481	0.542	0.525	1.991
M1,M2,M3	Ti	0.056	0.051	0.053	0.086	0.044	0.094	0.044	0.000	0.071	0.073	0.074	0.069	0.025
	Fe3+	0.762	0.639	0.721	0.638	0.521	0.593	0.644	0.000	0.859	0.780	0.590	0.746	0.000
	Mg	2.293	2.175	2.151	1.879	1.840	1.846	1.857	0.002	1.820	1.838	1.850	1.953	1.137
	Fe2+	1.521	1.658	1.575	1.868	1.827	1.860	1.758	1.172	1.743	1.795	1.913	1.669	1.846
	Mn	0.043	0.033	0.039	0.035	0.031	0.035	0.037	0.000	0.044	0.032	0.032	0.038	0.000
	total M1-M3	5.000	5.000	5.000	5.000	5.000	5.000	5.000	5.000	5.000	5.000	5.000	5.000	5.000
Octahedral	Ca	1.880	1.883	1.866	1.902	1.880	1.867	1.902	0.609	1.860	1.883	1.914	1.803	1.636
M4	Na	0.120	0.117	0.134	0.098	0.120	0.133	0.098	0.000	0.140	0.117	0.086	0.197	0.000
	Fe2+	0.000	0.000	0.000	0.000	0.000	0.000	0.000	4.808	0.000	0.000	0.000	0.000	1.289
	Mn	0.000	0.000	0.000	0.000	0.000	0.000	0.000	0.002	0.000	0.000	0.000	0.000	0.036
	Mg	0.000	0.000	0.000	0.000	0.000	0.000	0.000	0.000	0.000	0.000	0.000	0.000	0.000
	total M4 site	2.000	2.000	2.000	2.000	2.000	2.000	2.000	5.419	2.000	2.000	2.000	2.000	2.961
A site	Na	0.198	0.198	0.168	0.313	0.229	0.265	0.270	2.627	0.285	0.271	0.287	0.187	1.068
	K	0.048	0.045	0.058	0.076	0.066	0.077	0.070	0.012	0.102	0.080	0.079	0.075	0.067
	total A site	0.246	0.243	0.226	0.389	0.295	0.342	0.340	2.639	0.387	0.351	0.367	0.262	1.135
	Mg/Fe2+ + Mg	0.601	0.568	0.577	0.501	0.502	0.498	0.514	0.000	0.511	0.506	0.492	0.539	0.266

APPENDIX A: Amphibole Compositions; S898 Mylonitic Amphibolite

		898.5a4.2	898.5a4.3	898.5a4.4	898.5a4.5	898.5a4.6	898.5a1.1	898.5a1.2	898.5a1.3	898.5a1.4	898.5a5.1	898.5a5.2
	SiO2	46.155	43.556	43.442	44.047	42.052	44.005	43.016	43.882	43.399	43.729	43.276
	Al2O3	19.392	10.589	11.510	11.677	13.539	11.454	11.094	10.919	10.934	10.761	11.139
	TiO2	0.249	0.493	0.391	0.395	0.393	0.493	0.551	0.484	0.586	0.949	0.869
	FeO	13.825	19.040	18.524	18.625	18.988	19.409	20.234	19.434	19.091	19.070	19.295
	MnO	0.156	0.326	0.297	0.266	0.264	0.215	0.291	0.283	0.322	0.294	0.290
	MgO	4.719	9.083	9.111	9.046	8.201	9.013	8.812	8.674	8.973	8.850	8.787
	CaO	11.453	11.896	11.505	11.894	11.756	12.165	11.703	11.915	11.520	11.656	11.771
	Na2O	2.870	1.227	1.230	1.170	1.379	1.209	1.405	1.219	1.331	1.174	1.129
	K2O	0.318	0.351	0.346	0.354	0.369	0.349	0.373	0.330	0.347	0.330	0.374
	Cl	0.158	0.327	0.278	0.235	0.255	0.301	0.396	0.342	0.389	0.340	0.371
	F	0.000	0.007	0.000	0.049	0.003	0.042	0.088	0.051	0.052	0.000	0.016
	Total	99.295	96.895	96.634	97.758	97.199	98.655	97.963	97.533	96.944	97.153	97.317
Tetrahedral	Si	6.824	6.573	6.519	6.552	6.310	6.521	6.442	6.592	6.534	6.571	6.501
	Al	1.176	1.427	1.481	1.448	1.690	1.479	1.558	1.408	1.466	1.429	1.499
	Fe3+	0.000	0.000	0.000	0.000	0.000	0.000	0.000	0.000	0.000	0.000	0.000
	total T site	8.000	8.000	8.000	8.000	8.000	8.000	8.000	8.000	8.000	8.000	8.000
Octahedral	Al	2.203	0.456	0.555	0.599	0.705	0.522	0.400	0.525	0.475	0.477	0.473
M1,M2,M3	Ti	0.028	0.056	0.044	0.044	0.044	0.055	0.062	0.055	0.066	0.107	0.098
	Fe3+	0.000	0.586	0.714	0.564	0.644	0.571	0.800	0.519	0.686	0.580	0.640
	Mg	1.040	2.043	2.038	2.006	1.835	1.991	1.967	1.943	2.014	1.982	1.968
	Fe2+	1.729	1.817	1.611	1.753	1.738	1.834	1.734	1.922	1.718	1.817	1.784
	Mn	0.000	0.042	0.038	0.034	0.034	0.027	0.037	0.036	0.041	0.037	0.037
	total M1-M3	5.000	5.000	5.000	5.000	5.000	5.000	5.000	5.000	5.000	5.000	5.000
Octahedral	Ca	1.814	1.923	1.850	1.896	1.890	1.931	1.878	1.918	1.858	1.877	1.895
M4	Na	0.000	0.077	0.150	0.104	0.110	0.069	0.122	0.082	0.142	0.123	0.105
	Fe2+	1.574	0.000	0.000	0.000	0.000	0.000	0.000	0.000	0.000	0.000	0.000
	Mn	0.020	0.000	0.000	0.000	0.000	0.000	0.000	0.000	0.000	0.000	0.000
	Mg	0.000	0.000	0.000	0.000	0.000	0.000	0.000	0.000	0.000	0.000	0.000
	total M4 site	3.408	2.000	2.000	2.000	2.000	2.000	2.000	2.000	2.000	2.000	2.000
A site	Na	0.823	0.282	0.208	0.233	0.291	0.279	0.286	0.273	0.247	0.219	0.223
	K	0.060	0.068	0.066	0.067	0.071	0.066	0.071	0.063	0.067	0.063	0.072
	total A site	0.883	0.350	0.274	0.300	0.362	0.345	0.357	0.336	0.314	0.282	0.295
	Mg/Fe2+ + Mg	0.239	0.529	0.559	0.534	0.513	0.521	0.531	0.503	0.540	0.522	0.524

APPENDIX B: Plagioclase Feldspar Compositions

Plagioclase analyses are normalized to 8 oxygens. Compositions are separated into categories based on relative strain magnitude as discussed in the text. Label schemes for analyses follow similar patterns as illustrated for amphibole.

APPENDIX B: Plagioclase Compositions; S62 Undeformed Amphibolite

	Sample 62 spot 5													
	f1.1	f1.2	f1.3	f1.4	f1.5	f1.6	f1.7	f1.8	f1.9	S1FS1.2	S1AFS1.2	S1AFS2	S1AFS3	S2FS1
SiO2	55.664	55.758	56.133	58.652	55.357	59.383	56.849	57.175	60.063	60.092	56.452	56.226	54.443	58.711
Al2O3	27.738	27.657	27.580	26.384	27.880	25.211	26.465	26.706	24.293	24.299	27.542	27.038	28.651	23.788
TiO2	0.081	0.047	0.032	0.013	0.000	0.000	0.017	0.000	0.000	0.000	0.000	0.000	0.000	0.000
FeO	0.153	0.098	0.139	0.000	0.013	0.112	0.074	0.066	0.109	0.000	0.000	0.000	0.000	0.000
MnO	0.000	0.051	0.000	0.008	0.000	0.015	0.058	0.000	0.009	0.000	0.000	0.000	0.000	0.000
MgO	0.014	0.000	0.036	0.027	0.024	0.061	0.011	0.012	0.030	0.000	0.000	0.000	0.000	0.000
CaO	10.541	10.352	10.196	8.333	10.636	6.784	8.750	8.697	6.168	6.501	10.123	9.737	11.170	6.961
Na2O	5.523	5.555	5.773	6.392	5.328	7.173	6.367	6.631	7.632	8.107	6.081	6.381	5.358	7.398
K2O	0.042	0.027	0.040	0.222	0.141	0.257	0.052	0.055	0.147	0.015	0.000	0.005	0.000	0.328
Total	99.756	99.545	99.929	100.031	99.379	98.996	98.643	99.342	98.451	99.013	100.198	99.386	99.621	97.187
cat Si	2.511	2.519	2.526	2.617	2.506	2.670	2.581	2.578	2.710	2.701	2.532	2.543	2.465	2.694
cat Al	1.475	1.472	1.463	1.388	1.488	1.336	1.416	1.419	1.292	1.290	1.459	1.444	1.532	1.289
cat Ti	0.003	0.002	0.001	0.000	0.000	0.000	0.001	0.000	0.000	0.000	0.000	0.000	0.000	0.000
cat Fe	0.006	0.004	0.005	0.000	0.000	0.004	0.003	0.002	0.004	0.000	0.000	0.000	0.000	0.000
cat Mn	0.000	0.002	0.000	0.000	0.000	0.001	0.002	0.000	0.000	0.000	0.000	0.000	0.000	0.000
cat Mg	0.001	0.000	0.002	0.002	0.002	0.004	0.001	0.001	0.002	0.000	0.000	0.000	0.000	0.000
cat Ca	0.510	0.501	0.492	0.398	0.516	0.327	0.426	0.420	0.298	0.313	0.487	0.472	0.542	0.342
cat Na	0.483	0.487	0.504	0.553	0.468	0.625	0.560	0.580	0.668	0.707	0.529	0.560	0.470	0.658
cat K	0.002	0.002	0.002	0.013	0.008	0.015	0.003	0.003	0.008	0.001	0.000	0.000	0.000	0.019
Total cations	4.991	4.988	4.995	4.971	4.988	4.982	4.992	5.004	4.982	5.011	5.007	5.019	5.009	5.003
Mole% Ab	48.552	49.189	50.492	57.364	47.158	64.675	56.664	57.796	68.528	69.237	52.084	54.241	46.466	64.553
Mole% An	51.206	50.654	49.278	41.325	52.021	33.801	43.032	41.889	30.604	30.681	47.916	45.733	53.534	33.562
Mole% Or	0.243	0.157	0.230	1.311	0.821	1.525	0.304	0.315	0.868	0.082	0.000	0.027	0.000	1.885
Sum	100.000	100.000	100.000	100.000	100.000	100.000	100.000	100.000	100.000	100.000	100.000	100.000	100.000	100.000

APPENDIX B: Plagioclase Compositions; S62 Undeformed Amphibolite

									Sample 62 Spot 6					
	S2FS2	S5FS1	S5FS2	S1AFS1.2	S1AFS2	S1AFS3	S5FS1	S5FS2	62SP6	fs tr3	fs tr3	fs tr3	fs tr3	fs tr3
SiO2	56.660	59.106	57.699	56.452	56.226	54.443	59.106	57.699	60.176	59.427	59.335	59.129	58.899	57.471
Al2O3	24.761	24.427	25.632	27.542	27.038	28.651	24.427	25.632	24.483	24.814	24.965	25.389	25.675	26.312
TiO2	0.000	0.000	0.000	0.000	0.000	0.000	0.000	0.000	0.000	0.045	0.020	0.000	0.009	0.024
FeO	0.000	0.000	0.000	0.000	0.000	0.000	0.000	0.000	0.072	0.108	0.090	0.000	0.064	0.052
MnO	0.000	0.000	0.000	0.000	0.000	0.000	0.000	0.000	0.000	0.009	0.000	0.027	0.013	0.000
MgO	0.000	0.000	0.000	0.000	0.000	0.000	0.000	0.000	0.007	0.000	0.000	0.001	0.008	0.024
CaO	8.911	7.135	8.574	10.123	9.737	11.170	7.135	8.574	6.971	7.303	7.362	7.694	8.143	9.400
Na2O	6.921	7.730	6.949	6.081	6.381	5.358	7.730	6.949	7.709	7.392	7.432	7.248	6.893	6.405
K2O	0.052	0.000	0.002	0.000	0.005	0.000	0.000	0.002	0.051	0.051	0.049	0.065	0.054	0.051
Total	97.305	98.398	98.856	100.198	99.386	99.621	98.398	98.856	99.469	99.149	99.253	99.553	99.758	99.739
cat Si	2.614	2.678	2.613	2.532	2.543	2.465	2.678	2.613	2.694	2.672	2.666	2.650	2.637	2.585
cat Al	1.349	1.307	1.371	1.459	1.444	1.532	1.307	1.371	1.292	1.315	1.322	1.341	1.355	1.395
cat Ti	0.000	0.000	0.000	0.000	0.000	0.000	0.000	0.000	0.000	0.002	0.001	0.000	0.000	0.001
cat Fe	0.000	0.000	0.000	0.000	0.000	0.000	0.000	0.000	0.003	0.004	0.003	0.000	0.002	0.002
cat Mn	0.000	0.000	0.000	0.000	0.000	0.000	0.000	0.000	0.000	0.000	0.000	0.001	0.000	0.000
cat Mg	0.000	0.000	0.000	0.000	0.000	0.000	0.000	0.000	0.000	0.000	0.000	0.000	0.001	0.002
cat Ca	0.441	0.346	0.416	0.487	0.472	0.542	0.346	0.416	0.334	0.352	0.354	0.370	0.391	0.453
cat Na	0.619	0.679	0.610	0.529	0.560	0.470	0.679	0.610	0.669	0.644	0.648	0.630	0.598	0.558
cat K	0.003	0.000	0.000	0.000	0.000	0.000	0.000	0.000	0.003	0.003	0.003	0.004	0.003	0.003
Total cations	5.026	5.011	5.010	5.007	5.019	5.009	5.011	5.010	4.996	4.992	4.997	4.996	4.987	4.998
Mole% Ab	58.259	66.225	59.455	52.084	54.241	46.466	66.225	59.455	66.487	64.496	64.444	62.794	60.315	55.059
Mole% An	41.451	33.775	40.536	47.916	45.733	53.534	33.775	40.536	33.223	35.211	35.276	36.835	39.374	44.652
Mole% Or	0.290	0.000	0.009	0.000	0.027	0.000	0.000	0.009	0.289	0.293	0.280	0.371	0.311	0.288
Sum	100.000	100.000	100.000	100.000	100.000	100.000	100.000	100.000	100.000	100.000	100.000	100.000	100.000	100.000

APPENDIX B: Plagioclase Compositions; S62 Undeformed Amphibolite

	fs tr3	fs tr3	fs tr3	fs tr3	fs tr3	fs tr3	fs tr3	fs tr3	fs tr3	fs tr3	fs tr3	fs tr3	fs tr3	fs tr3
SiO2	56.746	56.688	56.780	56.734	57.914	59.050	57.256	56.037	56.308	56.747	56.874	56.955	56.835	55.842
Al2O3	26.906	26.944	26.868	26.646	26.228	24.907	26.481	26.700	26.922	26.843	26.785	26.622	26.729	26.769
TiO2	0.000	0.034	0.000	0.009	0.007	0.030	0.000	0.035	0.000	0.000	0.000	0.000	0.000	0.007
FeO	0.000	0.010	0.032	0.039	0.089	0.045	0.000	0.036	0.000	0.000	0.050	0.029	0.000	0.207
MnO	0.006	0.000	0.009	0.040	0.000	0.000	0.000	0.000	0.026	0.046	0.002	0.024	0.000	0.012
MgO	0.000	0.002	0.015	0.000	0.000	0.006	0.003	0.000	0.000	0.002	0.025	0.001	0.010	0.190
CaO	9.735	9.715	10.024	9.455	8.709	7.456	9.430	9.691	9.944	9.721	9.909	9.538	9.470	7.297
Na2O	6.004	6.035	6.183	6.280	6.583	7.384	6.185	6.010	6.119	6.181	6.193	6.218	6.375	5.725
K2O	0.050	0.049	0.025	0.041	0.056	0.065	0.058	0.037	0.039	0.057	0.044	0.025	0.045	1.565
Total	99.447	99.477	99.936	99.244	99.586	98.943	99.413	98.546	99.358	99.597	99.882	99.412	99.464	97.614
cat Si	2.560	2.557	2.554	2.566	2.602	2.663	2.581	2.553	2.547	2.559	2.559	2.570	2.565	2.570
cat Al	1.430	1.432	1.424	1.420	1.389	1.324	1.407	1.434	1.435	1.426	1.420	1.416	1.421	1.452
cat Ti	0.000	0.001	0.000	0.000	0.000	0.001	0.000	0.001	0.000	0.000	0.000	0.000	0.000	0.000
cat Fe	0.000	0.000	0.001	0.001	0.003	0.002	0.000	0.001	0.000	0.000	0.002	0.001	0.000	0.008
cat Mn	0.000	0.000	0.000	0.002	0.000	0.000	0.000	0.000	0.001	0.002	0.000	0.001	0.000	0.000
cat Mg	0.000	0.000	0.001	0.000	0.000	0.000	0.000	0.000	0.000	0.000	0.002	0.000	0.001	0.013
cat Ca	0.471	0.469	0.483	0.458	0.419	0.360	0.455	0.473	0.482	0.470	0.478	0.461	0.458	0.360
cat Na	0.525	0.528	0.539	0.551	0.574	0.646	0.541	0.531	0.537	0.540	0.540	0.544	0.558	0.511
cat K	0.003	0.003	0.001	0.002	0.003	0.004	0.003	0.002	0.002	0.003	0.003	0.001	0.003	0.092
Total cations	4.989	4.991	5.004	5.000	4.991	4.999	4.987	4.995	5.005	5.000	5.003	4.995	5.005	5.006
Mole% Ab	52.591	52.773	52.672	54.458	57.582	63.948	54.092	52.768	52.570	53.329	52.942	54.046	54.779	53.073
Mole% An	47.121	46.945	47.188	45.308	42.096	35.682	45.574	47.019	47.209	46.347	46.810	45.811	44.967	37.381
Mole% Or	0.288	0.282	0.140	0.234	0.322	0.370	0.334	0.214	0.220	0.324	0.247	0.143	0.254	9.546
Sum	100.000	100.000	100.000	100.000	100.000	100.000	100.000	100.000	100.000	100.000	100.000	100.000	100.000	100.000

APPENDIX B: Plagioclase Compositions; S143 Undeformed Amphibolite

	143.1f1.1	143.1f1.2	143.1f1.3	143.1f1.4	143.3f1.1	143.3f1.2	143.3a1.3	143.3f1.4	143.5ftr	143.5ftr	143.5ftr	143.5ftr	143.5ftr	143.5ftr
SiO2	55.786	54.741	55.313	53.348	54.339	55.029	53.992	54.512	59.035	54.976	54.416	54.771	55.999	56.846
Al2O3	27.894	27.480	28.114	27.863	26.326	27.777	28.352	27.770	25.204	27.929	27.893	28.168	26.993	26.513
TiO2	0.000	0.000	0.000	0.007	0.049	0.024	0.000	0.002	0.000	0.000	0.000	0.010	0.000	0.017
FeO	0.081	0.239	0.028	0.142	1.970	0.049	0.041	0.611	0.018	0.000	0.000	0.027	0.076	0.156
MnO	0.000	0.000	0.025	0.000	0.000	0.047	0.000	0.000	0.053	0.000	0.000	0.025	0.000	0.000
MgO	0.002	0.052	0.009	0.000	0.839	0.000	0.000	0.174	0.000	0.000	0.000	0.000	0.005	0.033
CaO	10.288	10.398	10.673	10.545	9.002	10.157	10.954	10.614	6.718	10.387	10.655	10.709	9.257	8.244
Na2O	6.036	5.834	6.020	5.761	5.859	6.170	5.510	5.663	7.740	5.810	5.804	5.780	6.397	6.555
K2O	0.035	0.021	0.054	0.011	0.508	0.020	0.032	0.049	0.074	0.041	0.035	0.059	0.092	0.389
Total	100.122	98.765	100.236	97.677	98.892	99.273	98.881	99.395	98.842	99.143	98.803	99.549	98.819	98.753
cat Si	2.509	2.500	2.490	2.467	2.501	2.499	2.465	2.481	2.662	2.497	2.485	2.482	2.546	2.581
cat Al	1.479	1.479	1.492	1.519	1.428	1.487	1.525	1.489	1.339	1.495	1.501	1.505	1.446	1.419
cat Ti	0.000	0.000	0.000	0.000	0.002	0.001	0.000	0.000	0.000	0.000	0.000	0.000	0.000	0.001
cat Fe	0.003	0.009	0.001	0.005	0.076	0.002	0.002	0.023	0.001	0.000	0.000	0.001	0.003	0.006
cat Mn	0.000	0.000	0.001	0.000	0.000	0.002	0.000	0.000	0.002	0.000	0.000	0.001	0.000	0.000
cat Mg	0.000	0.004	0.001	0.000	0.058	0.000	0.000	0.012	0.000	0.000	0.000	0.000	0.000	0.002
cat Ca	0.496	0.509	0.515	0.523	0.444	0.494	0.536	0.518	0.325	0.506	0.521	0.520	0.451	0.401
cat Na	0.526	0.517	0.526	0.517	0.523	0.543	0.488	0.500	0.677	0.512	0.514	0.508	0.564	0.577
cat K	0.002	0.001	0.003	0.001	0.030	0.001	0.002	0.003	0.004	0.002	0.002	0.003	0.005	0.023
Total cations	5.016	5.019	5.028	5.032	5.060	5.029	5.017	5.026	5.009	5.012	5.023	5.021	5.016	5.009
Mole% Ab	51.396	50.320	50.362	49.684	52.464	52.306	47.565	48.986	67.298	50.187	49.544	49.248	55.276	57.669
Mole% An	48.408	49.560	49.340	50.254	44.543	47.582	52.253	50.735	32.278	49.580	50.260	50.421	44.201	40.079
Mole% Or	0.196	0.119	0.297	0.062	2.993	0.112	0.182	0.279	0.423	0.233	0.197	0.331	0.523	2.252
Sum	100.000	100.000	100.000	100.000	100.000	100.000	100.000	100.000	100.000	100.000	100.000	100.000	100.000	100.000

APPENDIX B: Plagioclase Compositions; S143 Undeformed Amphibolite

	143.5ftr	143.5ftr	143.5ftr	143.5f1.1	143.5f1.2	143.5f1.3	143.5f1.4	143.6f3tr	143.6f3tr	143.6f3tr	143.6f3tr	143.6f3tr	143.6f3tr	143.6f3tr
SiO2	60.803	55.279	53.411	54.888	52.459	56.005	54.767	56.230	55.161	54.017	54.011	54.385	47.445	54.136
Al2O3	24.441	28.083	28.941	27.934	26.994	27.441	27.065	27.462	28.469	28.506	28.345	28.557	15.479	28.651
TiO2	0.028	0.009	0.000	0.000	0.029	0.000	0.047	0.000	0.005	0.007	0.002	0.000	0.549	0.000
FeO	0.099	0.114	0.089	0.114	0.105	0.032	0.240	0.187	0.032	0.041	0.000	0.091	13.268	0.053
MnO	0.000	0.000	0.000	0.000	0.004	0.029	0.000	0.003	0.000	0.000	0.030	0.000	0.210	0.000
MgO	0.000	0.014	0.000	0.000	1.041	0.003	0.083	0.016	0.000	0.009	0.046	0.012	7.429	0.002
CaO	6.335	10.930	11.658	10.170	9.519	9.528	9.755	10.076	10.969	11.178	10.093	10.681	11.925	11.534
Na2O	8.241	5.713	5.034	5.935	6.110	6.362	5.885	6.125	5.333	5.459	5.422	5.515	2.072	5.185
K2O	0.062	0.028	0.018	0.028	0.133	0.048	0.093	0.015	0.045	0.038	0.481	0.160	0.317	0.003
Total	100.009	100.170	99.151	99.069	96.394	99.448	97.935	100.114	100.014	99.255	98.430	99.401	98.694	99.564
cat Si	2.706	2.490	2.436	2.496	2.461	2.532	2.518	2.528	2.484	2.458	2.475	2.469	2.366	2.456
cat Al	1.282	1.491	1.555	1.497	1.492	1.462	1.467	1.455	1.511	1.529	1.531	1.528	0.910	1.532
cat Ti	0.001	0.000	0.000	0.000	0.001	0.000	0.002	0.000	0.000	0.000	0.000	0.000	0.021	0.000
cat Fe	0.004	0.004	0.003	0.004	0.004	0.001	0.009	0.007	0.001	0.002	0.000	0.003	0.553	0.002
cat Mn	0.000	0.000	0.000	0.000	0.000	0.001	0.000	0.000	0.000	0.000	0.001	0.000	0.009	0.000
cat Mg	0.000	0.001	0.000	0.000	0.073	0.000	0.006	0.001	0.000	0.001	0.003	0.001	0.552	0.000
cat Ca	0.302	0.528	0.570	0.496	0.478	0.461	0.481	0.485	0.529	0.545	0.495	0.519	0.637	0.561
cat Na	0.711	0.499	0.445	0.523	0.556	0.558	0.525	0.534	0.466	0.482	0.482	0.485	0.200	0.456
cat K	0.004	0.002	0.001	0.002	0.008	0.003	0.005	0.001	0.003	0.002	0.028	0.009	0.020	0.000
Total cations	5.009	5.015	5.010	5.018	5.074	5.018	5.012	5.012	4.994	5.019	5.015	5.015	5.269	5.006
Mole% Ab	69.943	48.533	43.820	51.282	53.327	54.569	51.911	52.338	46.682	46.815	47.915	47.863	23.359	44.851
Mole% An	29.711	51.310	56.077	48.559	45.909	45.160	47.549	47.578	53.059	52.971	49.288	51.224	74.290	55.132
Mole% Or	0.346	0.157	0.103	0.159	0.764	0.271	0.540	0.084	0.259	0.214	2.797	0.914	2.351	0.017
Sum	100.000	100.000	100.000	100.000	100.000	100.000	100.000	100.000	100.000	100.000	100.000	100.000	100.000	100.000

APPENDIX B: Plagioclase Compositions; S143 Undeformed Amphibolite

	143.6f3tr	143.6f3tr	143.6f3tr	143.6f2tr	143.6f2tr	143.6f2tr	143.6f2tr	143.6f2tr	143.6f2tr	143.6f2tr	143.6f2tr	143.6f2tr
SiO2	53.760	54.177	54.008	54.989	54.918	54.908	56.029	54.204	53.266	53.910	55.103	59.458
Al2O3	28.571	28.317	28.783	28.077	27.996	28.237	27.606	28.619	28.926	28.464	27.928	24.508
TiO2	0.001	0.027	0.025	0.000	0.016	0.000	0.040	0.009	0.023	0.023	0.000	0.000
FeO	0.068	0.106	0.159	0.043	0.044	0.032	0.000	0.215	0.053	0.000	0.205	0.013
MnO	0.000	0.017	0.002	0.023	0.001	0.015	0.025	0.006	0.000	0.016	0.000	0.016
MgO	0.018	0.013	0.008	0.016	0.000	0.000	0.077	0.055	0.000	0.000	0.030	0.019
CaO	11.024	11.258	11.315	10.690	10.640	11.045	8.458	10.200	11.885	10.936	10.380	6.266
Na2O	5.505	5.320	5.170	5.735	5.795	5.522	5.770	5.249	5.279	5.403	5.789	8.268
K2O	0.035	0.028	0.036	0.046	0.031	0.023	0.888	0.635	0.019	0.031	0.074	0.035
Total	98.982	99.263	99.506	99.619	99.441	99.782	98.893	99.192	99.451	98.783	99.509	98.583
cat Si	2.454	2.465	2.452	2.489	2.490	2.482	2.543	2.468	2.427	2.462	2.497	2.687
cat Al	1.537	1.519	1.540	1.498	1.496	1.504	1.477	1.536	1.553	1.532	1.491	1.305
cat Ti	0.000	0.001	0.001	0.000	0.001	0.000	0.001	0.000	0.001	0.001	0.000	0.000
cat Fe	0.003	0.004	0.006	0.002	0.002	0.001	0.000	0.008	0.002	0.000	0.008	0.000
cat Mn	0.000	0.001	0.000	0.001	0.000	0.001	0.001	0.000	0.000	0.001	0.000	0.001
cat Mg	0.001	0.001	0.001	0.001	0.000	0.000	0.005	0.004	0.000	0.000	0.002	0.001
cat Ca	0.539	0.549	0.550	0.518	0.517	0.535	0.411	0.498	0.580	0.535	0.504	0.303
cat Na	0.487	0.469	0.455	0.503	0.509	0.484	0.508	0.463	0.466	0.478	0.509	0.724
cat K	0.002	0.002	0.002	0.003	0.002	0.001	0.051	0.037	0.001	0.002	0.004	0.002
Total cations	5.023	5.010	5.006	5.015	5.017	5.008	4.997	5.014	5.030	5.011	5.014	5.024
Mole% Ab	47.376	46.023	45.167	49.133	49.551	47.438	52.321	46.438	44.514	47.120	50.019	70.344
Mole% An	52.426	53.818	54.626	50.608	50.275	52.432	42.381	49.866	55.380	52.703	49.560	29.460
Mole% Or	0.198	0.159	0.207	0.259	0.174	0.130	5.298	3.696	0.105	0.178	0.421	0.196
Sum	100.000	100.000	100.000	100.000	100.000	100.000	100.000	100.000	100.000	100.000	100.000	100.000

APPENDIX B: Plagioclase Compositions; S81 Full Strain amphibolite

	Undeformed	Undeformed	Undeformed	Undeformed	Undeformed	Mylonitic	Mylonitic	Mylonitic	Mylonitic	Mylonitic	Mylonitic	Mylonitic	Mylonitic	Mylonitic
	8FS1.2	8FS2.1	8FS2.2	12FS1.	12FS1.	16FS1.	16FS1.	16FS2.	16FS2.	16F22.	17FS1.	17FS1.	17FS2.	17FS2.
SiO2	53.560	52.960	60.640	53.210	50.450	54.150	53.020	51.780	51.310	50.930	54.570	54.210	54.450	54.030
Al2O3	28.520	28.350	23.600	27.680	28.470	28.370	28.190	28.640	29.930	29.480	28.220	28.290	28.150	28.020
TiO2	0.070	0.080	0.060	0.090	0.070	0.060	0.070	0.070	0.090	0.100	0.080	0.070	0.050	0.060
FeO	0.190	0.160	0.090	0.280	0.700	0.060	0.120	0.110	0.020	0.080	0.190	0.080	0.090	0.140
MnO	0.030	0.050	0.050	0.050	0.030	0.040	-0.010	0.010	0.010	-0.020	0.090	0.050	0.020	0.030
MgO	-0.010	0.010	-0.010	0.010	0.070	0.040	0.040	0.040	0.030	0.050	0.040	0.050	0.000	0.030
CaO	11.340	11.950	6.070	11.420	9.080	11.320	11.150	12.740	12.720	12.600	10.780	10.980	10.650	11.310
Na2O	4.950	4.630	7.760	4.800	5.750	5.130	4.740	4.040	4.180	4.140	5.270	5.130	5.360	5.010
K2O	0.030	0.060	0.040	0.030	0.060	0.050	0.050	0.010	0.040	0.040	0.050	0.050	0.050	0.030
Total	98.680	98.250	98.300	97.570	94.680	99.220	97.370	97.440	98.330	97.400	99.290	98.910	98.820	98.660
cat Si	2.452	2.439	2.737	2.465	2.411	2.464	2.456	2.408	2.367	2.372	2.479	2.471	2.482	2.472
cat Al	1.538	1.539	1.255	1.511	1.604	1.521	1.539	1.570	1.627	1.618	1.511	1.520	1.513	1.511
cat Ti	0.002	0.003	0.002	0.003	0.003	0.002	0.002	0.002	0.003	0.004	0.003	0.002	0.002	0.002
cat Fe	0.007	0.006	0.003	0.011	0.028	0.002	0.005	0.004	0.001	0.003	0.007	0.003	0.003	0.005
cat Mn	0.001	0.002	0.002	0.002	0.001	0.002	0.000	0.000	0.000	-0.001	0.003	0.002	0.001	0.001
cat Mg	-0.001	0.001	-0.001	0.001	0.005	0.003	0.003	0.003	0.002	0.003	0.003	0.003	0.000	0.002
cat Ca	0.556	0.590	0.294	0.567	0.465	0.552	0.553	0.635	0.629	0.629	0.525	0.536	0.520	0.554
cat Na	0.439	0.413	0.679	0.431	0.533	0.453	0.426	0.364	0.374	0.374	0.464	0.453	0.474	0.444
cat K	0.002	0.004	0.002	0.002	0.004	0.003	0.003	0.001	0.002	0.002	0.003	0.003	0.003	0.002
Total cations	4.997	4.997	4.974	4.993	5.053	5.001	4.986	4.987	5.005	5.004	4.997	4.995	4.998	4.994
Mole% Ab	44.054	41.072	69.655	43.125	53.206	44.928	43.350	36.440	37.204	37.200	46.803	45.680	47.526	44.416
Mole% An	55.770	58.578	30.108	56.697	46.429	54.784	56.349	63.500	62.562	62.563	52.904	54.027	52.182	55.409
Mole% Or	0.176	0.350	0.236	0.177	0.365	0.288	0.301	0.059	0.234	0.236	0.292	0.293	0.292	0.175
Sum	100.000	100.000	100.000	100.000	100.000	100.000	100.000	100.000	100.000	100.000	100.000	100.000	100.000	100.000

	Mylonitic 17FS3.	Mylonitic 17FS3.	Mylonitic 17FS4.	Mylonitic 17FS4.	Trans 13FS1.	Trans 13FS1.	Trans 13FS2.	Trans 13FS2.	Mylonitic 15FS1.	Mylonitic 15FS1.	Mylonitic 15FS2.	Mylonitic 15FS2.
SiO2	55.260	55.080	54.880	55.190	54.200	56.380	54.140	54.780	55.900	54.490	54.530	52.860
Al2O3	26.720	27.610	27.530	28.520	27.380	26.620	27.200	27.750	27.040	27.800	28.000	28.410
TiO2	0.060	0.070	0.050	0.100	0.050	0.060	0.070	0.080	0.060	0.050	0.080	0.030
FeO	0.100	0.110	0.100	0.190	0.140	0.120	0.090	0.080	0.040	0.000	0.090	0.090
MnO	0.020	0.030	0.000	0.000	0.030	0.030	0.060	0.040	0.020	0.030	-0.010	0.000
MgO	0.040	0.030	0.030	-0.010	0.040	0.010	0.030	-0.010	0.060	0.020	0.030	0.030
CaO	9.540	10.850	10.740	10.520	10.560	9.310	10.370	9.810	10.120	11.110	10.760	11.180
Na2O	5.650	5.260	5.320	5.260	5.400	5.830	5.700	5.740	5.250	5.000	5.160	4.780
K2O	0.030	0.040	0.020	0.040	0.040	0.030	0.050	0.040	0.040	0.030	0.060	0.030
Total	97.420	99.080	98.670	99.810	97.840	98.390	97.710	98.310	98.530	98.530	98.700	97.410
cat Si	2.545	2.504	2.504	2.488	2.497	2.567	2.499	2.505	2.544	2.491	2.488	2.448
cat Al	1.450	1.479	1.481	1.515	1.487	1.429	1.480	1.496	1.450	1.498	1.505	1.551
cat Ti	0.002	0.002	0.002	0.003	0.002	0.002	0.002	0.003	0.002	0.002	0.003	0.001
cat Fe	0.004	0.004	0.004	0.007	0.005	0.005	0.003	0.003	0.002	0.000	0.003	0.003
cat Mn	0.001	0.001	0.000	0.000	0.001	0.001	0.002	0.002	0.001	0.001	0.000	0.000
cat Mg	0.003	0.002	0.002	-0.001	0.003	0.001	0.002	-0.001	0.004	0.001	0.002	0.002
cat Ca	0.471	0.528	0.525	0.508	0.521	0.454	0.513	0.481	0.493	0.544	0.526	0.555
cat Na	0.504	0.464	0.471	0.460	0.482	0.515	0.510	0.509	0.463	0.443	0.456	0.429
cat K	0.002	0.002	0.001	0.002	0.002	0.002	0.003	0.002	0.002	0.002	0.003	0.002
Total cations	4.981	4.987	4.990	4.983	5.000	4.975	5.015	5.000	4.962	4.981	4.987	4.991
Mole% Ab	51.638	46.623	47.213	47.389	47.950	53.027	49.724	51.308	48.304	44.807	46.297	43.543
Mole% An	48.181	53.144	52.670	52.374	51.816	46.793	49.989	48.456	51.453	55.017	53.349	56.278
Mole% Or	0.180	0.233	0.117	0.237	0.234	0.180	0.287	0.235	0.242	0.177	0.354	0.180
Sum	100.000	100.000	100.000	100.000	100.000	100.000	100.000	100.000	100.000	100.000	100.000	100.000

APPENDIX B: Plagioclase Compositions; S81 Full Strain Transition: Undeformed Section

	Sample 81a spot 5 undeformed															
	f6.1	f6.2	f6tr	f6tr	f6tr	f6tr	f6tr	f6tr	f6tr	f6tr	f6tr	f6tr	f6tr	f6tr	f6tr	f6tr
SiO2	54.832	54.993	60.461	57.628	53.757	53.28	53.766	53.263	53.503	53.282	53.008	53.053	53.413	52.564	55.897	56.35
Al2O3	27.872	27.898	24.418	26.272	28.528	29.005	28.827	29.161	29.21	28.956	29.112	28.987	29.019	29.125	27.469	26.983
TiO2	0.034	0.009	0.02	0.019	0.001	0	0	0.017	0.018	0.007	0	0.028	0.006	0.018	0	0
FeO	0.099	0	0.01	0.116	0.071	0.066	0.046	0.085	0.025	0.07	0.032	0.026	0.029	0.057	0.065	0.043
MnO	0.041	0	0	0	0	0	0.046	0.01	0	0	0.062	0.037	0	0	0	0
MgO	0	0.008	0.003	0.019	0.013	0.003	0	0.004	0.021	0	0.014	0	0	0	0.013	0.009
CaO	11.339	11.172	6.711	9.09	12.087	12.454	12.503	12.689	12.801	13.134	12.993	12.588	12.834	12.969	10.473	10.067
Na2O	5.393	5.507	7.817	6.351	4.837	4.737	4.894	4.554	4.489	4.791	4.396	4.646	4.684	4.615	5.819	6.09
K2O	0.041	0.042	0.038	0.034	0.044	0.03	0.033	0.03	0.027	0.057	0.04	0.044	0.04	0.035	0.13	0.053
Total	99.65	99.63	99.48	99.53	99.34	99.58	100.12	99.81	100.09	100.30	99.66	99.41	100.03	99.38	99.87	99.60
cat Si	2.485	2.490	2.703	2.593	2.448	2.424	2.434	2.418	2.421	2.414	2.412	2.419	2.421	2.402	2.521	2.544
cat Al	1.489	1.489	1.287	1.393	1.531	1.555	1.538	1.560	1.558	1.546	1.561	1.558	1.550	1.568	1.460	1.436
cat Ti	0.001	0.000	0.001	0.001	0.000	0.000	0.000	0.001	0.001	0.000	0.000	0.001	0.000	0.001	0.000	0.000
cat Fe	0.004	0.000	0.000	0.004	0.003	0.003	0.002	0.003	0.001	0.003	0.001	0.001	0.001	0.002	0.002	0.002
cat Mn	0.002	0.000	0.000	0.000	0.000	0.000	0.002	0.000	0.000	0.000	0.002	0.001	0.000	0.000	0.000	0.000
cat Mg	0.000	0.001	0.000	0.001	0.001	0.000	0.000	0.000	0.001	0.000	0.001	0.000	0.000	0.000	0.001	0.001
cat Ca	0.551	0.542	0.321	0.438	0.590	0.607	0.606	0.617	0.621	0.638	0.634	0.615	0.623	0.635	0.506	0.487
cat Na	0.474	0.484	0.678	0.554	0.427	0.418	0.430	0.401	0.394	0.421	0.388	0.411	0.412	0.409	0.509	0.533
cat K	0.002	0.002	0.002	0.002	0.003	0.002	0.002	0.002	0.002	0.003	0.002	0.003	0.002	0.002	0.007	0.003
Total cations	5.007	5.008	4.993	4.987	5.002	5.008	5.013	5.003	4.997	5.025	5.002	5.008	5.010	5.019	5.007	5.006
Mole% Ab	46.15	47.04	67.68	55.73	41.90	40.70	41.39	39.31	38.76	39.64	37.89	39.94	39.69	39.09	49.77	52.11
Mole% An	53.62	52.73	32.11	44.08	57.85	59.13	58.43	60.52	61.08	60.05	61.88	59.81	60.09	60.71	49.50	47.60
Mole% Or	0.23	0.24	0.22	0.20	0.25	0.17	0.18	0.17	0.15	0.31	0.23	0.25	0.22	0.20	0.73	0.30
Sum	100	100	100	100	100	100	100	100	100	100	100	100	100	100	100	100

APPENDIX B: Plagioclase Compositions; S81 Full Strain Transition: Undeformed Section

							81a.s5ud									
	f6tr	f6tr	f6tr	f6tr	f6tr	f6tr	f2.1 rlfs	f2.2 rlfs	f2.3 rlfs	f2.4 e	f3.1 c	f3.2 e	f4.1 c	f4.2 c	f5.1 c	f1.1 Core
SiO2	52.937	52.979	58.744	59.086	58.87	59.154	53.74	56.71	52.47	62.32	52.3	60.15	54.82	53.6	52.3	52.862
Al2O3	29.107	29.005	25.252	25.195	25.249	25.092	28.63	26.93	29.33	22.5	29.4	24.03	27.03	28	28.8	23.615
TiO2	0	0.008	0.014	0	0	0.009	0	0	0	0	0	0	0	0	0	0.1
FeO	0	0	0.033	0.023	0	0.025	0	0	0	0	0	0	0	0	0	4.819
MnO	0.001	0.022	0	0	0	0.005	0	0	0	0	0	0	0	0	0	0.081
MgO	0.006	0.006	0	0.001	0	0	0	0	0	0	0	0	0	0	0	2.662
CaO	12.64	12.248	7.687	7.636	7.982	7.524	12.25	9.85	13.23	5.87	13.03	6.35	10	11.64	12.73	10.607
Na2O	4.639	4.809	7.271	7.264	7.457	7.509	4.97	6.11	4.23	7.79	4.55	8.23	6.6	5.13	4.65	4.464
K2O	0.037	0.028	0.058	0.058	0.062	0.054	0.0413	0.055	0.055	0.028	0.036	0.05	0.02	0.04	0.04	0.188
Total	99.37	99.11	99.06	99.26	99.62	99.37	99.63	99.66	99.32	98.51	99.32	98.81	98.47	98.41	98.52	99.40
cat Si	2.414	2.421	2.648	2.656	2.643	2.657	2.442	2.555	2.397	2.797	2.391	2.710	2.513	2.462	2.409	2.466
cat Al	1.565	1.562	1.341	1.335	1.336	1.328	1.533	1.430	1.579	1.190	1.584	1.276	1.460	1.516	1.563	1.298
cat Ti	0.000	0.000	0.000	0.000	0.000	0.000	0.000	0.000	0.000	0.000	0.000	0.000	0.000	0.000	0.000	0.004
cat Fe	0.000	0.000	0.001	0.001	0.000	0.001	0.000	0.000	0.000	0.000	0.000	0.000	0.000	0.000	0.000	0.188
cat Mn	0.000	0.001	0.000	0.000	0.000	0.000	0.000	0.000	0.000	0.000	0.000	0.000	0.000	0.000	0.000	0.003
cat Mg	0.000	0.000	0.000	0.000	0.000	0.000	0.000	0.000	0.000	0.000	0.000	0.000	0.000	0.000	0.000	0.185
cat Ca	0.618	0.600	0.371	0.368	0.384	0.362	0.596	0.476	0.648	0.282	0.638	0.306	0.491	0.573	0.628	0.530
cat Na	0.410	0.426	0.635	0.633	0.649	0.654	0.438	0.534	0.375	0.678	0.403	0.719	0.586	0.457	0.415	0.404
cat K	0.002	0.002	0.003	0.003	0.004	0.003	0.002	0.003	0.003	0.002	0.002	0.003	0.001	0.002	0.002	0.011
Total cations	5.009	5.012	5.001	4.995	5.015	5.007	5.012	4.998	5.002	4.948	5.019	5.013	5.051	5.010	5.018	5.089
Mole% Ab	39.83	41.47	62.91	63.05	62.62	64.17	42.24	52.72	36.54	70.48	38.64	69.91	54.37	44.27	39.71	42.72
Mole% An	59.96	58.37	36.76	36.62	37.04	35.53	57.53	46.97	63.15	29.35	61.15	29.81	45.52	55.50	60.07	56.09
Mole% Or	0.21	0.16	0.33	0.33	0.34	0.30	0.23	0.31	0.31	0.17	0.20	0.28	0.11	0.23	0.22	1.18
Sum	100	100	100	100	100	100	100	100	100	100	100	100	100	100	100	100.000

APPENDIX B: Plagioclase Compositions; S81 Full Strain Transition: Undeformed Section

	Sample 81a Spot 5 Undeformed									
	f1.2	f1.3	f1.4	f1.5	f1.6	f1.7	f1.8	f1.9	f1.10	f1.11
						Rim		Core	Core	Rim
SiO2	54.893	56.069	54.539	55.294	55.776	56.027	54.658	53.802	54.939	53.288
Al2O3	28.083	28.073	28.241	28.445	27.853	27.115	28.07	28.837	28.588	28.047
TiO2	0.007	0	0.004	0.02	0.004	0.013	0	0.02	0.015	0.02
FeO	0.141	0.066	0	0.011	0.036	0.039	0.02	0	0.02	0.106
MnO	0	0	0	0.01	0.048	0	0	0.024	0.025	0.041
MgO	0.007	0.009	0.005	0.014	0.024	0.007	0.018	0.001	0.018	0.075
CaO	10.701	10.722	10.907	11.156	10.386	9.561	10.541	11.354	11.413	9.551
Na2O	5.314	5.526	5.436	5.242	5.465	5.91	5.431	4.998	5.046	5.148
K2O	0.056	0.065	0.056	0.061	0.268	0.162	0.046	0.051	0.053	0.367
Total	99.20	100.53	99.19	100.25	99.86	98.83	98.78	99.09	100.12	96.64
cat Si	2.492	2.510	2.479	2.485	2.514	2.545	2.491	2.450	2.474	2.480
cat Al	1.503	1.481	1.513	1.507	1.479	1.452	1.507	1.548	1.517	1.538
cat Ti	0.000	0.000	0.000	0.001	0.000	0.000	0.000	0.001	0.001	0.001
cat Fe	0.005	0.002	0.000	0.000	0.001	0.001	0.001	0.000	0.001	0.004
cat Mn	0.000	0.000	0.000	0.000	0.002	0.000	0.000	0.001	0.001	0.002
cat Mg	0.000	0.001	0.000	0.001	0.002	0.000	0.001	0.000	0.001	0.005
cat Ca	0.520	0.514	0.531	0.537	0.502	0.465	0.515	0.554	0.551	0.476
cat Na	0.468	0.480	0.479	0.457	0.478	0.520	0.480	0.441	0.441	0.465
cat K	0.003	0.004	0.003	0.003	0.015	0.009	0.003	0.003	0.003	0.022
Total cations	4.992	4.991	5.006	4.991	4.993	4.994	4.997	4.998	4.989	4.993
Mole% Ab	47.18	48.08	47.27	45.79	48.02	52.30	48.12	44.21	44.31	48.26
Mole% An	52.50	51.55	52.41	53.86	50.43	46.76	51.61	55.50	55.38	49.48
Mole% Or	0.33	0.37	0.32	0.35	1.55	0.94	0.27	0.30	0.31	2.26
Sum	100.000	100.000	100.000	100.000	100.000	100.000	100.000	100.000	100.000	100.000

APPENDIX B: Plagioclase Compositions; S81 Full Strain Transition: Transitional Section

	Sample 81 spot II transitional section													
	f1.1	f1.2	f1.3	f1.4	f1.5	f1.6	f2.2	f2.3	f2.4	f3.1	f3.2	f3.3	f3.4	f3.5
	Rim	Core		Edge	Edge	Edge	Core	Core	Edge					
SiO2	54.062	51.253	49.690	52.441	55.712	55.383	56.087	53.568	52.078	57.751	55.605	59.557	54.742	57.664
Al2O3	27.534	28.082	28.953	28.682	27.062	27.276	27.375	28.244	27.881	25.879	26.854	24.989	28.039	24.897
TiO2	0.000	0.007	0.000	0.040	0.004	0.019	0.014	0.000	0.034	0.052	0.000	0.000	0.000	0.000
FeO	0.106	0.000	0.071	0.031	0.004	0.155	0.014	0.024	0.200	0.922	0.162	0.000	0.114	0.000
MnO	0.000	0.000	0.008	0.032	0.005	0.043	0.022	0.000	0.021	0.000	0.055	0.000	0.000	0.017
MgO	0.005	0.009	0.016	0.000	0.000	0.067	0.018	0.003	0.058	0.370	0.000	0.026	0.000	0.036
CaO	10.057	10.500	11.536	11.359	9.096	9.175	9.838	10.714	10.133	8.617	9.170	6.473	10.586	6.542
Na2O	5.657	5.497	5.016	4.986	6.143	5.730	5.713	5.320	5.317	6.239	6.185	7.854	5.522	7.340
K2O	0.050	0.048	0.047	0.025	0.032	0.120	0.036	0.053	0.140	0.059	0.026	0.055	0.033	0.055
Total	97.471	95.396	95.337	97.596	98.058	97.968	99.117	97.926	95.862	99.889	98.057	98.954	99.036	96.551
cat Si	2.497	2.429	2.368	2.429	2.547	2.536	2.539	2.466	2.453	2.596	2.546	2.678	2.490	2.658
cat Al	1.499	1.569	1.626	1.566	1.458	1.472	1.460	1.533	1.548	1.371	1.449	1.324	1.503	1.352
cat Ti	0.000	0.000	0.000	0.001	0.000	0.001	0.000	0.000	0.001	0.002	0.000	0.000	0.000	0.000
cat Fe	0.004	0.000	0.003	0.001	0.000	0.006	0.001	0.001	0.008	0.035	0.006	0.000	0.004	0.000
cat Mn	0.000	0.000	0.000	0.001	0.000	0.002	0.001	0.000	0.001	0.000	0.002	0.000	0.000	0.001
cat Mg	0.000	0.001	0.001	0.000	0.000	0.005	0.001	0.000	0.004	0.025	0.000	0.002	0.000	0.002
cat Ca	0.498	0.533	0.589	0.564	0.446	0.450	0.477	0.529	0.511	0.415	0.450	0.312	0.516	0.323
cat Na	0.507	0.505	0.463	0.448	0.544	0.509	0.501	0.475	0.486	0.544	0.549	0.685	0.487	0.656
cat K	0.003	0.003	0.003	0.001	0.002	0.007	0.002	0.003	0.008	0.003	0.002	0.003	0.002	0.003
Total cations	5.008	5.040	5.053	5.011	4.997	4.986	4.982	5.006	5.019	4.990	5.004	5.004	5.003	4.996
Mole% Ab	50.296	48.514	43.917	44.205	54.895	52.670	51.132	47.182	48.299	56.515	54.883	68.491	48.466	66.780
Mole% An	49.411	51.208	55.813	55.650	44.917	46.604	48.656	52.508	50.864	43.133	44.965	31.193	51.343	32.890
Mole% Or	0.292	0.279	0.271	0.146	0.188	0.726	0.212	0.309	0.837	0.352	0.152	0.316	0.191	0.329
Sum	100.000	100.000	100.000	100.000	100.000	100.000	100.000	100.000	100.000	100.000	100.000	100.000	100.000	100.000

APPENDIX B: Plagioclase Compositions; S81 Full Strain Transition: Mylonitic Section

Sample 81a spot 15 Mylonitic

	f2.1 edge	f2.2 edge	f2.3 core	f2.4 edge	f2.5 edge	f2.6 center	f2.7 near chl	Fs tr1	Fs tr1	Fs tr1	Fs tr1	Fs tr1	Fs tr1	Fs tr1
SiO2	56.736	56.273	54.535	59.964	55.220	55.377	53.707	57.323	57.455	57.126	55.803	56.278	56.229	56.081
Al2O3	25.663	25.939	27.939	25.081	22.909	27.954	27.539	26.442	26.326	27.161	27.378	27.761	27.607	27.363
TiO2	0.021	0.008	0.000	0.000	0.012	0.010	0.005	0.004	0.023	0.000	0.003	0.000	0.021	0.000
FeO	0.211	0.075	0.092	0.252	4.439	0.163	1.000	0.052	0.000	0.074	0.075	0.004	0.060	0.065
MnO	0.000	0.000	0.048	0.016	0.050	0.000	0.017	0.000	0.047	0.016	0.001	0.013	0.000	0.001
MgO	0.040	0.120	0.013	0.074	2.388	0.002	0.546	0.052	0.068	0.010	0.000	0.017	0.000	0.014
CaO	7.489	7.882	10.701	6.902	4.229	10.579	10.071	8.706	8.576	9.487	10.133	10.344	10.193	10.011
Na2O	6.788	6.369	5.482	7.375	6.725	5.524	5.488	6.395	6.239	6.087	5.672	5.695	5.746	5.944
K2O	0.242	0.366	0.026	0.067	0.227	0.037	0.056	0.098	0.136	0.046	0.059	0.024	0.054	0.059
Total	97.190	97.032	98.836	99.731	96.199	99.646	98.429	99.072	98.870	100.007	99.124	100.136	99.910	99.538
cat Si	2.611	2.595	2.487	2.677	2.607	2.502	2.470	2.589	2.598	2.561	2.530	2.525	2.529	2.533
cat Al	1.392	1.410	1.502	1.320	1.275	1.489	1.493	1.408	1.403	1.435	1.463	1.468	1.463	1.456
cat Ti	0.001	0.000	0.000	0.000	0.000	0.000	0.000	0.000	0.001	0.000	0.000	0.000	0.001	0.000
cat Fe	0.008	0.003	0.004	0.009	0.175	0.006	0.038	0.002	0.000	0.003	0.003	0.000	0.002	0.002
cat Mn	0.000	0.000	0.002	0.001	0.002	0.000	0.001	0.000	0.002	0.001	0.000	0.000	0.000	0.000
cat Mg	0.003	0.008	0.001	0.005	0.168	0.000	0.037	0.004	0.005	0.001	0.000	0.001	0.000	0.001
cat Ca	0.369	0.389	0.523	0.330	0.214	0.512	0.496	0.421	0.415	0.456	0.492	0.497	0.491	0.484
cat Na	0.606	0.569	0.485	0.638	0.616	0.484	0.489	0.560	0.547	0.529	0.499	0.495	0.501	0.520
cat K	0.014	0.022	0.002	0.004	0.014	0.002	0.003	0.006	0.008	0.003	0.003	0.001	0.003	0.003
Total cations	5.003	4.996	5.005	4.984	5.070	4.996	5.029	4.990	4.978	4.987	4.990	4.989	4.991	5.001
Mole% Ab	61.233	58.083	48.035	65.654	73.008	48.481	49.486	56.742	56.372	53.584	50.149	49.839	50.341	51.620
Mole% An	37.331	39.721	51.815	33.953	25.370	51.306	50.182	42.686	42.819	46.150	49.508	50.023	49.348	48.043
Mole% Or	1.436	2.196	0.150	0.392	1.621	0.214	0.332	0.572	0.809	0.266	0.343	0.138	0.311	0.337
Sum	100.000	100.000	100.000	100.000	100.000	100.000	100.000	100.000	100.000	100.000	100.000	100.000	100.000	100.000

APPENDIX B: Plagioclase Compositions; S81 Full Strain Transition: Mylonitic Section

	Fs tr1	Fs tr1	Fs tr1	Fs tr1	Fs tr1	Fs tr1	Fs tr1	Fs tr1	Fs tr1	Fs tr1	Fs tr1	Fs tr1	Fs tr1
SiO2	56.436	56.551	56.278	56.442	56.404	56.479	56.396	54.321	54.033	54.083	51.963	54.941	0.119
Al2O3	27.437	27.490	27.381	27.403	27.565	27.583	27.479	27.082	26.267	25.638	24.680	24.932	58.013
TiO2	0.045	0.001	0.020	0.001	0.000	0.000	0.001	0.000	0.009	0.001	0.000	0.038	0.071
FeO	0.000	0.059	0.067	0.036	0.134	0.067	0.044	0.115	0.160	0.179	0.205	0.292	0.000
MnO	0.011	0.000	0.000	0.045	0.031	0.000	0.000	0.000	0.013	0.011	0.036	0.017	0.000
MgO	0.016	0.003	0.000	0.005	0.000	0.018	0.000	0.000	0.000	0.009	0.021	0.024	25.150
CaO	9.953	9.848	9.760	9.879	9.880	10.126	10.119	10.611	11.594	11.830	12.506	9.601	0.000
Na2O	5.780	5.726	5.842	5.748	5.758	5.728	5.762	5.858	5.818	5.854	6.164	6.736	0.057
K2O	0.037	0.029	0.034	0.050	0.043	0.031	0.035	0.022	0.053	0.029	0.073	0.112	6.930
Total	99.715	99.707	99.382	99.609	99.815	100.032	99.836	98.009	97.947	97.634	95.648	96.693	90.340
cat Si	2.540	2.543	2.541	2.543	2.537	2.535	2.537	2.502	2.502	2.515	2.486	2.567	0.007
cat Al	1.455	1.457	1.457	1.455	1.461	1.459	1.457	1.470	1.434	1.405	1.392	1.373	3.776
cat Ti	0.002	0.000	0.001	0.000	0.000	0.000	0.000	0.000	0.000	0.000	0.000	0.001	0.003
cat Fe	0.000	0.002	0.003	0.001	0.005	0.003	0.002	0.004	0.006	0.007	0.008	0.011	0.000
cat Mn	0.000	0.000	0.000	0.002	0.001	0.000	0.000	0.000	0.001	0.000	0.001	0.001	0.000
cat Mg	0.001	0.000	0.000	0.000	0.000	0.001	0.000	0.000	0.000	0.001	0.001	0.002	2.070
cat Ca	0.480	0.475	0.472	0.477	0.476	0.487	0.488	0.524	0.575	0.589	0.641	0.481	0.000
cat Na	0.504	0.499	0.511	0.502	0.502	0.499	0.503	0.523	0.522	0.528	0.572	0.610	0.006
cat K	0.002	0.002	0.002	0.003	0.002	0.002	0.002	0.001	0.003	0.002	0.004	0.007	0.488
Total cations	4.984	4.979	4.987	4.982	4.985	4.985	4.987	5.025	5.043	5.047	5.106	5.053	6.350
Mole% Ab	51.131	51.184	51.893	51.139	51.201	50.494	50.647	49.915	47.456	47.171	46.972	55.600	1.235
Mole% An	48.654	48.645	47.908	48.568	48.548	49.326	49.150	49.962	52.259	52.676	52.662	43.792	0.000
Mole% Or	0.215	0.171	0.199	0.293	0.252	0.180	0.202	0.123	0.284	0.154	0.366	0.608	98.765
Sum	100.000	100.000	100.000	100.000	100.000	100.000	100.000	100.000	100.000	100.000	100.000	100.000	100.000

APPENDIX B: Plagioclase Compositions; S142 Full Strain Transition

	142.3mf3tr	142.3mf3tr	142.3mf3tr	142.3mf3tr	142.3mf3tr	142.3mf1tr	142.3mf1tr	142.3mf1tr	142.3mf1tr	142.3mf1tr	142.3tf1tr	142.3tf1tr	142.3tf1tr	142.3tf5tr	142.3tf5tr	142.3tf5tr
SiO2	52.903	53.054	52.966	55.099	59.455	53.211	54.373	53.992	54.099	57.063	55.719	51.739	52.357	58.585	54.265	52.073
Al2O3	28.508	28.368	28.61	27.53	25.086	28.813	28.305	28.299	28.4	26.844	27.285	29.573	29.583	25.509	28.742	29.427
TiO2	0.041	0.041	0	0.019	0.03	0	0	0.009	0.031	0	0.018	0	0.03	0	0.022	0
FeO	0.202	0.149	0.057	0.038	0.063	0.373	0.132	0.121	0.154	0.075	0.087	0.164	0.171	0.076	0	0.149
MnO	0	0	0.001	0	0.003	0.041	0.042	0.017	0.026	0.001	0.026	0.014	0	0.001	0	0
MgO	0.008	0.005	0.005	0	0.035	0.103	0	0	0	0.003	0	0.006	0	0	0.123	0
CaO	11.421	11.127	10.996	9.794	7.321	8.468	10.775	10.857	11.109	9.096	9.649	12.731	12.318	7.385	11.174	12.183
Na2O	5.223	5.411	5.437	6.066	7.644	5.343	5.419	5.698	5.466	6.595	6.026	4.439	4.847	7.575	4.943	4.928
K2O	0.019	0.04	0.023	0.033	0.053	1.346	0.027	0.028	0.03	0.033	0.045	0.031	0.027	0.056	0.119	0.013
Total	98.33	98.20	98.09	98.58	99.69	97.70	99.07	99.02	99.31	99.71	98.86	98.70	99.33	99.19	99.39	98.77
cat Si	2.436	2.444	2.440	2.514	2.662	2.461	2.475	2.464	2.462	2.567	2.533	2.380	2.392	2.639	2.461	2.392
cat Al	1.547	1.540	1.554	1.481	1.324	1.571	1.519	1.522	1.523	1.423	1.462	1.604	1.593	1.354	1.536	1.593
cat Ti	0.001	0.001	0.000	0.001	0.001	0.000	0.000	0.000	0.001	0.000	0.001	0.000	0.001	0.000	0.001	0.000
cat Fe	0.008	0.006	0.002	0.001	0.002	0.014	0.005	0.005	0.006	0.003	0.003	0.006	0.007	0.003	0.000	0.006
cat Mn	0.000	0.000	0.000	0.000	0.000	0.002	0.002	0.001	0.001	0.000	0.001	0.001	0.000	0.000	0.000	0.000
cat Mg	0.001	0.000	0.000	0.000	0.002	0.007	0.000	0.000	0.000	0.000	0.000	0.000	0.000	0.000	0.008	0.000
cat Ca	0.563	0.549	0.543	0.479	0.351	0.420	0.526	0.531	0.542	0.438	0.470	0.628	0.603	0.356	0.543	0.600
cat Na	0.466	0.483	0.486	0.537	0.664	0.479	0.478	0.504	0.482	0.575	0.531	0.396	0.429	0.661	0.435	0.439
cat K	0.001	0.002	0.001	0.002	0.003	0.079	0.002	0.002	0.002	0.002	0.003	0.002	0.002	0.003	0.007	0.001
Total cations	5.023	5.027	5.026	5.014	5.009	5.033	5.006	5.028	5.018	5.010	5.003	5.017	5.026	5.017	4.991	5.031
Mole% Ab	45.23	46.70	47.16	52.75	65.20	48.98	47.57	48.63	47.02	56.64	52.92	38.62	41.53	64.78	44.15	42.23
Mole% An	54.66	53.07	52.71	47.06	34.51	42.90	52.27	51.21	52.81	43.17	46.82	61.20	58.32	34.90	55.15	57.69
Mole% Or	0.11	0.23	0.13	0.19	0.30	8.12	0.16	0.16	0.17	0.19	0.26	0.18	0.15	0.32	0.70	0.07
Sum	100	100	100	100	100	100	100	100	100	100	100	100	100	100	100	100

APPENDIX B: Plagioclase Compositions; S142 Full Strain Transition

	142.3tf6tr	142.3tf6tr	142.3tf6tr	142.3tf6tr	142.3tf6tr	142.3tf6tr	142.3tf6tr	142.3tf6tr	142.3tf6tr	142.3tf6tr	142.3tf7tr	142.3tf7tr	142.3tf7tr	142.3tf7tr	142.2tf3tr	142.2tf3tr
SiO2	59.594	54.878	54.216	56.063	53.449	55.999	57.945	57.626	58.72	59.169	55.608	56.678	56.458	54.451	54.377	54.642
Al2O3	24.496	28.438	27.678	27.525	28.985	24.905	25.016	26.5	25.398	25.064	27.219	27.146	27.652	28.551	28.484	27.771
TiO2	0.011	0	0.012	0	0.032	0	0	0	0	0	0.015	0.007	0.015	0.007	0.026	0.02
FeO	0.171	0.067	0.027	0.095	0.111	0.298	0.131	0.096	0.1	0.161	0.296	0.222	0.124	0.08	0.108	0.085
MnO	0.041	0	0	0	0	0	0.003	0	0.018	0	0.002	0.027	0.005	0	0.005	0
MgO	0.004	0	0.006	0	0.012	0.281	0.027	0.013	0.013	0.009	0.012	0.031	0	0	0.005	0
CaO	6.166	10.781	10.236	9.996	11.498	6.878	6.623	8.452	7.05	7.002	9.412	9.667	9.954	11.542	11.345	10.075
Na2O	8.197	5.531	5.879	5.907	4.962	7.262	7.876	6.855	7.663	7.935	6.496	6.208	6.165	5.164	5.373	5.928
K2O	0.056	0.02	0.035	0.036	0.121	0.158	0.059	0.024	0.028	0.08	0.053	0.02	0.04	0.041	0.035	0.04
Total	98.74	99.72	98.09	99.62	99.17	95.78	97.68	99.57	98.99	99.42	99.11	100.01	100.41	99.84	99.76	98.56
cat Si	2.689	2.480	2.491	2.529	2.436	2.617	2.648	2.591	2.647	2.659	2.527	2.547	2.529	2.463	2.463	2.497
cat Al	1.303	1.515	1.499	1.464	1.557	1.372	1.348	1.404	1.349	1.327	1.458	1.438	1.460	1.522	1.520	1.496
cat Ti	0.000	0.000	0.000	0.000	0.001	0.000	0.000	0.000	0.000	0.000	0.001	0.000	0.001	0.000	0.001	0.001
cat Fe	0.006	0.003	0.001	0.004	0.004	0.012	0.005	0.004	0.004	0.006	0.011	0.008	0.005	0.003	0.004	0.003
cat Mn	0.002	0.000	0.000	0.000	0.000	0.000	0.000	0.000	0.001	0.000	0.000	0.001	0.000	0.000	0.000	0.000
cat Mg	0.000	0.000	0.000	0.000	0.001	0.020	0.002	0.001	0.001	0.001	0.001	0.002	0.000	0.000	0.000	0.000
cat Ca	0.298	0.522	0.504	0.483	0.562	0.344	0.324	0.407	0.341	0.337	0.458	0.466	0.478	0.559	0.551	0.493
cat Na	0.717	0.485	0.524	0.517	0.439	0.658	0.698	0.598	0.670	0.691	0.572	0.541	0.535	0.453	0.472	0.525
cat K	0.003	0.001	0.002	0.002	0.007	0.009	0.003	0.001	0.002	0.005	0.003	0.001	0.002	0.002	0.002	0.002
Total cations	5.019	5.005	5.022	4.998	5.007	5.031	5.029	5.006	5.014	5.026	5.031	5.005	5.010	5.003	5.013	5.018
Mole% Ab	70.41	48.09	50.86	51.57	43.54	65.03	68.05	59.40	66.19	66.92	55.37	53.69	52.73	44.64	46.06	51.45
Mole% An	29.27	51.80	48.94	48.22	55.76	34.04	31.62	40.47	33.65	32.63	44.33	46.20	47.05	55.13	53.74	48.32
Mole% Or	0.32	0.11	0.20	0.21	0.70	0.93	0.34	0.14	0.16	0.44	0.30	0.11	0.23	0.23	0.20	0.23
Sum	100	100	100	100	100	100	100	100	100	100	100	100	100	100	100	100

APPENDIX B: Plagioclase Compositions; S142 Full Strain Transition

	142.2tf3tr	142.2tf2tr	142.2tf2tr	142.2tf2tr	142.2tf2tr	142.2tf2tr	142.2tf2tr	142.2tf2tr	142.2tf2tr
SiO2	53.052	59.262	54.139	49.572	54.934	53.736	53.726	52.586	53.272
Al2O3	28.362	24.502	28.143	18.825	27.757	27.856	28.468	27.489	28.564
TiO2	0.002	0.007	0.02	0.379	0	0.025	0	0	0
FeO	0.116	0.48	0.102	8.338	0.099	0.147	0.014	0.114	0.03
MnO	0.033	0.044	0	0.148	0	0	0.023	0.025	0
MgO	0.005	0.095	0	5.527	0.006	0.001	0	0.032	0.001
CaO	10.966	6.209	10.543	11.16	10.251	10.672	10.715	9.841	11.51
Na2O	5.507	7.767	5.852	3.565	6.028	5.715	5.628	5.471	5.44
K2O	0.031	0.029	0.044	0.176	0.04	0.033	0.034	0.385	0.02
Total	98.07	98.40	98.84	97.69	99.12	98.19	98.61	95.94	98.84
cat Si	2.446	2.684	2.473	2.420	2.499	2.472	2.459	2.474	2.440
cat Al	1.541	1.308	1.515	1.083	1.488	1.511	1.536	1.524	1.542
cat Ti	0.000	0.000	0.001	0.014	0.000	0.001	0.000	0.000	0.000
cat Fe	0.004	0.018	0.004	0.340	0.004	0.006	0.001	0.004	0.001
cat Mn	0.001	0.002	0.000	0.006	0.000	0.000	0.001	0.001	0.000
cat Mg	0.000	0.006	0.000	0.402	0.000	0.000	0.000	0.002	0.000
cat Ca	0.542	0.301	0.516	0.584	0.500	0.526	0.526	0.496	0.565
cat Na	0.492	0.682	0.518	0.337	0.532	0.510	0.499	0.499	0.483
cat K	0.002	0.002	0.003	0.011	0.002	0.002	0.002	0.023	0.001
Total cations	5.030	5.004	5.029	5.198	5.024	5.027	5.024	5.025	5.032
Mole% Ab	47.53	69.24	49.99	36.20	51.44	49.12	48.64	49.01	46.05
Mole% An	52.30	30.59	49.77	62.62	48.34	50.69	51.17	48.72	53.84
Mole% Or	0.18	0.17	0.25	1.18	0.22	0.19	0.19	2.27	0.11
Sum	100	100	100	100	100	100	100	100	100

APPENDIX B: Plagioclase Compositions; S75 Mylonitic Amphibolite

	751 FS1.1	751 FS1.2	751 FS1.3	751 FS2.1	751 FS2.2	751 FS2.3	751 FS2.4	751 FS3.1	751 FS3.2	751 FS3.3	753 FS1.1	753 FS1.2	753 FS1.3	753 FS2.1
SiO2	57.225	55.929	57.814	57.557	58.091	60.605	57.342	57.456	52.116	56.691	56.592	56.301	58.857	56.784
Al2O3	25.449	27.394	26.331	26.262	25.995	24.176	26.224	26.557	27.264	26.558	26.873	26.226	25.935	26.877
TiO2	0.000	0.000	0.000	0.040	0.034	0.000	0.000	0.000	0.000	0.000	0.000	0.000	0.000	0.007
FeO	0.139	0.118	0.142	0.219	0.098	0.071	0.103	0.257	0.509	0.210	0.068	0.047	0.089	0.033
MnO	0.000	0.000	0.000	0.000	0.000	0.000	0.018	0.000	0.000	0.000	0.000	0.000	0.000	0.000
MgO	0.000	0.001	0.000	0.008	0.000	0.000	0.005	0.002	0.203	0.019	0.003	0.016	0.000	0.000
CaO	8.878	10.155	8.446	8.460	8.292	5.956	8.200	8.859	8.436	7.786	9.195	8.763	7.905	9.621
Na2O	6.854	5.880	6.925	6.906	6.956	8.454	7.021	6.644	5.948	6.450	6.363	6.591	7.144	6.199
K2O	0.051	0.033	0.043	0.033	0.051	0.048	0.051	0.063	0.054	0.697	0.047	0.039	0.036	0.040
Total	98.596	99.509	99.700	99.484	99.515	99.309	98.963	99.838	94.529	98.411	99.141	97.983	99.966	99.561
cat Si	2.605	2.528	2.597	2.593	2.612	2.714	2.595	2.582	2.482	2.583	2.561	2.576	2.630	2.560
cat Al	1.365	1.459	1.394	1.394	1.377	1.276	1.399	1.406	1.530	1.426	1.433	1.414	1.366	1.428
cat Ti	0.000	0.000	0.000	0.001	0.001	0.000	0.000	0.000	0.000	0.000	0.000	0.000	0.000	0.000
cat Fe	0.005	0.004	0.005	0.008	0.004	0.003	0.004	0.010	0.020	0.008	0.003	0.002	0.003	0.001
cat Mn	0.000	0.000	0.000	0.000	0.000	0.000	0.001	0.000	0.000	0.000	0.000	0.000	0.000	0.000
cat Mg	0.000	0.000	0.000	0.001	0.000	0.000	0.000	0.000	0.014	0.001	0.000	0.001	0.000	0.000
cat Ca	0.433	0.492	0.406	0.408	0.399	0.286	0.398	0.426	0.430	0.380	0.446	0.430	0.378	0.465
cat Na	0.605	0.515	0.603	0.603	0.606	0.734	0.616	0.579	0.549	0.570	0.558	0.585	0.619	0.542
cat K	0.003	0.002	0.002	0.002	0.003	0.003	0.003	0.004	0.003	0.041	0.003	0.002	0.002	0.002
Total cations	5.016	5.001	5.009	5.011	5.003	5.016	5.015	5.007	5.029	5.009	5.003	5.010	4.998	4.998
Mole% Ab	58.115	51.073	59.597	59.522	60.112	71.785	60.602	57.368	55.874	57.532	55.451	57.514	61.930	53.707
Mole% An	41.599	48.739	40.162	40.291	39.600	27.948	39.110	42.272	43.794	38.376	44.278	42.260	37.863	46.064
Mole% Or	0.286	0.187	0.241	0.187	0.288	0.267	0.288	0.360	0.332	4.092	0.272	0.226	0.206	0.229
Sum	100.000	100.000	100.000	100.000	100.000	100.000	100.000	100.000	100.000	100.000	100.000	100.000	100.000	100.000

APPENDIX B: Plagioclase Compositions; S75 Mylonitic Amphibolite

	753 FS2.2	753 FS2.3	753 FS2.4	755 FS1.1	755 FS1.2	755 FS1.3	755 FS1.4	755 FS1.5	755 FS1.6	755 FS1.7	755 FS1.8	755 FS2.1	755 FS2.2	755 FS2.3
SiO2	55.568	54.911	55.958	57.457	54.909	56.084	56.691	55.979	56.489	56.486	44.613	58.281	58.238	56.678
Al2O3	27.263	27.496	27.406	26.367	27.394	27.526	26.781	27.560	26.595	27.440	14.845	26.080	25.509	26.590
TiO2	0.000	0.000	0.001	0.000	0.000	0.007	0.001	0.040	0.000	0.000	0.298	0.000	0.000	0.000
FeO	0.047	0.059	0.103	0.000	0.036	0.006	0.044	0.038	0.047	0.044	16.659	0.041	0.018	0.021
MnO	0.000	0.000	0.000	0.000	0.000	0.000	0.000	0.000	0.000	0.000	0.205	0.000	0.000	0.000
MgO	0.000	0.000	0.000	0.001	0.002	0.005	0.000	0.000	0.001	0.000	8.107	0.016	0.000	0.009
CaO	9.773	10.096	9.878	8.904	9.815	10.044	9.487	9.969	9.499	9.868	10.794	8.331	7.746	8.741
Na2O	6.220	5.835	6.024	6.668	5.969	5.854	6.260	6.107	6.221	6.097	1.991	7.019	7.173	6.603
K2O	0.044	0.051	0.055	0.085	0.037	0.030	0.039	0.043	0.043	0.059	0.343	0.044	0.036	0.084
Total	98.915	98.448	99.425	99.482	98.160	99.556	99.304	99.736	98.894	99.994	97.856	99.812	98.719	98.726
cat Si	2.527	2.510	2.530	2.588	2.516	2.530	2.562	2.524	2.564	2.538	2.290	2.612	2.634	2.573
cat Al	1.461	1.482	1.461	1.400	1.479	1.464	1.426	1.465	1.423	1.453	0.898	1.378	1.360	1.423
cat Ti	0.000	0.000	0.000	0.000	0.000	0.000	0.000	0.001	0.000	0.000	0.012	0.000	0.000	0.000
cat Fe	0.002	0.002	0.004	0.000	0.001	0.000	0.002	0.001	0.002	0.002	0.715	0.002	0.001	0.001
cat Mn	0.000	0.000	0.000	0.000	0.000	0.000	0.000	0.000	0.000	0.000	0.009	0.000	0.000	0.000
cat Mg	0.000	0.000	0.000	0.000	0.000	0.000	0.000	0.000	0.000	0.000	0.620	0.001	0.000	0.001
cat Ca	0.476	0.495	0.479	0.430	0.482	0.486	0.459	0.482	0.462	0.475	0.594	0.400	0.375	0.425
cat Na	0.548	0.517	0.528	0.582	0.530	0.512	0.548	0.534	0.547	0.531	0.198	0.610	0.629	0.581
cat K	0.003	0.003	0.003	0.005	0.002	0.002	0.002	0.002	0.002	0.003	0.022	0.002	0.002	0.005
Total cations	5.018	5.009	5.005	5.005	5.011	4.994	5.000	5.010	5.000	5.003	5.359	5.005	5.001	5.009
Mole% Ab	53.390	50.968	52.297	57.264	52.282	51.241	54.299	52.449	54.105	52.612	24.339	60.241	62.502	57.477
Mole% An	46.360	48.737	47.392	42.255	47.505	48.588	45.476	47.307	45.652	47.055	72.902	39.513	37.295	42.044
Mole% Or	0.249	0.295	0.311	0.481	0.213	0.171	0.224	0.245	0.243	0.333	2.758	0.246	0.204	0.479
Sum	100.000	100.000	100.000	100.000	100.000	100.000	100.000	100.000	100.000	100.000	100.000	100.000	100.000	100.000

APPENDIX B: Plagioclase Compositions; S75 Mylonitic Amphibolite

	755	756	756	756	756	756	756	756	756	756	756	756
	FS2.4	FS1.1	FS1.2	FS1.3	FS2.1	FS2.2	FS2.3	FS2.4	FS3.1	FS3.2	FS3.3	FS3.4
SiO2	55.938	55.912	56.552	58.756	57.993	54.026	54.843	54.977	56.625	57.021	55.679	56.134
Al2O3	26.857	26.957	26.504	24.826	26.164	26.587	27.352	27.685	25.982	26.126	27.469	26.561
TiO2	0.020	0.000	0.027	0.040	0.000	0.034	0.034	0.000	0.053	0.000	0.000	0.000
FeO	0.000	0.192	0.080	0.113	0.071	0.225	0.056	0.053	0.039	0.000	0.115	0.044
MnO	0.000	0.000	0.000	0.000	0.000	0.000	0.000	0.000	0.000	0.000	0.000	0.000
MgO	0.000	0.004	0.023	0.000	0.000	0.060	0.008	0.016	0.000	0.000	0.000	0.000
CaO	9.396	10.381	8.972	7.279	8.621	9.306	10.644	10.519	9.341	9.305	10.431	9.765
Na2O	6.241	5.692	6.387	7.559	6.772	5.883	5.647	5.729	6.332	6.617	5.781	6.036
K2O	0.041	0.048	0.056	0.044	0.051	0.052	0.036	0.071	0.030	0.043	0.026	0.474
Total	98.493	99.185	98.600	98.615	99.671	96.173	98.618	99.051	98.402	99.113	99.501	99.014
cat Si	2.549	2.537	2.571	2.660	2.604	2.526	2.506	2.501	2.582	2.582	2.519	2.553
cat Al	1.443	1.442	1.420	1.325	1.385	1.465	1.473	1.484	1.396	1.395	1.465	1.424
cat Ti	0.001	0.000	0.001	0.001	0.000	0.001	0.001	0.000	0.002	0.000	0.000	0.000
cat Fe	0.000	0.007	0.003	0.004	0.003	0.009	0.002	0.002	0.001	0.000	0.004	0.002
cat Mn	0.000	0.000	0.000	0.000	0.000	0.000	0.000	0.000	0.000	0.000	0.000	0.000
cat Mg	0.000	0.000	0.002	0.000	0.000	0.004	0.001	0.001	0.000	0.000	0.000	0.000
cat Ca	0.459	0.505	0.437	0.353	0.415	0.466	0.521	0.513	0.456	0.452	0.506	0.476
cat Na	0.552	0.501	0.563	0.663	0.590	0.533	0.500	0.505	0.560	0.581	0.507	0.532
cat K	0.002	0.003	0.003	0.003	0.003	0.003	0.002	0.004	0.002	0.003	0.001	0.028
Total cations	5.005	4.994	5.001	5.009	4.999	5.008	5.007	5.011	4.999	5.012	5.003	5.015
Mole% Ab	54.461	49.667	56.117	65.108	58.537	53.192	48.878	49.438	54.997	56.137	50.001	51.396
Mole% An	45.304	50.057	43.562	34.645	41.175	46.497	50.917	50.157	44.833	43.620	49.853	45.948
Mole% Or	0.235	0.276	0.321	0.247	0.288	0.311	0.205	0.405	0.170	0.242	0.146	2.656
Sum	100.000	100.000	100.000	100.000	100.000	100.000	100.000	100.000	100.000	100.000	100.000	100.000

APPENDIX B: Plagioclase Compositions; S910a Mylonitic Amphibolite

	910a.2f2.1	910a.2f2.2	910a.2f2.3	910a.2f3.1	910a.2f3.2	910a.2f3.3	910a.2f3.4	910a.2f3.5	910a.2f4.1	910a.2f4.2	910a.2f5.1	910a.2f5.2	910a.2f5.3
SiO2	54.930	56.624	55.720	54.960	55.671	56.696	55.703	57.067	56.532	56.095	56.155	55.617	55.064
Al2O3	27.297	27.030	27.392	26.349	27.849	27.312	26.998	25.915	26.542	25.867	27.442	27.146	27.965
TiO2	0.000	0.000	0.000	0.000	0.000	0.008	0.000	0.033	0.023	0.043	0.000	0.003	0.036
FeO	0.044	0.111	0.127	0.182	0.106	0.139	0.298	0.202	0.386	2.058	0.214	0.228	0.260
MnO	0.005	0.040	0.000	0.000	0.000	0.009	0.000	0.000	0.000	0.042	0.000	0.010	0.083
MgO	0.000	0.000	0.000	0.000	0.000	0.000	0.086	0.002	0.014	0.657	0.000	0.000	0.008
CaO	9.811	9.273	9.867	10.198	10.260	9.469	8.650	8.135	8.627	9.178	9.931	9.517	10.400
Na2O	6.125	6.509	5.976	6.518	6.099	6.458	6.223	7.153	6.721	5.987	6.089	6.403	5.776
K2O	0.060	0.036	0.036	0.035	0.031	0.063	0.438	0.037	0.102	0.297	0.044	0.115	0.048
Total	98.272	99.623	99.118	98.242	100.016	100.154	98.396	98.544	98.947	100.224	99.875	99.039	99.640
cat Si	2.516	2.553	2.528	2.528	2.508	2.544	2.545	2.596	2.567	2.542	2.530	2.529	2.493
cat Al	1.474	1.436	1.464	1.428	1.479	1.445	1.454	1.390	1.420	1.381	1.457	1.455	1.492
cat Ti	0.000	0.000	0.000	0.000	0.000	0.000	0.000	0.001	0.001	0.001	0.000	0.000	0.001
cat Fe	0.002	0.004	0.005	0.007	0.004	0.005	0.011	0.008	0.015	0.078	0.008	0.009	0.010
cat Mn	0.000	0.002	0.000	0.000	0.000	0.000	0.000	0.000	0.000	0.002	0.000	0.000	0.003
cat Mg	0.000	0.000	0.000	0.000	0.000	0.000	0.006	0.000	0.001	0.044	0.000	0.000	0.001
cat Ca	0.482	0.448	0.480	0.503	0.495	0.455	0.423	0.397	0.420	0.446	0.479	0.464	0.505
cat Na	0.544	0.569	0.526	0.581	0.533	0.562	0.551	0.631	0.592	0.526	0.532	0.565	0.507
cat K	0.004	0.002	0.002	0.002	0.002	0.004	0.026	0.002	0.006	0.017	0.003	0.007	0.003
Total cations	5.021	5.014	5.004	5.049	5.020	5.016	5.016	5.024	5.021	5.038	5.009	5.029	5.014
Mole% Ab	52.866	55.838	52.182	53.530	51.735	55.046	55.114	61.280	58.164	53.198	52.465	54.551	49.989
Mole% An	46.794	43.959	47.611	46.281	48.092	44.601	42.334	38.512	41.256	45.065	47.285	44.805	49.738
Mole% Or	0.341	0.203	0.207	0.189	0.173	0.353	2.552	0.209	0.581	1.736	0.249	0.645	0.273
Sum	100.000	100.000	100.000	100.000	100.000	100.000	100.000	100.000	100.000	100.000	100.000	100.000	100.000

APPENDIX B: Plagioclase Compositions; S141 & S899 Mylonitic Amphibolite

	141.4f2tr	141.4f2tr	141.4f2tr	141.4f2tr	141.4f2tr	141.4f1tr	141.4f1tr	141.4f1tr	141.4f1tr	141.4f1tr	899.1f1tr	899.1f1tr	899.1f1tr
SiO2	59.358	56.207	53.980	54.150	56.993	54.604	53.033	52.567	52.833	52.622	54.509	55.030	55.381
Al2O3	24.883	27.052	28.721	28.610	26.215	28.095	29.449	29.322	29.459	29.460	27.537	27.322	27.355
TiO2	0.017	0.000	0.015	0.000	0.036	0.010	0.002	0.005	0.000	0.011	0.019	0.002	0.008
FeO	0.121	0.058	0.064	0.171	0.156	0.170	0.169	0.091	0.037	0.029	0.173	0.121	0.169
MnO	0.016	0.010	0.065	0.008	0.000	0.001	0.002	0.033	0.000	0.000	0.000	0.005	0.000
MgO	0.026	0.016	0.000	0.097	0.000	0.016	0.015	0.002	0.000	0.008	0.006	0.013	0.000
CaO	6.665	9.424	11.689	9.947	8.683	10.714	12.208	12.056	12.204	12.148	9.848	9.648	9.648
Na2O	8.153	6.232	5.051	5.314	6.827	5.697	4.685	4.923	4.663	4.669	5.824	6.136	5.896
K2O	0.058	0.029	0.054	0.647	0.040	0.035	0.043	0.031	0.036	0.032	0.042	0.045	0.126
Total	99.297	99.028	99.639	98.944	98.950	99.342	99.606	99.030	99.232	98.979	97.958	98.322	98.583
cat Si	2.668	2.548	2.449	2.470	2.584	2.481	2.411	2.406	2.410	2.406	2.505	2.518	2.526
cat Al	1.318	1.445	1.536	1.538	1.401	1.504	1.578	1.582	1.584	1.588	1.491	1.474	1.470
cat Ti	0.001	0.000	0.001	0.000	0.001	0.000	0.000	0.000	0.000	0.000	0.001	0.000	0.000
cat Fe	0.005	0.002	0.002	0.007	0.006	0.006	0.006	0.003	0.001	0.001	0.007	0.005	0.006
cat Mn	0.001	0.000	0.002	0.000	0.000	0.000	0.000	0.001	0.000	0.000	0.000	0.000	0.000
cat Mg	0.002	0.001	0.000	0.007	0.000	0.001	0.001	0.000	0.000	0.001	0.000	0.001	0.000
cat Ca	0.321	0.458	0.568	0.486	0.422	0.522	0.595	0.591	0.596	0.595	0.485	0.473	0.471
cat Na	0.711	0.548	0.444	0.470	0.600	0.502	0.413	0.437	0.412	0.414	0.519	0.544	0.521
cat K	0.003	0.002	0.003	0.038	0.002	0.002	0.002	0.002	0.002	0.002	0.002	0.003	0.007
Total cations	5.029	5.004	5.006	5.015	5.016	5.019	5.007	5.022	5.006	5.007	5.010	5.018	5.003
Mole% Ab	68.661	54.386	43.747	47.293	58.593	48.941	40.884	42.420	40.794	40.945	51.569	53.370	52.129
Mole% An	31.017	45.447	55.945	48.919	41.181	50.861	58.870	57.405	58.999	58.870	48.186	46.372	47.138
Mole% Or	0.321	0.167	0.308	3.789	0.226	0.198	0.247	0.176	0.207	0.185	0.245	0.258	0.733
Sum	100.000	100.000	100.000	100.000	100.000	100.000	100.000	100.000	100.000	100.000	100.000	100.000	100.000

APPENDIX B: Plagioclase Compositions; S898 & 895 Mylonitic Amphibolite

	898.1f1.1	898.1f1.2	898.1f1.3	898.1f1.4	898.1f1.5	898.1f1.6	898.1f1.7	898.1f1.8	898.5f1.1	898.5f1.2	898.5f1.3	898.5f1.4	898.5f1.5	898.5f1.6
SiO2	54.661	58.819	59.741	59.732	58.433	51.587	54.872	60.267	56.021	59.170	55.905	56.167	52.865	54.172
Al2O3	27.851	24.831	25.123	25.054	25.305	29.589	27.858	24.824	26.977	25.908	26.427	26.319	29.149	27.364
TiO2	0.017	0.000	0.000	0.005	0.000	0.000	0.013	0.014	0.000	0.010	0.024	0.016	0.032	0.000
FeO	0.005	0.625	0.033	0.056	0.066	0.059	0.143	0.052	0.141	0.150	0.264	1.140	0.095	0.342
MnO	0.000	0.000	0.001	0.000	0.000	0.055	0.000	0.000	0.000	0.009	0.000	0.050	0.059	0.001
MgO	0.000	0.177	0.006	0.000	0.003	0.000	0.000	0.006	0.000	0.008	0.000	0.208	0.004	0.000
CaO	10.646	6.551	7.106	7.019	7.248	12.425	10.696	6.356	11.415	7.561	8.049	9.205	12.568	9.283
Na2O	5.796	8.196	7.684	7.759	7.700	4.522	5.602	8.012	4.183	7.482	7.039	6.363	4.744	6.573
K2O	0.047	0.064	0.060	0.056	0.083	0.081	0.059	0.024	0.056	0.058	0.043	0.117	0.058	0.084
Total	99.023	99.263	99.754	99.681	98.838	98.318	99.243	99.555	98.793	100.356	97.751	99.585	99.574	97.819
cat Si	2.490	2.654	2.669	2.671	2.642	2.381	2.493	2.692	2.544	2.634	2.567	2.549	2.409	2.500
cat Al	1.495	1.320	1.323	1.320	1.348	1.610	1.492	1.307	1.444	1.359	1.430	1.408	1.566	1.488
cat Ti	0.001	0.000	0.000	0.000	0.000	0.000	0.000	0.000	0.000	0.000	0.001	0.001	0.001	0.000
cat Fe	0.000	0.024	0.001	0.002	0.002	0.002	0.005	0.002	0.005	0.006	0.010	0.043	0.004	0.013
cat Mn	0.000	0.000	0.000	0.000	0.000	0.002	0.000	0.000	0.000	0.000	0.000	0.002	0.002	0.000
cat Mg	0.000	0.012	0.000	0.000	0.000	0.000	0.000	0.000	0.000	0.001	0.000	0.014	0.000	0.000
cat Ca	0.520	0.317	0.340	0.336	0.351	0.614	0.521	0.304	0.555	0.361	0.396	0.448	0.614	0.459
cat Na	0.512	0.717	0.666	0.673	0.675	0.405	0.494	0.694	0.368	0.646	0.627	0.560	0.419	0.588
cat K	0.003	0.004	0.003	0.003	0.005	0.005	0.003	0.001	0.003	0.003	0.003	0.007	0.003	0.005
Total cations	5.020	5.047	5.004	5.006	5.024	5.019	5.009	5.001	4.920	5.010	5.032	5.030	5.018	5.053
Mole% Ab	49.497	69.117	65.956	66.461	65.477	39.524	48.496	69.428	39.733	63.958	61.128	55.203	40.453	55.902
Mole% An	50.239	30.528	33.705	33.223	34.058	60.011	51.168	30.436	59.917	35.716	38.626	44.129	59.222	43.628
Mole% Or	0.264	0.355	0.339	0.316	0.464	0.466	0.336	0.137	0.350	0.326	0.246	0.668	0.325	0.470
Sum	100.000	100.000	100.000	100.000	100.000	100.000	100.000	100.000	100.000	100.000	100.000	100.000	100.000	100.000

APPENDIX B: Plagioclase Compositions; S898 & 895 Mylonitic Amphibolite

	898.5f1.7	898.5f1.8	898.5f1.9	895.3f1.1	895.3af1.2	895.3f2.1	895.3f2.2
SiO2	51.340	52.973	54.055	55.641	56.126	55.602	57.937
Al2O3	30.248	29.277	28.744	27.210	27.306	27.123	26.443
TiO2	0.000	0.000	0.013	0.000	0.000	0.000	0.008
FeO	0.175	0.000	0.000	0.396	0.371	0.245	0.255
MnO	0.000	0.015	0.000	0.036	0.051	0.000	0.000
MgO	0.013	0.000	0.011	0.009	0.022	0.000	0.015
CaO	13.453	12.417	11.479	9.516	9.579	9.955	8.636
Na2O	4.294	4.734	5.113	6.453	6.498	6.271	6.858
K2O	0.050	0.055	0.027	0.068	0.032	0.059	0.047
Total	99.573	99.471	99.442	99.329	99.985	99.255	100.199
cat Si	2.348	2.413	2.454	2.525	2.530	2.525	2.592
cat Al	1.630	1.572	1.538	1.456	1.450	1.452	1.394
cat Ti	0.000	0.000	0.000	0.000	0.000	0.000	0.000
cat Fe	0.007	0.000	0.000	0.015	0.014	0.009	0.010
cat Mn	0.000	0.001	0.000	0.001	0.002	0.000	0.000
cat Mg	0.001	0.000	0.001	0.001	0.001	0.000	0.001
cat Ca	0.659	0.606	0.558	0.463	0.463	0.484	0.414
cat Na	0.381	0.418	0.450	0.568	0.568	0.552	0.595
cat K	0.003	0.003	0.002	0.004	0.002	0.003	0.003
Total cations	5.029	5.012	5.003	5.033	5.030	5.027	5.009
Mole% Ab	36.511	40.699	44.562	54.890	55.010	53.095	58.811
Mole% An	63.210	58.990	55.284	44.729	44.812	46.576	40.924
Mole% Or	0.280	0.311	0.155	0.381	0.178	0.329	0.265
Sum	100.000	100.000	100.000	100.000	100.000	100.000	100.000

APPENDIX B: Plagioclase Compositions; S898 & 895 Mylonitic Amphibolite

	898.1f1.1	898.1f1.2	898.1f1.3	898.1f1.4	898.1f1.5	898.1f1.6	898.1f1.7	898.1f1.8	898.5f1.1	898.5f1.2	898.5f1.3	898.5f1.4	898.5f1.5	898.5f1.6
SiO2	54.661	58.819	59.741	59.732	58.433	51.587	54.872	60.267	56.021	59.170	55.905	56.167	52.865	54.172
Al2O3	27.851	24.831	25.123	25.054	25.305	29.589	27.858	24.824	26.977	25.908	26.427	26.319	29.149	27.364
TiO2	0.017	0.000	0.000	0.005	0.000	0.000	0.013	0.014	0.000	0.010	0.024	0.016	0.032	0.000
FeO	0.005	0.625	0.033	0.056	0.066	0.059	0.143	0.052	0.141	0.150	0.264	1.140	0.095	0.342
MnO	0.000	0.000	0.001	0.000	0.000	0.055	0.000	0.000	0.000	0.009	0.000	0.050	0.059	0.001
MgO	0.000	0.177	0.006	0.000	0.003	0.000	0.000	0.006	0.000	0.008	0.000	0.208	0.004	0.000
CaO	10.646	6.551	7.106	7.019	7.248	12.425	10.696	6.356	11.415	7.561	8.049	9.205	12.568	9.283
Na2O	5.796	8.196	7.684	7.759	7.700	4.522	5.602	8.012	4.183	7.482	7.039	6.363	4.744	6.573
K2O	0.047	0.064	0.060	0.056	0.083	0.081	0.059	0.024	0.056	0.058	0.043	0.117	0.058	0.084
Total	99.023	99.263	99.754	99.681	98.838	98.318	99.243	99.555	98.793	100.356	97.751	99.585	99.574	97.819
cat Si	2.490	2.654	2.669	2.671	2.642	2.381	2.493	2.692	2.544	2.634	2.567	2.549	2.409	2.500
cat Al	1.495	1.320	1.323	1.320	1.348	1.610	1.492	1.307	1.444	1.359	1.430	1.408	1.566	1.488
cat Ti	0.001	0.000	0.000	0.000	0.000	0.000	0.000	0.000	0.000	0.000	0.001	0.001	0.001	0.000
cat Fe	0.000	0.024	0.001	0.002	0.002	0.002	0.005	0.002	0.005	0.006	0.010	0.043	0.004	0.013
cat Mn	0.000	0.000	0.000	0.000	0.000	0.002	0.000	0.000	0.000	0.000	0.000	0.002	0.002	0.000
cat Mg	0.000	0.012	0.000	0.000	0.000	0.000	0.000	0.000	0.000	0.001	0.000	0.014	0.000	0.000
cat Ca	0.520	0.317	0.340	0.336	0.351	0.614	0.521	0.304	0.555	0.361	0.396	0.448	0.614	0.459
cat Na	0.512	0.717	0.666	0.673	0.675	0.405	0.494	0.694	0.368	0.646	0.627	0.560	0.419	0.588
cat K	0.003	0.004	0.003	0.003	0.005	0.005	0.003	0.001	0.003	0.003	0.003	0.007	0.003	0.005
Total cations	5.020	5.047	5.004	5.006	5.024	5.019	5.009	5.001	4.920	5.010	5.032	5.030	5.018	5.053
Mole% Ab	49.497	69.117	65.956	66.461	65.477	39.524	48.496	69.428	39.733	63.958	61.128	55.203	40.453	55.902
Mole% An	50.239	30.528	33.705	33.223	34.058	60.011	51.168	30.436	59.917	35.716	38.626	44.129	59.222	43.628
Mole% Or	0.264	0.355	0.339	0.316	0.464	0.466	0.336	0.137	0.350	0.326	0.246	0.668	0.325	0.470
Sum	100.000	100.000	100.000	100.000	100.000	100.000	100.000	100.000	100.000	100.000	100.000	100.000	100.000	100.000

APPENDIX B: Plagioclase Compositions; S898 & 895 Mylonitic Amphibolite

	898.5f1.7	898.5f1.8	898.5f1.9	895.3f1.1	895.3af1.2	895.3f2.1	895.3f2.2
SiO2	51.340	52.973	54.055	55.641	56.126	55.602	57.937
Al2O3	30.248	29.277	28.744	27.210	27.306	27.123	26.443
TiO2	0.000	0.000	0.013	0.000	0.000	0.000	0.008
FeO	0.175	0.000	0.000	0.396	0.371	0.245	0.255
MnO	0.000	0.015	0.000	0.036	0.051	0.000	0.000
MgO	0.013	0.000	0.011	0.009	0.022	0.000	0.015
CaO	13.453	12.417	11.479	9.516	9.579	9.955	8.636
Na2O	4.294	4.734	5.113	6.453	6.498	6.271	6.858
K2O	0.050	0.055	0.027	0.068	0.032	0.059	0.047
Total	99.573	99.471	99.442	99.329	99.985	99.255	100.199
cat Si	2.348	2.413	2.454	2.525	2.530	2.525	2.592
cat Al	1.630	1.572	1.538	1.456	1.450	1.452	1.394
cat Ti	0.000	0.000	0.000	0.000	0.000	0.000	0.000
cat Fe	0.007	0.000	0.000	0.015	0.014	0.009	0.010
cat Mn	0.000	0.001	0.000	0.001	0.002	0.000	0.000
cat Mg	0.001	0.000	0.001	0.001	0.001	0.000	0.001
cat Ca	0.659	0.606	0.558	0.463	0.463	0.484	0.414
cat Na	0.381	0.418	0.450	0.568	0.568	0.552	0.595
cat K	0.003	0.003	0.002	0.004	0.002	0.003	0.003
Total cations	5.029	5.012	5.003	5.033	5.030	5.027	5.009
Mole% Ab	36.511	40.699	44.562	54.890	55.010	53.095	58.811
Mole% An	63.210	58.990	55.284	44.729	44.812	46.576	40.924
Mole% Or	0.280	0.311	0.155	0.381	0.178	0.329	0.265
Sum	100.000	100.000	100.000	100.000	100.000	100.000	100.000

APPENDIX C: Chlorite Compositions

Chlorite analyses are normalized to 28 oxygens. Compositions are separated into categories based on relative strain magnitude as discussed in the text. Label schemes for analyses follow similar patterns as illustrated for amphibole.

APPENDIX C: Chlorite Compositions; S62 Undeformed Amphibolite

	S625 chl1.1	S625 chl1.2	S625 chl1.3	S625 chl1.4	S625 chl1.5	S625	S625
SiO2	25.642	25.572	25.619	25.990	25.502	24.352	24.510
Al2O3	20.778	20.665	20.473	20.570	20.583	18.800	19.037
TiO2	0.056	0.027	0.094	0.063	0.017	0.000	0.000
FeO	24.696	24.458	24.354	24.161	24.501	30.019	29.704
MnO	0.223	0.213	0.260	0.288	0.198	0.301	0.268
MgO	15.792	16.220	16.193	16.620	16.538	12.142	12.012
CaO	0.039	0.031	0.044	0.011	0.011	0.020	0.047
Total	87.226	87.186	87.037	87.703	87.350	85.634	85.578
cat Si	5.418	5.401	5.420	5.444	5.379	5.437	5.460
cat Al	5.174	5.144	5.105	5.078	5.117	4.946	4.998
cat Ti	0.009	0.004	0.015	0.010	0.003	0.000	0.000
cat Fe	4.364	4.320	4.309	4.232	4.322	5.605	5.533
cat Mn	0.040	0.038	0.047	0.051	0.035	0.057	0.051
cat Mg	4.974	5.107	5.107	5.190	5.201	4.041	3.989
cat Ca	0.009	0.007	0.010	0.002	0.002	0.005	0.011
Total cations	19.987	20.022	20.013	20.007	20.059	20.090	20.041
Fe/(Fe+Mg)	0.467	0.458	0.458	0.449	0.454	0.581	0.581

APPENDIX C: Chlorite Compositions; S8991 Undeformed Amphibolite

	S8991 Sp1 Chl	S8991 Sp1 Chl	S8991 Sp1 Chl	S8991 Sp1 Chl	S8991 Sp1 Chl	S8991 Sp1 Chl	S8991 Sp1 Chl	S8991 Sp1 Chl	S8991 Sp1 Chl	S8991 Sp1 Chl
SiO2	25.966	26.988	26.432	26.063	26.134	26.76	26.425	26.275	26.004	26.426
Al2O3	21.741	21.78	21.874	21.75	21.726	21.487	22.063	21.894	21.983	22.142
TiO2	0.042	0.042	0.062	0.053	0.075	0.081	0.046	0.05	0.062	0.094
FeO	22.763	22.487	22.562	22.915	22.663	22.739	22.756	22.766	22.496	22.599
MnO	0.166	0.249	0.114	0.183	0.128	0.192	0.109	0.166	0.243	0.197
MgO	18.263	17.667	17.982	18.463	18.129	18.562	18.348	18.189	18.085	18.402
CaO	0.038	0.467	0.013	0.007	0.037	0.032	0	0.019	0.04	0.098
Total	88.98	89.68	89.04	89.43	88.89	89.85	89.75	89.36	88.91	89.96
cat Si	5.312	5.460	5.386	5.307	5.345	5.409	5.346	5.345	5.315	5.333
cat Al	5.242	5.193	5.253	5.220	5.236	5.119	5.261	5.249	5.296	5.266
cat Ti	0.006	0.006	0.010	0.008	0.012	0.012	0.007	0.008	0.010	0.014
cat Fe	3.894	3.805	3.845	3.902	3.876	3.844	3.850	3.873	3.845	3.814
cat Mn	0.029	0.043	0.020	0.032	0.022	0.033	0.019	0.029	0.042	0.034
cat Mg	5.570	5.329	5.462	5.605	5.527	5.594	5.534	5.516	5.511	5.536
cat Ca	0.008	0.101	0.003	0.002	0.008	0.007	0.000	0.004	0.009	0.021
Total cations	20.061	19.937	19.978	20.075	20.026	20.019	20.017	20.023	20.027	20.019
Fe/(Fe+Mg)	0.411	0.417	0.413	0.410	0.412	0.407	0.410	0.413	0.411	0.408

APPENDIX B: Chlorite Compositions; S81 Full Strain Transition: Mylonitic Section

	S81 Fmy chl	S81 Fmy chl	S81a Fmy chl1	S81a Fmy chl1	S81a Fmy chl1	S81a Fmy chl1	S81a Fmy chl1
SiO2	24.272	24.755	25.478	25.515	25.492	25.394	25.972
Al2O3	21.100	20.702	20.717	20.772	20.617	20.677	20.602
TiO2	0.020	0.051	0.087	0.065	0.057	0.081	0.073
FeO	23.411	22.221	23.273	23.628	23.670	23.514	22.862
MnO	0.314	0.212	0.184	0.247	0.284	0.220	0.262
MgO	16.014	16.039	16.665	16.375	16.359	16.320	16.684
CaO	0.043	0.011	0.014	0.033	0.000	0.028	0.000
Total	85.174	83.991	86.418	86.635	86.479	86.234	86.455
cat Si	5.242	5.379	5.397	5.401	5.410	5.400	5.481
cat Al	5.371	5.301	5.172	5.183	5.157	5.182	5.124
cat Ti	0.003	0.008	0.014	0.010	0.009	0.013	0.012
cat Fe	4.229	4.038	4.123	4.183	4.201	4.182	4.035
cat Mn	0.057	0.039	0.033	0.044	0.051	0.040	0.047
cat Mg	5.156	5.195	5.262	5.168	5.175	5.174	5.249
cat Ca	0.010	0.003	0.003	0.007	0.000	0.006	0.000
Total cations	20.069	19.962	20.004	19.997	20.003	19.996	19.946
Fe/(Fe+Mg)	0.451	0.437	0.439	0.447	0.448	0.447	0.435

APPENDIX D: Epidote Compositions

Epidote analyses are normalized to 13 oxygens. Compositions are separated into categories based on relative strain magnitude as discussed in the text. Label schemes for analyses follow similar patterns as illustrated for amphibole.

APPENDIX D: Epidote Compositions; S8991 & S8998 Undeformed Amphibolite

	S8998 SP3 EPID1	S8998 SP3 EPID1	S8991 SP1 EPID3	S8991 SP1 EPID3	S8991 SP1 EPID3	S8991 SP4 EPID1	S8991 SP4 EPID1	S8991 SP4 EPID2	S8991 SP4 EPID2	S8991 SP4 EPID2	S8991 SP4 EPID2	S8991 SP4 EPID2
SiO2	38.483	38.357	38.649	40.302	38.820	38.544	38.314	38.181	39.479	38.630	40.313	40.174
Al2O3	26.716	26.509	26.614	27.407	26.574	26.504	26.079	25.529	26.600	28.217	28.842	28.721
TiO2	0.072	0.196	0.016	0.115	0.077	0.068	0.013	0.038	0.243	0.149	0.105	0.120
Fe2O3	8.324	8.233	8.505	6.749	8.850	8.124	8.862	9.509	7.119	5.632	4.353	4.781
MnO	0.126	0.083	0.101	0.025	0.000	0.131	0.121	0.096	0.044	0.065	0.036	0.120
MgO	0.059	0.014	0.001	0.021	0.030	0.023	0.021	0.026	0.014	0.022	0.024	0.014
CaO	23.327	24.380	24.128	23.044	23.704	23.582	23.613	23.617	23.355	24.229	23.296	23.358
Total	97.107	97.772	98.014	97.663	98.055	96.976	97.023	96.996	96.854	96.944	96.969	97.288
cat Si	3.028	3.008	3.021	3.118	3.030	3.037	3.028	3.026	3.095	3.022	3.116	3.103
cat Al	2.477	2.450	2.452	2.499	2.444	2.461	2.429	2.385	2.457	2.602	2.628	2.614
cat Ti	0.004	0.012	0.001	0.007	0.005	0.004	0.001	0.002	0.014	0.009	0.006	0.007
cat Fe3+	0.493	0.486	0.500	0.393	0.520	0.482	0.527	0.567	0.420	0.332	0.253	0.278
cat Mn	0.008	0.006	0.007	0.002	0.000	0.009	0.008	0.006	0.003	0.004	0.002	0.008
cat Mg	0.007	0.002	0.000	0.002	0.003	0.003	0.002	0.003	0.002	0.003	0.003	0.002
cat Ca	1.966	2.049	2.021	1.910	1.982	1.991	1.999	2.006	1.961	2.031	1.929	1.933
Total cations	7.983	8.012	8.002	7.930	7.984	7.987	7.994	7.996	7.952	8.002	7.937	7.944
% Pistacite	49.778	49.645	50.839	40.760	52.606	49.103	53.486	57.639	43.783	33.911	26.368	28.822

APPENDIX D: Epidote Compositions; S142 Full Strain Transition

	S142 Sp1 Ep1	S142 Sp1 Ep1	S142 Sp2 Ep1	S142 Sp2 Ep1	S142 Sp2 Ep1	S142 Sp2 Ep1	S142 Sp2 Ep1	S142 Sp2 Ep2	S142 Sp2 Ep2	S142 Sp2 Ep3	S142 Sp2 Ep3	S142 Sp2 Ep3	S142 Sp2 Ep3	S142 Sp2 Ep3
SiO2	39.809	41.403	38.665	38.519	39.230	38.843	39.545	38.476	38.799	38.845	39.033	39.384	38.831	39.311
Al2O3	31.279	30.489	30.184	30.187	31.157	31.520	31.269	27.330	28.247	31.713	30.646	30.538	30.485	30.580
TiO2	0.000	0.000	0.000	0.000	0.000	0.000	0.000	0.000	0.000	0.000	0.000	0.000	0.000	0.000
Fe2O3	2.246	2.200	3.439	3.670	2.679	1.789	2.739	6.599	5.205	1.479	2.823	3.265	3.024	2.359
MnO	0.071	0.093	0.126	0.070	0.082	0.078	0.096	0.045	0.000	0.183	0.198	0.148	0.021	0.069
MgO	0.056	0.039	0.020	0.007	0.007	0.025	0.248	0.060	0.045	0.047	0.036	0.060	0.045	0.032
CaO	24.623	23.168	24.610	24.630	24.741	25.040	24.437	24.657	24.551	24.863	24.745	24.491	24.747	24.261
Total	98.084	97.392	97.044	97.083	97.896	97.295	98.334	97.167	96.847	97.130	97.481	97.886	97.153	96.612
cat Si	3.035	3.153	3.001	2.991	3.006	2.991	3.012	3.020	3.035	2.992	3.009	3.022	3.004	3.044
cat Al	2.810	2.736	2.761	2.762	2.813	2.860	2.807	2.528	2.604	2.879	2.784	2.762	2.780	2.790
cat Ti	0.000	0.000	0.000	0.000	0.000	0.000	0.000	0.000	0.000	0.000	0.000	0.000	0.000	0.000
cat Fe3+	0.129	0.126	0.201	0.214	0.154	0.104	0.157	0.390	0.306	0.086	0.164	0.189	0.176	0.137
cat Mn	0.005	0.006	0.008	0.005	0.005	0.005	0.006	0.003	0.000	0.012	0.013	0.010	0.001	0.005
cat Mg	0.006	0.004	0.002	0.001	0.001	0.003	0.028	0.007	0.005	0.005	0.004	0.007	0.005	0.004
cat Ca	2.011	1.890	2.046	2.049	2.031	2.066	1.994	2.073	2.058	2.052	2.044	2.014	2.051	2.013
Total cations	7.996	7.916	8.019	8.021	8.010	8.028	8.005	8.021	8.009	8.026	8.017	8.003	8.018	7.992
% Pistacite	13.131	13.185	20.287	21.577	15.585	10.474	15.857	40.031	31.580	8.640	16.592	19.108	17.861	14.061

APPENDIX D: Epidote Compositions; S142 Full Strain Transition

	S142 Sp2 Ep4	S142 Sp2 Ep5	S142 Sp2 Ep5	S142 Sp2 Ep5	S142 Sp2 Ep5	S142 Sp2 Ep5
SiO2	38.089	38.796	38.897	38.877	38.286	38.188
Al2O3	27.896	29.160	28.914	28.950	28.940	28.578
TiO2	0.000	0.000	0.000	0.000	0.000	0.000
Fe2O3	6.130	4.567	5.111	5.239	4.981	5.107
MnO	0.000	0.073	0.020	0.116	0.079	0.046
MgO	0.029	0.025	0.024	0.030	0.025	0.035
CaO	24.678	24.804	24.655	24.560	24.629	24.219
Total	96.822	97.425	97.621	97.772	96.940	96.173
cat Si	2.996	3.013	3.017	3.013	2.994	3.008
cat Al	2.586	2.669	2.643	2.644	2.667	2.653
cat Ti	0.000	0.000	0.000	0.000	0.000	0.000
cat Fe3+	0.363	0.267	0.298	0.306	0.293	0.303
cat Mn	0.000	0.005	0.001	0.008	0.005	0.003
cat Mg	0.003	0.003	0.003	0.003	0.003	0.004
cat Ca	2.080	2.064	2.049	2.039	2.064	2.044
Total cations	8.029	8.020	8.012	8.013	8.026	8.014
% Pistacite	36.913	27.228	30.412	30.993	29.651	30.693

APPENDIX D: Epidote Compositions; S910a & 895 Mylonitic Amphibolite

	S910A Sp4 Ep1	S910A Sp4 Ep1	S910A Sp4 Ep1	S910A Sp4 Ep1	S910A Sp4 Ep1	S910a Sp4 Ep Tr	S910a Sp4 Ep Tr	S910a Sp4 Ep Tr	S910a Sp4 Ep Tr	S910a Sp4 Ep Tr	S910a Sp4 Ep Tr	S910a Sp4 Ep Tr	S910a Sp4 Ep Tr
SiO2	40.170	39.691	38.509	38.858	39.006	38.019	37.815	38.044	38.154	38.548	39.564	38.734	38.592
Al2O3	33.125	33.155	27.437	28.077	28.308	26.796	25.451	25.639	26.457	27.760	26.542	28.483	27.662
TiO2	0.046	0.017	0.013	0.000	0.003	0.000	0.026	0.075	0.057	0.015	0.016	0.000	0.260
Fe2O3	0.461	0.104	7.344	6.428	6.197	8.331	9.812	9.895	8.453	7.275	7.809	6.451	6.943
MnO	0.008	0.054	0.202	0.063	0.087	0.060	0.086	0.009	0.000	0.126	0.025	0.055	0.050
MgO	0.013	0.000	0.018	0.044	0.000	0.000	0.004	0.013	0.021	0.014	0.017	0.016	0.028
CaO	25.009	24.435	24.011	24.205	23.974	23.985	23.923	24.056	24.310	24.405	23.283	24.073	24.558
Total	98.832	97.456	97.534	97.675	97.575	97.191	97.117	97.731	97.452	98.143	97.256	97.812	98.093
cat Si	3.019	3.019	3.013	3.023	3.032	2.997	3.002	3.000	3.004	2.999	3.093	3.008	3.002
cat Al	2.934	2.972	2.530	2.575	2.593	2.490	2.381	2.383	2.455	2.545	2.446	2.607	2.536
cat Ti	0.003	0.001	0.001	0.000	0.000	0.000	0.002	0.004	0.003	0.001	0.001	0.000	0.015
cat Fe3+	0.026	0.006	0.432	0.376	0.362	0.494	0.586	0.587	0.501	0.426	0.459	0.377	0.406
cat Mn	0.001	0.003	0.013	0.004	0.006	0.004	0.006	0.001	0.000	0.008	0.002	0.004	0.003
cat Mg	0.001	0.000	0.002	0.005	0.000	0.000	0.000	0.002	0.002	0.002	0.002	0.002	0.003
cat Ca	2.014	1.991	2.013	2.018	1.997	2.026	2.035	2.033	2.050	2.034	1.950	2.003	2.047
Total cations	7.998	7.992	8.005	8.001	7.990	8.011	8.012	8.010	8.015	8.015	7.953	8.000	8.012
% Pistacite	2.642	0.600	43.788	38.260	36.790	49.689	59.259	59.310	50.830	43.003	47.443	37.902	41.437

APPENDIX D: Epidote Compositions; S910a & 895 Myl

	S895 Sp7 Ep1	S895 Sp7 Ep1	S895 Sp7 Ep1	S895 Sp7 Ep1	S895 Sp7 Ep1
SiO2	37.822	53.789	40.946	38.137	38.279
Al2O3	26.928	19.894	25.779	27.058	28.706
TiO2	0.043	0.100	0.008	0.036	0.000
Fe2O3	7.758	6.253	8.052	7.455	6.182
MnO	0.097	0.038	0.074	0.071	0.136
MgO	0.032	0.027	0.003	0.006	0.011
CaO	24.003	18.569	23.382	24.068	24.388
Total	96.683	98.670	98.244	96.831	97.702
cat Si	2.994	3.957	3.166	3.009	2.980
cat Al	2.512	1.725	2.349	2.516	2.634
cat Ti	0.003	0.006	0.000	0.002	0.000
cat Fe3+	0.462	0.346	0.468	0.443	0.362
cat Mn	0.007	0.002	0.005	0.005	0.009
cat Mg	0.004	0.003	0.000	0.001	0.001
cat Ca	2.036	1.464	1.937	2.035	2.034
Total cations	8.017	7.502	7.925	8.010	8.021
% Pistacite	46.611	50.143	49.881	44.880	36.264

VITA

Matthew W. Nyman was born on April 25, 1961 in Fitchburg, Massachusetts approximately 7 minutes after his twin brother Martin. They were the third and fourth children of Richard and Beverly Nyman. Matthew's other siblings include an older sister, Marcia, and an older brother Mark. Matthew moved to Ashburnham, Massachusetts in 1968 and graduated from Oakmont Regional High School in 1979. In 1983 Matthew graduated from the University of Vermont, Burlington, Vermont with a Bachelor of Science degree in Geology. After a stint of carpentry and minerals consulting in Alaska and hydrogeology in Burlington, Vermont, Matthew attended The State University of New York at Binghamton starting in the Fall of 1985 and graduating in May, 1987 with a Masters of Arts in Geological Sciences. August of 1987 found Matthew at Virginia Polytechnic Institute and State University, Blacksburg, Virginia working towards a PhD in Metamorphic Petrology which was completed in January, 1992. After completion of this degree, Matthew (and his wife May) will move to Calgary, Alberta, Canada for postdoctoral work in geology at The University of Calgary.